SUPERCRITICAL GAS COOLING AND NEAR-CRITICAL-PRESSURE CONDENSATION OF REFRIGERANT BLENDS IN MICROCHANNELS

A Dissertation
Presented to
The Academic Faculty

by

Ulf Christian Andresen

In Partial Fulfillment
of the Requirements for the Degree
Doctor of Philosophy in
Mechanical Engineering

Georgia Institute of Technology
May 2007

SUPERCRITICAL GAS COOLING AND NEAR-CRITICAL-PRESSURE CONDENSATION OF REFRIGERANT BLENDS IN MICROCHANNELS

Approved by:

Dr. Srinivas Garimella, Advisor
G. W. Woodruff School of Mechanical
Engineering
Georgia Institute of Technology

Dr. S. Mostafa Ghiaasiaan
G. W. Woodruff School of Mechanical
Engineering
Georgia Institute of Technology

Dr. Samuel Graham
G. W. Woodruff School of Mechanical
Engineering
Georgia Institute of Technology

Dr. Donald R. Webster
School of Civil & Environmental
Engineering
Georgia Institute of Technology

Dr. Tom Fuller
School of Chemical and Biomolecular
Engineering
Georgia Institute of Technology

Date Approved:
1st of December 2006

ACKNOWLEDGEMENTS

First and foremost, I would like to thank to Dr. Srinivas Garimella who provided me with the opportunity of working in the Sustainable Thermal Systems Laboratory (STSL) at the Georgia Institute of Technology. His trust in my abilities, continuous encouragement and support in all aspects of life was the foundation of this work.

I would like to thank the members of STSL for providing me with a helping hand whenever it was needed: Lalit Bohra, Brian Fronk, Sangsoo Lee and Vishwanath Subramanium. Biswajit Mitra and Chris Goodman helped me in the start-up phase of this project. Matt Determan helped me monitor my experiments during short breaks. I highly value the discussions with Jesse D. Killion and Akhil Agarwal and their assistance during the most strenuous time in completing my dissertation.

Furthermore, I would like to thank my committee members for their guidance and suggestions: Drs. Tom Fuller, Mostafa Ghiaasiaan, Samuel Graham, and Don Webster.

Ulf C. Andresen

TABLE OF CONTENTS

LIST OF TABLES

LIST OF FIGURES

NOMENCLATURE

A	Area, [m^2]
D	Diameter, [mm]
c_P	Specific Heat, [J/kg-K]
E_0	Specific Work of Thermal Expansion, [-]
e	Surface Roughness, [mm]
f	Friction Factor, [-]
$f(\,,)$	Function of (,)
G	Mass Flux, [kg/m^2-s]
Gr	Grashof Number, [-]
g	Gravitational Acceleration = 9.81 m/s^2
h	Heat Transfer Coefficient, [W/m^2-K]
i	Enthalpy, [J/kg]
I.D.	Inner Diameter, [mm]
Ja	Jacob Number, [-]
J_G	Dimensionless Vapor Velocity, [-]
K	Loss Coefficient, [-]
k	Thermal Conductivity, [W/m-K]
L	Length, [m, mm]
LMTD	Log-Mean Temperature Difference, [°C, K]
M	Fin Parameter, [m^{-1}]
$\dot{m}$	Mass Flow Rate, [kg/s]
Nu	Nusselt Number, [-]

P	Pressure, [kPa]
P_r	Reduced Pressure (Ratio of Pressure to Saturation Pressure), [-]
Pr	Prandtl Number, [-]
$\dot{Q}$	Heat Duty, [W]
r	Radius, [mm]
r^*	Ratio of Outer and Inner Radii = r_{outer} / r_{inner} , [-]
Ra	Rayleigh Number, [-]
Re	Reynolds Number, [-]
STD	Standard Deviation
T	Temperature, [°C, K]
t	Thickness, [mm]
U	Uncertainty of ( )
$\dot{V}$	Volumetric Flow Rate, [m³/s]
V	Velocity, [m/s]
$\dot{W}$	Work Input, [W]
w	Width, [mm]
x	Quality, [-]
z	Height, [mm]

Greek Symbols

α	Void Fraction, [-]; Thermal Diffusivity, [m²/s]
β	Volumetric Thermal Expansion Coefficient, [1/K]
Δ	Change/ Difference, [-]
ε	Emissivity, [-]

μ	Dynamic Viscosity, [kg/m-s]
η	Efficiency, [-]
ρ	Density, [kg/m^3]
σ	Stefan-Boltzmann Constant = 5.67×10^{-8} W/m^2-K^4; Surface Tension, [N/m]
v	Kinematic Viscosity, [m^2/s]
ψ	Flow Multiplier, [-]; Surface Tension Parameter, [-]
X	Martinelli Parameter, [-]

Subscripts and Superscripts

Al	Aluminum
ambient	Surroundings
annulus	Annulus side
avg	Average
bulk	Bulk
CL	Critical-Lower
critical	Critical Point
CU	Critical-Upper
Cu	Copper
f	Friction
fin	Fins
flowmeter	Flowmeter
G	Gaseous or Vapor
H	Homogeneous Flow

hydraulic	Hydraulic
i	Inner
ideal	Ideal
in	Inlet
ins	Insulation
l, L	Liquid
laminar	Laminar Flow
o	Outer
out	Outlet
P	Constant Pressure
port	Individual Port in a Refrigerant or Water Tube
post	Post-Condenser
pre	Pre-Condenser
prim	Primary Loop
pump	Pump
r	Refrigerant; Reduced (i.e. P_r = Reduced Pressure)
s	Shell-and-Tube
S	Separated Flow
sat	Saturation
sec	Secondary Loop
shaft	Shaft
SS	Stainless Steel
t	Tube-in-Tube

test	Test Section
tube	Refrigerant or Water Tube
turbulent	Turbulent Flow
v	Vapor
w	Water
wall	Wall

SUMMARY

A study of heat transfer and pressure drop in zero ozone-depletion-potential (ODP) refrigerant blends in small diameter tubes was conducted. The azeotropic refrigerant blend R410A (equal parts of R32 and R125 by mass) has zero ODP and has properties similar to R22, and is therefore of interest for vapor compression cycles in high-temperature-lift space-conditioning and water heating applications. Smaller tubes lead to higher heat transfer coefficients and are better suited for high operating pressures.

Heat transfer coefficients and pressure drops for R410A were determined experimentally during condensation across the entire vapor-liquid dome at 0.8, $0.9 \times P_{\text{critical}}$ and gas cooling at 1.0, 1.1, $1.2 \times P_{\text{critical}}$ in three different round tubes (D = 3.05, 1.52, 0.76 mm) over a mass flux range of $200 < G < 800$ kg/m^2-s. A thermal amplification technique was used to accurately determine the heat duty for condensation in small quality increments or supercritical cooling across small temperature changes while ensuring low uncertainties in the refrigerant heat transfer coefficients.

The data from this study were used in conjunction with data obtained under similar operating conditions for refrigerants R404A and R410A in tubes of diameter 6.22 and 9.40 mm to develop models to predict heat transfer and pressure drop in tubes with diameters ranging from 0.76 to 9.40 mm during condensation. Similarly, in the supercritical states, heat transfer and pressure drop models were developed to account for the sharp variations in the thermophysical properties near the critical point.

The physical understanding and models resulting from this investigation provide the information necessary for designing and optimizing new components that utilize R410A for air-conditioning and heat pumping applications.

CHAPTER 1 - INTRODUCTION

This chapter discusses the need for an investigation of condensation heat transfer at high reduced pressures and gas cooling at supercritical pressures of refrigerant blend R410A in microchannels and its significance for the HVAC industry.

1.1 Need for Refrigerant Blend R410A

Certain refrigerants have an adverse effect on the ozone layer in the stratosphere by decomposing ozone at a higher rate than the creation of ozone. This has raised serious concerns about using HCFC (Hydrochlorofluorocarbon) and CFC (Chlorofluorocarbon) refrigerants in vapor compression cycles. In accordance with the Montreal Protocol, all CFC refrigerants were phased out by 1996, while HCFC refrigerants are to be phased out by 2030 (Gonzalez and Bankobeza, 2003). R410A is among the newer refrigerant blends with zero ozone-depletion-potential (ODP). It is an azeotropic refrigerant blend, composed of equal parts (by mass) of HFCs (Hydrofluorocarbon) R32 and R125. Table 1.1 compares the saturation properties of R410A and R22 at two different temperatures.

Table 1.1: Properties of R22 and R410A (Lemmon *et al.*, 2002)

	T (°C)	P (kPa)	i_{fg} (kJ/kg)	ρ (kg/m^3)		μ (µPa·s)		k (mW/m-K)	
				liquid	vapor	liquid	vapor	liquid	vapor
R22	60.0	2427	140.0	1030.4	111.6	108.0	14.8	67.04	15.93
	40.1	1537	166.5	1128.2	66.3	138.6	13.3	76.57	12.85
R410A	60.0	3837	107.6	815.5	200.8	68.8	19.7	74.45	32.77
	40.1	2427	162.5	975.2	103.7	98.0	16.0	85.65	19.57

The critical temperature and pressure for R22 and R410A are: 96.1°C/4990 kPa and 71.4°C/4903 kPa respectively. Figure 1.1 depicts the pressure-enthalpy diagrams for R22 and R410A. It is apparent that any refrigeration system using R410A operates at a significantly higher pressure. R410A is therefore considered a high-pressure-refrigerant and does not classify as a "drop-in" replacement for R22, without design modifications. Few models are available for the prediction of condensation heat transfer and pressure drop in refrigerant blends at near-critical pressures. Also, in the supercritical state, most available models have been developed for carbon-dioxide or steam.
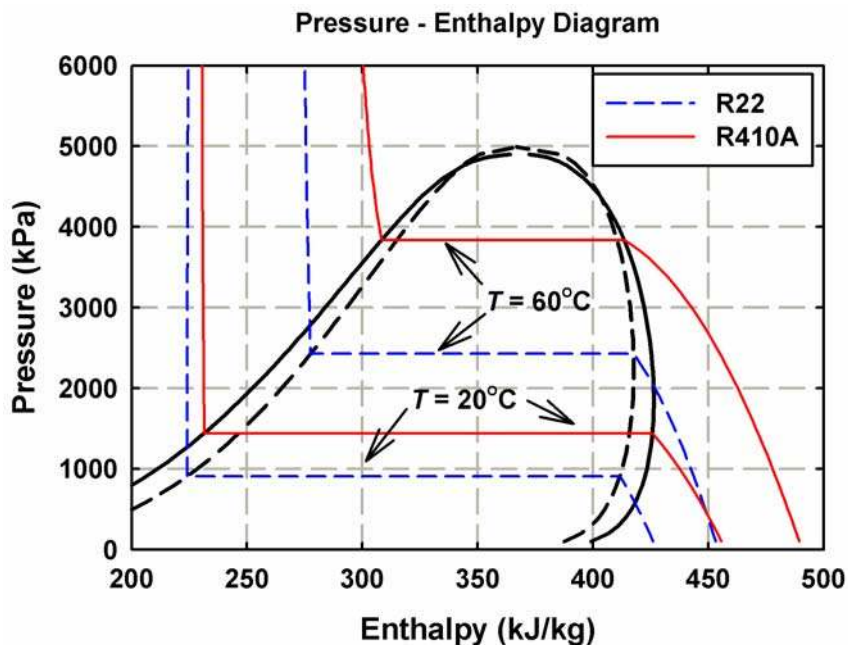
Figure 1.1: Pressure-Enthalpy Diagram for R22 and R410A (Lemmon *et al.*, 2002)

1.2 R410A in Microchannels

The need for understanding the behavior of refrigerant R410A in small diameter tubes at high operating pressures comes from the recent interest in using vapor compression

cycles for high temperature-lift space-conditioning and water-heating applications. To achieve the high temperatures required, the refrigerant blend must either undergo a condensation process at pressures close to the critical pressure ($P_{critical}$) or a gas cooling process at pressures exceeding the critical pressure. In the latter case, the refrigerant blend transitions from a gas-like phase to a liquid-like state as the temperature decreases across the critical region, without an isothermal phase change process.

It is particularly important to understand these near-critical-pressure phenomena in microchannels because these small diameter tubes are especially suitable for the high operating pressures. Furthermore, the physical mechanisms for heat transfer and pressure drop are different in small diameter tubes. Two-phase heat transfer in large diameter tubes is influenced by gravitational effects, resulting in a wavy flow at some conditions. With a decrease in diameter, gravitational effects are less significant such that annular flow becomes more prevalent. Annular flow is shear-driven flow, often corresponding to high heat transfer coefficients. Heat transfer and pressure drop data are available for tubes currently used in AC systems: 9.40 and 6.22 mm for refrigerants R410A and R404A (Jiang, 2004; Mitra, 2005). In this study, tubes of diameters 3.05, 1.52 and 0.76 mm were used, where the 3.05 mm tube is a standard copper tube. The 1.52 mm and 0.76 mm tubes are multiport extruded aluminum tubes provided by Modine Manufacturing Company. Such multiport tubes are already in use in automotive air-conditioning heat exchangers. The data from all these tubes are used to develop heat transfer and pressure drop models that span a diameter range from 9.40 to 0.76 mm for two different refrigerants (R410A and R404A), which is directly applicable to a wide range of conditions of interest to the

HVAC&R industry. In addition to varying the diameter, the effects of mass flux, operating pressure, quality (during condensation) and temperature (during supercritical cooling) are investigated.

1.3 Objectives of Present Study

The objectives of the present study are as follows:

- Experimentally determine the local heat transfer coefficient and pressure drop of R410A in three different smooth round tubes of 3.05, 1.52 and 0.76 mm internal diameter (I.D.) for the mass flux range $200 < G < 800$ kg/m^2-s under the following conditions:

  - Condensation: at pressures 0.8 and $0.9 \times P_{critical}$, where the entire vapor-liquid dome is traversed in small quality increments; typically $\Delta x < 0.3$.

  - Critical/Supercritical Cooling: at pressures 1.0, 1.1, and $1.2 \times P_{critical}$, where the temperature intervals are chosen to track the steep changes in heat transfer and pressure drop phenomena near the critical point with high resolution.

- Compare the heat transfer and pressure drop data for condensation and supercritical cooling with the limited correlations in the literature and provide explanations for agreement or disagreement with the existing models. The most significant parameters influencing heat transfer and pressure drop are identified and considered in the subsequent model development.

- Develop models for the heat transfer and pressure drop with validation based on the data from this study and data on 6.22 and 9.40 mm tubes available from

4

previous similar studies. The models account for the flow mechanisms during condensation and supercritical gas cooling.

The wide range of mass fluxes and tube diameters at the different pressures allows for a comprehensive understanding of the underlying physics driving the behavior of refrigerant blends such as R410A.

1.4 Organization of the Dissertation

This dissertation is organized as follows:

CHAPTER 2 provides a literature review of the most significant work on in-tube condensation and supercritical heat transfer and pressure drop. The deficiencies in the literature are identified.

CHAPTER 3 explains the experimental set-up and procedures for all tests.

CHAPTER 4 presents the analysis of the data with sample calculations and an estimation of the respective uncertainties.

CHAPTER 5 and **CHAPTER 6** discuss the experimental results for the condensation and supercritical studies, respectively. Comparisons of the data with the most applicable models from the literature are shown. This is followed by the development of models for heat transfer and pressure drop at near-critical pressures.

CHAPTER 7 provides the conclusions, summarizes the findings and provides recommendations for future work.

CHAPTER 2 - LITERATURE REVIEW

An overview of the most significant studies of in-tube condensation and supercritical gas-cooling is presented here.

2.1 Prior Investigations of In-Tube Condensation

Condensation studies can be classified into flow regime, pressure drop and heat transfer studies. The work proposed here falls into the latter two categories, but since prior work on flow regimes will be utilized to model the results, a brief review of all three types of investigations is provided here.

2.1.1 Flow Regimes

A combination of gravitational forces, inertial forces and interfacial shear stresses governs the flow regimes. Surface tension also assumes increasing significance at the smaller diameters. Annular flow is associated with high interfacial shear stresses. Gravitational effects are more significant in the wavy flow regime. Several researchers have tried to characterize and predict the transitions from one flow regime to another by flow visualization as well as by analytical approaches.

Taitel and Dukler (1976) developed a theoretical flow regime map for gas-liquid mixtures for horizontal and near horizontal pipe flow. In this study, five basic flow regimes were considered: smooth stratified, wavy stratified, intermittent (slug and plug), annular with dispersed liquid and dispersed bubble. The transition from one flow regime to another was based on dimensionless parameters, which are dependent on gas and liquid mass

flow rates, properties of the fluid, pipe diameter and angle of inclination with respect to the horizontal. Taitel and Dukler's flow map was developed for two-phase air-water flow and not for phase-change condensation, which is of interest in the present study. Additionally, surface tension effects were not accounted for in this study.

Breber *et al.* (1980) developed a flow regime map based on condensation data for several different refrigerants (R11, R12, R113) along with steam and n-Pentane for inside tube diameters ranging from 4.8 to 50.8 mm. The flow map consisted of four different regimes: Annular and annular mist, bubble, wavy and stratified, slug and plug flow. The transition from one regime to another was determined by the Martinelli parameter and the superficial gas velocity. The experimental results were compared with Taitel and Dukler's (1976) work. Overall, good agreement was found, except at small diameters. The authors concluded that transition criteria for adiabatic two-phase flow could also be applied to condensing flow.

Tandon *et al*. (1985) characterized the flow patterns of three different binary mixtures of R22 and R12 in a 10 mm inner diameter round tube. They categorized the flow patterns into annular, semiannular, wavy, slug and plug flow. Comparison with the literature showed that Breber *et al.*'s map did not represent the wavy flow pattern well. In addition, the comparison with semiannular flow data was also unsatisfactory. The annular and slug flow data, however, were depicted well.

Ewing *et al.* (1999) used flow visualization to test the applicability of Breber *et al.*'s (1980) flow map for adiabatic air and water mixtures. The flow channels were horizontal, round, transparent tubes with an inner diameter of 19 mm. The data were generally consistent with the results of Breber *et al.* and support the general applicability of the map.

Dobson and Chato (1998) analyzed four refrigerants (R12, R22, R134a, R32/R125 in 50/50 percent and 60/40 percent mass fraction) condensing in smooth tubes with inner diameters ranging from 3.14 to 7.04 mm. The flow regimes were broadly divided into two categories: gravity-dominated and shear dominated flows. In gravity dominated flows, the laminar film condensing at the top of the tube dominated, whereas in shear dominated flows, forced-convective condensation was the driving mode of heat transfer. Flow regimes were assigned based on the modified Froude number introduced by Soliman (1982). The Froude number captures the effects of inertial to gravitational forces. Further, the flow regimes were subdivided into five categories for high void fractions, listed in the order of increasing vapor velocity: stratified, wavy, wavy-annular, annular and annular-mist flow. For low void fractions, the flow is further divided into slug, plug, and bubbly flow, listed in order of increasing liquid inventory.

Coleman (2000) and Coleman and Garimella (2000a; 2000b; 2003) classified the flow regimes for condensing R134a in round and square tubes, for hydraulic diameters ranging from 1 to 5 mm and a mass flux range of $150 < G < 750$ kg/m^2-s. From flow visualization, the following major flow regimes were identified: annular, wavy,

intermittent and dispersed flow. Each flow regime was further divided into flow patterns to precisely describe the flow. The flow maps were plotted on mass flux versus quality graphs. Simple algebraic equations were used as transition criteria.

El Hajal *et al.* (2003) and Thome *et al.* (2003) developed a flow pattern map for condensation based on a prior map developed for evaporation by Kattan *et al.* (1998b; 1998a; 1998c). The different flow regimes were: fully-stratified, stratified-wavy, intermittent, annular, mist and bubbly flow. The flow map incorporates a new definition of the logarithmic mean void fraction: For high reduced pressures, the homogeneous void fraction model is proposed; at low reduced pressures, the model by Rouhani and Axelsson (1970) is used. For intermediate pressures, both models are combined to obtain a logarithmic mean void fraction. The flow map is built on a data bank of twenty different fluids (including R410A and R404A), with reduced pressures ranging $0.02 < P_r < 0.8$ and a diameter range of $3.14 < D < 21.4$ mm. This study was also used to develop a new heat transfer model, which is explained in a subsequent section.

2.1.2 Condensation Pressure Drop

The pressure drop during condensation arises from shear stresses imposed by the surrounding walls, the interaction of the two phases, and a deceleration component due to the change in density during condensation. As the low-density vapor condenses to a higher-density liquid, the overall flow velocity decreases, resulting in an increase in static pressure. The deceleration pressure change acts opposite to the frictional pressure drop, reducing the overall measured pressure drop. Researchers have correlated the frictional

9

pressure drop in two-phase studies to single-phase flow with the aid of two-phase multipliers (Lockhart and Martinelli, 1949; Chisholm, 1973; Friedel, 1979). These correlations, however, do not represent the physical phenomena well and often lead to significant errors and scatter. More recent studies have modified the above mentioned correlations to improve the agreement with their data (Mishima and Hibiki, 1996; Tran *et al.*, 2000; Lee and Lee, 2001; Cavallini *et al.*, 2002; Kawahara *et al.*, 2002; Jiang, 2004; Mitra, 2005).

Lockhart and Martinelli (1949) developed a widely used correlation for two-phase pressure drop by relating the Martinelli parameter, X, to the liquid and gas two-phase mulipliers. The Martinelli parameter relates the pressure drop in the pipe if the liquid phase flowed alone, to the pressure drop if the gas phase flowed alone. Their investigation included data for adiabatic two-phase flow in horizontal tubes for air, benzene, kerosene, water and various oils in round tubes ranging from 1.49 to 25.83 mm. The pressure drops were correlated based on whether the liquid flow and gas flow were laminar or turbulent. Chisholm (1967) developed the following correlations for the two-phase multipliers, which were found to be in good agreement with the predictions of Lockhart and Martinelli:

$$\phi_L = \left(1 + \frac{C}{X} + \frac{1}{X^2}\right)^{1/2}$$
(2.1)

$$\phi_G = \left(1 + CX + X^2\right)^{1/2}$$
(2.2)

The constant C depends on the flow regime of the liquid and gas phases.

Chisholm (1973) focused on convective evaporation of steam, water mercury and nitrogen mixtures. A new dimensionless parameter, Γ, was introduced, relating the gas-only pressure drop to the liquid-only pressure drop. Gas-only or liquid-only refers to flow through the entire tube at the same mass flux as the two-phase mixture. The resulting two-phase multiplier has the form:

$$\phi_{LO}^2 = 1 + \left(\Gamma^2 - 1\right) \cdot \left[B \cdot x^{(2-n)/2} \cdot (1-x)^{(2-n)/2} + x^{2-n} \right] \tag{2.3}$$

The exponent n depends on the flow regime (laminar or turbulent). The constant B is a function of mass flux and Γ. Typically, the exponent n is the same exponent as the Blasius friction factor correlation.

Tran *et al.* (2000) studied evaporating refrigerants (R134a, R12, R113) in two round ($D =$ 2.46 and 2.92 mm) and one rectangular (4.06 × 1.7 mm) tubes. Chisholm's (1973) model was modified to account for the effects of surface tension. The confinement number, N_{conf}, relates surface tension to buoyancy forces. The resulting two-phase multiplier is:

$$\phi_{LO}^2 = 1 + \left(4.3\Gamma^2 - 1\right) \cdot \left[N_{conf} \cdot x^{0.875} \cdot (1-x)^{0.875} + x^{1.725} \right] \tag{2.4}$$

Friedel (1979) used a data bank of over 25,000 points of horizontal and vertical up and downward flow in round and rectangular tubes. The data bank is dominated by flow of water, R12, air-water and air-oil mixtures and tubes of circular cross-section. A liquid-only two-phase multiplier is used to determine the frictional pressure drop.

$$\phi_{LO}^2 = C_{F1} + \frac{3.21 C_{F2}}{\text{Fr}^{0.045} \text{We}^{0.035}} \tag{2.5}$$

11

Besides the Froude number, Fr, and the Weber number, We, the constants C_{F1} and C_{F2} are functions of the quality and property ratios of the liquid and vapor phases. Friedel's correlation was considered to be applicable to all flow regimes. Other researchers, such as Cavallini *et al.* (2002), have tried to improve its predictive capabilities by modifying the exponents and constants in the expression for ϕ_{LO}^2, especially for the annular flow regime.

Cavallini *et al.* (2002) used the dimensionless vapor velocity, J_G, to distinguish between flow regimes and improve Friedel's (1979) correlation in the annular flow regime for condensing refrigerants. The data bank included refrigerants R22, R134a, R125, R32, R236ea, R407C and R410A in an 8 mm round tube with reduced pressures less than $P_r <$ 0.8 and a mass flux range $100 < G < 750$ kg/m²-s. For annular flow, new constants were fit to Friedel's original model. This two-phase multiplier correlation did not include the Froude number, because they reasoned that gravitational effects are not significant in the annular flow regime. It should be noted, however, that the predictions of these models display discontinuities as the flow transitions from annular flow to the other regimes.

Mitra (2005) also modified the empirical constants in Friedel's (1979) correlation to predict the pressure drop in all flow regimes present in his and Jiang's (2004) study (wavy and annular flow) on high pressure refrigerants (R410A and R404A) in tubes ranging from 6.22 – 9.40 mm I.D.

Garimella *et al.* (2005) investigated the pressure drop for condensing refrigerant (R134a) flow in microchannels, ranging from $0.5 < D < 4.91$ mm. The mass flux under

investigation ranged from $150 < G < 750$ kg/m^2-s. A pressure drop model for annular/ mist/disperse flow was developed by defining an interfacial friction factor correlation, which was a function of the Martinelli parameter, liquid-phase Reynolds number, and a non-dimensional surface tension parameter, originally introduced by Lee and Lee (2001). For intermittent flow, the model by Garimella *et al.* (2002; 2003), which accounts for pressure drop in the liquid slug, the film-bubble region, and in the transitions between them, was used. Smooth transitions between the predictions in the annular and intermittent regions were ensured through appropriate interpolation.

The friction factor, or shear stress, determined in the pressure drop analysis is often used in the heat transfer models, which are discussed next.

2.1.3 Condensation Heat Transfer

Some of the frequently cited heat transfer correlations for condensing flows inside round tubes by Kosky and Staub (1971), Traviss *et al.* (1973) and Shah (1979) were developed for purely annular flow. With the phasing out of HCFCs and CFCs, researchers have focused on newer refrigerants and refrigerant blends. Several studies (Eckels and Pate, 1991; Ebisu and Torikoshi, 1998; Kwon and Kim, 2000; Han and Lee, 2001) compare the heat transfer of CFCs, such as R12 and R22, to the proposed replacements, such as R134a and R410A. In more recent condensation studies (Sweeney, 1996; Dobson and Chato, 1998; Ebisu and Torikoshi, 1998; Boissieux *et al.*, 2000; Han and Lee, 2001; Cavallini *et al.*, 2002; El Hajal *et al.*, 2003; Thome *et al.*, 2003) flow regime based heat transfer models were developed.

Kosky and Staub (1971) studied annular condensation of steam in a 12.57 mm I.D. horizontal tube for pressures ranging from 20 – 152 kPa and a mass flux range of 2.7 – 150 kg/m^2-s. Since the flow was in the annular regime, orientation was not significant. The heat and momentum transfer analogy was applied to determine the annular flow heat transfer, where the two-phase gas multiplier was used to determine the shear stress and dimensionless temperature, which was related to the non-dimensional film thickness. This model is limited to Newtonian fluids with changes in thermophysical properties that are small with temperature variations.

Traviss *et al.* (1973) studied R12 and R22 during condensation, focusing on annular flow in horizontal 8 mm tubes. An analytical model was developed based on von Karman's universal velocity distribution to describe the liquid film. The turbulent vapor core was assumed to be at the saturation temperature without any radial temperature gradients. The data were obtained for mass fluxes $161 < G < 1530$ kg/m^2-s at saturation temperatures between 25 and 58°C. Good agreement was obtained between the data and their model, although, the authors pointed out that since the model assumes an annular condensation film around the tube wall with no entrainment, it underpredicts the data for disperse and mist flow.

Shah (1979) used data from 21 different studies to develop a heat transfer model for condensation based on a previous model for evaporation. In the condensation study, the mass flux ranged from $11 < G < 211$ kg/m^2-s and the reduced pressure $0.002 < P_r < 0.44$. The fluids in the reference studies were water, R11, R12, R22, R113, methanol, ethanol,

benzene, toluene and tricholoroethylene in horizontal, vertical and inclined pipes of diameters ranging from 7 to 40 mm. The heat transfer model includes a correction for the reduced pressure, although due to the limited P_r range in the data bank used, heat transfer predictions at pressures close to the critical pressure are not expected to be adequate.

Kwon *et al.* (2001) developed an analytical model for condensation heat transfer coefficients for turbulent annular film flow. Their model also accounted for liquid entrainment. The authors adopted the correlation proposed by Ishii and Mishima (1998) for determining the amount of entrained fluid in annular flow in the equilibrium and entrance regions. They accounted for liquid entrainment by including it in the development of the momentum and mass balance equations for their overall model. The predictions of their model were compared with the data from a previous study (Kwon and Kim, 2000), in which the heat transfer coefficients for R22 in smooth, horizontal tubes were obtained. The model was in good agreement with the experimental results, due to the improved prediction of the eddy viscosity model for turbulent annular film flow and the consideration of liquid entrainment.

Cavallini *et al.* (2002) developed a heat transfer and pressure drop model for halogenated refrigerants (including R410A) using a data bank from the literature. The model is only valid for pressures less than $0.75 \times P_{critical}$ (since no data were available at higher pressures) and tube diameters ranging from $3 < D < 21$ mm. The mass flux ranged from $100 < G < 750$ kg/m^2-s. Cavallini *et al.* suggested criteria similar to Breber *et al.* (1980) for the primary flow regimes in their investigation. Heat transfer models were developed

to predict the following: annular, annular stratifying, and slug flow. In addition, transitions between the flow regimes were addressed. The superficial gas velocity and Martinelli parameter served to distinguish between the flow regimes. To predict the annular flow heat transfer coefficient, the model by Kosky and Staub (1971) was proposed. In addition, a new correlation for the frictional pressure gradient based on Friedel's (1979) correlation was developed, as described in the previous section of this chapter. The stratified flow model considered the condensing the film on the inner tube in addition to the liquid pool at the bottom of the tube separately. It is stated by the authors that the contribution of the liquid pool to the total heat transfer is more significant at higher reduced pressures. In the slug flow region, the heat transfer coefficient was computed using a two-phase multiplier applied to the corresponding single-phase heat transfer coefficient.

El Hajal *et al.* (2003) and Thome *et al.* (2003) studied condensing refrigerants and refrigerant blends (15 different fluids) for pressures up to $0.8 \times P_{critical}$, however, the studies for R410A were only for $P < 0.63 \times P_{critical}$. The flow regime map and heat transfer model were built upon the work of Kattan *et al.* (1998b; 1998a; 1998c), who studied evaporating refrigerants. The flow patterns observed fell into the following regimes: annular, stratified-wavy, fully stratified, intermittent, mist and bubbly flow. Only the first five regimes were included in this model, as few or no data were available for the bubbly flow regime. The heat transfer was said to occur due to two types of mechanisms within the tube: convective condensation and film condensation. Annular, mist and intermittent flow were governed by convective condensation, whereas stratified-wavy and stratified

flow were composed of both, convective and film condensation. The relative composition is determined by knowing the portion of tube filled with the liquid pool. The heat transfer coefficients were correlated in terms of the Reynolds number, Prandtl number and interfacial friction factor.

Jiang (2004) studied R404A condensing in 9.40 mm tubes, while Mitra (2005) investigated R410A in 6.22 and 9.40 mm I.D. tubes under similar conditions as those in the present study. The heat transfer was said to occur due to two types of mechanisms: wavy flow and annular flow. The annular flow model was based on a two-phase multiplier approach, recognizing that the liquid film in the flow almost always exhibited fully turbulent behavior. In the wavy flow model, it was assumed that the local heat transfer was the sum of film condensation on the top portion of the tube and forced convection in the liquid pool at the bottom. Data were assigned to the different flow regimes based on the modified Soliman Froude number (Soliman, 1982). The effects of diameter were also modeled. However, because only two tube diameters were investigated these models may not accurately predict heat transfer and pressure drop in the smaller diameter tubes under consideration in the present work.

2.2 Supercritical Heat Transfer and Pressure Drop

During the flow of a fluid at supercritical pressures, significant property variations occur as the temperature of the fluid approaches the transition temperature. Below the transition temperature, the fluid is considered to behave as a liquid, while above the transition temperature, the fluid behaves as a gas. The transition temperature is uniquely defined for

17

each pressure. Figure 2.1 shows that the specific heat of the fluid spikes at the transition point, the density abruptly increases, and the viscosity and thermal conductivity increase as the fluid is cooled from a gas-like to a liquid-like state. It should also be noted that specific heat , c_p , drastically increases as the fluid transitions from a liquid-like to a gas-like state, where the peak in c_p marks $T_{pseudo\text{-}critical}$.
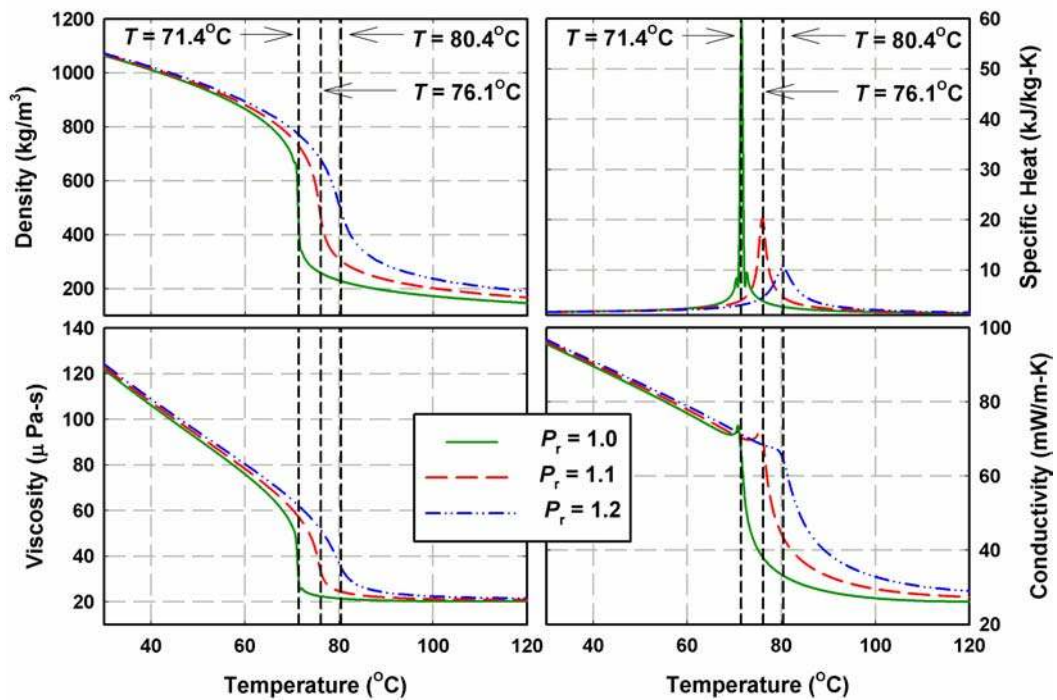
Figure 2.1: Properties of R410A at Critical and Supercritical Pressures

(Lemmon *et al.*, 2002)

With an increase in P_r further above the critical pressure, the magnitude of c_p gets smaller. The specific heat characterizes the energy required to increase the temperature of the fluid by a certain value. Inside the liquid-vapor dome (subcritical state), the c_p of the refrigerant is undefined or infinite, as heat addition or rejection occurs isothermally

during phase change. In the supercritical state, the refrigerant transitions from a liquid-like to a gas-like state, but the transition occurs over a small temperature range, which leads to a high value of c_P. These property variations lead to spikes in the heat transfer coefficient near the transition point. The decrease in density in the gas-like phase results in a larger pressure drop due to the higher flow velocities. Most prior research on supercritical heat transfer and pressure drop focuses on steam and carbon-dioxide studies. Only recently have refrigerant blends been studied by researchers (Jiang, 2004; Mitra, 2005) at supercritical pressures.

Ghajar and Asadi (1986) compared existing empirical approaches for forced convective heat transfer near the critical point for CO_2 and water in turbulent pipe flow. The most significant discrepancies according to Ghajar and Asadi are due to 1) property variations, 2) heat flux and buoyancy effects and 3) differences in values of the physical properties used by the different researchers. The mass fluxes in the CO_2 data bank ranged from 26 to 2500 kg/m^2-s and a reduced pressure range of 1 - 1.46. The water data ranged from 17 < G < 3000 kg/m^2-s and 0.018 < P_r < 1.88. To correct for the differences in physical properties, Ghajar and Asadi recomputed all constants in the cited models with the same property inputs. Then the heat transfer models were compared with all the available data. It was determined that the following Nusselt number correlation yielded the best results,

$$\text{Nu} = a\,\text{Re}^b\,\text{Pr}^c \left(\frac{\rho_w}{\rho_b}\right)^d \left(\frac{c_{P,w}}{c_{P,b}}\right)^n \tag{2.6}$$

where the constants a, b, c, d are determined by a non-linear least squares regression and n is chosen by the Jackson and Fewster (1975) criterion. It is apparent that the convective

heat transfer model follows a Dittus-Boelter (1930) type correlation with property ratio multipliers to account for the large property variations in the near-critical region.

Pitla *et al.* (1998) conducted a comprehensive literature review of heat transfer and pressure drop for supercritical carbon dioxide. Most of the research they reviewed was conducted by Russian scientists during the 1960s and 70s. The paper focuses on the thermophysical properties, factors influencing heat transfer, heat transfer correlations for heating and cooling, coefficient of friction and numerical methods used in the calculation of heat transfer at supercritical pressures. Pitla *et al.* state that Shitsman (1963), Tanaka et al. (1971) and Krasnoshchekov *et al.* (1970) observed an improvement in the heat transfer when the wall temperature was less than the critical temperature and the fluid bulk temperature was greater than the critical temperature. Krasnoshchekov *et al.* (1970) attributed the higher heat transfer rate to the formation of a liquid-like layer near the wall of the tube. The thermal conductivity of this layer is higher than the conductivity of the bulk fluid. Similarly, the heat transfer during heating decreases as a thin gas layer forms near the wall.

Kurganov (1998a; 1998b) investigated the heating of CO_2 at supercritical pressures. A dimensionless parameter was used to divide the flow into three different regions: liquid-like state, pseudo-phase transition and gas-like state. Heat transfer and pressure drop correlations were developed for each region. The dimensionless parameter is the specific work of thermal expansion:

$$E_0 = P\left(\frac{\partial(1/\rho)}{\partial i}\right)_P = \frac{P\beta}{\rho c_P} \tag{2.7}$$

E_0 represents the ratio of work done by the refrigerant during cooling to the heat convected out during flow.

In a two part paper, Pitla *et al.* (2001b; 2001a) undertook a numerical study of heat transfer and pressure drop during cooling of supercritical CO_2. The numerical simulations are based on Favre-averaged (density-weighted averaged), parabolized Navier-Stokes equations. The turbulent model also involved Nikuradse's mixing length model and the *k-ε* equation. Experiments were conducted to compare the numerical simulations. An average of the Nusselt number at the bulk and wall temperatures using the Gnielinski (1976) equation was used to model the results.

Only recently have researchers investigated the cooling of refrigerant blends at supercritical pressures. Jiang (2004) studied the pressure drop and heat transfer of refrigerant R404A at supercritical pressures in a 9.40 mm round tube. Mitra (2005) studied supercritical cooling of R410A in 9.40 and 6.22 mm I.D. round tubes. The data from both studies were combined by Mitra (2005) for model development. The specific work of thermal expansion (Kurganov, 1998a; 1998b) was used to divide the data into three different regions. The pressure drop was modeled using Churchill's equation (1977) where correction multipliers for the bulk and wall viscosity and a diameter ratio were used for each flow regime. Similarly, the heat transfer model incorporated a diameter ratio as well as a specific heat ratio (for wall and bulk properties) multiplier to modify the single phase Nusselt number correlation of Churchill (1977). The baseline diameter was

9.40 mm. It is not clear whether these models developed for 6.22 < D < 9.40 mm can be extrapolated to the much smaller tubes under consideration here.

Most researchers have recommended heat transfer correlations for single-phase flow with property corrections to account for the significant variations near the critical region. Prior investigations have focused on supercritical heating experiments where the inner wall temperature is higher than the temperature of the bulk fluid. The higher temperatures at the wall correspond to lower viscosities and lower thermal conductivities. For supercritical cooling, the opposite is expected. The temperatures at the wall are lower than the bulk flow, corresponding to higher thermal conductivities and viscosities characteristic of liquid-like fluids. It is expected that the bulk-to-wall temperature difference has a significant impact on heat transfer coefficients and frictional pressure drops and that correlations for supercritical heating will not adequately predict supercritical cooling data.

2.2 Summary of Literature Review

The relevant pressure drop models for condensation are summarized in Table 2.1. As mentioned in the previous sections, most pressure drop models were developed for adiabatic flow or water/air mixtures. The most commonly used two-phase pressure drop models correlate the frictional pressure drop in two-phase studies to single-phase flow with the aid of two-phase multipliers (Lockhart and Martinelli, 1949; Chisholm, 1973; Friedel, 1979). Only Jiang (2004) and Mitra (2005) have investigated high-pressure refrigerants (R404A and R410A) at conditions similar to those investigated in this study.

However, the tubes investigated by them (9.40 and 6.22 mm) were much larger than the
tubes under consideration here (0.76 – 3.05 mm).

Table 2.1: Summary of In-tube Condensation: ΔP

Author	Fluids	I.D. (mm)	G (kg/m²-s)	P_r or Tsat (°C)	Models
Lockhart and Martinelli (1949)	Air, benzene, kerosenes, water, oil	1.49-25.83		110.3 – 359.5 kPa	Liquid/vapor two-phase multiplier approach
Chisholm (1973)	Air/water, Steam		190-6770		Liquid-only two phase multiplier
Friedel (1979)	Various fluids from literature				Liquid-only two phase multiplier
Mishima and Hibiki (1996)	Air/water mixtures	1 - 4			Exponential diameter function in two-phase multiplier
Tran et al. (2000)	R134a, R12, R113	2.46, 2.92, 4.06 ×1.7	69 - 704	$0.04 < P_r < 0.23$	Modified Chisholm (1973) to include confinement number
Lee and Lee (2001)	Air/water mixture	0.4 – 4	$175 < Re_{LO} < 17,700$		Modified Lockhart and Martinelli (1949) approach
Cavallini et al. (2002)	R22, R134a, R125, R32, R410A, R236ea	3 – 21	100 – 750	$30 < T_{sat} < 60$ $P_r < 0.75$	Modified Friedel's (1979) correlation for annular flow
Jiang (2004)	R404A	9.40	200 - 800	$0.8 < P_r < 0.9$	Modified Friedel's (1979) correlation for wavy and annular flow
Mitra (2005)	R410A	6.22, 9.40			
Garimella et al. (2005)	R134a	0.5 – 4.91	150 - 750	$0.35 < P_r$	Annular and intermittent flow model

Table 2.2 summarizes the most relevant in-tube condensation heat transfer studies. Most prior investigations have focused on annular flow of pure refrigerants at low reduced pressures. Few models address condensation of R410A. In more recent studies, flow regimes have been considered to model the physical phenomena and improve the heat transfer predictions for flows spanning multiple flow regimes.

Table 2.2: Summary of In-tube Condensation: *h*

Author	Fluids	I.D. (mm)	G (kg/m^2-s)	P_r or Tsat (°C)	Models
Kosky and Staub (1971)	Steam	12.57	2.7-149.2	$0 < P_r < 0.007$	Annular heat transfer model
Traviss *et al.* (1973)	R12, R22	8.00	161 - 1532	$0.16 < P_r < 0.47$	Annular heat transfer model
Shah (1979)	R11, R12, R22, R113, water, methanol, ethanol, benzene, toluene, trichloroethylene	7– 40	7-40	11-211	Empirical heat transfer model for $1 < Pr_l < 13$
Kwon *et al.* (2001)	R22, R410A	9.52 O.D.	97, 144, 202	$T_{sat} = 31$	Analytical model for annular flow
Cavallini *et al.* (2002)	R22, R134a, R125, R32, R410A, R236ea	3 – 21	100 – 750	$30 < T_{sat} < 60$ $P_r < 0.75$	Kosky and Staub (1971) model for annular flow, Jaster and Kosky (1976) model for stratified flow
El Hajal *et al.* (2003), Thome *et al.* (2003)	Data from literature (including R410A)	3.1 – 21.4	24 - 1022	$0.02 < P_r < 0.8$	Annular, stratified-wavy and fully stratified flow. *h* model based on their flow regime model
Jiang (2004)	R404A	9.40	200 - 800	$0.8 < P_r < 0.9$	Annular and Wavy flow models
Mitra (2005)	R410A,	6.22, 9.40			

All relevant supercritical work is summarized in Table 2.3. Prior investigations have mostly focused on steam and CO_2 and heating applications, rather than cooling. As the thermophysical properties drastically change in the vicinity of the critical temperatures, researchers have proposed the use of property multipliers in conjunction with single-phase pressure drop and heat transfer correlations to capture the trends in their data.

Table 2.3: Summary of Supercritical: ΔP and h

Author	Fluids	Condition	P_r or Tsat (°C)	Models
Krasnoshchekov et al.(1970)	CO_2	Cooling	30-215°C	Single-phase turbulent correlation with property corrections
Ghajar and Asadi (1986)	Water, CO_2	Heating	$1.00 < P_r <$ 1.46 (CO_2); $0.018 < P_r <$ 1.88 (water)	Dittus-Boelter-type HT correlation with property corrections
Kurganov (1998a; 1998b)	CO_2	Heating		Flow regime transition criteria
Pitla et al. (1998)	Water, CO_2	Heating, cooling	7-29.4 MPa	Literature Review
Pitla et al. (2001b; 2001a)	CO_2	Cooling	$T_{wall} = 30°C$ $P_{in} = 10$ MPa $T_{in} = 120°C$ $T_{out} = 5°C$	Average of wall and bulk heat transfer coefficient based on Gnielinski (1976) correlation with property corrections
Jiang (2004)	R404A	Cooling	$1.0 < P_r < 1.2$	Modified Churchill's (1979) friction factor and Nusselt number equation
Mitra (2005)	R410A,			

Further investigation is needed to understand the effect of diameter on heat transfer and pressure drop in high pressure refrigerants such as R410A. Due to the deficiencies in the understanding of near-critical-pressure condensation and supercritical cooling of

refrigerant blends in microchannels, this study is proposed using the experimental setup and techniques described in the following chapters.

CHAPTER 3 - EXPERIMENTAL APPROACH

The Phase Change/Supercritical Heat Transfer and Pressure Drop Test Facility was first developed for investigations of flow regimes, pressure drop and heat transfer during condensation of refrigerant R134a (Coleman and Garimella, 2000a, 2003). Subsequently, Jiang (2004) and Mitra (2005) conducted condensation and supercritical cooling experiments for R404A and R410A in 6.22 and 9.40 mm tubes in a modified version of that facility. Minor modifications and re-calibrations were made by this author to allow testing of high-pressure refrigerant blends in the smaller tubes of interest in this study. The facility comprises a closed refrigerant loop constructed largely of 12.7 mm (½ in.) outer diameter stainless steel tubing. The wall thickness of the tubing is 1.24 mm (0.049 in.), allowing for a maximum system pressure of 25 MPa (3700 psig) (Swagelok, 2003). A total of 27 different temperature measurements, 6 pressure transducers, and 4 flowmeters are used to record the pertinent parameters through an IOtech data acquisition system (DAQ), which transfers the data to a Windows based computer. Figure 3.1 shows a photograph of the facility. The details of the equipment are provided in the following tables, which include the details of the DAQ in Table 3.1, and the model and serial numbers of the pressure transducers and RTD/Thermocouples in Table 3.2 and Table 3.3, respectively. The flowmeter specifications are provided in Table 3.4.

3.1 Phase-Change Tests

The test facility is described first, followed by detailed descriptions of the different test sections.
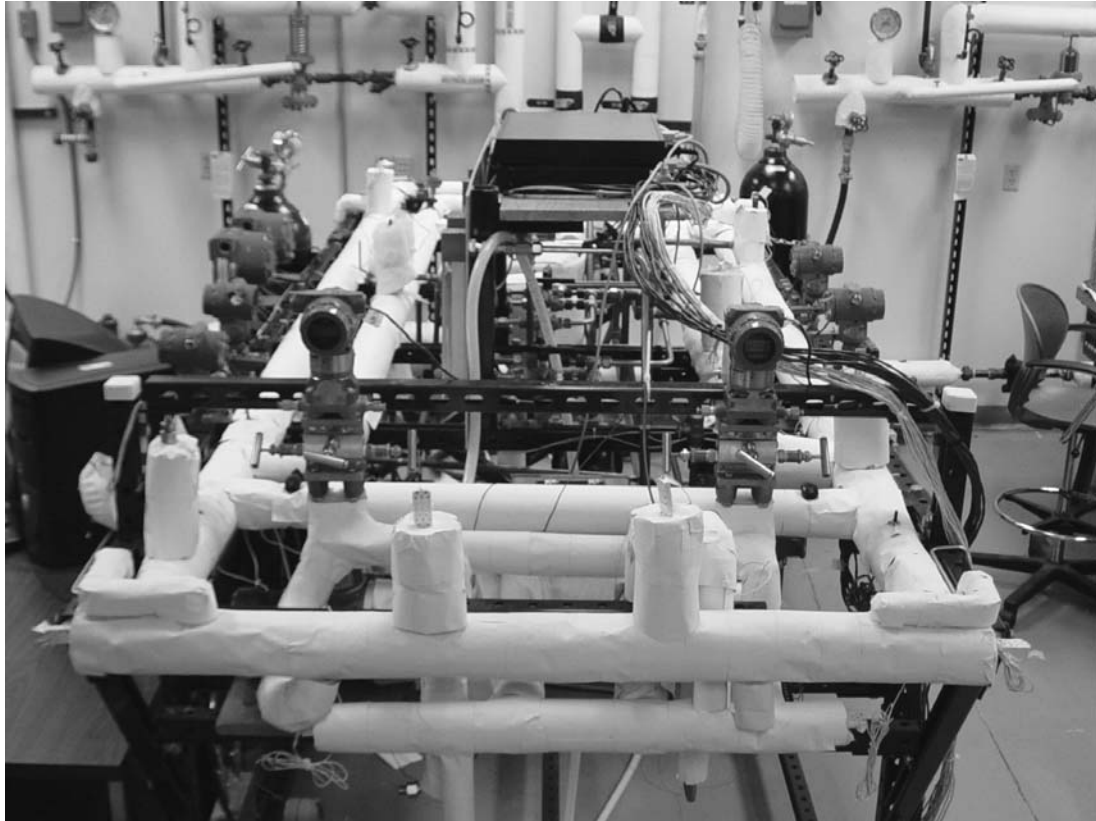
Figure 3.1: Photograph of Test Facility

3.1.1 Test Facility Details

A schematic of the test facility is shown in Figure 3.2. Subcooled liquid refrigerant (visually verified by a sight glass) flows through a Coriolis mass flowmeter (Micromotion CMF025, uncertainty: ± 0.10%) and is pumped through a coiled tube-in-tube evaporator that heats the refrigerant to a superheated state using steam. An accumulator (Accumulators Inc. A13100: max. operating pressure of 21 MPa) allows for adjustments to the refrigerant inventory to precisely control the desired pressure in the refrigerant loop.

28

Table 3.1: Data Acquisition System

Instrument	Manufacturer	Model	Serial No.	Range
Temperature Measurement System		TempScan/1100	126523	1 slot
Expansion Chassis		Exp/10A	147116	2 slots
Voltage Card	IOTech	TEMP V/32	231625	32 Channels
RTD Card		TEMP RTD/16B	151019	16 Channels
Thermocouple Card		TC/32B	250815	32 Channels

Table 3.2: Pressure Transducers

Instrument	Manufacturer	Model	Serial No.	Range	Uncertainty
Absolute Pressure Transducer	Rosemount	3051TA4A2 B21AE5M5	$P_{r,post,out}$:1021623 $P_{r,test,out}$: 1019353 $P_{r,test,in}$: 1019351 $P_{r,pre,in}$: 101352	0-4000 psi	± 0.075% of span
Differential Pressure Transducer, $\Delta P_{Mid-range}$	Rosemount	3051CD3A2 2A1AB4M5	0687134	0-9 psi	± 0.075% of span
Differential Pressure Transducer, $\Delta P_{low-range}$		3051CD1A2 2A1AM5	687133	0-25 in.H_2O = 0-0.9 psi	± 0.075% of span

Table 3.3: Temperature Measurements

Instrument	Manufacturer	Model	Range	Uncertainty
Refrigerant & Condenser Loop Thermocouples		TMQSS-125G-6	Max. Temperature = 220°C	± 1 ˚C
Test-Section Thermocouples	Omega	5TC-TT-T-36-72	Max. Temperature = 180°C	± 1 ˚C
RTDs		PR-13	Max. Temperature = 400˚C	± 0.5 ˚C

Table 3.4: Flowmeter Specifications

Instrument	Manufacturer	Model	Serial No.	Range	Uncertainty
Refrigerant Mass Flow Meter	Micromotion	CMF025M319NU	Sensor: 326974	0 - 8 lb_m/min	± 0.10% of reading
Basis Remote Flow Transmitter		IFT9701R6D3U	IFT:2114443 Sensor: 366359		
Secondary Loop Water Mass Flow Meter	Micromotion	DS006S100SU	Sensor: 205104	0 - 2 lb_m/min	± 0.15% of reading
Basis Remote Flow Transmitter		IFT9701R6D3U	IFT:2114848 Sensor: 366366		
Post-Condenser Rotameter	Gilmont Accucal	GF-4541-1220		0-125 mL/min	± 2% of reading
		GF-4541-1240		0-2.2 L/min	
		GF-4541-1250		0-4.8 L/min	
Primary Loop Volumetric Flow Tube	Rosemount	8711TSE30FS1	80675	0-6.610 gpm	± 0.5% of reading
Magnetic Flow Transmitter		8712CT12M4	0860087272		
Pre-Condenser Volumetric Flow Tube	Rosemount	8711: RRE15FS1	0071955	0-6.256 L/min	± 0.5% of reading
Magnetic Flow Transmitter		8712CT12M4	63610		

Temperature and pressure measurements, along with another sight glass, ensure the superheated state of the refrigerant before it enters one of two pre-condensers (either a tube-in-tube or a shell-and-tube heat exchanger, depending on the heat duty required). The pre-condenser condenses the refrigerant to the desired thermodynamic state at the inlet of the test section. The dimensions of the condensers are provided in Table 3.5. The

pressure measurement at the test section inlet, along with heat duty in the pre-condenser and the temperature and pressure measurements at the superheated state, accurately determine the inlet condition (i.e. quality) at the test section. All absolute pressure transducers (Rosemount, model 3051) have an uncertainty of ± 0.075% of the span.
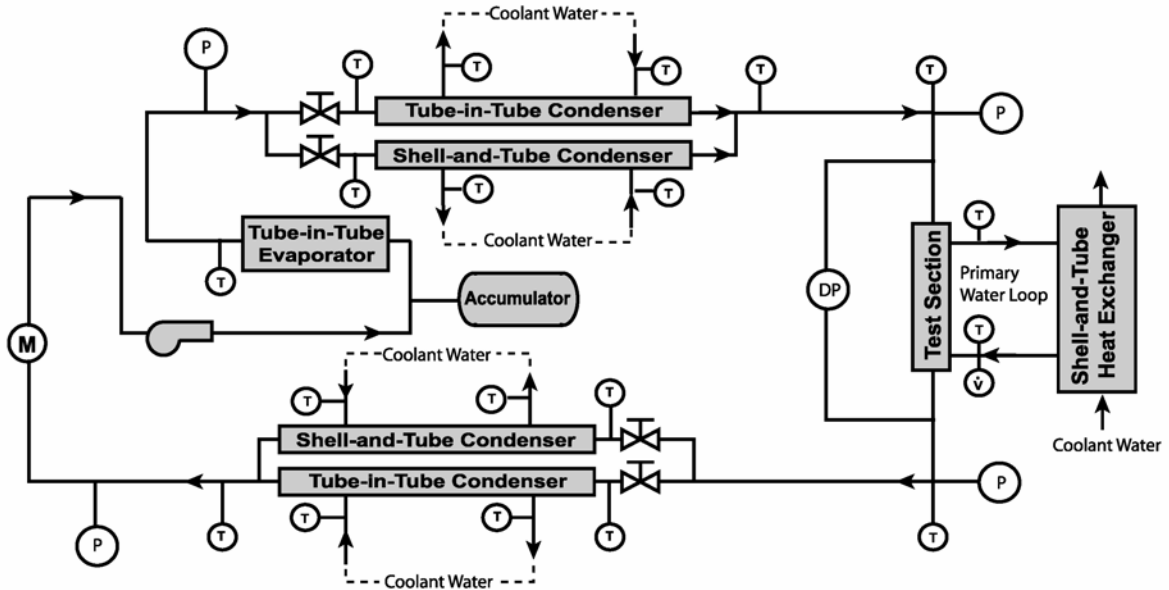
Figure 3.2: Schematic of Test Facility

The condition of the refrigerant at the test section outlet is calculated in the same manner as the inlet condition, using the temperature/pressure measurements at the subcooled state at the post-condenser outlet, and the heat duty of the post-condenser. The subcooled refrigerant is pumped through the evaporator to complete the flow loop.

The pressure drop across the test section is determined with one of two differential pressure transducers (Rosemount 3051, uncertainty ±0.075% of the span).

Table 3.5: Pre- and Post-Condensers Dimensions

PRE-CONDENSER					
SHELL-AND-TUBE Exergy Inc.: 35 Series Model 00256-1			TUBE-IN-TUBE (in-house)		
Length	$L_{pre,s}$ (mm)	460	Length	$L_{pre,t}$ (mm)	432
Insulation diameter	$D_{pre,ins,s}$ (mm)	100	Insulation diameter	$D_{pre,ins,t}$ (mm)	100
Shell, outer diameter	$D_{pre,o,s}$ (mm)	38.1	Outer tube, outer diameter	$D_{pre,o,t}$ (mm)	12.7
Shell, inner diameter	$D_{pre,i,s}$ (mm)	34.8	Outer tube, inner diameter	$D_{pre,i,t}$ (mm)	10.9
Tube outer diameter	(mm)	3.18	Inner tube, outer diameter	(mm)	6.35
Wall thickness	(mm)	0.32	Inner tube, inner diameter	(mm)	4.57
Heat Transfer Area	(m²)	0.27			
Tube Length: Condenser to Test Section	$L_{r,pre-to-test}$ (mm)	914	Tube Length: Condenser to Test Section	$L_{r,pre-to-test}$ (mm)	914
Tube/Baffle Count		55/11			
POST-CONDENSER					
SHELL-AND-TUBE Exergy Inc.: 35 Series Model 00256-2			TUBE-IN-TUBE (in-house)		
Length	$L_{post,s}$ (mm)	206	Length	$L_{post,t}$ (mm)	1295
Insulation diameter	$D_{post,ins,s}$ (mm)	100	Insulation diameter	$D_{post,ins,t}$ (mm)	100
Shell, outer diameter	$D_{post,o,s}$ (mm)	38.1	Outer tube, outer diameter	$D_{post,o,t}$ (mm)	12.7
Shell, inner diameter	$D_{post,i,s}$ (mm)	34.8	Outer tube, inner diameter	$D_{post,i,t}$ (mm)	10.9
Tube outer diameter	(mm)	3.18	Inner tube, outer diameter	(mm)	6.35
Wall thickness	(mm)	0.32	Inner tube, inner diameter	(mm)	4.57
Heat Transfer Area	(m²)	0.13			
Length of Tubing: Condenser to Test Section	$L_{r,test-to-post}$ (mm)	914	Length of Tubing: Condenser to Test Section	$L_{r,test-to-post}$ (mm)	914
Tube/Baffle Count		55 / 7			

The pressure transducers have different operating ranges (0 - 6.2 kPa and 0 – 62 kPa) and the appropriate one for each test is selected to minimize measurement uncertainties.

The heat duty in the test section could be determined using the difference between the inlet and outlet conditions of the refrigerant, which are deduced from the pre- and post-condenser energy balances. This, however, would lead to unreasonably high uncertainties because the heat duty in the test section is intentionally small to capture *local* variations during the condensation/cooling process. With a nominal quality drop of $\sim 5 - 10\%$, the corresponding inlet and outlet enthalpies are two very similar quantities; if subtracted from one-another, the overall uncertainty would be on the same order as the calculated value. Therefore, an alternate method of obtaining the test section heat duty directly from the test section coolant-side measurements is used. To accurately determine the heat duty of the refrigerant from the coolant-side energy balance, it is necessary to have a large temperature rise in the coolant. With a low heat duty in the test section, this would require a low coolant flow rate. This poses a problem, however, because with a low coolant flow rate, the coolant-side heat transfer coefficient would be low and would dominate the overall heat transfer process, masking the variations in the refrigerant-side heat transfer coefficient. To decouple the conflicting requirements, the heat transfer coefficient of the refrigerant in the test section is determined with the aid of the thermal amplification technique introduced by Garimella and Bandhauer (2001). Figure 3.3 shows the schematic of the thermal amplification technique, which allows for the determination of the refrigerant heat transfer coefficient with relatively low uncertainties

by ensuring that the dominant heat transfer resistance in the test section is on the refrigerant side.
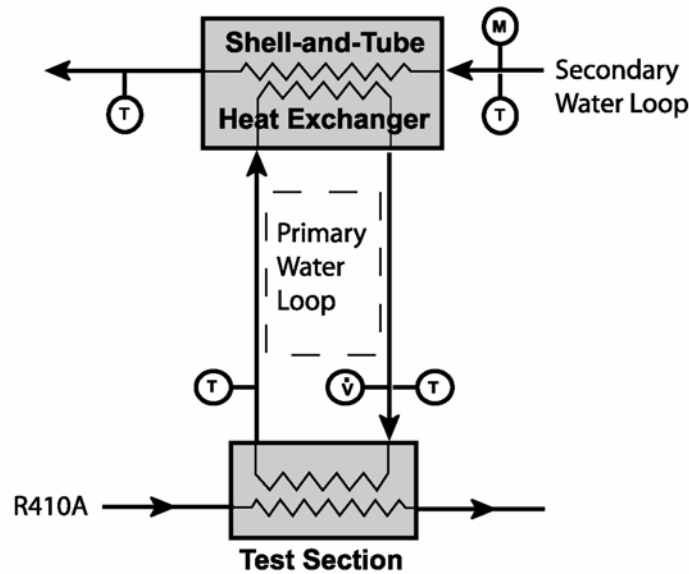
Figure 3.3: Thermal Amplification Technique

The heat rejected by the refrigerant in the test section is transferred to a high-flow rate (high heat transfer coefficient) closed water loop (primary loop) in counter flow with the refrigerant. This makes the heat transfer rate relatively insensitive to the coolant-side h, because the high flow rate results in a high heat transfer coefficient, making the refrigerant-side resistance dominant. The temperature rise of the coolant in this loop is relatively small. Heat from the primary loop is then rejected in a small shell-and-tube heat exchanger to a secondary water loop. The flow rate in the secondary water loop is relatively low to allow for a large temperature rise in the secondary heat exchanger, allowing accurate determination of the heat duty. The flow rate is determined with a Coriolis mass flowmeter (Micromotion DS006, uncertainty $\pm$ 0.15%). The specifications
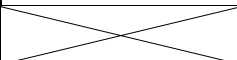
for the primary loop and secondary loop heat exchanger are shown in Table 3.6 and Table 3.7, respectively.

Table 3.6: Primary Loop Dimensions

Primary loop		
Equivalent length (for heat loss)	L_{prim} (mm)	4548
Actual length	$L_{prim,tube}$ (mm)	2540
Insulation diameter	$D_{prim,ins}$ (mm)	76
Outer diameter	$D_{prim,o}$ (mm)	12.70
Inner diameter	$D_{prim,i}$ (mm)	10.92
Relative surface roughness	e_{prim} (-)	0.0015

The equivalent length for heat loss calculations, L_{prim}, was determined by summing the surface area of the flow meter, water pump and tubing in the primary loop and dividing the value by the inner diameter of the water tubing. Detailed calculations are shown in Chapter 4.

Table 3.7: Secondary Loop Heat Exchanger Dimensions

SHELL-AND-TUBE Exergy Inc.: 23 Series Model 00540-4		
Length	L_{sec} (mm)	173
Insulation diameter	$D_{sec,ins}$ (mm)	100
Shell, outer diameter	$D_{sec,o}$ (mm)	25.4
Shell, inner diameter	$D_{sec,i}$ (mm)	22.9
Tube diameter	(mm)	3.18
Wall Thickness	(mm)	0.32
Heat Transfer Area	(m^2)	0.04
Tube/ Baffle Count		19 / 9

3.1.2 Test Section Details

Table 3.8 shows an overview of the three different test sections used in this study. The 3.05 mm I.D. test section is a tube-in-tube heat exchanger, with refrigerant flowing through the inner copper tube and water flowing in counter flow through the annulus between this copper tube and an outer stainless steel tube.

Table 3.8: Test Section Details

D (mm)	$L_{heat-transfer}$ (m)	Channels	Geometry
3.05	0.1524	1	Single Tube
1.52	0.3048	10	Multiport
0.76	0.3048	17	Multiport

The 3.05 mm test section is shown in Figure 3.4. The corresponding dimensions are given in Table 3.9. Five T-type thermocouples are soldered on the outer wall of the refrigerant tube. The spacing between the thermocouples (TC) is 38 mm (1.5 in.) along the direction of the refrigerant flow. In addition, the location from one thermocouple to the next is rotated by 90 degrees, spanning one entire revolution from the first to the last TC.
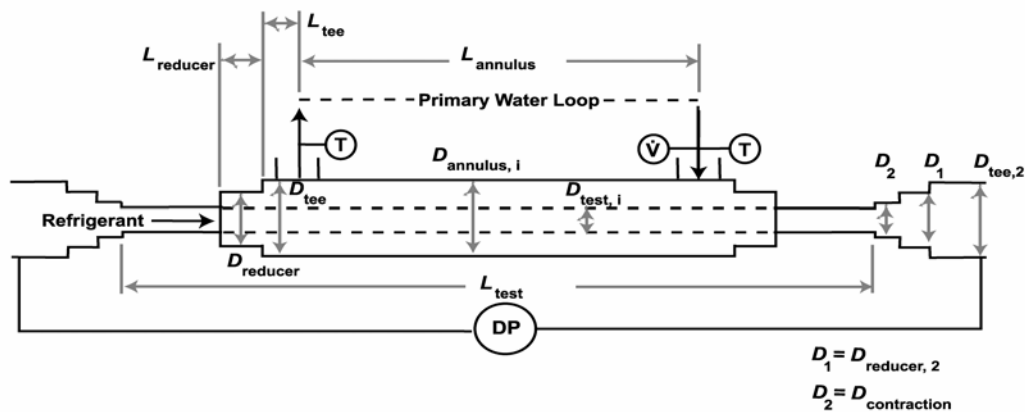
Figure 3.4: Schematic of 3.05 mm Test Section

The other two test sections (1.52 and 0.76 mm I.D.) are multiport tubes extruded from aluminum. For the multiport test sections, the refrigerant tube is brazed between two water tubes. Again, the water flows in counter-flow with respect to the refrigerant.

Table 3.9: 3.05 mm Test Section Dimensions

3.05 mm Tube-in-tube Test section		
Length of Annulus	$L_{annulus}$ (mm)	152.4
Length of inner tube	L_{test} (mm)	323.8
Length of reducer	$L_{reducer}$ (mm)	22.86
Length of Tee	L_{tee} (mm)	13.21
Insulation diameter	$D_{test,ins}$ (mm)	100
Outer tube, outer diameter	$D_{annulus,o}$ (mm)	12.7
Outer tube, inner diameter	$D_{annulus,i}$ (mm)	10.2
Inner tube, outer diameter	$D_{test,o}$ (mm)	6.35
Inner tube, inner diameter	$D_{test,i}$ (mm)	3.05
Swagelok Tee-Fitting, inner diameter	$D_{tee} = D_{tee,2}$ (mm)	10.41
Swagelok Reducer-Fitting, inner diameter	$D_{reducer} = D_{reducer,2}$ (mm)	9.25
Swagelok Reducer-Contraction, inner diameter	$D_{contraction}$ (mm)	4.83

Figure 3.5 shows the multiport test section. Figure 3.6 shows the cross-sectional view of the 0.76 mm test section. It is noted that only the refrigerant tube is different between the two multiport test sections. The water channels have rectangular ports. The determination of the heat transfer coefficient from the measured data is explained in Chapter 4. All relevant dimensions for the multiport test sections are provided in Table 3.10.
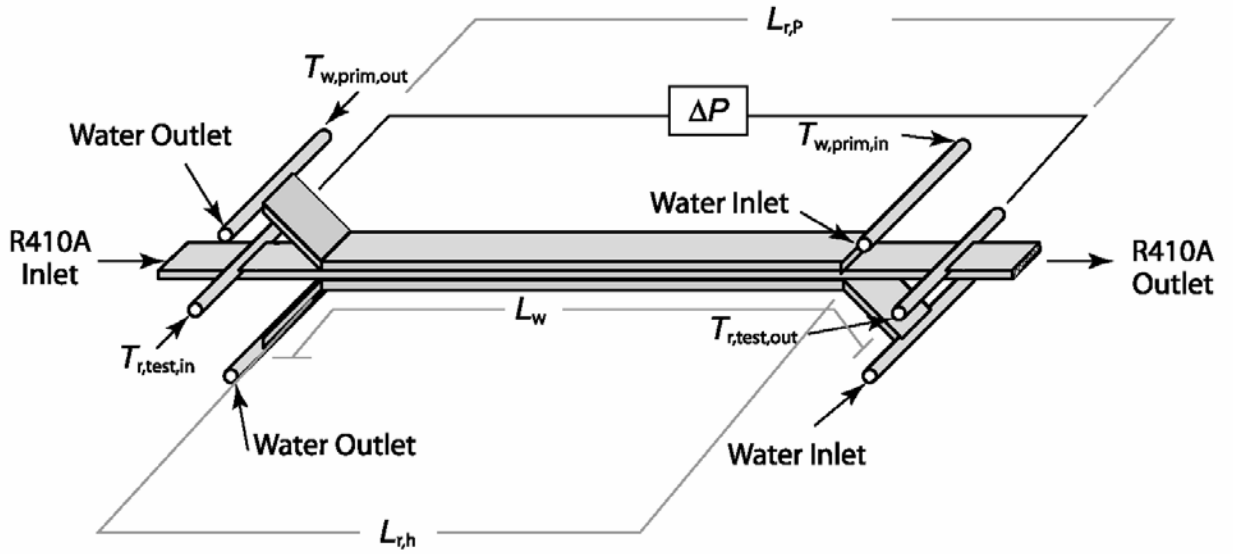
Figure 3.5: Multiport Test Section
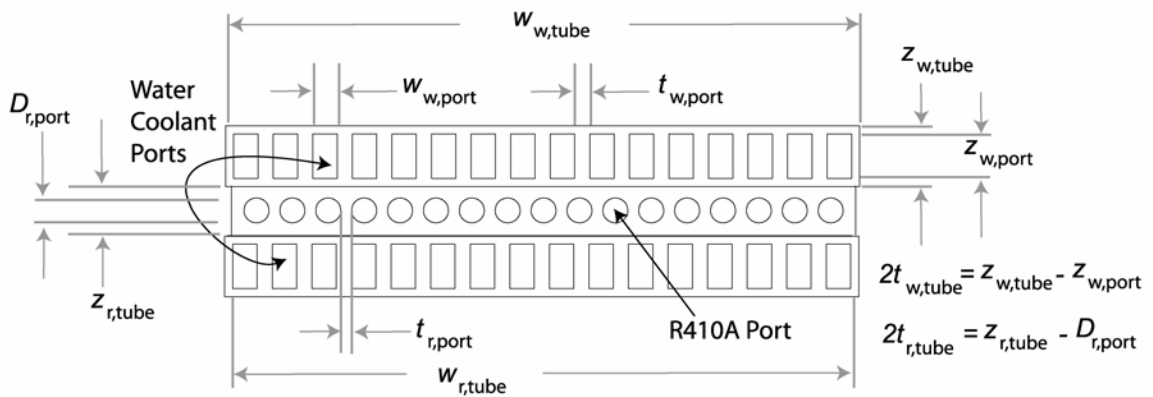
Figure 3.6: Cross Section of 0.76 mm Test Section

3.2 Supercritical Tests

For supercritical tests, the refrigerant flows through the same loop as described above. The pre-condenser now is a pre-cooler as it simply cools the refrigerant to the desired test

Table 3.10: Multiport Test Section Dimensions

	Variables		0.76 mm Test Section	1.52 mm Test Section
Refrigerant Tube	Refrigerant Port Diameter	$D_{r,port}$ (mm)	0.76	1.52
	Number of Refrigerant Ports	n_r	17	10
	Height of Refrigerant Tube	$z_{r,tube}$ (mm)	1.524	2.290
	Width of Refrigerant Tube	$w_{r,tube}$ (mm)	19.05	19.05
	Length of Heat Transfer Section	$L_{r,h}$ (mm)	304.8	304.8
	Length for ΔP Analysis	$L_{r,P}$ (mm)	508.0	508.0
	Spacing between ports	$t_{r,port}$ (mm)	0.333	0.338
	Thickness above Ports	$t_{r,tube}$ (mm)	0.381	0.383
	Cross-section Area at In/ Outlet	$A_{contraction}$ (mm^2)	34.37	34.37
Water Tube	Height of Water Port	$z_{w,port}$ (mm)	1.397	
	Width of Water Port	$w_{w,port}$ (mm)	0.762	
	Number of Water Ports	n_w	16	
	Height of Water Tube	$z_{w,tube}$ (mm)	1.905	
	Width of Water Tube	$w_{w,tube}$ (mm)	19.84	
	Total Length	L_w (mm)	457.2	
	Spacing between ports	$t_{w,port}$ (mm)	0.476	
	Thickness above Ports	$t_{w,tube}$ (mm)	0.254	

section inlet temperature. Similarly, the post-cooler ensures that the refrigerant is at a liquid-like state as it enters the refrigerant pump. Heat transfer coefficients in the supercritical tests are also obtained using the thermal amplification technique described above for the condensation tests.

3.3 Charging Refrigerant Loop with R410A

The entire refrigerant loop was evacuated using a 3 cfm rotary vane vacuum pump (J.B. Industries, Model: DV-85N) in conjunction with a digital vacuum gage (Sealed Units Parts Co. VG64). Once the refrigerant loop reached a vacuum of 150 microns (150 microns = 20 Pa; where 1 torr = 1000 microns), the pump was turned off and the system's pressure was monitored to identify any pressure changes. A potential pressure rise would indicate a leak. Upon ensuring a leak-free system, the refrigerant loop was charged with approximately 3 kg of R410A.

3.4 Test Procedures

At start up, the refrigerant in the entire loop is a sub-cooled liquid (which is observed in both sight glasses). Initial flow rates for the pre and post-condensers are set, as well the flow rate of the primary loop. The primary loop flow rate is carefully chosen to ensure a significantly high heat transfer coefficient on the water side but minimizing the pump heat input. The refrigerant flow rate is set to correspond to the desired mass flux. Then, the steam lines are opened. The system pressure is closely monitored and adjusted with the aid of the accumulator to the desired operating pressure. Meanwhile, the refrigerant mass flow rate is continuously fine-tuned.

Real-time charting of the refrigerant temperature, pressure in the test section and mass flow rate allows for determination of steady state. Once the system reaches steady-state

(which takes between $2 - 3$ hours, depending upon the mass flux and quality under consideration), a data point is taken by recording measurements every second over a two minute period in an MS Excel spreadsheet. The data are then averaged to represent that test condition. The data are also analyzed at this time to ensure energy balances and the establishment of the desired test conditions. Two such points are recorded to ensure that the conditions do not change with time. The flow conditions are then changed to obtain the next data point. The EES data analysis program is discussed in the following chapter.

CHAPTER 4 - DATA ANALYSIS

The derivation of the heat transfer coefficients and their associated uncertainties from the experimental data, and sample calculations for two-phase and supercritical tests are described here. The thermodynamic states and properties of water, air and R410A are evaluated using Engineering Equation Solver (EES) software (Klein, 2005) along with the EES-REFPROP interface to access the properties for the refrigerant in REFPROP Version 7.0 (Lemmon *et al.*, 2002). The uncertainty propagation in EES assumes that all measurements are uncorrelated and random (Taylor and Kuyatt, 1994). Appendix A shows sample uncertainty calculations. This chapter is divided into three major sections which address: 4.1 In-tube Condensation in the Annular Test Section, 4.2 Condensation in the Multiport Test Sections, and 4.3 Supercritical Heat Transfer and Pressure Drop.

4.1 In-tube Condensation for the 3.05 mm Test Section

The following discussion pertains to the conditions summarized in Table 4.1 and Table 4.2. A detailed analysis of the refrigerant heat transfer coefficient and frictional pressure gradient are presented. All details of the calculations are shown in Appendix B.

4.1.1 Test Section Quality

At the evaporator outlet, the refrigerant is superheated, such that the temperature and pressure measurement at the pre-condenser inlet yields the enthalpy of the refrigerant:

$$i_{r, \text{pre, in}} = f\left(T_{r, \text{pre, in}}, P_{r, \text{pre, in}}\right) = f\left(100.30°\text{C}, 3927 \text{ kPa}\right) = 486.0 \pm 0.7 \text{ kJ/kg} \quad (4.1)$$

Table 4.1: Refrigerant Measurements, $\dot{m}_r$ = 5.847 ×10^{-3} kg/s

		Temperature (°C)		Pressure		
					(psia)	(kPa)
Pre - Condenser	**inlet**	$T_{r, pre, in}$	100.30 ± 0.5	$P_{r, pre, in}$	569.6 ± 0.75	3927 ± 5
	outlet	$T_{r, pre, out}$	62.17 ± 0.5			
Test section	**inlet**	$T_{r, test, in}$	61.37 ± 0.5	$P_{r, test, in}$	569.4 ± 0.75	3926 ± 5
	outlet	$T_{r, test, out}$	61.01 ± 0.5	$P_{r, test, out}$	569.4 ± 0.75	3926 ± 5
Post - Condenser	**inlet**	$T_{r, post, in}$	60.20 ± 0.5			
	outlet	$T_{r, post, out}$	56.78 ± 0.5	$P_{r, post, out}$	569.1 ± 0.75	3924 ± 5

Table 4.2: Water Measurements

		Temperature (°C)		Flow Rate		
Pre - Condenser	**inlet**	$T_{w, pre, in}$	30.07 ± 0.5	$\dot{V}_{w, pre}$	0.2272 ± 0.001 L/min	3.787 ± 0.019 × 10^{-6} m^3/s
	outlet	$T_{w, pre, out}$	66.54 ± 0.5			
Primary Loop	**inlet**	$T_{w, test, in}$	49.69 ± 0.5	$\dot{V}_{w, prim}$	1.049 ± 0.006 gpm	6.618 ± 0.033 × 10^{-5} m^3/s
	outlet	$T_{w, test, out}$	50.01 ± 0.5			
Secondary Loop	**inlet**	$T_{w, sec, in}$	36.84 ± 0.5	$\dot{m}_{w, sec}$	0.2245 ± 0.0004 lb$_m$/min	1.697 ± 0.002 × 10^{-3} kg/s
	outlet	$T_{w, sec, out}$	49.05 ± 0.5			
Post - Condenser	**inlet**	$T_{w, post, in}$	30.10 ± 1.0	$\dot{V}_{w, post}$	0.20 ± 0.04 L/min	3.33 ± 0.06 × 10^{-6} m^3/s
	outlet	$T_{w, post, out}$	59.32 ± 1.0			

A significant temperature difference is desired at the pre-condenser inlet to ensure that the refrigerant is superheated. Table 4.3 compares the measured temperatures with the saturation temperatures deduced from the pressure transducers. Similarly, at the post-condenser outlet, at significant temperature difference is needed to ensure that the refrigerant is at a sub-cooled state, so that it can be pumped without damaging the refrigerant pump, and also to ensure that temperature and pressure measurements can be used to obtain the refrigerant enthalpy.

Table 4.3: Refrigerant Saturation Temperatures at Condensers

	Measured T (°C)	Saturation T (°C)	Temperature Difference (°C)
Pre-condenser Inlet	100.30 ± 0.5	61.09 ± 0.06	39.21 ± 0.5
Post-condenser outlet	56.78 ± 0.5	60.97 ± 0.06	4.19 ± 0.5

At the pre-condenser outlet, the refrigerant is a two-phase fluid, whose enthalpy cannot be directly determined from a pressure and temperature measurement. Therefore, to determine the enthalpy at the test section inlet, the water-side heat duty (Equation 4.2) and an energy balance on the refrigerant side at the pre-condenser (Equation 4.3) are used. Detailed calculations of the heat losses $\dot{Q}_{loss}$ will be shown in a subsequent subsection. It will be shown (Table 4.4) that $\dot{Q}_{loss,pre}$ = 2.9 W and $\dot{Q}_{loss, \text{pre-to-test}}$ = 4.4 W. Here, the subscript "pre-to-test" refers to the plumbing between the pre-condenser and the test section. The water-side heat duty yields:

$$\dot{Q}_{\text{pre}} = \dot{m}_{w, \text{pre}} \left(i_{w, \text{pre, out}} - i_{w, \text{pre, in}} \right) + \dot{Q}_{\text{loss, pre}} \tag{4.2}$$

$$\dot{Q}_{pre} = (0.003770 \text{ kg/s})(278.8 - 126.3) \text{kJ/kg} + 2.9 \text{ W} = 577.9 \pm 12 \text{ W}$$

Detailed calculations of the intermediate steps, such as determination of $\dot{m}_{w, \text{pre}}$ are shown in Appendix B. The refrigerant enthalpy at the test section inlet is a function of refrigerant mass flow rate, the pre-condenser inlet enthalpy and the heat losses.

$$i_{r,\text{test,in}} = \left(i_{r, \text{pre, in}} - \frac{\dot{Q}_{pre}}{\dot{m}_r} - \frac{\dot{Q}_{\text{loss, pre-to-test}}}{\dot{m}_r} \right) \tag{4.3}$$

$$i_{r,\text{test,in}} = \left(486.0 \text{ kJ/kg} - \frac{577.9 \text{ W}}{0.005847 \text{ kg/s}} - \frac{4.4 \text{ W}}{0.005847 \text{ kg/s}} \right) = 386.4 \pm 2.1 \text{ kJ/kg}$$

The refrigerant enthalpy, along with the pressure measurement at the test section inlet, yields the quality.

$$x_{r, \text{ test, in}} = f \left(P_{r, \text{ test, in}}, i_{r, \text{ test, in}} \right) \tag{4.4}$$

$$x_{r, \text{ test, in}} = f \left(3926 \text{ kPa}, 386.4 \text{ kJ/kg} \right) = 0.73 \pm 0.02$$

Similar calculations on the post-condenser result in the quality at the test section outlet: $x_{r, \text{ test, out}} = 0.57 \pm 0.03$. For each data point, the test section quality is taken as the average of the calculated inlet and outlet qualities:

$$x_{r, \text{ test, avg}} = \frac{x_{r, \text{ test, in}} + x_{r, \text{ test, out}}}{2} \tag{4.5}$$

$$x_{r, \text{ test, avg}} = \frac{0.73 + 0.57}{2} = 0.65 \pm 0.02$$

The decrease in quality, and therefore, the test section heat duty, could simply be calculated from the difference between the inlet and outlet qualities. This, however, results in relatively high uncertainties, especially for tests with small changes in quality

across the test section. Therefore, the test section heat duty is calculated using an alternative approach described in section 4.1.5.

4.1.2 Heat Losses to the Environment

The heat losses to the ambient are minimized by fiberglass insulation of low thermal conductivity (k_{ins} = 0.043 W/m-K) surrounding the test section, as well as the primary and secondary water loops. The heat losses on the outside of the insulation are due to natural convection and radiation. The computation of heat losses in the pre- and post-condenser, the secondary loop heat exchanger, as well as the losses in the refrigerant and primary loop tubing are all similar; therefore, only the calculations for the pre-condenser losses are shown in detail here. Other heat loss calculations are shown in Appendix B.

It is assumed that the temperature of the inner wall of the outer shell of the pre-condenser is equal to the average of the water temperature at the inlet and outlet of the condenser. The heat loss to the environment, $\dot{Q}_{loss,\,pre}$, is calculated as follows:

$$\dot{Q}_{loss,\,pre} = \frac{\left(T_{inner\,wall} - T_{ambient}\right)}{R_{wall} + R_{ins} + \left(\dfrac{R_{nat.conv.}\,R_{radiation}}{R_{nat.conv.} + R_{radiation}}\right)} \tag{4.6}$$

The corresponding resistance network is shown in Figure 4.1. The conductive resistances R_{wall} and R_{ins} are given by Equation 4.7 and 4.8, respectively. The appropriate values for all variables are given in Table 3.5.

$$R_{wall} = \frac{\ln\left(\dfrac{D_{pre,o,s}}{D_{pre,i,s}}\right)}{2\pi k_{pre,s} L_{pre,s}} \tag{4.7}$$
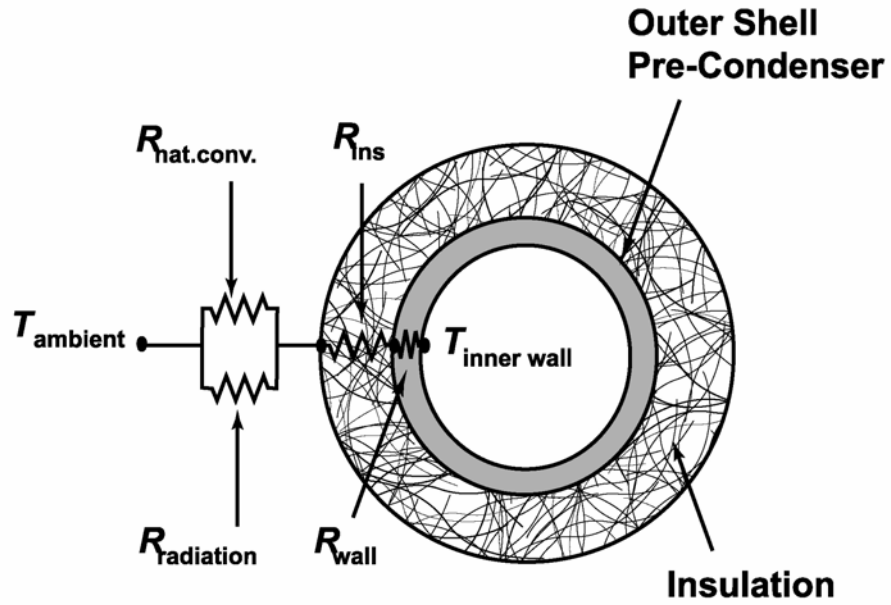
Figure 4.1: Thermal Resistance Network for Pre-Condenser

$$R_{wall} = \frac{\ln\left(\dfrac{38.1 \text{ mm}}{34.8 \text{ mm}}\right)}{2\pi\left(14.9 \text{ W/m-K}\right)\left(0.460 \text{ m}\right)} = 2.103 \times 10^{-3} \text{ K/W}$$

$$R_{ins} = \frac{\ln\left(\dfrac{D_{pre,ins,s}}{D_{pre,o,s}}\right)}{2\pi k_{ins} L_{pre,s}} \tag{4.8}$$

$$R_{ins} = \frac{\ln\left(\dfrac{100 \text{ mm}}{38.1 \text{ mm}}\right)}{2\pi\left(0.043 \text{ W/m-K}\right)\left(0.460 \text{ m}\right)} = 7.756 \text{ K/W}$$

The radiative resistance is given in Equation 4.9, where the emissivity of the outside surface of the insulation is assumed to be $\varepsilon_{ins} = 0.85$ and $\sigma = 5.67 \times 10^{-8}$ W/m²-K⁴ is the Stefan-Boltzmann constant. The temperature of the surroundings is assumed to be $T_{ambient}$, which is 23.0°C, and the temperature of to the outside wall of the surface is T_{ins}, which is unknown. Equations 4.6 to 4.12 are solved iteratively, resulting in $T_{ins} = 25.64$°C.

$$R_{radiation} = \frac{1}{\pi D_{pre,o,s} L_{pre,s} \varepsilon_{ins} \sigma \left(T^2_{ins} + T^2_{ambient} \right) \left(T_{ins} + T_{ambient} \right)} \tag{4.9}$$

$$R_{radiation} = 1.362 \text{ K/W}$$

To determine the natural convection heat transfer coefficient, the Rayleigh number, Ra, has to be calculated. The thermal properties are evaluated at the average air temperature, $T_{avg} = (T_{ins} + T_{ambient})/2 = (25.64 + 23.0)$°C / 2 = 24.32°C.

$$\text{Ra} = \frac{g \beta_{air} \left(T_{ins} - T_{ambient} \right) D^3_{pre, ins, s}}{\nu_{air} \alpha_{air}} \tag{4.10}$$

$$\text{Ra} = \frac{\left(9.81 \text{ m/s}^2 \right) \left(0.003362 \text{ K}^{-1} \right) \left(25.64 - 23.0 \right) °\text{C} \left(0.100 \text{ m} \right)^3}{\left(1.560 \text{ x } 10^{-5} \text{ m}^2/\text{s} \right) \left(2.128 \text{ x } 10^{-5} \text{m}^2/\text{s} \right)} = 261200$$

The Nusselt number for natural convection around a horizontal cylinder is given by Churchill and Chu (1975):

$$\text{Nu} = \left(0.60 + \frac{0.387 \text{Ra}^{1/6}}{\left(1 + \left(\frac{0.559}{\text{Pr}} \right)^{9/16} \right)^{8/27}} \right)^2 \tag{4.11}$$

$$\text{Nu} = \left(0.60 + \frac{0.387(261200)^{1/6}}{\left(1 + \left(\frac{0.559}{0.7297} \right)^{9/16} \right)^{8/27}} \right)^2 = 10.08$$

The heat transfer coefficient is determined using $h_{\text{nat.conv.}} = \text{Nu} \cdot k_{\text{air}} / D_{\text{pre,ins,s}}$, which is calculated to be $h_{\text{nat.conv.}} = 2.565$ W/m^2-K. The natural convection resistance is given by:

$$R_{\text{nat.conv.}} = \frac{1}{h_{\text{nat.conv.}} \pi D_{\text{pre,ins,s}} L_{\text{pre,ins,s}}} \tag{4.12}$$

$$R_{\text{nat.conv.}} = \frac{1}{(2.565 \text{ W/m}^2\text{-K}) \pi (0.100 \text{ m})(0.460 \text{ m})} = 2.695 \text{ K/W}$$

Finally, the heat loss as presented in Equation 4.6 can be calculated:

$$\dot{Q}_{\text{loss, pre}} = \frac{(48.31 - 23.0)\,°\text{C}}{\left[(2.103 \times 10^{-3}) + (7.756) + \left(\frac{(2.695)(1.362)}{(2.695) + (1.362)} \right) \right] \text{ K/W}} = 2.9 \text{ W}$$

4.1.3 Heat Loss in the Test Section

The heat loss in the test section is calculated in a manner similar to that described above for the pre-condenser losses. Since the heat duties in the test section are much smaller than in the condensers, the losses to the environment represent a more significant fraction of the overall energy balance. Instead of assuming an inner wall temperature, $T_{\text{inner wall}}$, a convective resistance, $R_{\text{annulus,o}}$, is added to the resistance network as outlined in Equation 4.13.

$$\dot{Q}_{\text{loss, test}} = \frac{\left(T_{\text{r,test,avg}} - T_{\text{ambient}}\right)}{R_{\text{annulus,o}} + R_{\text{wall}} + R_{\text{ins}} + \left(\dfrac{R_{\text{nat.conv.}} R_{\text{radiation}}}{R_{\text{nat.conv.}} + R_{\text{radiation}}}\right)} \tag{4.13}$$

The additional convective resistance, $R_{\text{annulus,o}}$, is defined in 4.14.

$$R_{\text{annulus, o}} = \frac{1}{h_{\text{annulus}} \pi D_{\text{annulus, i}} L_{\text{test}}} \tag{4.14}$$

The water-side heat transfer coefficient in the annulus, h_{annulus}, is calculated using curve-fits by Garimella and Christensen (1995) for the laminar and turbulent Nusselt numbers in annuli reported by Kays and Leung (1963). The Reynolds number in the annulus for this data point is 9171, which indicates turbulent flow according to Walker et al. (1957). The Prandtl number and diameter ratio are Pr = 3.562, $r^* = 0.6225$ respectively, which yields the following Nusselt number:

$$\text{Nu}_{\text{turbulent}} = 0.025 \left(\text{Re}_{\text{annulus}}^{0.78} \ \text{Pr}^{0.48} \left(r^*\right)^{-0.14}\right) \tag{4.15}$$

The Nusselt number is determined to be $\text{Nu}_{\text{turbulent}} = 60.58$. The corresponding water-side heat transfer coefficient, h_{annulus}, is 10100 ± 2525 W/m^2-K, where a conservative $\pm 25\%$ uncertainty is assumed. With a total resistance of 53.03 K/W and the temperature difference between the environment and the water of $\Delta T = 26.85°$C, the heat loss in the test section is $\dot{Q}_{\text{loss, test}} = 0.5$ W. Table 4.4 summarizes all heat loss calculations in the refrigerant loop for this data point.

Table 4.4: Heat Losses

	Surface Area (m^2)	Radiation Loss $\dot{Q}_{loss,radiation}$ (W)	Nat. Conv. Loss $\dot{Q}_{loss,nat.conv}$ (W)	Total Heat Loss $\dot{Q}_{loss,total}$ (W)
Primary Loop	1.086	11.3	5.7	**17.0**
Pre-Condenser	0.144	1.9	1.0	**2.9**
Pre-Condenser to Test Section	0.287	3.0	1.4	**4.4**
Test Section	0.048	0.3	0.2	**0.5**
Test Section to Post-Condenser	0.287	2.9	1.4	**4.3**
Post-Condenser	0.065	0.7	0.4	**1.1**
Secondary Heat Exchanger	0.054	0.4	0.2	**0.6**

It should be noted that the surface areas in Table 4.4 are based on the diameter of the insulation and the length of the components. In the primary loop, the heat transfer length is comprised of the length of the tubing in the water loop (1.782 m), the equivalent length of the circulation pump housing (1.286 m), and the equivalent length of the flow meter (1.477 m), to yield L_{prim} = 4.548 m. The equivalent lengths in the flow meter and pump housing are the respective surface areas divided by the product of π and the outer diameter of the tubing (12.7 mm) as described by Mitra (2005).

4.1.4 Heat Dissipation into Primary Loop by Water Circulation Pump

The heat duty in the test section, $\dot{Q}_{test}$, is calculated as follows:

$$\dot{Q}_{test} = \dot{Q}_{sec} + \dot{Q}_{loss,ambient} - \dot{Q}_{pump} \qquad (4.16)$$

To accurately determine the heat duty in the test section, it is necessary to characterize the heat input to the primary loop by the water circulation pump (Micromotion 5000-750, S/N 365623). By determining the efficiency of the pump and calculating the shaft work required to achieve the volumetric flow rate of water, the net heat gain is calculated. It is assumed that all of the heat is rejected into the water circulating in the primary loop.

The pump efficiency, η, is defined as the ratio of the ideal work, $\dot{W}_{ideal}$, to the actual work, $\dot{W}_{shaft}$, required to move the water in the primary loop (Equation 4.17). The heat gain, $\dot{Q}_{pump}$, can be related to the efficiency using Equation 4.18.

$$\eta = \frac{\dot{W}_{ideal}}{\dot{W}_{shaft}} \tag{4.17}$$

$$\frac{\dot{Q}_{pump}}{\dot{W}_{shaft}} = 1 - \eta \tag{4.18}$$

The ideal work input to the pump, $\dot{W}_{ideal}$, represents the power supplied to the pump to move the water in the primary loop without any losses in the pump. $\dot{W}_{ideal}$ is a function of the pressure drop and the volumetric flow rate in the primary loop, $\dot{V}_{w,\,prim}$.

$$\dot{W}_{ideal} = \left(\Delta P_{prim}\right) \dot{V}_{w,\,prim} \tag{4.19}$$

The pressure drop in the primary loop across the pump is characterized with a pressure gage for different flow rates, ranging from 0.1 to 2.5 gpm. The shaft work, or actual work supplied to the pump, is the product of the rotational speed, ω, and the torque, τ:

$$\dot{W}_{shaft} = \tau \omega \tag{4.20}$$

From the pump manufacturer's specification curves (Figure 4.2), the torque and the rotational speed can be related to the flowrate and pressure drop as shown in Equations 4.21 and 4.22.

The following equations were estimated from Figure 4.2 using a linear curve fit:

$$\tau(\text{Nm}) = \frac{0.8}{700} \Delta P_{\text{prim}}(\text{kPa}) + 0.1 \tag{4.21}$$

$$\omega(\text{rpm}) = 860 \dot{V}(\text{gpm}) + 300 \frac{\Delta P_{\text{prim}}(\text{kPa})}{220} \tag{4.22}$$

The pressure drop data, along with Equations 4.21 and 4.22 is used to fit a 3rd order polynomial correlating the volumetric flow rate to the heat input by the water pump.
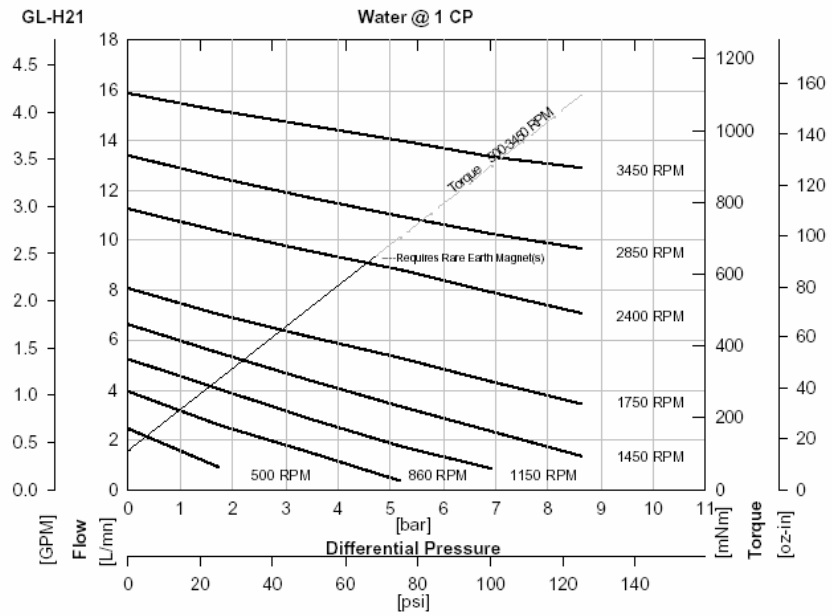
Figure 4.2: Primary Loop Pump Performance (Micropump, 2000)

Figure 4.3 shows the heat input to the primary loop for all three test sections under investigation. It should be noted that the multiport test sections have the same geometry on the water side, and therefore use the same heat input correlation.
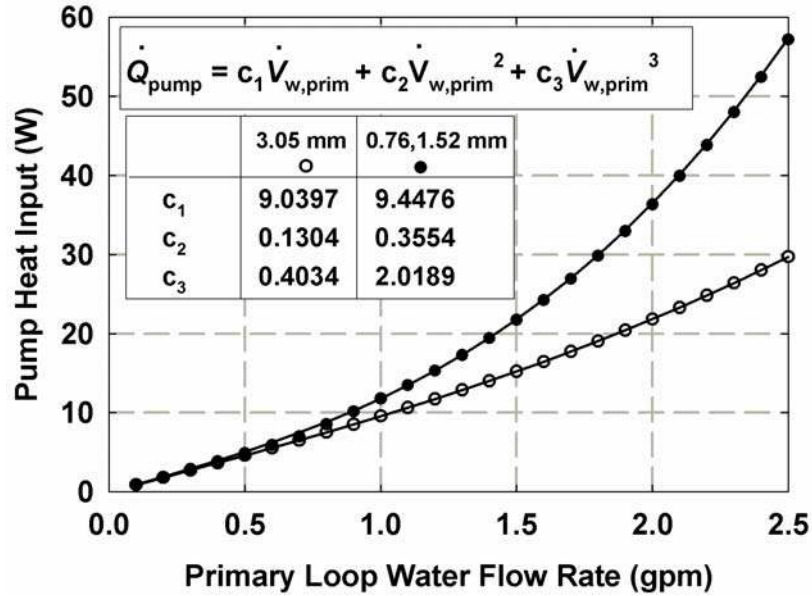
Figure 4.3: Pump Heat Input in Primary Loop

For the data under consideration, the volumetric flow rate is 1.049 gpm. The corresponding heat input is calculated using Equation 4.23, yielding a pump heat input of 10.09 ± 5.04 W, where a conservative 50% uncertainty is assumed.

$$\dot{Q}_{pump} = 9.0397\dot{V}_{w,prim,gpm} + 0.1304\dot{V}^2_{w,prim,gpm} + 0.4034\dot{V}^3_{w,prim,gpm} \tag{4.23}$$

$$\dot{Q}_{pump} = 9.0397(1.049) + 0.1304(1.049)^2 + 0.4034(1.049)^3 = 10.09 \pm 5.04 \text{ W}$$

4.1.5 Calculation of the Heat Duty in the Test Section

To determine the heat duty in the test section, as shown in Equation 4.16, the heat transfer rate in the secondary loop needs to be determined. This is done by the mass

flowrate of the secondary water loop, and temperature measurements at the heat exchanger inlet and outlet, which yield the respective enthalpies. Thus,

$$\dot{Q}_{sec} = \dot{m}_{w,\,sec}\left(i_{w,\,sec,\,out} - i_{w,\,sec,\,in}\right) \tag{4.24}$$

$$\dot{Q}_{sec} = \left(1.697 \times 10^{-3}\,\text{kg/s}\right)\left(205.6 - 154.6\right)\text{kJ/kg} = 86.61 \pm 5.02\ \text{W}$$

Due to the high accuracy of the water mass flow measurement, $1.697 \pm 0.002 \times 10^{-3}$ kg/s, and the significant temperature rise, $\Delta T_{sec} = 13.00 \pm 0.71°C$, in the secondary loop, the heat duty of the coolant in the secondary loop is determined with a relatively small uncertainty, $\dot{Q}_{sec} = 86.61 \pm 5.02$ W. It should be noted that the corresponding temperature rise in the primary water loop is only $\Delta T_{prim} = 0.32°C$, demonstrating the gain achieved by the thermal amplification technique.

The heat losses to the ambient, $\dot{Q}_{loss,ambient}$, are the sum of the losses in the test section, and primary and secondary water loops.

$$\dot{Q}_{loss,\,ambient} = \dot{Q}_{loss,\,test} + \dot{Q}_{loss,\,primary} + \dot{Q}_{loss,\,sec} \tag{4.25}$$

The temperature difference between the outer tube wall of the test section and the ambient is relatively small, 20°C, in almost all cases. For this data point, the combined losses (Table 4.4) were estimated to be 18.1 ± 9 W, where a conservative $\pm\ 50\%$ uncertainty is assumed. The heat transfer rate in the test section (Equation 4.16) is then determined to be $\dot{Q}_{test} = 86.61 + 18.14 - 10.09 = 94.6 \pm 11.5$ W. The log-mean temperature difference between the refrigerant and water in the primary loop is given by:

$$\text{LMTD} = \frac{\left(T_{r,\,test,\,in,\,sat} - T_{w,test,\,out}\right) - \left(T_{r,\,test,\,out,\,sat} - T_{w,\,test,\,in}\right)}{\ln\left[\dfrac{\left(T_{r,\,test,\,in,\,sat} - T_{w,\,test,\,out}\right)}{\left(T_{r,\,test,\,out,\,sat} - T_{w,\,test,\,in}\right)}\right]} \tag{4.26}$$

which yields LMTD = 11.22 ± 0.35°C. It should be noted that the saturation temperatures of the refrigerant at the measured inlet and outlet pressures are used, rather than the measured test section inlet and outlet temperatures, which differs from the approach used shown by Jiang (2004) for similar experiments with R404A on 9.4 mm tubes and Mitra (2005) for similar experiments with R410A on 9.4 and 6.2 mm tubes. This is because saturation temperatures obtained from pressures measured using the transducers used in this study yield lower uncertainties than those resulting from RTD measurements. For example, at the test section inlet, the measured pressure is 3926 ± 5 kPa. This yields a saturation temperature, $T_{r,test,in,sat} = f\left(P_{r,test,in}, i_{r,test,in}\right) = 61.07 \pm 0.06^{\circ}C$, where the enthalpy is: $i_{r,test,in} = 386.4 \pm 2.0$ kJ/kg. In contrast, the measured temperature is know only within 0.5°C, i.e., $T_{r,test,in} = 61.37 \pm 0.5^{\circ}C$.

Similarly, at the test section outlet, $T_{r,test,out,sat} = 61.07 \pm 0.06^{\circ}C$, whereas $T_{r,test,out} = 61.01 \pm 0.5^{\circ}C$. These much lower uncertainties led to the decision to use the saturation temperatures. The measured temperatures were then used primarily to validate the data. Thus, any data with significant discrepancies between the measured and saturation temperatures were not considered valid. These considerations are summarized in Table 4.5.

Table 4.5: Refrigerant Saturation Temperatures

	Measured T (°C)	Pressure (kPa)	Enthalpy (kJ/kg)	Saturation T (°C)	Temperature Difference (°C)
Test section inlet	61.37 ± 0.5	3926 ± 5	386.4 ± 2.0	61.07 ± 0.06	0.30 ± 0.5
Test section outlet	61.01 ± 0.5	3926 ± 5	370.6 ± 3.6	61.07 ± 0.06	0.06 ± 0.5

4.1.6 Refrigerant Heat Transfer Coefficient in Test Section

The measured heat duty and the LMTD are used to calculate the overall heat transfer conductance *UA*, as follows:

$$\dot{Q}_{\text{test}} = (UA)(\text{LMTD}) \tag{4.27}$$

From Equation 4.27, *UA* = 8.433 ± 1.061 W/K. Figure 4.4 shows the thermal resistance network for the test section. This network depicts the heat transfer in the main portion of the test section between the inlet and the outlet, and also accounts for the additional area within the assembly (but beyond the inlet and outlet fittings), which also participate to some extent in the heat transfer.
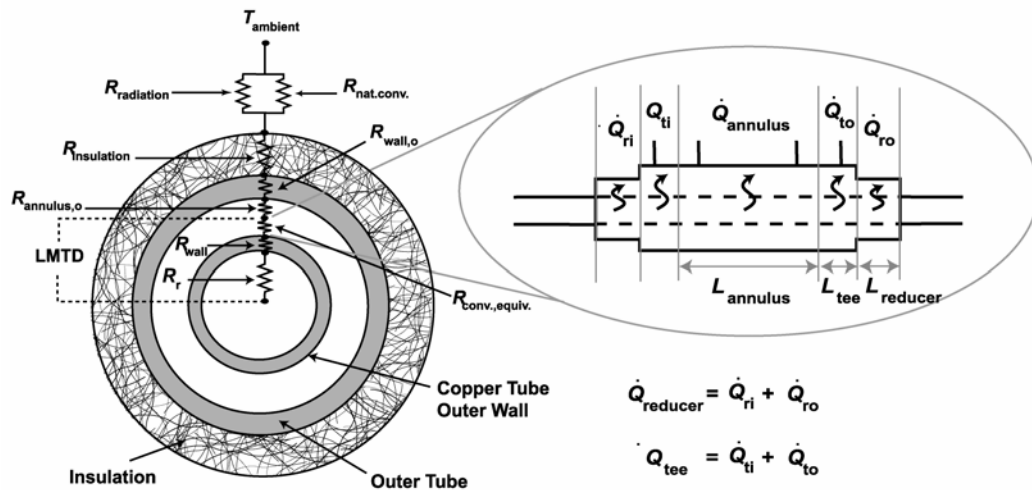
Figure 4.4: Resistance Network for Test Section

The heat transfer in the reducer and the tee fittings is in parallel with the forced convection in the primary annular portion of the test section between the inlet and outlet. The refrigerant heat transfer coefficient can then be deduced from Figure 4.4 as follows:

$$UA = \frac{1}{R_{\text{r}} + R_{\text{wall}} + R_{\text{conv.,equiv.}}} \tag{4.28}$$

where the conductive resistance in the copper tube, R_{wall}, is presented in Equation 4.29. It should be noted that the heat transfer area spans the test section's annulus portion, as well as the length of the Swagelok fittings at the ends.

The conductive resistance is:

$$R_{\text{wall}} = \frac{\ln\left(\dfrac{D_{\text{test,o}}}{D_{\text{test,i}}}\right)}{2\pi k_{\text{test}}\left(L_{\text{annulus}} + 2\cdot\left(L_{\text{reducer}} + L_{\text{tee}}\right)\right)} \tag{4.29}$$

$$R_{\text{wall}} = \frac{\ln\left(\dfrac{6.35 \text{ mm}}{3.048 \text{ mm}}\right)}{2\pi\left(398.3 \text{ W/m-K}\right)\left(0.1524 + 2\left(0.02286 + 0.01321\right)\right)\text{m}} = 1.306 \times 10^{-2} \text{ K/W}$$

The equivalent convective resistance on the water-side, $R_{\text{conv.,equiv.}}$, defined in Equation 4.30, considers forced convection in the annulus, and approximates as natural convection the heat transfer in the Swagelok fittings at the test section ends (Equations 4.32 and 4.33):

$$\frac{1}{R_{\text{conv,equiv.}}} = \frac{1}{R_{\text{annulus,i}}} + 2\cdot\left(\frac{1}{R_{\text{tee}}} + \frac{1}{R_{\text{reducer}}}\right) \tag{4.30}$$

The forced convective resistance is defined in Equation 4.31:

$$R_{\text{annulus,i}} = \frac{1}{h_{\text{annulus}} \pi D_{\text{test,o}} L_{\text{annulus}}} \qquad (4.31)$$

The water-side heat transfer coefficient was previously calculated (to determine the heat losses in the test section): $h_{\text{annulus}} = 10100$ W/m^2-K, resulting in $R_{\text{annulus,i}} = 3.258 \times 10^{-2}$ K/W.

The thermal resistances in the Swagelok tee fitting and reducer are given in Equations 4.32 and 4.33 where natural convection between horizontal cylinders is approximated using an effective thermal conductivity (Incropera and DeWitt, 1996):

$$R_{\text{tee}} = \frac{\ln\left(\dfrac{D_{\text{tee}}}{D_{\text{test, o}}}\right)}{2\pi k_{\text{eff}} L_{\text{tee}}} \qquad (4.32)$$

$$R_{\text{reducer}} = \frac{\ln\left(\dfrac{D_{\text{reducer}}}{D_{\text{test, o}}}\right)}{2\pi k_{\text{eff}} L_{\text{reducer}}} \qquad (4.33)$$

The effective conductivity, k_{eff}, is based on the geometry and a modified Rayleigh number, Ra^*, as follows:

$$\frac{k_{\text{eff}}}{k_{\text{water}}} = 0.386 \left(\frac{\text{Pr}}{0.861 + \text{Pr}}\right)^{0.25} \left(\text{Ra}^*\right)^{0.25} \qquad (4.34)$$

The modified Rayleigh number for the Tee-fitting is given here; for the reducer, the appropriate diameter is similarly substituted into Equation 4.35.

$$\text{Ra}^*_{\text{tee}} = \frac{\left[\ln\left(D_{\text{tee}} \middle/ D_{\text{test, o}}\right)\right]^4}{\left(D_{\text{test, o}}^{-3/5} + D_{\text{tee}}^{-3/5}\right)^5} \cdot \frac{g\beta_{\text{w}}\left(T_{\text{wall,o}} - T_{\text{w,test,avg}}\right)}{\nu_{\text{w}} \alpha_{\text{w}}} \qquad (4.35)$$

$$\text{Ra}^*_{\text{tee}} = \frac{\left[\ln\left(10.41/6.350\right)\right]^4}{\left(0.00635^{-3/5} + 0.01041^{-3/5}\right)^5} \cdot \frac{9.81 \cdot 4.567 \times 10^{-4} \left(52.97 - 49.85\right)}{\left(1.558 \cdot 5.548\right) \times 10^{-4}} = 154.2$$

From the modified Rayleigh number, the resulting thermal resistances in the tee and reducer are: $R_{\text{tee}} = 7.188$ K/W and $R_{\text{reducer}} = 4.070$ K/W, where the effective thermal conductivities in the reducer and tee are $k_{\text{reducer}} = 0.6435$ W/m-K $k_{\text{tee}} = 0.8293$ W/m-K respectively. It should be noted that the corresponding thermal conductivity of water at this temperature is 0.6435 W/m-K. Furthermore, it should be noted that the resistance in the annulus, $R_{\text{annulus,i}}$, constitutes 0.8% of the resistance when compared to R_{reducer} and only 0.45% when compared with R_{tee}, indicating that the reducer and the tee participate minimally in the heat transfer compared to the main annulus section.

For this data point, $\dot{Q}_{\text{reducer}} = 1.47$ W and $\dot{Q}_{\text{tee}} = 0.83$ W, whereas the heat duty for the forced convection in the annulus is: $\dot{Q}_{\text{annulus}} = 92.35$ W. Even though the heat duties at the ends are low in comparison to the heat duty in the primary heat transfer portion of the annulus, they should not be neglected. If the ends were not considered in the analysis, the heat transfer area for the refrigerant would be underestimated, thereby, increasing the heat transfer coefficient.

From Equation 4.28, all known values can be substituted to calculated R_{r}:

$$8.433 = \frac{1}{R_{\text{r}} + 1.306 \times 10^{-3} + 3.178 \times 10^{-2}}$$

This yields a refrigerant-side resistance of $R_r = 8.550 \times 10^{-2}$ K/W. This resistance is used to obtain the refrigerant heat transfer coefficient as follows:

$$R_r = \frac{1}{h_r \pi D_{test,\,i} \left(L_{test} + 2L_{reducer} + 2L_{tee} \right)} \tag{4.36}$$

This yields a condensation heat transfer coefficient of $h_r = 5440 \pm 1069$ W/m²-K. It can also be seen from this analysis that for this data point, the resistance ratio is:

$$R_{ratio} = \frac{R_r}{R_{wall} + R_{conv.equiv.}} = 2.584 \tag{4.37}$$

which minimizes the dependence of the computed refrigerant heat transfer coefficient on the approach used to obtain the other resistances, especially the annulus-side resistance.

4.1.7 Heat Transfer Coefficient based on Measured Wall Temperature

The refrigerant heat transfer coefficient calculations in the previous section were also verified using temperature measurements with thermocouples soldered onto the outer surface of the inner tube of the test section. The refrigerant saturation temperatures and the measured outer wall temperatures were then used in calculating the refrigerant-to-wall LMTD.

$$\text{LMTD} = \frac{\left(T_{r,\,test,\,in,\,sat} - T_{wall,avg} \right) - \left(T_{r,\,test,\,out,\,sat} - T_{wall,avg} \right)}{\ln \left[\dfrac{\left(T_{r,\,test,\,in,\,sat} - T_{wall,avg} \right)}{\left(T_{r,\,test,\,out,\,sat} - T_{wall,avg} \right)} \right]} \tag{4.38}$$

For the data point under consideration, the average wall temperature measured by the five thermocouples is $T_{wall,avg} = 51.83°C$, with a minimum and maximum temperature of 51.06°C and 52.72°C. The overall conductance determined using Equation 4.27:

$\dot{Q}_{\text{test}} = (UA)(\text{LMTD})$, yields $UA = 10.24$ W/K. In the present case, the overall heat transfer conductance is given by Equation 4.39:

$$UA = \frac{1}{R_{\text{r}} + R_{\text{wall}}} \tag{4.39}$$

The resistances in the above equation were defined in the previous section (Equations 4.29 and 4.36). The resulting heat transfer coefficient for the refrigerant (based on the measured wall temperature) is $h_{\text{r,wall}} = 4828 \pm 641$ W/m²-K. This heat transfer coefficient agrees well with the heat transfer coefficient determined using the thermal amplification technique, $h_{\text{r}} = 5440 \pm 1069$ W/m²-K, i.e. a difference of $(h_{\text{r}} - h_{\text{r,wall}})/h_{\text{r}} = 11.25\%$. For all condensation data, the difference ranges from -1.24 to 13.26%, with an average of 5.86%. This second approach for obtaining the heat transfer coefficient provides additional, independent validation for the thermal amplification technique used in this study. With the annular 3.05 mm test section data being validated in this manner, test on the brazed tube heat exchangers for the 0.76 and 1.52 mm tubes were only conducted using the thermal amplification technique.

4.1.8 Pressure Drop across Test Section

The measured pressure drop, $\Delta P_{\text{measured}}$, in the test section is composed of the frictional pressure drop: ΔP_{f}, the deceleration pressure drop: $\Delta P_{\text{deceleration}}$, and the contraction and expansion pressure drops at the inlet and outlet of the test section, $\Delta P_{\text{contraction}}$ and $\Delta P_{\text{expansion}}$.

$$\Delta P_{\text{measured}} = \Delta P_{\text{f}} - \left| \Delta P_{\text{deceleration}} \right| + \Delta P_{\text{contraction}} - \Delta P_{\text{expansion}} \tag{4.40}$$

The contraction pressure drop is calculated using a model given in Hewitt *et al.* (1994). The contraction losses consist of a pressure drop due to the area reduction, as well due to frictional losses as follows:

$$\Delta P_{\text{contraction}} = \frac{G^2}{2\rho_1} \left(\underbrace{1 - A_{\text{ratio}}^2}_{\substack{\text{Kinetic} \\ \text{Energy} \\ \text{Change}}} + \underbrace{\left(\frac{1}{C_C} - 1\right)^2}_{\substack{\text{Frictional} \\ \text{Pressure Loss}}} \right) \psi_H \tag{4.41}$$

The ratio of the test section cross-sectional area to the cross-sectional area of the refrigerant tubing is given below:

$$A_{\text{ratio}} = \frac{A_{\text{test}}}{A_{\text{r}}} \tag{4.42}$$

For the annular test section, there are three sequential contractions (see Figure 3.4) which sum up to the total contraction pressure drop. The coefficient of contraction is given by Chisholm (1983):

$$C_C = \frac{1}{0.639 \left[1 - \left(A_{\text{ratio}}\right)\right]^{1/2} + 1} \tag{4.43}$$

$$\psi_H = 1 + \left(\frac{\rho_{\text{l,test,in}}}{\rho_{\text{v,test,in}}} - 1\right) x_{\text{r,test,in}} \tag{4.44}$$

For a test section inlet quality $x_{\text{r,test,in}} = 0.73$, the homogeneous flow multiplier is $\psi_H = 3.075$. Hewitt *et al.* (1994) state that for a sudden contraction, the homogeneous multiplier yields better agreement with experimental data than the separated flow multiplier. For the data point under consideration, the total contraction pressure drop is $\Delta P_{\text{contraction}} = 1.579$ kPa. As defined in Equation 4.41, 77% of this pressure drop is to due

the kinetic energy change ($\Delta P_{\text{contraction,kinetic-energy}} = 1.216$ kPa) and 23% ($\Delta P_{\text{contraction,loss}} = 0.363$ kPa) is due to frictional losses.

The expansion pressure drop recommended by Hewitt *et al.* (1994) is:

$$\Delta P_{\text{expansion}} = \frac{G^2}{2\rho_l}\left(\underbrace{\left(1 - A_{\text{ratio}}^2\right)}_{\substack{\text{Kinetic} \\ \text{Energy} \\ \text{Change}}} - \underbrace{\left(1 - A_{\text{ratio}}\right)^2}_{\text{Frictional Loss}} \right)\psi_S = \frac{G^2 A_{\text{ratio}}\left(1 - A_{\text{ratio}}\right)\psi_S}{\rho_l} \qquad (4.45)$$

Again, three sequential expansion terms are considered due to changing flow area in the fittings (Figure 3.4). The separated flow multiplier, ψ_S, is given in Equation 4.46; the quality at the test section outlet is used for its calculation, with $B = 0.25$ given by Chisholm (1983). It should be noted that a B-coefficient of unity reduces Equation 4.46 to the homogeneous multiplier, ψ_H.

$$\psi_s = 1 + \left(\frac{\rho_{l,\text{test,out}}}{\rho_{v,\text{test,out}}} - 1 \right)\left[Bx_{r,\text{test,out}}\left(1 - x_{r,\text{test,out}}\right) + x_{r,\text{test,out}}^2 \right] \qquad (4.46)$$

In this case, for $x_{r,\text{test,out}} = 0.57$, $\Psi_S = 2.110$. The combined expansion pressure drop is:

$$\Delta P_{\text{expansion}} = \Delta P_{\text{expansion,kinetic energy}} - \Delta P_{\text{expansion,loss}}$$

$$= (0.8361 - 0.3758)\text{kPa} = 0.4604 \text{ kPa}$$

The deceleration pressure drop due to decreasing velocities resulting from condensation can be derived from an axial momentum balance in the test section as shown by Carey (1992).

64

$$\left|\Delta P_{\text{deceleration}}\right| = \left\|G^2\left[\frac{x^2}{\rho_v\alpha} + \frac{(1-x)^2}{\rho_l(1-\alpha)}\right]\right|_{\substack{\alpha = \alpha_{\text{r, test, out}} \\ x = x_{\text{r, test, out}}}} - \left|G^2\left[\frac{x^2}{\rho_v\alpha} + \frac{(1-x)^2}{\rho_l(1-\alpha)}\right]\right|_{\substack{\alpha = \alpha_{\text{r, test, in}} \\ x = x_{\text{r, test, in}}}}\right\| \quad (4.47)$$

The void fraction, α, is a function the refrigerant quality along with the vapor and liquid densities and their corresponding dynamic viscosities. In the absence of other reliable correlations for void fraction in microchannels, the Baroczy correlation (1965), given below, is used to compute the void fraction:

$$\alpha = \left[1 + \left(\frac{1-x}{x}\right)^{0.74}\left(\frac{\rho_v}{\rho_l}\right)^{0.65}\left(\frac{\mu_l}{\mu_v}\right)^{0.13}\right]^{-1} \quad (4.48)$$

For this representative data point, the void fractions at the inlet and outlet are $\alpha_{\text{in}} = 0.81$ and $\alpha_{\text{out}} = 0.72$, respectively, yielding a pressure rise due to deceleration of 0.4050 kPa. Finally, the frictional pressure drop is determined from Equation 4.40: $4.362\ \text{kPa} = \left(\Delta P_f - 0.4050 + 1.579 - 0.4604\right)\ \text{kPa}$, $\Delta P_f = 3.648$ kPa, and the corresponding pressure gradient for a test section length of $L_{\text{test}} = 323.8$ mm is $\nabla P_f = 11.27$ kPa/m. The ratio of the deceleration pressure drop to the measured pressure is 9.3%. Similarly, the contraction, expansion and frictional pressure drops are 36.2%, 10.6% and 86.6% of the measured pressure drop, respectively.

4.2 Condensation in the Multiport Test Sections

For the 1.52 and 0.76 mm I.D. test sections, the heat transfer analysis is similar to the procedure described in the previous sections. However, the water in the test section is not flowing through an annulus but rather through the microchannel tubes. The resistance network to determine the refrigerant h_r incorporates a fin analysis to use the appropriate

heat transfer area of the side walls of the refrigerant and water ports as described by Bandhauer (2002). The pressure drop analysis is the same as shown for the annular test sections (with only one contraction and expansion term instead of three terms as in the annular test section).

4.2.1 Heat Transfer Coefficient in 1.52 mm Test Section

The following discussion pertains to the conditions summarized in Table 4.6. The water-side heat transfer coefficient for the rectangular water channels is determined using Churchill's Nusselt number (Equation 4.49) and friction factor (Equation 4.50) correlations (1977). All detailed calculations are also shown in Appendix C.

The Reynolds number in the water ports, Re_w, is turbulent. In this case $Re_w = 5950$ and Pr = 3.10.

$$\text{Nu}_w = \left[4.364^{10} + \left(\frac{\exp\left[\frac{2200 - \text{Re}_w}{365} \right]}{4.364^2} + \left(6.3 + \frac{0.079 \cdot \left(\frac{f}{8} \right)^{1/2} \cdot \text{Re}_w \cdot \text{Pr}}{\left(1 + \text{Pr}^{0.8} \right)^{5/6}} \right)^{-2} \right)^{-5} \right]^{1/10} \quad (4.49)$$

$$f = 8 \left[\left(\frac{8}{\text{Re}_w} \right)^{12} + \left\{ 2.457 \ln\left(\left[\frac{7}{\text{Re}_w} \right]^{0.9} + 0.27 \left(\frac{e_{w,port}}{D_{w,port,hydraulic}} \right) \right)^{16} + \left[\frac{37530}{\text{Re}_w} \right]^{16} \right\}^{-1.5} \right]^{1/12} \quad (4.50)$$

The relative surface roughness is $(e_{w,port}/D_{w,port,hydraulic}) = 0.0009$ (Coleman, 2000), yielding a friction factor, $f = 0.03717$ and $\text{Nu}_w = 41.45$. The resulting water-side heat transfer coefficient is $h_w = 27410$ W/m²-K. Again, a ± 25% uncertainty is assumed for h_w.

Table 4.6: Variable Values for Sample Calculation

	Variable	Value
Calculated Values	G (kg/m²-s)	800.0
	x_{avg} (-)	0.2962
	P_r (-)	0.8021
	$\dot{Q}_{test}$ (W)	233.3
	$\dot{Q}_{pump}$ (W)	27.36
	$\dot{Q}_{sec}$ (W)	236.4
	$\dot{Q}_{loss,ambient}$ (W)	24.23
Measured Values	$\dot{V}_{w,\,prim}$ (m³/s)	1.01×10^{-4}
	$T_{r,test,in,sat}$ (°C)	61.10
	$T_{r,test,out,sat}$ (°C)	61.07
	$T_{r,test,in}$ (°C)	61.11
	$T_{r,test,out}$ (°C)	60.80
	$T_{w,prim,in}$ (°C)	57.37
	$T_{w,prim,out}$ (°C)	57.92

A cross-sectional view of the 1.52 mm test section is shown in Figure 4.5. The heat transfer area for the water-side, A_w, is composed of the direct, $A_{w,direct}$, and indirect heat transfer area, $A_{w,indirect}$, as follows:

$$A_w = A_{w,direct} + \eta_{w,fin} A_{w,indirect} \tag{4.51}$$

The direct heat transfer area corresponds to both water tubes (on top and bottom of the refrigerant tube).

$$A_{w,direct} = 2 \cdot n_w \cdot L_{r,h} \cdot w_{w,port} \tag{4.52}$$
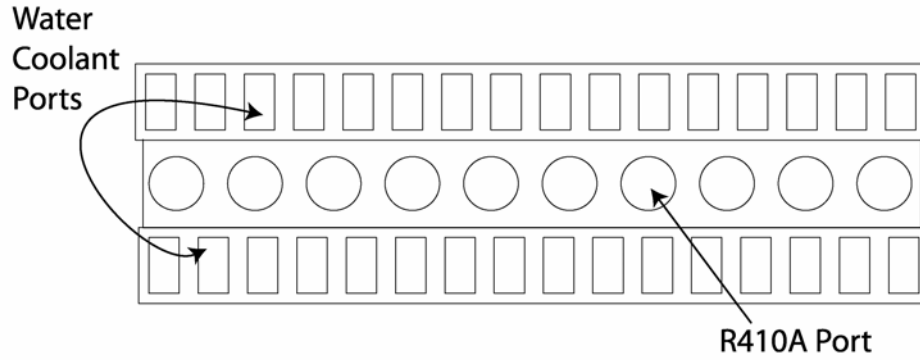
Figure 4.5: Cross Section of 1.52 mm Test Section

For 16 ports of 304.8 mm length and a width of 0.762 mm, $A_{w,direct} = 0.007432$ m^2. Figure 4.6 shows the cross-sectional view of the test section, with the direct heat transfer area marked in thick lines.
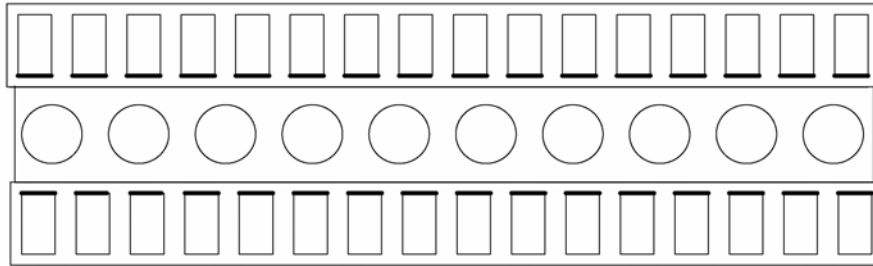
Figure 4.6: Direct Heat Transfer Area

The indirect heat transfer area includes the area of the side walls of the ports, as well as the top area in each port. The factor of two is needed to include the top and bottom water tube. From these calculations, $A_{w,indirect} = 0.03468$ m^2.

$$A_{w,indirect} = 2n_w \cdot L_{r,h} \cdot \left(2z_{w,port} + w_{w,port}\right) \tag{4.53}$$

Figure 4.7 illustrates the indirect heat transfer area with thick lines.
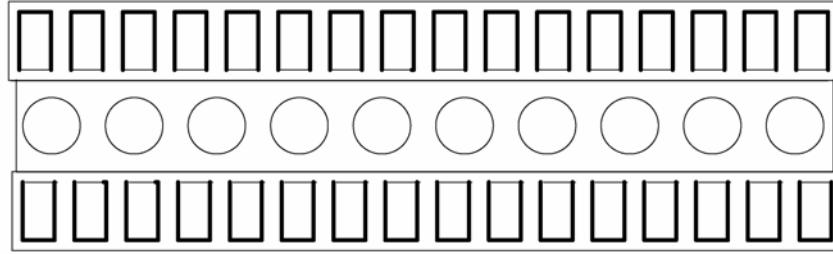
Figure 4.7: Indirect Heat Transfer Area

The fin efficiency is defined as follows:

$$\eta_{w,fin} = \frac{\tanh\left(M \cdot \left(z_{w,port} + w_{w,port}/2\right)\right)}{M \cdot \left(z_{w,port} + w_{w,port}/2\right)} \tag{4.54}$$

The fin parameter, M, is calculated as follows:

$$M = \sqrt{\frac{h_w \cdot 2\left(L_{r,h} + t_{w,port}\right)}{k_{Al} \cdot \left(L_{r,h} \cdot t_{w,port}\right)}} \tag{4.55}$$

M is calculated to be 696.4 m^{-1}, resulting in a fin efficiency of 68.2%. The total area

transfer area, determined by Equation 4.51, is

$A_w = \left(0.007432 + 0.682 \cdot 0.03468\right) \text{ m}^2 = 0.03108 \text{ m}^2$ and the water-side heat transfer

resistance is $R_w = 11.73 \times 10^{-4}$ K/W.

For the heat loss calculation, the multiport test section assembly is approximated as a

circular tube with 1-D heat transfer in the radial direction as illustrated in Figure 4.9.
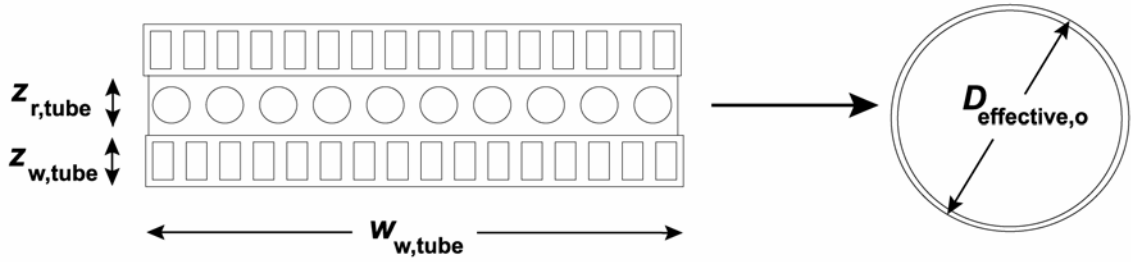
Figure 4.8: Effective Diameter for Heat Loss Calculations

The effective outer diameter is given as:

$$D_{effective,o} = \frac{\left(2w_{w,tube} + 4z_{w,tube} + 2z_{r,tube}\right)L_{r,h}}{\pi L_{r,h}}$$ (4.56)

For this test section, the effective outside and inside diameters are 16.51 and 16.00 mm. (Here, the tube thickness, $t_{w,tube}$ = 0.254 mm, is used to deduce the inner diameter.) The corresponding conductive wall resistance is 6.858×10^{-5} K/W.

As shown in a previous section, a heat transfer analysis between the average water temperature and the ambient temperature is used to determine the heat losses in the test section. For this case, the heat lost to the ambient is 1.489 W. The heat transfer coefficient of the refrigerant can be deduced by the analysis outlined in Equations 4.27 and 4.28,

$$\dot{Q}_{test} = (UA)(\text{LMTD})$$

$$UA = \frac{1}{R_r + R_{conduction} + R_w}$$

where the convective resistance on the water-side is $R_w = 11.73 \times 10^{-4}$ K/W and the conductive resistance is:

70

$$R_{\text{conduction}} = \frac{t_{\text{r,tube}} + t_{\text{w,tube}}}{k_{\text{Al}} \cdot A_{\text{conduction}}} \tag{4.57}$$

where $A_{\text{conduction}}$ is defined in 4.58, as proposed by Bandhauer (2002):

$$A_{\text{conduction}} = \frac{A_{\text{r,tube,i}} + A_{\text{r,tube,o}} + A_{\text{w,tube,i}} + A_{\text{w,tube,o}}}{4} \tag{4.58}$$

$$A_{\text{r,tube,i}} = 2 \cdot L_{\text{r,h}} \left((n_{\text{r}} - 1) t_{\text{r,port}} + D_{\text{r}} \cdot n_{\text{r}} \right) = 0.01645 \text{ m}^2 \tag{4.59}$$

$$A_{\text{r,tube,o}} = 2 \cdot L_{\text{r,h}} \cdot w_{\text{r,tube}} = 0.01161 \text{ m}^2 \tag{4.60}$$

$$A_{\text{w,tube,i}} = 2 \cdot L_{\text{r,h}} \left((n_{\text{w}} - 1) t_{\text{w,port}} + w_{\text{w,port}} \cdot n_{\text{w}} \right) = 0.01178 \text{ m}^2 \tag{4.61}$$

$$A_{\text{w,tube,o}} = 2 \cdot L_{\text{r,h}} \cdot w_{\text{w,tube}} = 0.01209 \text{ m}^2 \tag{4.62}$$

The total area of interest for conduction is 0.01298 m^2, resulting in a conductive resistance of 3.303×10^{-4} K/W.

The LMTD for this case is 3.493 K, yielding a *UA* value of 66.8 W/K, or a total resistance of 1.497×10^{-2} K/W. The resulting refrigerant resistance is 13.57×10^{-3} K/W. The resistance ratio of the refrigerant resistance to the water-side resistance is $R_{\text{ratio}} = 8.9$ The effective heat transfer area on the refrigerant side is determined by Equation 4.63:

$$A_{\text{r,surface}} = \pi \cdot D_{\text{r}} \cdot L_{\text{r,h}} \cdot n_{\text{r}} \tag{4.63}$$

For 10 ports and a length and diameter of 0.3048m and 1.524 mm, respectively, $A_{\text{r,surface}} =$ 0.01459m^2. It should be noted that the treatment to obtain the refrigerant-side area is not the same as what was needed for the water side, because there is only one refrigerant tube

instead of the two water tubes. In addition, the ports in the refrigerant tube are circular instead of rectangular. The resulting heat transfer coefficient is $h_r = 5088$ W/m²-K.

For the above calculation, the microchannel port walls in the water tubes have been treated as fins with their corresponding efficiencies, reflecting the fact that the heat transfer area is not in direct contact with the cooling water side. For the refrigerant tubes, the fin efficiency approaches unity, thereby allowing for the indirect area to be treated as a direct heat transfer area without any loss of accuracy. Figure 4.9 shows a comparison of the fin efficiencies on the water side and on the refrigerant side for all condensation experiments in the 1.52 mm test section.
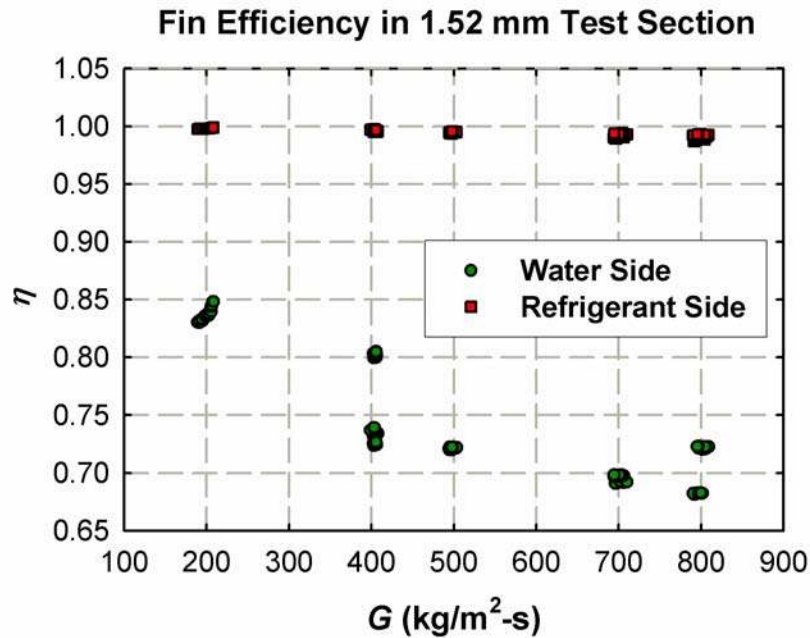
Figure 4.9: Fin Efficiency in 1.52 mm Test Section

It is observed that the water-side efficiencies are about 20 - 30% lower than those on the refrigerant side, with the exception of the lower mass flux cases. In order to minimize the

quality drop at $G = 200$ kg/m^2-s, the coolant flow rate was reduced, resulting in a lower h_w, which in turn leads to higher fin efficiencies on the water side. Based on the results shown in this figure, the fin efficiencies were taken into account for calculating the water-side effective area, whereas on the refrigerant side, the entire surface area in contact with the refrigerant was treated as a direct area.

4.2.2 Pressure drop in 1.52 mm Test Section

The frictional pressure drop in the multiport test section is determined as outlined in Equations 4.40 - 4.48 for the annular test section. For this data point, the measured pressure drop is $\Delta P_{measured} = 7.444$ kPa and the deceleration pressure drop is $\left|\Delta P_{deceleration}\right| = 0.2755$ kPa, which represents 3.7% of the measured pressure drop (for a change in quality from $x_{r,test,in} = 0.37$ to $x_{r,test,out} = 0.22$). The contraction and expansion pressure drops are $\Delta P_{contraction} = 0.7444$ kPa and $\Delta P_{expansion} = 0.2492$ kPa, corresponding to 10% and 3.3% of the measured pressure drop. This results in a frictional pressure drop of 7.224 kPa, and for a test section length of 0.508 m, a frictional pressure gradient of $\nabla P_f = 14.22$ kPa/m.

4.3 Supercritical Heat Transfer and Pressure Drop

4.3.1 Heat Transfer

The calculation of the refrigerant heat transfer coefficient is done in the same manner as described for the two-phase condensation experiments with the aid of the thermal amplification technique. For a given P_r and G, the refrigerant temperature in the test section is varied, ranging from 35 to 110°C. The deduced heat transfer coefficient is assumed to represent heat transfer at the average refrigerant temperature in the test

section. For a sample data point (Run 12 on 21 September 2005) in the 3.05 mm test section at $P_r = 1.112$, $G = 790.8$ kg/m²-s and an average refrigerant temperature of $T_{r,avg} = 86.62°C$, the heat duty in the test section was $\dot{Q}_{test} = 151.7$ W. The refrigerant to coolant log-mean temperature difference and overall conductance were LMTD = 17.5°C and UA = 8.671 W/K (equivalent to a total resistance of 0.1153 K/W), resulting in a refrigerant resistance of $R_r = 0.08627$ K/W. The resistance ratio, as given by:

$$R_{ratio} = R_r / \left(R_{wall} + R_{conv.equiv} \right),$$ is 2.969. The deduced refrigerant heat transfer coefficient is $h_r = 5103$ W/m²-K. This value agrees well with the heat transfer coefficient based on the measured wall temperatures, $h_{r,wall} = 5150$ W/m²-K, the difference between the two heat transfer coefficients being $\left(h_r - h_{r,wall} \right) / h_r = -0.9\%$.

4.3.2 Pressure Drop

The frictional pressure drop is computed in a similar fashion as outlined for the two-phase analysis, and Equation 4.40 still applies. However, the deceleration (Equation 4.64), contraction (Equation 4.65) and expansion pressure changes are derived from momentum balances for single phase flow.

$$\left| \Delta P_{deceleration} \right| = \left| \frac{G^2}{\rho_{out}} - \frac{G^2}{\rho_{in}} \right| \tag{4.64}$$

The contraction coefficients, $K_{contraction}$, are functions of the area ratio (Munson *et al.*, 1998). The area ratio represents the ratio of the cross-sectional flow at the smaller area to the larger one and therefore is less than unity.

$$\Delta P_{\text{contraction}} = \frac{G^2}{2\rho_{\text{in}}} \left(\underbrace{\left(1 - A_{\text{ratio}}^2\right)}_{\substack{\text{Kinetic} \\ \text{Energy} \\ \text{Change}}} + \underbrace{K_{\text{contraction}}}_{\substack{\text{Frictional} \\ \text{Pressure Loss}}} \right) \tag{4.65}$$

$$\Delta P_{\text{expansion}} = \frac{G^2}{2\rho_{\text{out}}} \left(\underbrace{\left(1 - A_{\text{ratio}}^2\right)}_{\substack{\text{Kinetic} \\ \text{Energy} \\ \text{Change}}} - \underbrace{K_{\text{expansion}}}_{\substack{\text{Frictional} \\ \text{Pressure Loss}}} \right) \tag{4.66}$$

The expansion coefficient, $K_{\text{expansion}}$, is also a function of the cross-sectional area ratio and is defined as:

$$K_{\text{expansion}} = \left(1 - A_{\text{ratio}}\right)^2 \tag{4.67}$$

All loss coefficients are summarized in Table 4.7.

Table 4.7: Contraction and Expansion Loss Coefficients

Test Section	Geometry	A_{ratio}	$K_{\text{contraction}}$	$K_{\text{expansion}}$
Annular	Tee - Reducer	0.7889	0.10	0.0445
	Reducer - Contraction	0.2722	0.38	0.5296
	Manifold -Test Section	0.3989	0.30	0.3613
Multiport	Inlet/ Test Section	0.5307	0.50	0.2202

 For the data mentioned above (Run 12 on 21 September 2005) in the 3.05 mm test section, the measured pressure drop is 4.686 kPa, whereas the pressure drop due to contraction, expansion and deceleration are: 1.848, 0.553 and 0.6964 kPa, respectively. The resulting frictional pressure drop is 4.090 kPa, resulting in pressure gradient of $\nabla P_{\text{f}} =$ 12.63 kPa/m (for a test section length of 323.8 mm). The ratio of the frictional to measured pressure drop is 87.9 %.

CHAPTER 5 - CONDENSATION PRESSURE DROP AND HEAT TRANSFER RESULTS AND MODEL DEVELOPMENT

This chapter provides a detailed discussion of the experimental results for the phase-change pressure drop and heat transfer tests on all three test sections. The results are compared with the literature, and models for predicting ΔP and h are presented. To enable the models to address a larger range of geometric parameters and working fluids, the data taken previously by Jiang (2004) for refrigerant R404A on 9.40 mm tubes and by Mitra (2005) for refrigerant R410A on 6.22 and 9.40 mm tubes were also included in the experimental database with some modifications.

5.1 In-tube Condensation Results

This section focuses on the pressure drops, heat transfer coefficients and flow regime assignments for the experimental data.

5.1.1 Pressure Drop

The frictional pressure gradient for all test sections at both reduced pressures ($P_r = 0.8$ and 0.9) is shown in Figure 5.1. The higher shear rate between the liquid and vapor phases at higher flow velocities results in an increase in the pressure gradient at high qualities and mass fluxes. The increase in reduced pressure, however, results in a decrease in the frictional pressure gradient. This can be explained by the diminishing difference in the properties of the liquid and vapor phases.
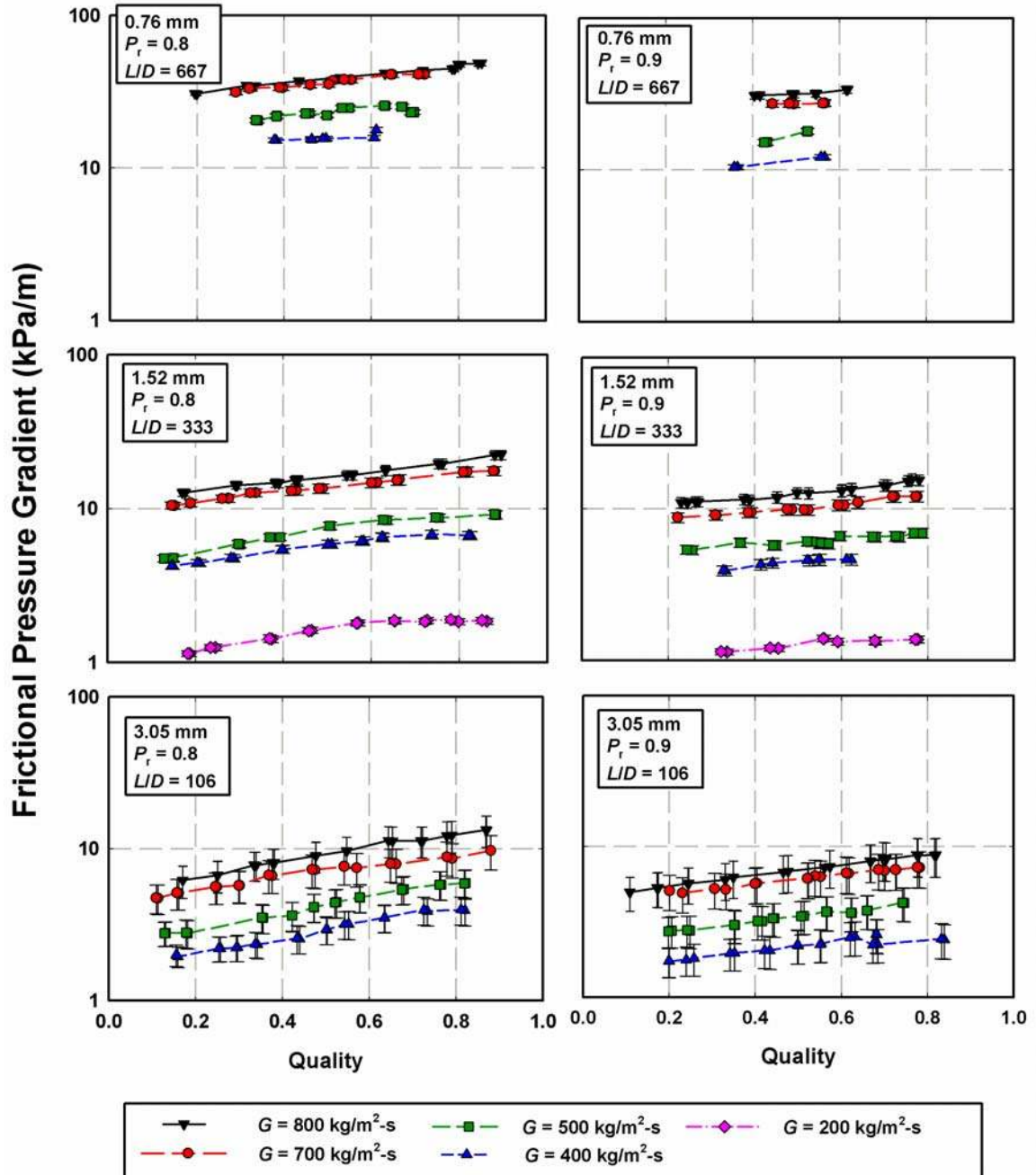
Figure 5.1: Frictional Pressure Gradient versus Quality

As P_r increases from 0.8 to 0.9, the viscosity ratio, μ_v / μ_l, increases from 0.30 to 0.40.

Similarly, the density ratio, ρ_v / ρ_l, increases from 0.26 to 0.37 (Lemmon *et al.*, 2002).

As the liquid-vapor dome converges to the critical pressure, the ratios of the vapor and liquid properties converge to unity, which decreases the vapor-liquid shear and the two-phase pressure drops. For example, in the 1.52 mm tube (for $G = 800$ kg/m^2-s, $x = 0.39$), the frictional pressure gradient changes from 14.63 kPa/m at $P_r = 0.8$ to 11.46 kPa/m at $P_r = 0.9$. The corresponding velocities for the liquid and vapor phase are $V_G = 2.46$ m/s and $V_L = 1.48$ m/s at $P_r = 0.8$, and $V_G = 1.91$ m/s and $V_L = 1.46$ m/s at $P_r = 0.9$. It should be noted that the vapor and liquid velocities decrease by 0.55 m/s and 0.02 m/s, respectively, with an increase in pressure. Also, as expected, the pressure gradient increases with a decrease in diameter. Figure 5.2 shows a direct comparison of the pressure gradient for two different test sections at $G = 800$ kg/m^2-s for the two reduced pressures in this study.
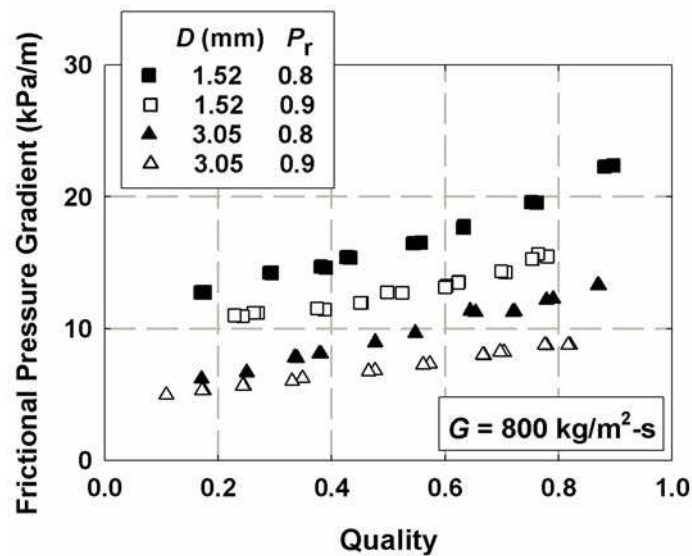
Figure 5.2: Frictional Pressure Gradient versus *x* for different *D* and *P*$_r$

The relative contributions of the frictional, deceleration and end effect ($\Delta P_{endeffect} = \Delta P_{contraction} - \Delta P_{expansion}$) pressure drops are shown in Table 5.1.

Table 5.1 : Relative Pressure Drop Contributions and Uncertainties

Test Section	P_r	$\dfrac{\Delta P_f}{\Delta P_{measured}}(\%)$	$\dfrac{\Delta P_{deceleration}}{\Delta P_{measured}}(\%)$	$\dfrac{\Delta P_{endeffects}}{\Delta P_{measured}}(\%)$	$\dfrac{U_{\Delta P_f}}{\Delta P_{measured}}(\%)$
0.76 mm	0.8	**98.6**	4.0	5.4	3.8
	0.9	**99.3**	5.9	6.6	4.8
1.52 mm	0.8	**98.7**	5.1	6.4	5.7
	0.9	**100.6**	8.7	8.1	7.5
3.05 mm	0.8	**84.7**	9.5	24.8	18.5
	0.9	**87.1**	16.8	29.7	22.5
Average	**All**	**94.1**	**8.7**	**14.6**	**11.5**

It should be noted that the frictional component, which is of interest in this study, dominates in all test sections. The values presented in the table are the average magnitudes of the ΔP fractions across the entire data set for each tube, for all G and x. The uncertainties in $\Delta P_{deceleration}$, $\Delta P_{contraction}$ and $\Delta P_{expansion}$ are estimated conservatively at $\pm$ 50%. The average uncertainty for ΔP_f in all test sections is 11.5%, with the highest uncertainties in the 3.05 mm test section, due to the lower contribution of frictional pressure drop in this larger diameter test section compared to the end effects, as shown in Table 5.1.

5.1.2 Heat Transfer Coefficient

The local heat transfer coefficients for all test conditions are presented in Figure 5.3. It is seen that the heat transfer coefficients increase with an increase in quality and mass flux. Additionally, the heat transfer coefficient increases as the diameter decreases.
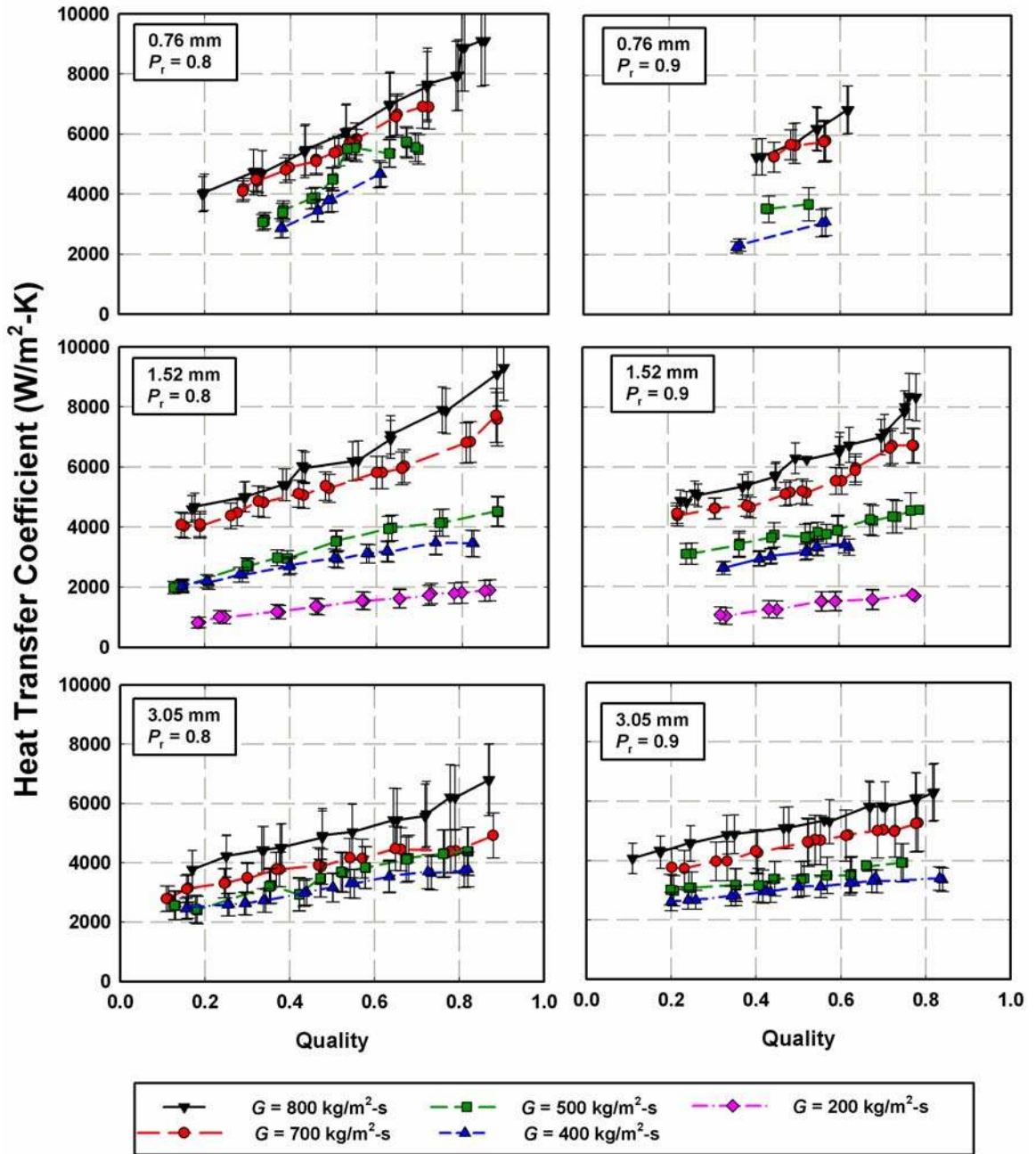
Figure 5.3: Heat Transfer Coefficients versus Quality

Table 5.2 summarizes the average quality change, resistance ratio, and uncertainty in the heat transfer coefficient, denoted as U_{h_r}, for each reduced pressure. The standard deviation, STD, is defined in Equation 5.1.

$$STD = \sqrt{\frac{1}{n}\sum_{j=1}^{n}\left(h_j - \overline{h}\right)^2} \qquad (5.1)$$

Table 5.2: Average Resistance Ratio, Quality Drop and Uncertainty in h_r

Test Section	P_r	$R_{ratio} \pm STD$	$\Delta x \pm STD$	$\dfrac{U_{h_r}}{h_r} \pm STD$ (%)
0.76 mm	0.8	8.8 ± 2.1	0.46 ± 0.17	11.1 ± 3.1
	0.9	9.7 ± 2.5	0.61 ± 0.06	11.6 ± 1.8
1.52 mm	0.8	14.2 ± 4.3	0.20 ± 0.02	12.1 ± 4.0
	0.9	13.1 ± 5.0	0.30 ± 0.06	10.9 ± 5.0
3.05 mm	0.8	3.4 ± 0.6	0.22 ± 0.05	16.8 ± 1.7
	0.9	3.0 ± 0.7	0.38 ± 0.10	15.1 ± 2.3
Average	**All**	$\mathbf{8.7 \pm 3.2}$	$\mathbf{0.32 \pm 0.09}$	$\mathbf{13.2 \pm 3.4}$

It can be seen from Table 5.2 that data were obtained for quality changes of 0.32 on average, thus capturing the variation of heat transfer coefficients and pressure drop with quality. Figure 5.4 shows a representative plot demonstrating the effects of diameter and reduced pressure. With an increase in reduced pressure from $P_r = 0.8$ to 0.9, the latent heat decreases from 103.6 kJ/kg to 76.9 kK/kg; however, the specific heat of the liquid and vapor phases increase from $c_{P,l} = 3.33$ kJ/kg-K to 5.89 kJ/kg-K and $c_{P,v} = 4.21$ kJ/kg-K to 8.04 kJ/kg-K, respectively. The heat transfer coefficients essentially remain unaffected by the competing property effects with an increase in reduced pressure. It should also be noted that with an increase in diameter, h decreases. This will be explored further in a following discussion.
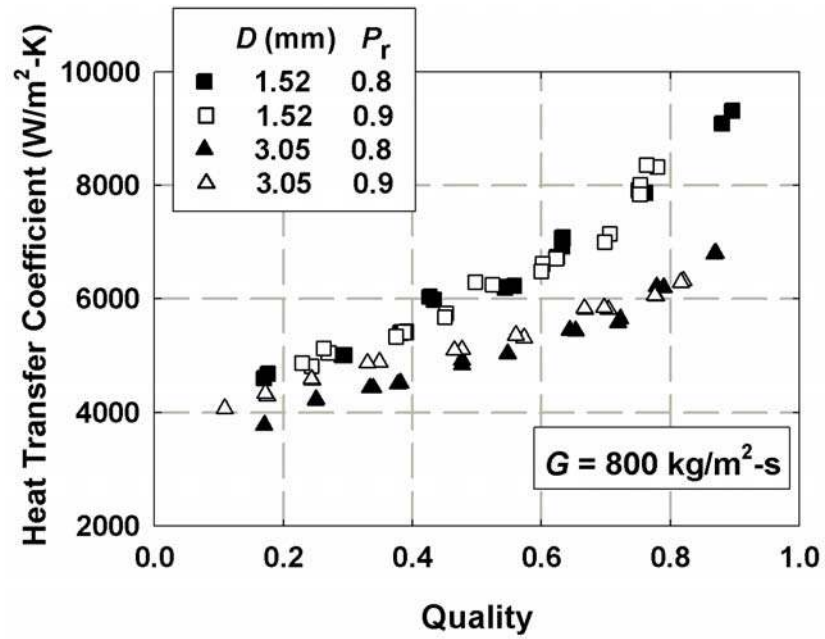
Figure 5.4: Heat Transfer Coefficient versus Quality for different *D* and *P*r

Figure 5.5 shows the resistance ratios for all condensation data for all test sections.
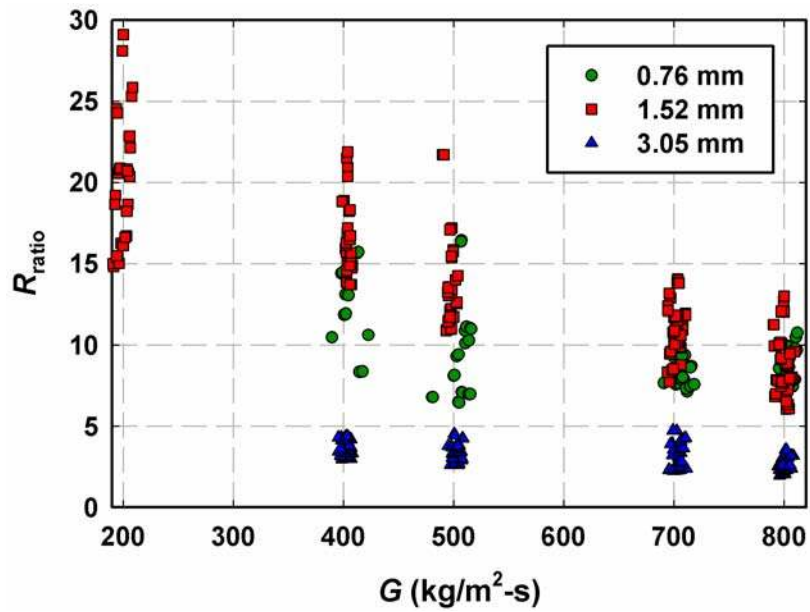
Figure 5.5: Resistance Ratio for all Condensation Data

The lowest resistance ratio was $R_{ratio} = 1.98$ (3.05 mm test section: $G = 795.9$ kg/m^2-s, P_r = 0.90 $x = 0.82$), the highest $R_{ratio} = 29.1$ (1.52 mm test section: $G = 200.0$ kg/m^2-s, P_r = 0.91 $x = 0.34$). The average resistance ratio for all data was 8.7. It should be noted that the resistance ratio in the 0.76 mm test section is lower than it is in the 1.52 mm test section due to an increase in h_r, which results in a decrease in R_r. The average resistance ratios in the single-tube test section (3.05 mm) are lower than the values in the multiport test sections, due to a different geometry of the test section design. The average heat transfer coefficient on the water side for the single-tube test section is $h_w = 8914$ W/m^2-K due to the flow of water through an annulus of flow area 50.0×10^{-6} m^2 compared to a refrigerant flow area of 7.3×10^{-6} m^2. However, in the 1.52 mm test section, $h_w = 21460$ W/m^2-K and in the 0.76 mm test section, $h_w = 26250$ W/m^2-K because of water flow through $D_h = 0.99$ mm multiport channels. In addition, the multiport geometry provides an effective indirect area of 3.468×10^{-2} m^2 in addition to the direct area of 7.432×10^{-3} m^2, which reduces the water-side resistance considerably.

For the 3.05 mm test section, the heat transfer coefficients were also verified using measurements of wall temperatures, as described in Section 4.1.7. Figure 5.6 shows representative wall-temperatures in the 3.05 mm test section for two different mass fluxes at both reduced pressures, plotted along with the refrigerant and coolant temperatures. The average deviation of all wall-temperature measurements was 0.82°C, with a minimum and maximum deviation ranging from 0 to 3.0°C. It should be noted that the slight variations in the average temperature corresponds to adjustments in the primary loop coolant flow rate.
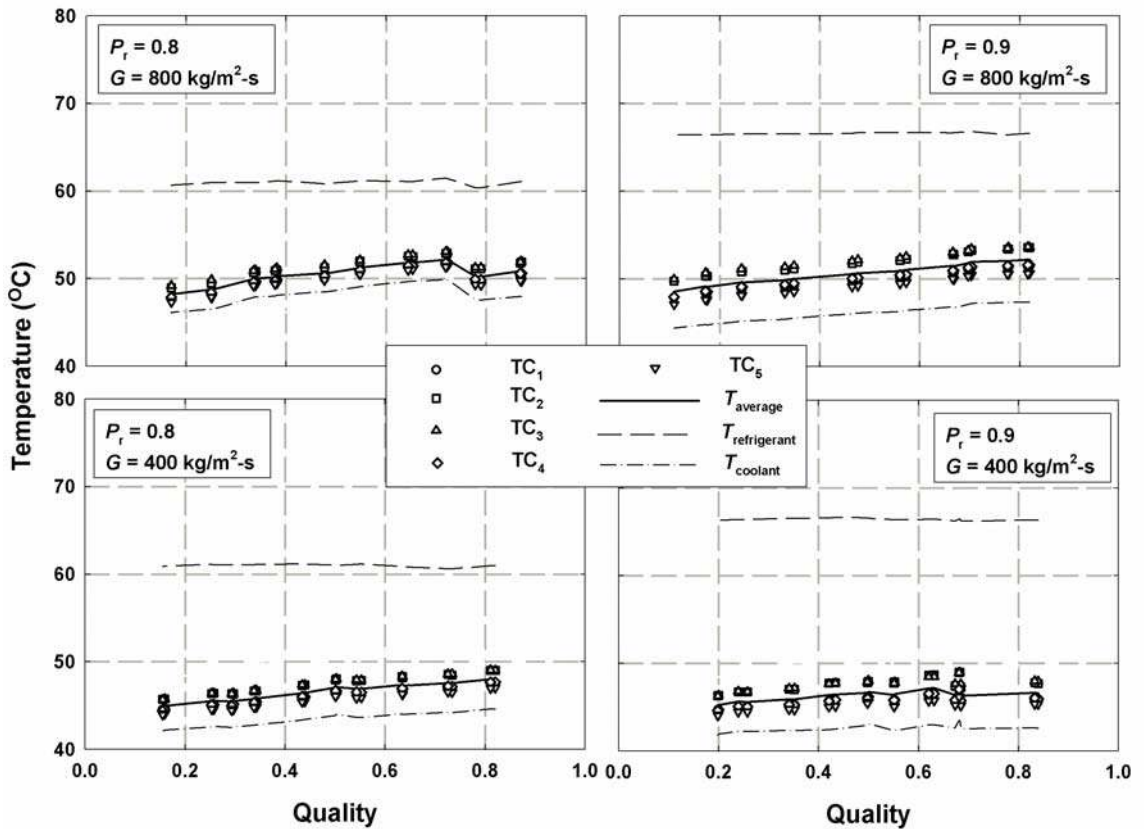
Figure 5.6: Representative Wall-Temperature Measurements, *D* = 3.05 mm

It can also be seen that the slight variations in the wall mounted thermocouple readings are quite small compared to the refrigerant-to-coolant ΔT.

As seen in Figure 5.7, the two independent methods of determining the refrigerant-side heat transfer coefficient agree well, with a deviation ranging from -1.25 to 13.26% and an average deviation of 5.86%.

Figure 5.8 shows a representative comparison of all R410A data for a high and a low mass flux case ($G = 800$ and 400 kg/m^2-s at $P_r = 0.9$).
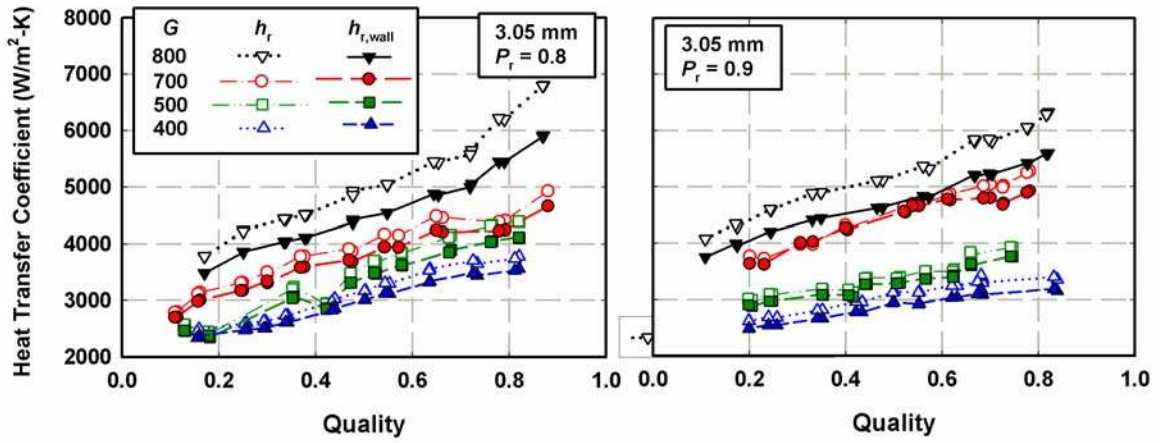
Figure 5.7: Wall-Temperature based *h* versus Quality
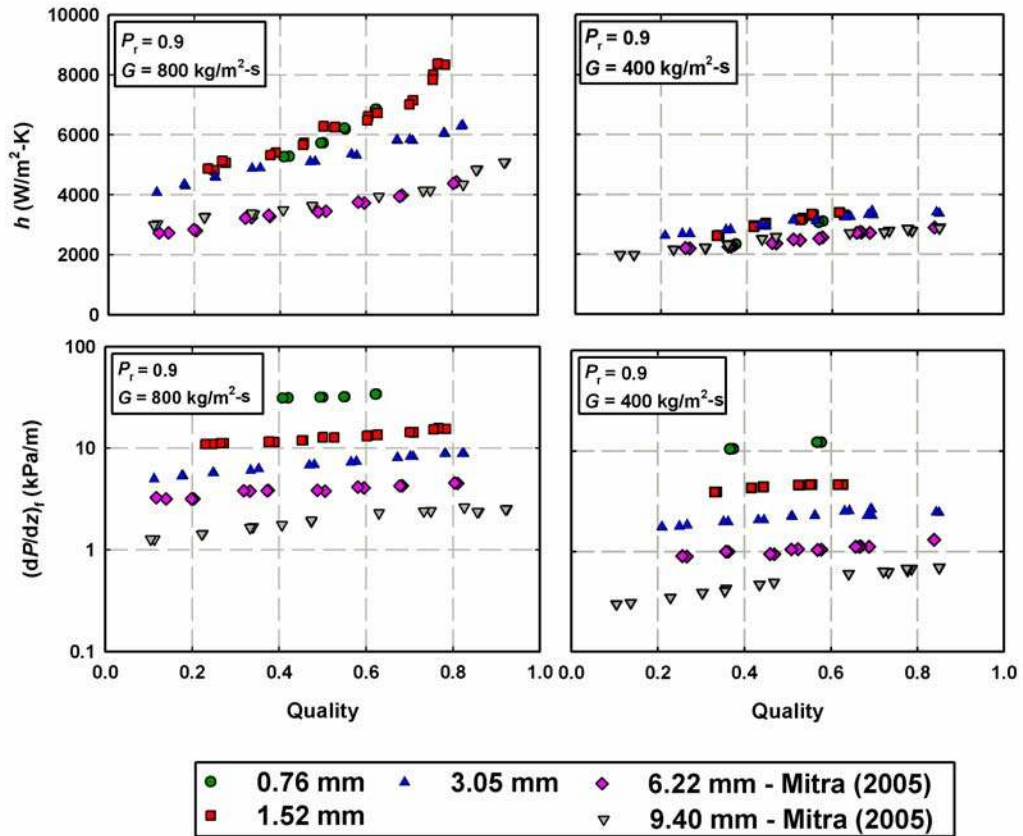
Figure 5.8: Diameter Comparison for Condensation Data

85

In Figure 5.8, the data from Mitra (2005) are also shown. It should be noted that the heat transfer coefficients are different than previously reported by Mitra because the data of Mitra (2005) and Jiang (2004) were reanalyzed here as outlined in Chapter 4. Specifically, the following modified analyses were conducted on their data: 1) using the saturation temperature of the refrigerant instead of the measured temperatures due to the better accuracy of the pressure transducers to determine the LMTD and 2) including the heat transfer in the near stagnant zones at the ends of the test section on the coolant side of the annulus. From the pressure gradient results, it is apparent that a decrease in diameter results in an increase in the frictional pressure gradient, regardless of mass flux. The heat transfer coefficient plots, however, show that the experimental results for the two smallest (0.76 and 1.52 mm) and two largest test tubes (6.22 and 9.40 mm) are almost indistinguishable. The applicable flow regimes must be considered to correctly interpret these results. The following section describes the assignment of flow regimes to the data.

5.1.3 Flow Regimes

Coleman (2000), Coleman and Garimella (2000a; 2000b; 2003)

Coleman (2000) and Coleman and Garimella (2000a; 2000b; 2003) classified the flow regimes for condensing R134a in round, square, and rectangular tubes, for hydraulic diameters ranging from 1 to 5 mm for the mass flux range $150 < G < 750$ kg/m^2-s. Since the experiments were conducted at a lower reduced pressure ($P_r \leq 0.35$), their test conditions do not strictly match those of interest in the present study, and may not be directly applicable to the present data. However, these flow regime transition criteria

were in fact developed for condensing refrigerant flow (instead of boiling or adiabatic flow; or water – air mixtures) for a diameter range similar to that of interest in this study. In addition, the mass flux range matches with that for the present study as well. Therefore, their flow regime maps should provide useful guidance in characterizing the flow regimes for the present study. Figure 5.9 shows the data from the present study plotted on their flow regime maps. The 3.05 mm data are plotted on their flow regime map for square 3×3 tubes. Coleman and Garimella (2003) showed that for the hydraulic diameters under consideration, a change from circular to square tubes did not significantly affect the flow regimes.

It can be seen in Figure 5.9 that the data from the current study fall within two primary flow regimes: wavy flow (discrete and disperse waves), and annular flow (annular film/mist flow and mist flow). The data for the 0.76 mm and 1.52 mm tubes are plotted on the flow regime maps of Coleman and Garimella for 1×1 mm and 2×2 mm square tubes, respectively. It can be seen that most of the data fall in the annular/mist flow regimes. There are only 10 points (out of 404 total condensation points in this study) for the 1.52 mm tube in the intermittent flow (plug/slug and discrete waves), and 16 points in the discrete wave flow regime on the 2×2 mm flow map. As the wavy flow regime vanishes at smaller diameters, it is assumed these points fall into a region of transition between plug/slug and annular film flow.
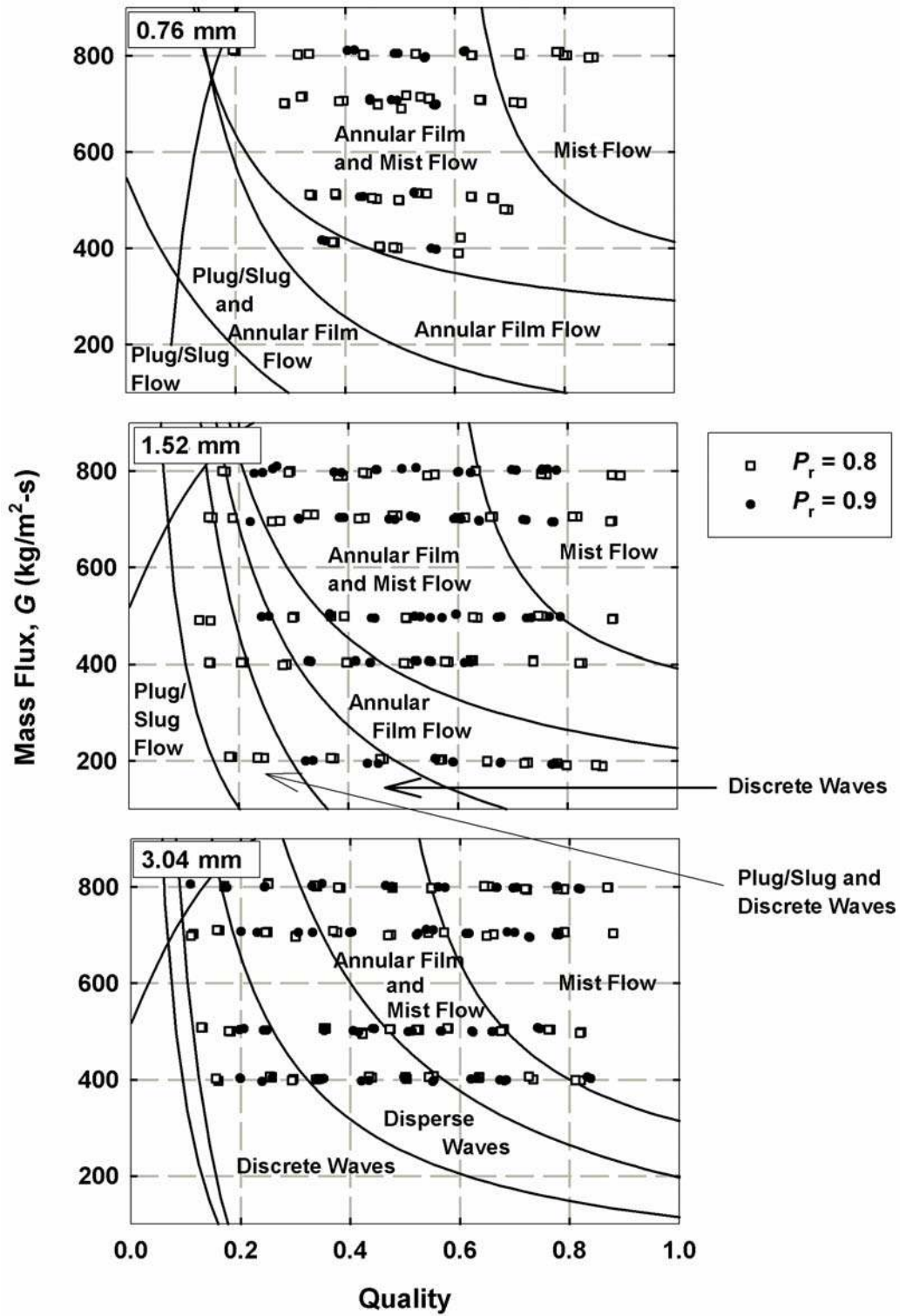
Figure 5.9: Data from Present Study plotted on Flow Regime Maps of Coleman and Garimella (2000, 2003)

Jiang (2004) and Mitra (2005)

Jiang (2004) and Mitra (2005) considered flow regime maps by several investigators (Breber *et al.*, 1980; Dobson and Chato, 1998; Coleman and Garimella, 2003; El Hajal *et al.*, 2003) to assign flow regimes to their condensation data for 6.22 and 9.40 mm tubes at conditions similar to those investigated in the present study. They found that the predictions by Coleman and Garimella (2003) and Dobson and Chato (1998) yielded the best predictions. Based on their investigations, they used a transition criterion based on the modified Soliman Froude number (Soliman, 1982) to distinguish between annular and wavy flow. None of their data points were in the intermittent flow regime. However, in the present study, particularly due to the smaller diameter tubes under consideration, assignment of the data to gravity dominated wavy flow regime using the Soliman Froude number would not be appropriate.

Cavallini et al. (2002)

Cavallini *et al.* (2002) analyzed different flow regime maps found in the literature (Breber *et al.*, 1980; Sardesai *et al.*, 1981; Tandon *et al.*, 1982; Tandon *et al.*, 1985; Dobson and Chato, 1998; Rabas and Arman, 2000) to develop a new pressure drop and heat transfer model for condensing refrigerants. Cavallini *et al.* determined that for a dimensionless vapor velocity of $J_G > 2.5$, annular flow prevails. Here J_G is defined as:

$$J_G = \frac{xG}{\left[gD\rho_v \left(\rho_l - \rho_v \right) \right]^{0.5}} \tag{5.2}$$

The flow for $J_G < 2.5$ is either "Transition and Wavy-Stratified" or "Slug Flow." To divide these two flow regimes, the Martinelli parameter as defined in Equation 5.3 is used:

$$X_{tt} = \left(\frac{\mu_l}{\mu_v}\right)^{0.1} \left(\frac{\rho_v}{\rho_l}\right)^{0.5} \left(\frac{1-x}{x}\right)^{0.9} \tag{5.3}$$

For $X_{tt} > 1.6$, the flow is considered to be slug flow and for $X_{tt} < 1.6$, the flow corresponds to the wavy flow regime. Figure 5.10 shows the data from this study plotted on the flow regime maps of Cavallini *et al.* It can be seen that this flow regime map agrees well with the predictions of Coleman and Garimella for all flow regimes: wavy flow, annular flow and intermittent flow. For the smallest two diameters (0.76 and 1.52 mm), the flow is mostly annular. Only a few data points (out of 404 total condensation points in this study) fall in the intermittent (35 points) and wavy (17 points) regimes (in the 1.52 and 3.05 mm diameter tubes). Figure 5.11 shows the data from Jiang (2004) and Mitra (2005) plotted on the flow regime maps by Cavallini *et al.*

5.2 Comparison of Heat Transfer and Pressure Drop Results with the Literature

In this section, the experimental results from this study are compared with the predictions of applicable pressure drop and heat transfer coefficient models. Even though the literature is compared with all data to be modeled (including the data obtained by Jiang (2004) and Mitra (2005)), the discussion will mostly focus on the data taken by this author, unless stated otherwise. It should be noted that there are no models in the literature for the diameter range of interest at the high reduced pressures under consideration.
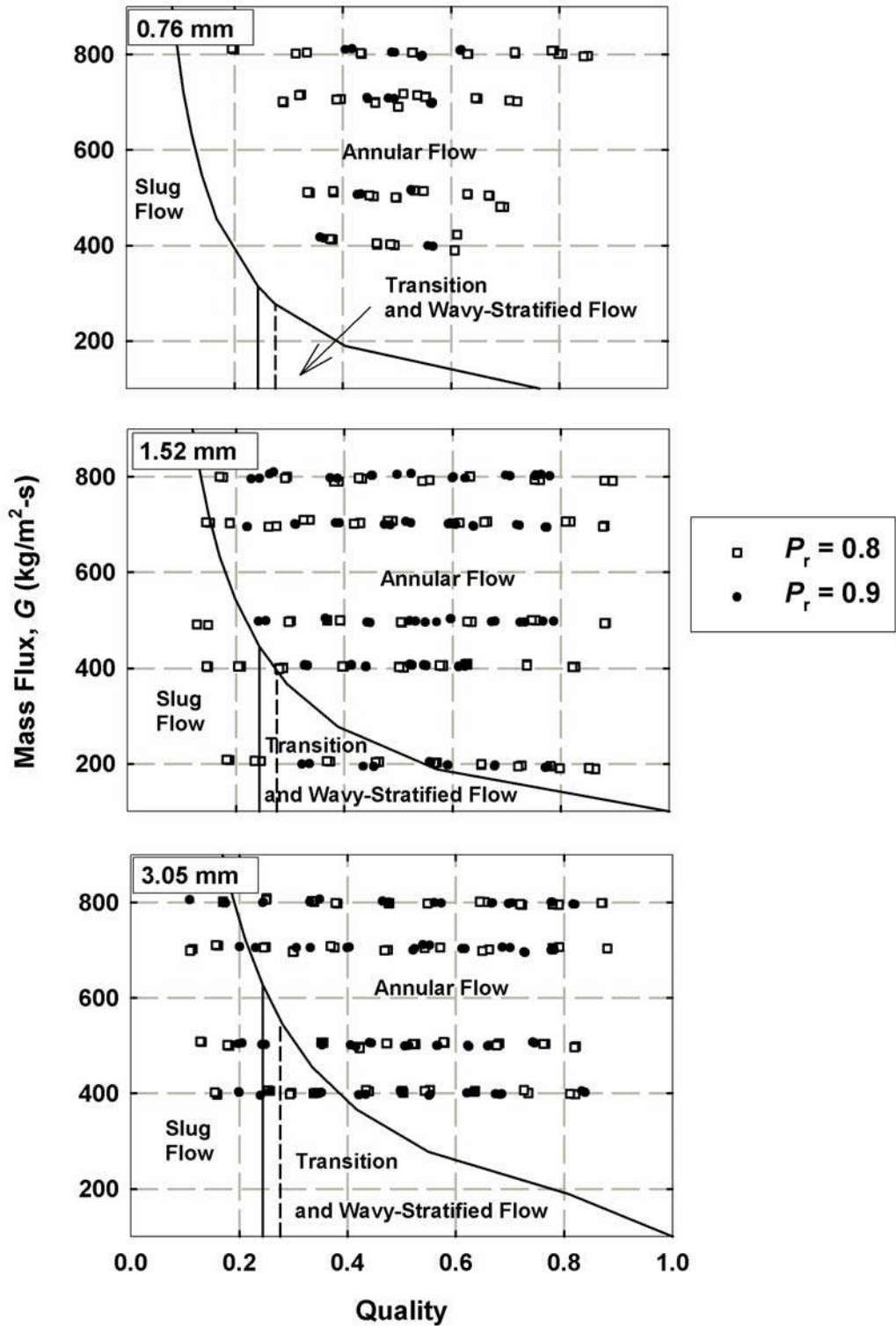
Figure 5.10: Data from Present Study plotted on Flow Regime Maps of Cavallini *et al.* (2002)
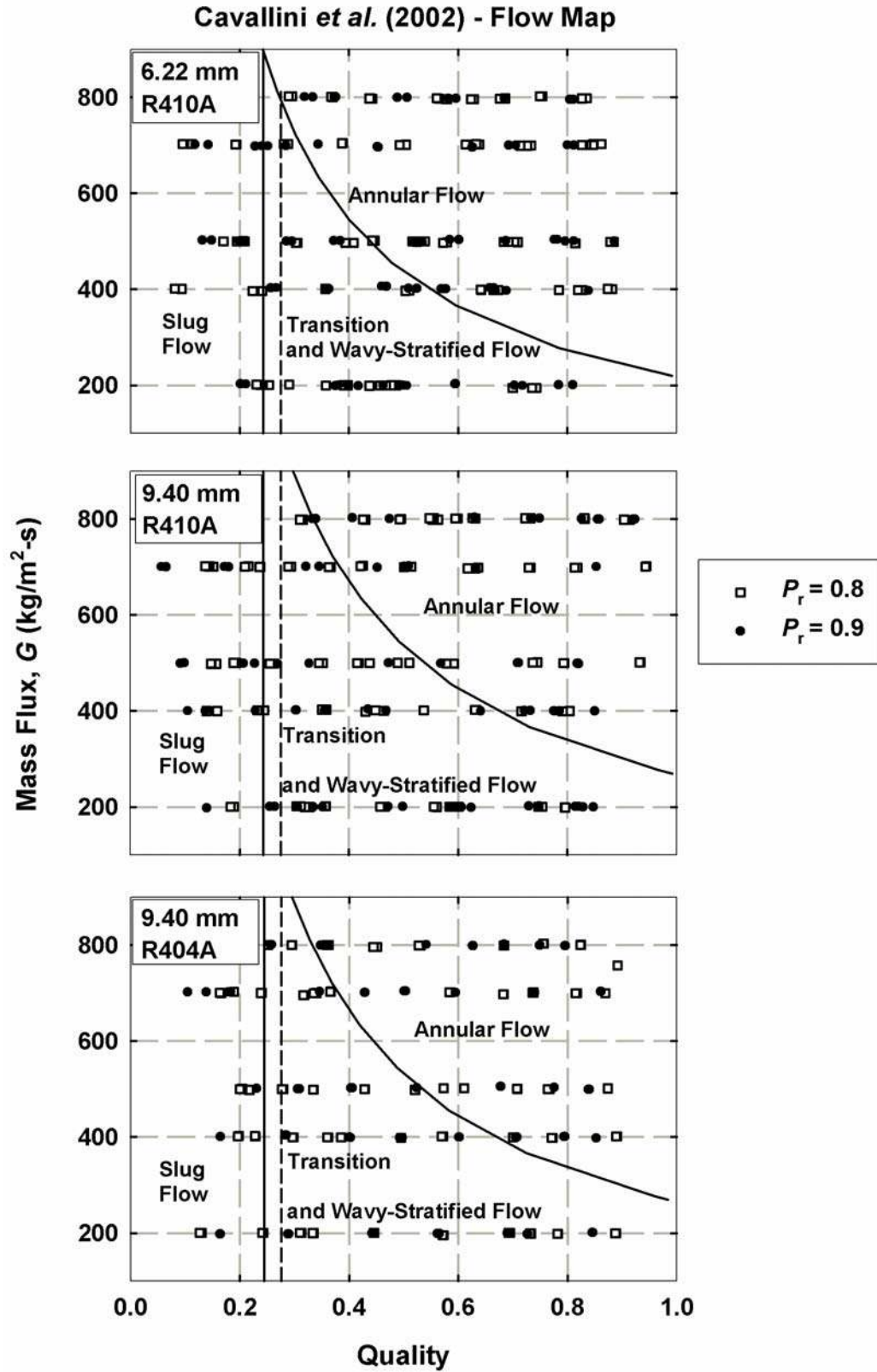
Figure 5.11: Data from Jiang (2004) and Mitra (2005) plotted on Flow Regime Maps of Cavallini *et al.* (2002)

5.2.1 Pressure Drop

Researchers have long been relating the frictional pressure drop in two-phase flow to single-phase flow with the aid of two-phase multipliers. The three well-known correlations by Lockhart and Martinelli (1949), Chisholm (1973) and Friedel (1979) are often modified to account for different geometries or flow conditions. Some of the frequently cited models and their modifications will be compared here with the data from the present study.

Lockhart and Martinelli (1949)/Chisholm (1967)

Lockhart and Martinelli used pressure drop results for adiabatic two-phase flow in horizontal tubes to correlate the pressure gradient in the liquid and vapor by means of the Martinelli parameter, where the Martinelli parameter is given by

$$X = \left(\frac{\left(dP_f / dz \right)_L}{\left(dP_f / dz \right)_G} \right)^{1/2} \tag{5.4}$$

The subscript "L" refers to flow of the liquid through the whole channel; similarly "G" refers to the vapor phase. Chisholm (1967) proposed correlations for the two-phase multipliers ϕ_L^2 and ϕ_G^2 in terms of the Martinelli parameter by means of a constant C.

$$\phi_L = \left(1 + \frac{C}{X} + \frac{1}{X^2} \right)^{1/2} \tag{5.5}$$

$$\phi_G = \left(1 + CX + X^2 \right)^{1/2} \tag{5.6}$$

The recommended value for C depends on the flow regimes of the vapor and the liquid phases. The liquid and vapor Reynolds numbers,

$$\mathrm{Re_L} = \frac{G(1-x)D}{\mu_l} \tag{5.7}$$

$$\mathrm{Re_G} = \frac{GxD}{\mu_v} \tag{5.8}$$

are used to assign flow regimes (turbulent and laminar) to the corresponding liquid and gas phases, respectively. The four possible constants for C are presented below:

$$
\begin{aligned}
\mathrm{Re_L} &\le 2000, \mathrm{Re_G} \le 2000 : C = 5 \\
\mathrm{Re_L} &> 2000, \mathrm{Re_G} \le 2000 : C = 10 \\
\mathrm{Re_L} &\le 2000, \mathrm{Re_G} > 2000 : C = 12 \\
\mathrm{Re_L} &> 2000, \mathrm{Re_G} > 2000 : C = 20
\end{aligned} \tag{5.9}
$$

The pressure gradient in the channel is then determined by:

$$\frac{dP_f}{dz} = \phi_L^2 \left(\frac{dP}{dz} \right)_L \tag{5.10}$$

where,

$$\left(\frac{dP}{dz} \right)_L = \frac{1}{2} \cdot f_L \cdot \frac{\left((1-x)G \right)^2}{\rho_l \cdot D} \tag{5.11}$$

By substituting X and ϕ_L^2 into Equation 5.10, the relative contributions of the liquid-only and gas-only pressure drops become apparent:

$$\frac{dP_f}{dz} = \left(\frac{dP}{dz} \right)_L + C \left[\left(\frac{dP}{dz} \right)_L \cdot \left(\frac{dP}{dz} \right)_G \right]^{1/2} + \left(\frac{dP}{dz} \right)_G \tag{5.12}$$

Figure 5.12 shows representative plots comparing the data with the predictions of this model, as well as the deviations for all tubes.
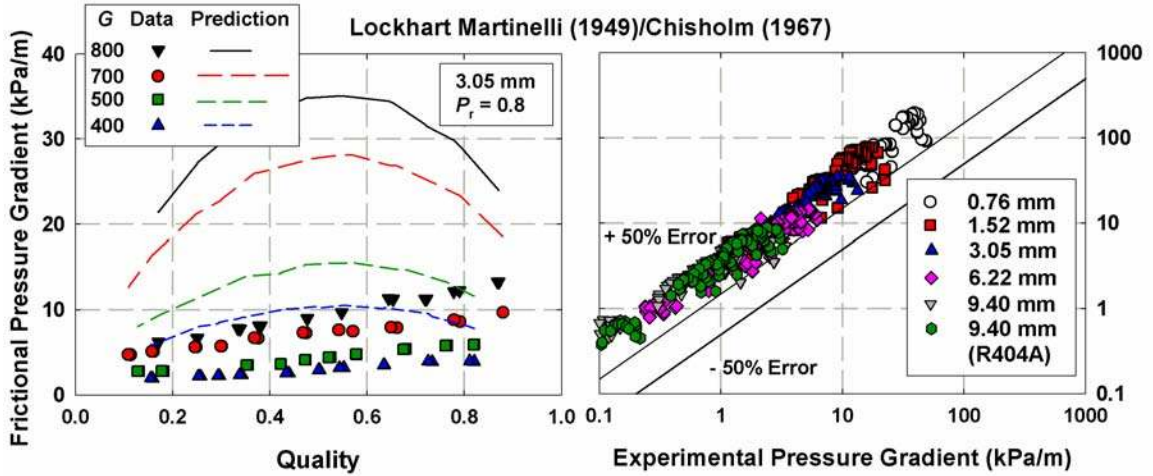
Figure 5.12: Comparison with Lockhart-Martinelli (1949)/Chisholm (1967)

Here, the friction factor f_L is determined by the Churchill (1977) correlation (Equation 4.50) and is a function of Re_L. It can be seen that this model fails to capture the trend of the data in addition to drastically overpredicting all data by 263%. Lee and Lee (2001) as well as Mishima and Hibiki (1996) developed new correlations for the parameter C in Equation 5.5 for small diameter tubes. Lee and Lee (2001) proposed that the parameter C should be a function of the liquid-only Reynolds number, and two other dimensionless parameters to capture the effects of viscosity and surface tension as presented in Equation 5.13:

$$C = a \cdot Re_{LO}^{b} \cdot \left(\frac{J \cdot \mu_L}{\sigma} \right)^{c} \cdot \left(\frac{\mu_L^2}{\sigma \cdot \rho_L \cdot D} \right)^{d} \tag{5.13}$$

where J is the liquid-slug velocity. The values of these parameters depend on the liquid and gas phase flow regimes (laminar/turbulent) as in Equation 5.9. On average, the model overpredicts the data by 738% for all data. Lee and Lee developed their correlation for Re_{LO} range from $175 - 17,700$, whereas in the current study, Re_{LO} varies from $4340 -$

127,000. The experimental Reynolds numbers in this study are higher than the reported Reynolds numbers in other studies due to the low viscosities at the high reduced pressures. Mishima and Hibiki (1996) proposed that C varies exponentially with D, as shown below :

$$C = 21\big(1 - \exp(-0.319D)\big) \tag{5.14}$$

This model overpredicts the data by 174%. The overall comparison plots for the predictions by Mishima and Hibiki and Lee and Lee are shown in Figure 5.13.
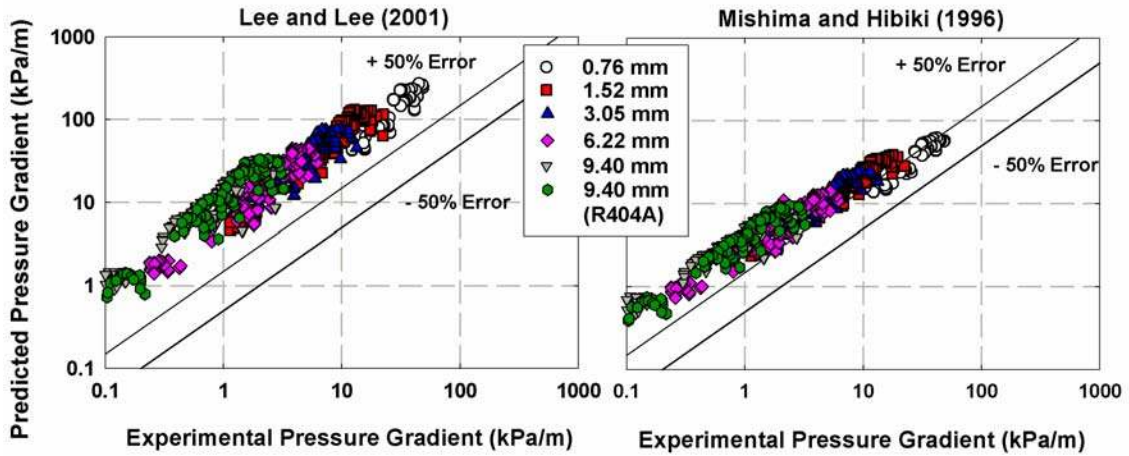
Figure 5.13: Comparison with Lee and Lee (2001) and Mishima and Habiki (1996)

Chisholm (1973), Tran et al. (2000)

Chisholm (1973) developed a correlation for a liquid-only two-phase multiplier ϕ_{LO}^2. Liquid-only refers to the flow conditions as if the entire flow channel were filled with liquid at the same mass flux as the two-phase flow. This model, however, was developed for evaporating flow, rather than condensing flow.

$$\phi_{LO}^2 = 1 + \big(\Gamma^2 - 1\big) \cdot \left[B \cdot x^{(2-n)/2} \cdot (1-x)^{(2-n)/2} + x^{2-n} \right] \tag{5.15}$$

The parameter Γ relates the gas-only and liquid-only pressure gradients, and is used to assign appropriate values for B.

$$\Gamma = \left(\frac{(dP_f / dz)_{GO}}{(dP_f / dz)_{LO}} \right)^{1/2} \tag{5.16}$$

$$\begin{array}{ll} 0 < \Gamma \le 9.5 & : \quad B = \dfrac{55}{G^{1/2}} \\[2mm] 9.5 < \Gamma < 28 & : \quad B = \dfrac{520}{\Gamma G^{1/2}} \\[2mm] 28 \le \Gamma & : \quad B = \dfrac{15000}{\Gamma^2 G^{1/2}} \end{array} \tag{5.17}$$

The exponent $n = 1$ is used for laminar flow, and $n = 0.25$ for turbulent flow (determined with $\mathrm{Re}_{LO} = GD / \mu_l$). The frictional pressure gradient is related to the liquid-only pressure gradient by means of the two-phase multiplier.

$$\frac{dP_f}{dz} = \phi_{LO}^2 \left(\frac{dP}{dz} \right)_{LO} = \phi_{LO}^2 \left(\frac{1}{2} \cdot f_{LO} \cdot \frac{G^2}{\rho_l \cdot D} \right) \tag{5.18}$$

The friction factor f_{LO} is a function of the liquid-only Reynolds number, Re_{LO}. Figure 5.14 shows a representative comparison plot, as well as the overall model predictions. This model also fails to capture the trends in the data, especially at high qualities. It, however, predicts the data well on average for the smaller tubes (0.76 and 1.52 mm). The average deviations for the 0.76 and 1.52 mm tubes are 10% and 16%, respectively. For the larger tubes ($D > 1.52$ mm), the model underpredicts the data. For the data by Jiang (2004) and Mitra (2005), the deviation is 30% on average.
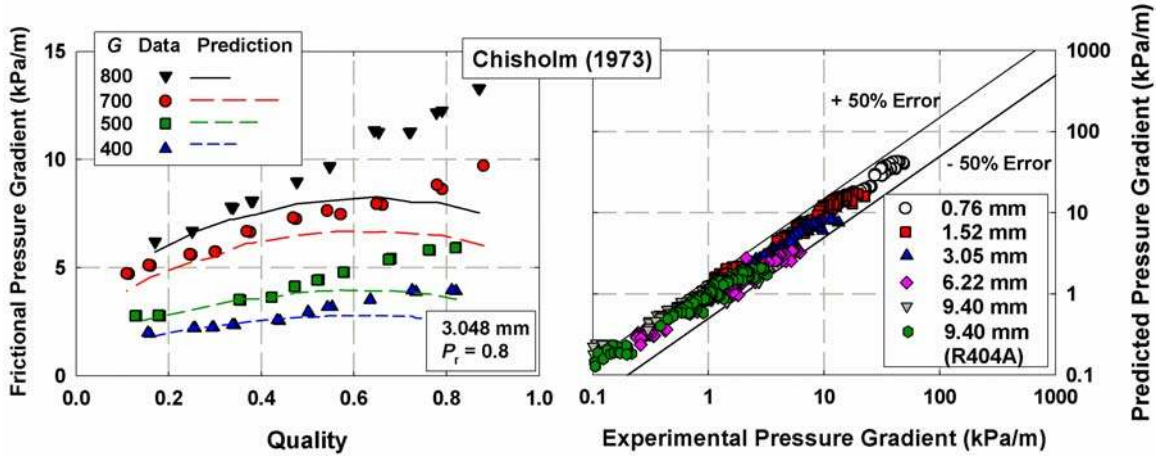
Figure 5.14: Comparison with Chisholm (1973)

Tran *et al.* (2000) modified the above model of Chisholm (1973) to include the effects of surface tension and geometry by including a confinement number, N_{conf}.

$$N_{\text{conf}} = \frac{\left[\dfrac{\sigma}{g\left(\rho_l - \rho_v\right)}\right]^{1/2}}{D} \qquad (5.19)$$

The numerator in Equation 5.19 represents the effects of surface tension and buoyancy forces, while the denominator characterizes the geometry. The modified liquid-only multiplier now is:

$$\phi_{\text{LO}}^2 = 1 + \left(4.3\Gamma^2 - 1\right)\cdot\left[N_{\text{conf}} \cdot x^{0.875} \cdot \left(1 - x\right)^{0.875} + x^{1.725}\right] \qquad (5.20)$$

Figure 5.15 shows comparisons of the data with the predictions of this model. The model captures the trends better than the original Chisholm (1973) model; however, it significantly overpredicts the data (by 87% on average), especially for the higher mass fluxes.
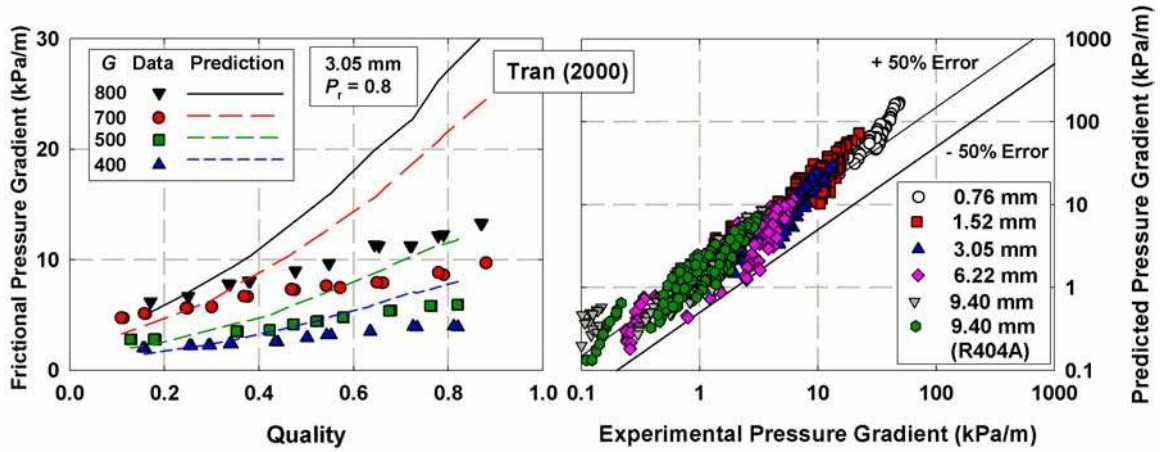
Figure 5.15: Comparison with Tran (2000)

Friedel (1979), Cavallini et al. (2002) , Mitra (2005)

Friedel (1979) used a data bank of over 25,000 points to predict a liquid-only two-phase multiplier as follows:

$$\phi_{LO}^2 = C_{F1} + \frac{3.21 C_{F2}}{Fr^{0.045} We^{0.035}} \tag{5.21}$$

where, C_{F1} and C_{F2} are:

$$C_{F1} = (1-x)^2 + x^2 \left(\frac{\rho_l}{\rho_v}\right)\left(\frac{f_{GO}}{f_{LO}}\right) \tag{5.22}$$

$$C_{F2} = x^{0.78}(1-x)^{0.224}\left(\frac{\rho_l}{\rho_v}\right)^{0.91}\left(\frac{\mu_v}{\mu_l}\right)^{0.19}\left(1-\frac{\mu_v}{\mu_l}\right)^{0.7} \tag{5.23}$$

In Equation 5.21, Fr and We are the Froude and Weber numbers respectively. Friedel's correlation is stated to cover all flow regimes. As seen in Figure 5.16, the model follows trends in the present data well; however, it mostly overpredicts the data on average by 17% for $D = 0.76$, 1.52 and 3.05 mm. The deviation for $D = 6.22$ and 9.40 mm is 27% on average.
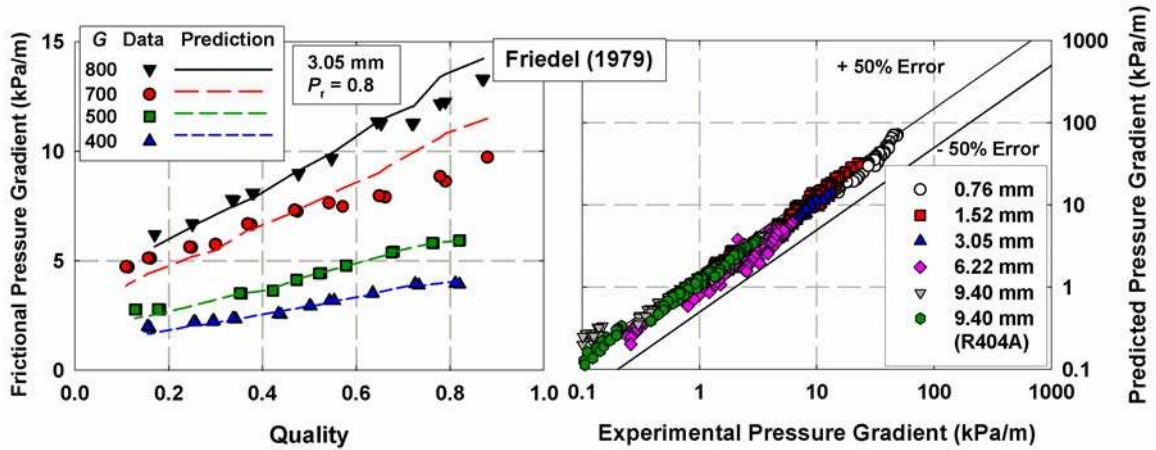
Figure 5.16: Comparison with Friedel (1979)

Cavallini *et al.* (2002) modified the Friedel correlation to make it applicable to high pressure refrigerants. They recommended that for dimensionless vapor velocity, $J_G < 2.5$ (Equation 5.2), Friedel's original correlation should be used. For flows corresponding to higher J_G values, new constants were fitted to the original model. It should be noted that the Froude number is not present as a parameter in Cavallini's annular flow model, because gravitational effects are not predominant in annular flow. This model does not yield a smooth transition between predictions for $J_G < 2.5$ and $J_G > 2.5$. This can be observed in Figure 5.17, where the model predicts a sudden increase in pressure gradient at the low qualities and low mass fluxes. The annular flow model underpredicts the data for all diameters investigated by 38% on average.
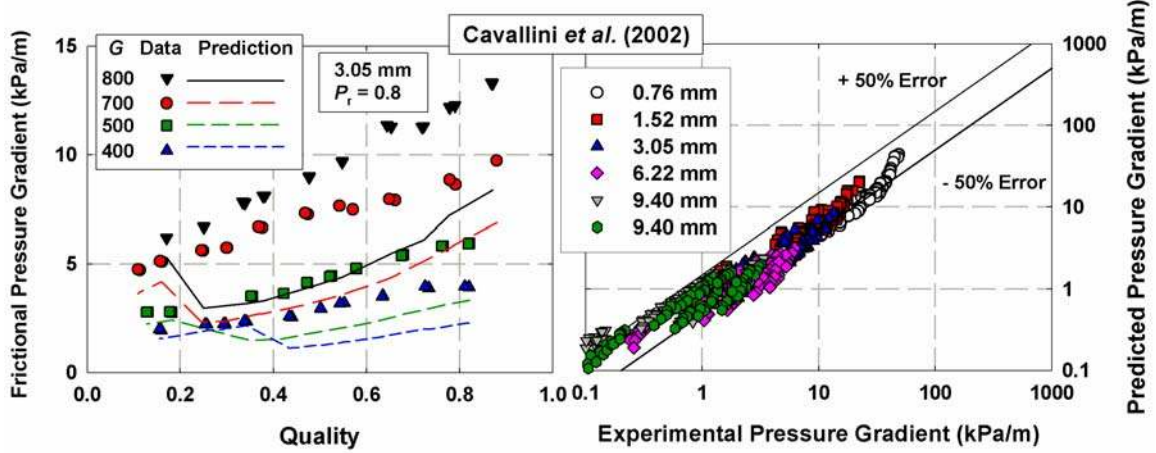
Figure 5.17: Comparison with Cavallini *et al.* (2002)

Mitra (2005) also proposed new constants and exponents to Friedel's original model. As seen in Figure 5.18, Mitra's model drastically overpredicts the pressure gradient in smaller tubes, because too much emphasis was given to the exponent corresponding to the Froude number. Thus, Mitra proposed that $\phi^2_{LO,\,Mitra} \sim Fr^{0.416}$, whereas Friedel's original model suggests $\phi^2_{LO,\,Friedel} \sim Fr^{-0.045}$. With a decrease in diameter, $\phi^2_{LO,\,Mitra}$ $\left(\sim D^{-0.416} \right)$ increases considerably, by a factor of 1.8 as the diameter changes from 6.22 mm to 1.52 mm. Therefore, further modifications are required before his model can be extended to diameters smaller than the 6.22 mm investigated by Mitra. The average deviation between the current data (D = 0.76, 1.52 and 3.05 mm) and the predictions of Mitra's model is 197%.
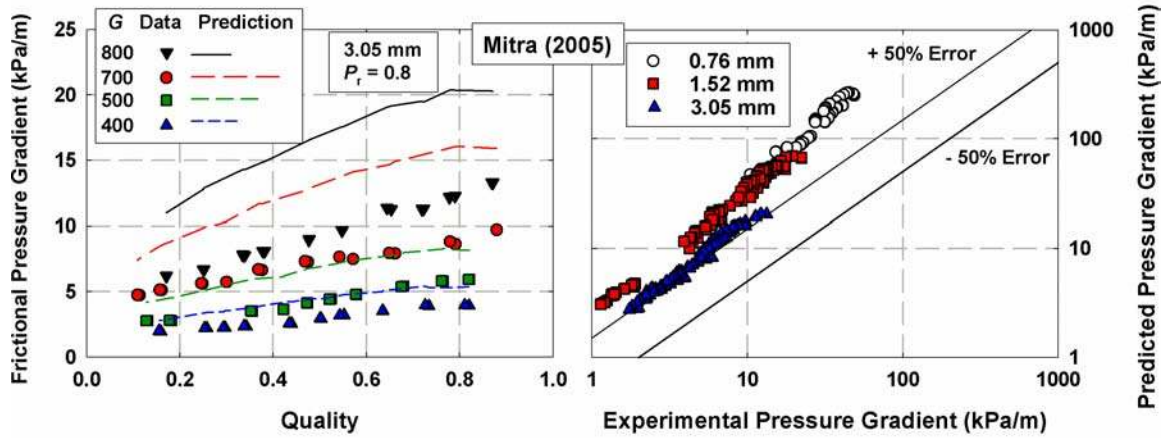
Figure 5.18: Comparison with Mitra (2005)

Garimella et al. (2005)

Garimella *et al.* (2005) proposed an annular/mist/disperse flow model for pressure drop during condensation in terms of the interfacial friction factor, f_{int}.

$$\frac{dP_f}{dz} = \frac{1}{2} \cdot f_{int} \cdot \frac{G^2 \cdot x^2}{\rho_v \cdot \alpha^{2.5} \cdot D} \qquad (5.24)$$

The interfacial friction factor characterized the friction between the vapor core and the surrounding liquid film, and is a function of the Martinelli parameter, X, the Reynolds number, Re_α, and the dimensionless surface tension parameter, ψ.

$$\frac{f_{int}}{f_L} = A \cdot X^a \cdot Re_\alpha^b \cdot \psi^c \qquad (5.25)$$

The empirical constants (*A, a, b, c*) in Equation 5.25 depend on the whether the flow is laminar or turbulent, which is determined by the Reynolds number defined as follows:

$$Re_\alpha = \frac{GD(1-x)}{(1+\sqrt{\alpha})\mu_l} \qquad (5.26)$$

The surface tension parameter, ψ, originally introduced by Lee and Lee (2001), captures the relative importance of viscous and surface tension effects:

$$\psi = \frac{G(1-x)\mu_1}{\rho_1(1-\alpha)\sigma}$$ (5.27)

Garimella *et al.* (2005) also proposed an interpolation technique to yield a smooth transition from their earlier intermittent flow model (Garimella *et al.*, 2002) to annular flow. Since only a few data points in the study (26 points out of 404) fall in the intermittent flow regime, this comparison focuses on the annular flow model applied to all experimental data. The model overpredicts the data by 35% on average. The deviation increases with a decrease in diameter, even though the diameter range studied by Garimella *et al.* (2005) was similar to the diameters under consideration. It should be noted that their model was developed for R134a condensing at $P_r \leq 0.35$. Furthermore, it is observed in Figure 5.19 that the transition from the turbulent to the laminar flow regime (based on Equation 5.26) results in a peak in the prediction. The authors state that only 24 points were used in developing the turbulent model (Re_α>3400), whereas 249 points were used in the laminar model (Re_α<2100). In the current study, however, only 10% of all data fall within the laminar regime, as defined by the authors, due to the larger diameter tubes used in this study. The rest of the data are turbulent or transitional.

Summary of Pressure Drop Correlations

Table 5.3 summarizes the average deviations for data collected by this author and by Jiang (2004) and Mitra (2005) from the relevant pressure drop correlations in the literature.
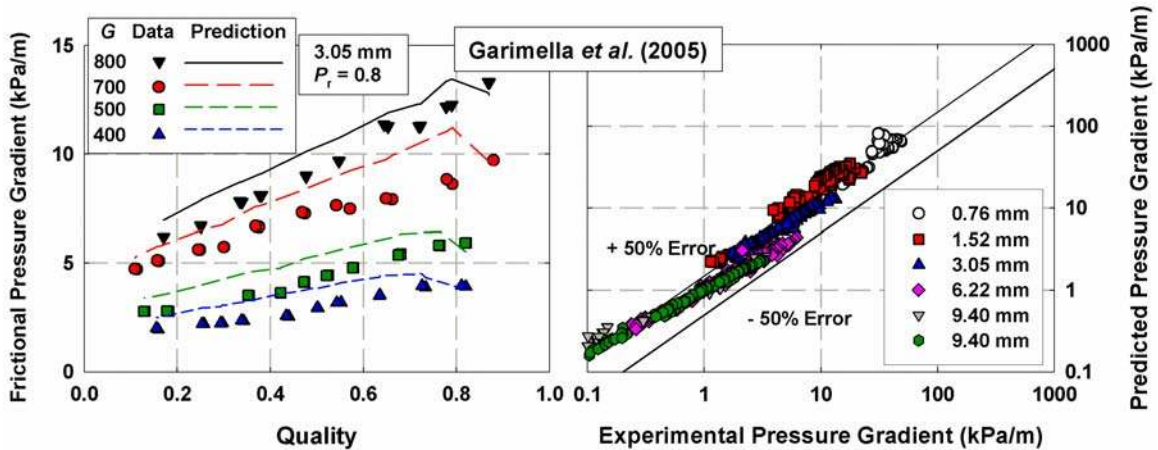
Figure 5.19: Comparison with Garimella *et al.* (2005)

Table 5.3: Deviation of available Pressure Drop Correlations

Study	Flow Regime	Avg. Deviation (%)	Comments
Lockhart and Martinelli (1949)/ Chisholm (1967)	All	263	Overpredicts Data significantly at medium range qualities
Mishima and Hibiki (1996)	All	174	Deviation increases with increase in D
Lee and Lee (2001)	All	738	Deviation increases with increase in D
Chisholm (1973)	All	20	Deviation increases with increase in D
Tran *et al.* (2000)	All	87	Deviation increases with increase in x
Friedel (1979)	All	19	Deviation increases with increase in D
Cavallini *et al.* (2002)	Annular, Wavy	38	Underpredicts annular flow regime
Mitra (2005)	Annular, Wavy	197	Compared to 0.76, 1.52 and 3.05 mm
Garimella *et al.* (2005)	Annular, Intermittent	35	Deviation increases as D decreases

5.2.2 Heat Transfer Coefficient

Some of the frequently cited heat transfer correlations for condensing flows inside round tubes for purely annular flow were developed by Kosky and Staub (1971), Traviss *et al.* (1973) and Shah (1979). These correlations are usually the basis for the heat transfer models spanning different flow regimes to include annular, wavy and intermittent flow (Cavallini *et al.*, 2002; Bandhauer *et al.*, 2005; Mitra, 2005). The subsequent discussion compares the data with predictions of 1) annular flow 2) wavy flow 3) multiflow regime and 4) mini/microchannel correlations from the literature.

Annular Flow Correlations

Kosky and Staub (1971)

Kosky and Staub (1971) used the Martinelli analogy to determine the thermal resistance of the condensate film in annular flow. The resulting heat transfer correlation is

$$h = \frac{\rho_l c_p V}{T^+} \tag{5.28}$$

where the dimensionless temperature, T^+, is related to the non-dimensional film thickness δ^+ by means of the Prandtl number, Pr, as seen in Equation 5.29.

$$
\begin{aligned}
T^+ &= \delta^+ \Pr && \text{for } \delta^+ \leq 5 \\
T^+ &= 5\left[\Pr + \ln\left(1 + \Pr\left(\delta^+/5 - 1\right)\right)\right] && \text{for } 5 < \delta^+ \leq 30 \\
T^+ &= 5\left[\Pr + \ln\left(1 + 5\Pr\right) + 0.495\ln\left(\delta^+/30\right)\right] && \text{for } 30 < \delta^+
\end{aligned}
\tag{5.29}
$$

The film thickness and corresponding Reynolds number are defined below:

$$
\begin{aligned}
\delta^+ &= \sqrt{\mathrm{Re}_L/2} && \text{for } \mathrm{Re}_L <\sim 1000 \\
\delta^+ &= 0.0504\,\mathrm{Re}_L^{7/8} && \text{for } \mathrm{Re}_L >\sim 1000
\end{aligned}
\tag{5.30}
$$

$$\mathrm{Re_L} = \frac{(1-x)GD}{\mu_l} \tag{5.31}$$

The shear velocity, *V*, is expressed as:

$$V = \sqrt{\frac{D}{4\rho_l}\left(\frac{\mathrm{d}P}{\mathrm{d}z}\right)_f} \tag{5.32}$$

where the frictional pressure gradient in Equation 5.32 is determined by a modified version of the Lockhart and Martinelli pressure drop model (1949). The heat transfer model, as seen in Figure 5.20, consistently overpredicts the data, on average by 263%, for all mass fluxes and qualities. Additionally, with an increase in reduced pressure, the model predicts an increase in *h*, whereas in the present study, the heat transfer coefficient decreases with an increase in P_r due to the associated decrease in i_{fg}.
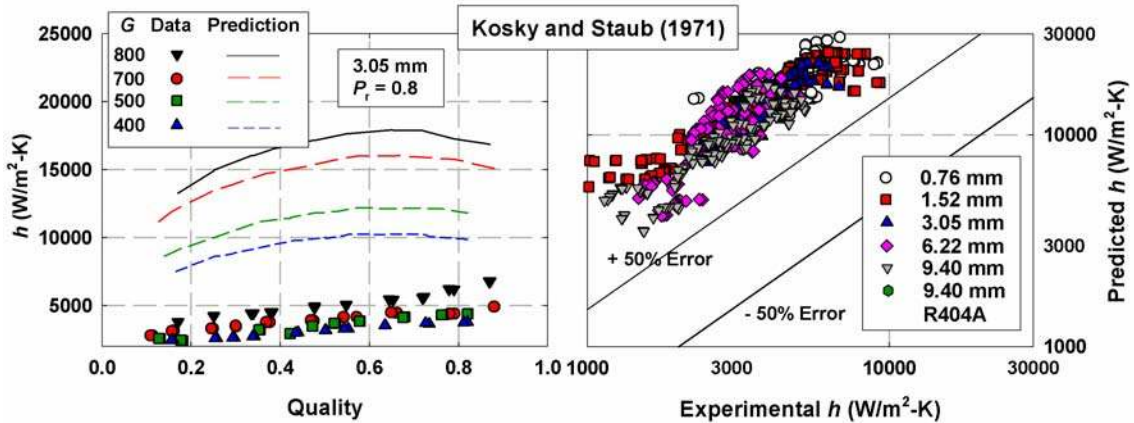
Figure 5.20: Comparison with Kosky and Staub (1971)

Traviss et al. (1973)

Traviss *et al.* (1973) assumed that the von Karman momentum-heat transfer analogy is applicable in the liquid layer in annular flow, as seen in Kosky and Staub (1971). As the

vapor core is usually very turbulent, temperature gradients in the vapor are neglected and the liquid-vapor interface was assumed to be at the saturation temperature. The shear stress was determined with the Lockhart–Martinelli correlation (1949) and the Zivi (1964) void fraction model. The resulting heat transfer correlation is as follows:

$$h = \frac{k_1}{D} \cdot 0.15 \left[\frac{1}{X_{tt}} + \frac{2.85}{X_{tt}^{0.476}} \right] \cdot \frac{\text{Pr} \cdot \text{Re}_L^{0.9}}{T^+}$$

(5.33)

The dimensionless film thickness is defined in a somewhat different manner than in Kosky and Staub (1971) as seen in Equation 5.34.

$$\begin{aligned}
\delta^+ &= 0.7071 \cdot \text{Re}_L^{0.5} && \text{for } \text{Re}_L < 50 \\
\delta^+ &= 0.4818 \cdot \text{Re}_L^{0.585} && \text{for } 50 \le \text{Re}_L \le 1125 \\
\delta^+ &= 0.095 \cdot \text{Re}_L^{0.812} && \text{for } 1125 < \text{Re}_L
\end{aligned}$$

(5.34)

To determine the dimensionless temperature, the definition of δ^+ is substituted into Equation 5.29. Again, the model consistently overpredicts the data by 138.7% on average. The decrease in h with an increase in P_r is not captured in the predictions. A sample comparison plot is shown in Figure 5.21.
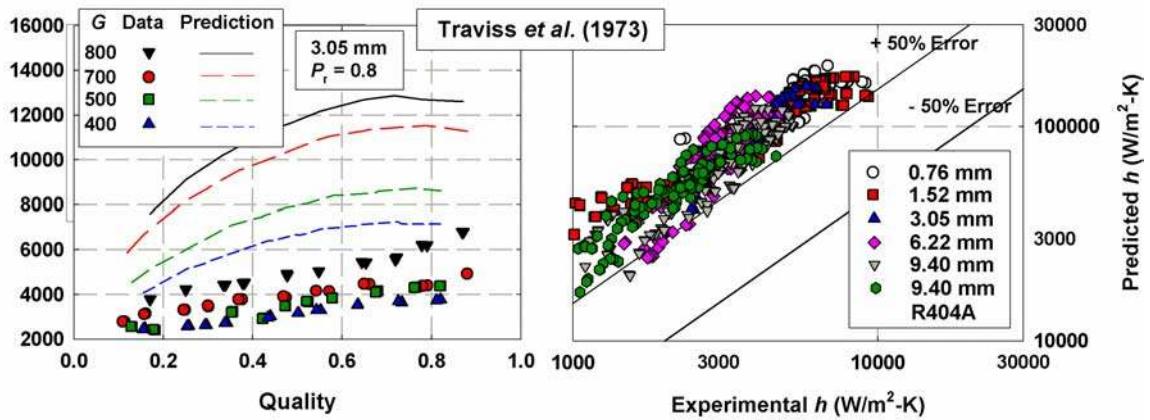
Figure 5.21: Comparison with Traviss (1973)

Shah (1979)

Shah (1979) modified the Dittus-Boelter correlation for single-phase flow (1930) with a multiplier to account for condensing flow. The Dittus-Boelter correlation is given in Equation 5.35.

$$h_{\text{D-B}} = 0.023 \, \text{Re}_{\text{LO}}^{0.8} \, \text{Pr}_{\text{L}}^{0.4} \, \frac{k_{\text{l}}}{D}$$ (5.35)

The resulting condensation heat transfer correlation is given in Equation 5.36.

$$h = h_{\text{D-B}} \left[\left(1-x\right)^{0.8} + \frac{3.8 x^{0.76} \left(1-x\right)^{0.04}}{P_{\text{r}}^{0.38}} \right]$$ (5.36)

It should be noted that Shah's model does not rely on any pressure drop correlation. This model overpredicts the data on average by 144.7% for all tubes of interest at all qualities. Even though the multiplier to the Dittus-Boelter correlation in Equation 5.36 decreases with an increase of P_{r}, the properties imbedded in Re_{L} and Pr_{L} in the single-phase correlation dominate and result in an increase in h with an increase in P_{r}, which does not agree with the experimental results from the present study. The model predictions are shown in Figure 5.22.
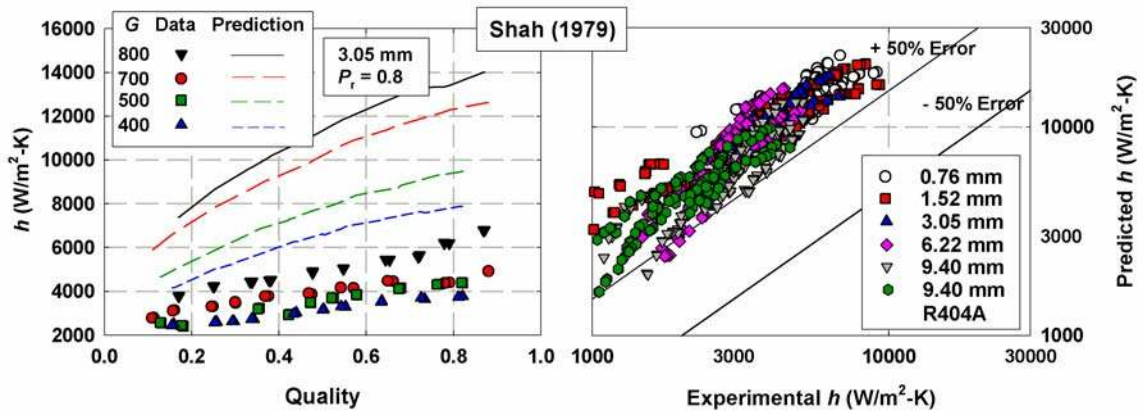
Figure 5.22: Comparison with Shah (1979)

Moser et al. (1998)

Moser *et al.* (1998) proposed an equivalent Reynolds number to correlate shear-controlled condensation heat transfer inside smooth tubes with 3.14 < *D* < 20 mm to single phase expressions based on a heat-momentum analogy. Moser *et al.* noticed that equivalent mass velocity model by Akers *et al.* (1959) underpredicts the data of several researchers due to the following reasons: 1) the driving temperature difference is not represented accurately and 2) the friction factors of the liquid and vapor phases should not be constant and equal. To correct this, Moser *et al.* related the friction factors by means of a two-phase multiplier, which led to the definition of an equivalent Reynolds number:

$$\text{Re}_{\text{eq}} = \phi_{\text{LO}}^{8/7} \, \text{Re}_{\text{LO}} \tag{5.37}$$

The temperature difference correction factor is a function of dimensionless radius, R^+, as well as Re_L, and Pr_L, where C_1 and C_2 are functions of Pr_L:

$$F = \frac{T_{\text{bulk}} - T_{\text{wall}}}{T_\delta - T_{\text{wall}}} = 1.31 \left(R^+ \right)^{C_1} \text{Re}_\text{L}^{C_2} \, \text{Pr}_\text{L}^{-0.185} \tag{5.38}$$

The above equations, along with the Petukhov (1970) correlation, result in the following Nusselt number correlation:

$$\text{Nu} = \frac{0.0994^{C_1} \cdot \text{Re}_\text{L}^{C_2} \cdot \text{Re}_{\text{eq}}^{1+0.875C_1} \cdot \text{Pr}^{0.815}}{\left(1.58 \ln \text{Re}_{\text{eq}} - 3.28 \right) \cdot \left(2.58 \ln \text{Re}_{\text{eq}} + 13.7 \, \text{Pr}^{2/3} - 19.1 \right)} \tag{5.39}$$

Overall, the data from the present study are overpredicted on average by 53% by this correlation as shown in Figure 5.23.
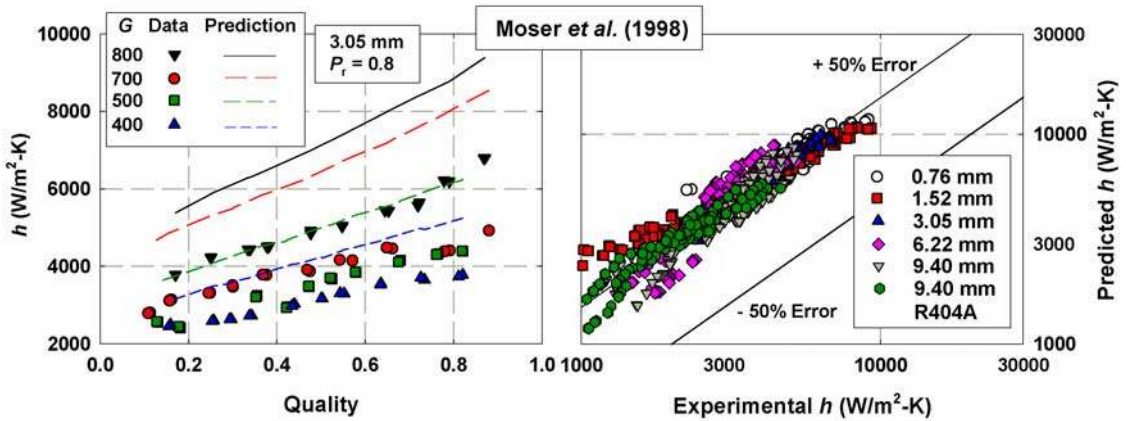
Figure 5.23: Comparison with Moser *et al.* (1998)

Wavy Flow Correlations

Chato (1962)

In wavy flow, a condensate layer forms on the inner perimeter of the tube. Due to low vapor velocities, the condensate film is dominated by gravitational forces, leading to the formation of a liquid pool at the bottom of the tube. Chato (1962) assumed the heat transfer contribution of the liquid pool in the bottom to be negligible in comparison with the film condensation on the upper part of the tube. In his analytical derivation, Chato developed a momentum-energy integral method to predict the laminar condensation heat transfer. To predict the depth of the liquid pool in the bottom, he assumed a constant vapor half-angle of 120° spanning the inner tube, thereby simplifying his correlation to:

$$h = 0.468K \left[\frac{g\rho_l (\rho_l - \rho_v) i_{fg} (1 + 0.68 \mathrm{Ja}) k_l^3}{\mu_l (D/2)(\Delta T)} \right]^{1/4} \tag{5.40}$$

where *K* is a correction factor for low Prandtl numbers. Several researchers have modified Chato's derivation or used it in conjunction with a heat transfer correlation for

the liquid pool in the bottom (Dobson and Chato, 1998; Cavallini *et al.*, 2002; Mitra, 2005) as shown in the subsequent comparisons.

Multi Flow Regime Correlations

Dobson and Chato (1998)

Dobson and Chato (1998) subdivided condensing flows into gravity dominated and shear dominated regimes. The gravity dominated flow, or wavy flow, consists of a laminar film condensation on the upper part of the tube (Chato, 1962) in conjunction with a forced convective term at the bottom of the tube to yield the following correlation:

$$Nu_{wavy} = \frac{0.23 \, \text{Re}_{GO}^{0.12}}{1+1.11 X_{tt}^{0.58}} \left[\frac{\text{Ga} \cdot \text{Pr}_l}{\text{Ja}} \right]^{1/4} + \left(1 - \frac{\theta}{\pi} \right) Nu_{bottom} \tag{5.41}$$

where Nu_{bottom} is the Dittus-Boelter equation, modified with a two-phase multiplier:

$$Nu_{bottom} = 0.0195 \cdot \text{Re}_L^{0.8} \cdot \text{Pr}_L^{0.4} \cdot \sqrt{1.376 + \frac{c_1}{X_{tt}^{c_2}}} \tag{5.42}$$

The values for c_1 and c_2 are functions of the modified Froude number, Fr_{SO}, where the modified Froude number also serves as a transition criterion between the flow regimes. For all $G > 500$ kg/m²-s, the flow is considered to be annular. For $G < 500$ kg/m²-s and $Fr_{SO} > 20$, the flow is annular, whereas for $Fr_{SO} < 20$, the flow is considered wavy. The half-angle θ was estimated by a void fraction model. The annular flow Nusselt number was computed using a modified version of the Dittus-Boelter equation:

$$Nu_{annular} = 0.023 \cdot \text{Re}_L^{0.8} \cdot \text{Pr}_L^{0.4} \cdot \left[1 + \frac{2.22}{X_{tt}^{0.89}} \right] \tag{5.43}$$

Overall, the model overpredicts the data from this study on average by 97%. It should be noted in Figure 5.24, however, that the predictions in the wavy flow regime are

111

reasonably good. However, the transition from wavy to annular flow is abrupt, and the predictions from the wavy and annular models do not agree with each other at the transition point. On average the model deviates by 18% for the wavy flow regime. The annular flow data are overpredicted by 121% on average.

Cavallini et al. (2002)

Cavallini *et al.* (2002) used the prediction by Kosky and Staub (1971) in conjunction with their pressure drop model (which is a modified version of the Friedel correlation) in the annular flow regime.
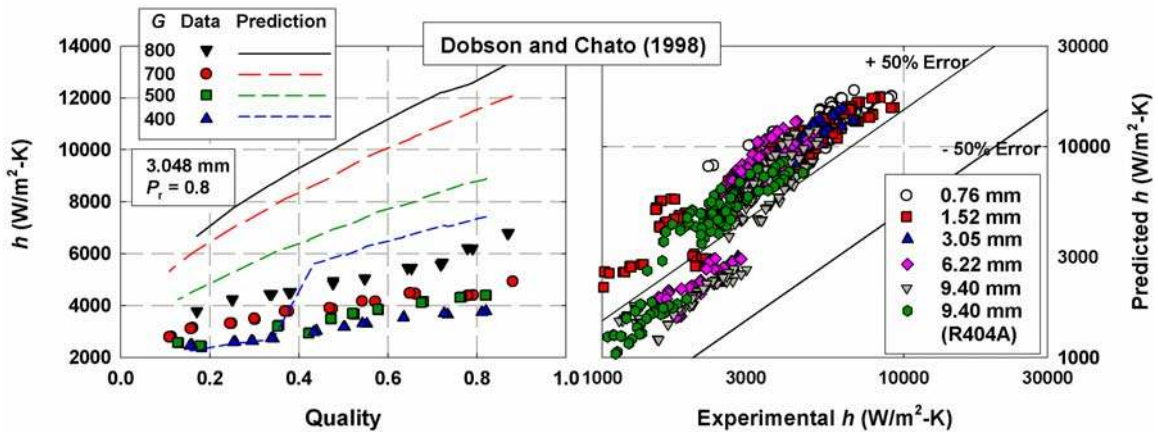
Figure 5.24: *h* Comparison with Dobson and Chato (1998)

In the wavy-stratified flow regime, the heat is transferred in the upper part of the tube through a thin film and in the lower part of the tube through the liquid pool. The heat transfer coefficient is sum of the two as seen in Equation 5.44.

$$h_{\text{stratified}} = \frac{0.725}{1+0.82\left(1-x/x\right)^{0.268}} \cdot \left(\frac{k_1^3 \rho_1 \left(\rho_1 - \rho_v\right) g i_{\text{lv}}}{\mu D \left(T_{\text{bulk}} - T_{\text{wall}}\right)}\right)^{0.25} + h_{\text{D-B}} \left(1-x\right)^{0.8} \left(1 - \frac{\theta}{\pi}\right) \quad (5.44)$$

It should be noted that the single-phase Dittus-Boelter correlation, as defined in Equation 5.35, is used in the liquid pool at the bottom. For the transition between the annular and wavy flow, linear interpolation is recommended. Overall, the comparison, especially in the annular flow regime seems to predict the data of this study well (average deviation is 17.6%), as seen in Figure 5.25. This, however, is misleading as the pressure drop model recommended by Cavallini *et al.* (2002) in the previous section of this chapter underpredicts the data.

Mitra (2005)

Mitra (2005) developed separate correlations for heat transfer in the annular and wavy flow regimes using his data for R410A on 6.22 mm and 9.40 mm tubes and Jiang's (2004) data for R404A on 9.40 mm tubes. He based his annular flow model on the approach taken by Shah (1979). Mitra's model consists of three components which resemble a single-phase correlation, a two-phase flow multiplier and a diameter ratio as seen in Equation 5.45:

$$h_{\mathrm{annular}} = 0.0134 \cdot \mathrm{Re}_{\mathrm{L}}^{0.84} \cdot \mathrm{Pr}_{\mathrm{L}}^{0.3} \left[1 + \left(\left(\frac{x}{1-x} \right) \left(\frac{\rho_{\mathrm{l}}}{\rho_{\mathrm{v}}} \right) \right)^{0.80} \right] \left(\frac{D}{D_{\mathrm{baseline}}} \right)^{-0.32} \tag{5.45}$$

The wavy flow model consists of a summation of the following two parts: film condensation on the upper part of the tube and forced convection in the liquid pool at the bottom of the tube. For the film condensation, subcooling of the liquid was assumed to be negligible. The two parts are summed based the angle θ, which represents the area fraction in the tube occupied by condensation and forced convection, respectively. It should be noted that the Nusselt number for the liquid pool, $\mathrm{Nu}_{\mathrm{Pool}}$, is based on a

hydraulic diameter, D_h, for the pool geometry, which explains the need for a diameter ratio multiplier in Equation 5.46

$$\mathrm{Nu}_{wavy} = \frac{\theta}{\pi} \mathrm{Nu}_{Film} + \left(1 - \frac{\theta}{\pi}\right)\left(\frac{D}{D_h}\right) \mathrm{Nu}_{Pool} \tag{5.46}$$

A transition region between the annular and wavy flow regimes was identified, in which interpolation between the two flow models was used to predict the heat transfer. Since these models were based only on data for only two different diameters, it appears that extrapolating this model for use in tubes tested in the present study leads to significant deviations due to the large variation in the diameter ratio term across the wider range of diameters. When predicting the heat transfer for the smaller tubes in this study, heat transfer coefficients are overpredicted, by 132% on average, as seen in Figure 5.25.
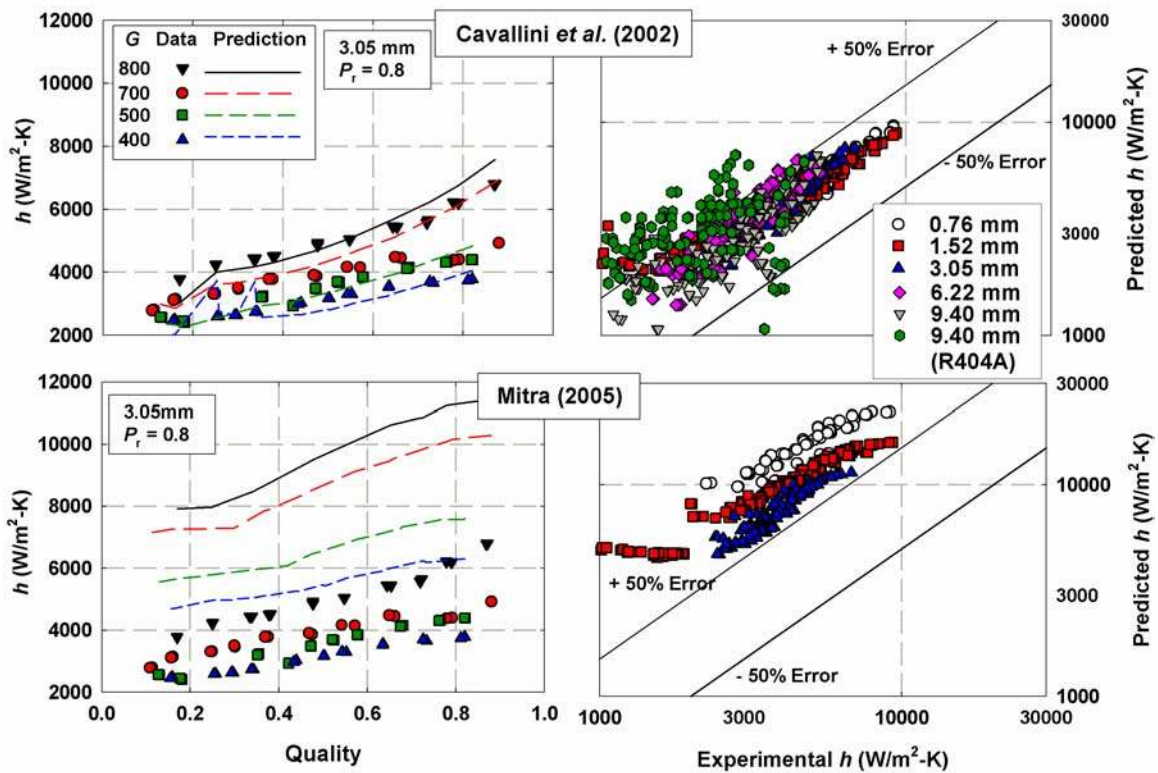
Figure 5.25: *h* Comparison with Cavallini *et al.* (2002) and Mitra (2005)

114

Minichannel Correlations

Kim *et al.* (2003) investigated heat transfer of R410A and R22 in smooth and finned multi-port tubing with hydraulic diameters of D_h = 1.41 and 1.56 mm for 200 < G < 600 kg/m²-s. For smooth tubing, they recommended the use of the heat transfer model by Webb (1998) to predict their data. This model is a modified version of the Dittus-Boelter equation, where h_{D-B} is determined by Equation 5.35 with Re_L instead of Re_{LO}, such that:

$$h = h_{D-B} \left[\frac{1.31(R^+)^A Re_L^B}{Pr^{0.185}} \right] \tag{5.47}$$

The parameters: R^+, A, and B are functions of the equivalent Reynolds number and liquid Prandtl number. It should be noted in Figure 5.26 that the heat transfer model predicts very little increase in h with increasing x and therefore does not predict the trends in the data well. The average deviation for all data is 19%.
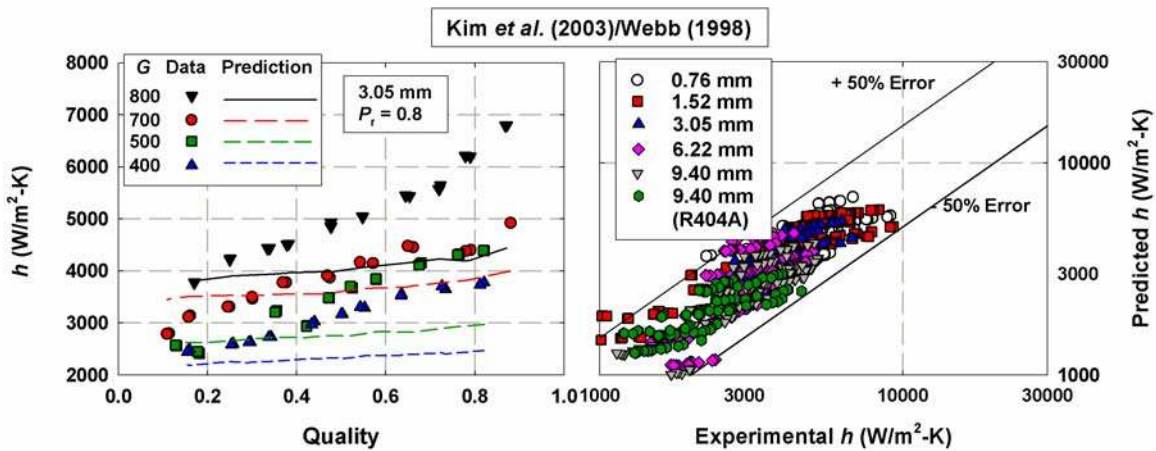
Figure 5.26: *h* Comparison with Kim (2003)/Webb (1998)

<u>**Summary of Heat Transfer Correlations**</u>

All the above comparisons with the literature are summarized in Table 5.4. It is clear that most correlations in the literature fail to capture the trends in the data, or drastically overpredict the experimental results. Only the model by Cavallini *et al.* (2002) yields reasonable predictions on average. It should be noted, however, that the embedded pressure gradient model is not representative of the current pressure drop data. Therefore, the model does not adequately account for the underlying physics of condensing flows near the critical pressure.

Table 5.4: Summary of Predictive Capabilities of Condensation Heat Transfer Models in the Literature

Study	Flow Regime	Avg. Deviation (%)	Comments
Kosky and Staub (1971)	Annular	262	Embedded ΔP model overpredicts data – leads to overprediction in h
Traviss *et al.* (1973)	Annular	139	Predicts increase in h with increase in P_r
Shah (1979)	Annular	145	Predicts increase in h with increase in P_r
Moser *et al.* (1998)	Annular	53	
Chato (1962)	Wavy	49	Neglects liquid pool in bottom of tube
Dobson and Chato (1998)	Annular, Wavy	97	Used modified Fr to divide flow regimes
Cavallini *et al.* (2002)	Annular, Wavy	18	Prediction seems reasonable, but the suggested ΔP model underpredicts data.
Mitra (2005)	Annular, Wavy	132	Only compared to $D = 0.76, 3.05, 1.52$ mm, since model is based on 6.22 and 9.40 mm data
Kim *et al.*(2003)/ Webb (1998)	All	19	h predictions does not vary much with changes in x

5.3 Model Development

The flow map by Coleman (2000) was used to divide the data in the study by Jiang (2004) and Mitra (2005) for high pressure refrigerant R404A and R410A. It should also be noted that the flow regime predictions by Coleman (2000) and Cavallini *et al.* (2002) for wavy and annular are in good agreement for all diameters of interest in this study (0.76 – 9.40 mm). However, Cavallini *et al.* do not consider a transition region to intermittent flow, as Coleman does. Only 26 points (out of 404 points) from this study fall within the intermittent region. Furthermore, no intermittent flow was observed in the data (549 points) of Jiang (2004) and Mitra (2005). This is not sufficient to develop a reliable correlation. The flow regime transition from wavy to annular flow outlined by Cavallini *et al.* (2002) is defined in terms of the dimensionless vapor velocity and their study included data on R410A for reduced pressures up to $0.63 \times P_{critical}$. However, the transition criteria of Coleman and Garimella (2000, 2003) were based only on data for the low pressures refrigerant R134a, and their transition criteria were simple algebraic expressions in terms of the mass flux, G, and quality, x. Therefore, the criteria of Cavallini *et al.* (2002) are used here to assign flow regimes to all condensation data from the present study. Furthermore, it should be noted that the data used in the model development consist of the data taken by this author, as well as the data for the same conditions (P_r and G) from Jiang (2004) and Mitra (2005) for R404A and R410A. Not enough data from any of these three studies are in the intermittent regime to support the development of a distinct model for this flow regime. The models developed here for annular and wavy flow regimes are presented here.

5.3.1 Pressure Drop Model

The correlation proposed by Lockhart and Martinelli (1949) and later modified by Chisholm (1967) will used as a starting point to develop a new pressure drop model to predict the data for all flow regimes and diameters. The frictional pressure gradient is modeled by means of a two-phase multiplier and the liquid phase pressure gradient as introduced in Equation 5.10:

$$\frac{dP_{\mathrm{f}}}{dz} = \phi_{\mathrm{L}}^2 \left(\frac{dP}{dz} \right)_{\mathrm{L}}$$

The liquid pressure gradient is evaluated with the Churchill friction factor correlation for single-phase flow. It was shown in the literature comparison section, that upon substitution of ϕ_{L}^2 and the Martinelli parameter, X, into the above equation, the friction pressure gradient can be expressed as (Equation 5.12):

$$\frac{dP_{\mathrm{f}}}{dz} = \left(\frac{dP}{dz} \right)_{\mathrm{L}} + C \left[\left(\frac{dP}{dz} \right)_{\mathrm{L}} \cdot \left(\frac{dP}{dz} \right)_{\mathrm{G}} \right]^{1/2} + \left(\frac{dP}{dz} \right)_{\mathrm{G}}$$

The parameter C in the equation accounts for the cross-term of the liquid and gas pressure drops (i.e. the interactions between the phases) and has been modified by several researchers to account for different flow regimes and geometries (Mishima and Hibiki, 1996; Lee and Lee, 2001; Kawahara *et al.*, 2002). Chisholm (1967) proposed different constants for C as a function of Reynolds number. For microchannels, an exponential dependence of C has been proposed (Mishima and Hibiki, 1996). An exponential dependence, however, was not observed in this study. The confinement number, as proposed by Tran *et al.* (2000) (Equation 5.19), is believed to be significant as it captures

the competing effects of gravitational and surface tension forces across all diameters in this study.

$$N_{conf} = \frac{\left[\dfrac{\sigma}{g(\rho_l - \rho_v)}\right]^{1/2}}{D}$$

As seen in Figure 5.27, N_{conf} ranges from 0.026 to 0.488 for all diameters, reduced pressures and refrigerants in this study.
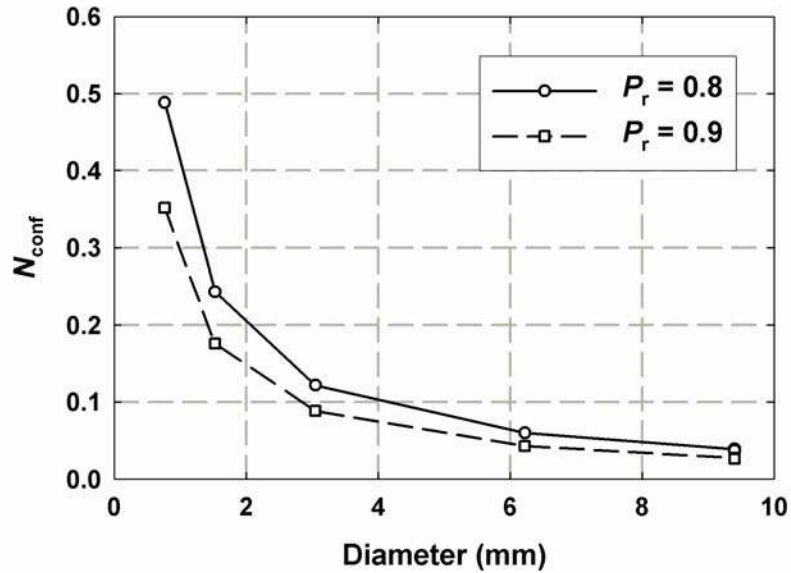
Figure 5.27: Confinement Number for different Diameters and P_r

A continuous function for C is proposed, which depends on the liquid Reynolds number to capture the effects of inertia, and the confinement number, as follows:

$$C = a \cdot \mathrm{Re}_L^b \cdot N_{conf}^c \qquad (5.48)$$

From regression analysis, the values for *a*, *b* and *c* were determined to be *a* = 24, *b* = -0.3 and *c* = -0.4:

$$C = 24 \cdot \text{Re}_{\text{L}}^{-0.3} \cdot N_{\text{conf}}^{-0.4}$$

The two-phase multipliers, ϕ_{L}^2, derived from the data from the current study, and the predictions of Equation 5.49, are shown in Figure 5.28.

$$\phi_{\text{L}}^2 = 1 + \frac{24 \cdot \text{Re}_{\text{L}}^{-0.3} \cdot N_{\text{conf}}^{-0.4}}{X} + \frac{1}{X^2} \tag{5.49}$$
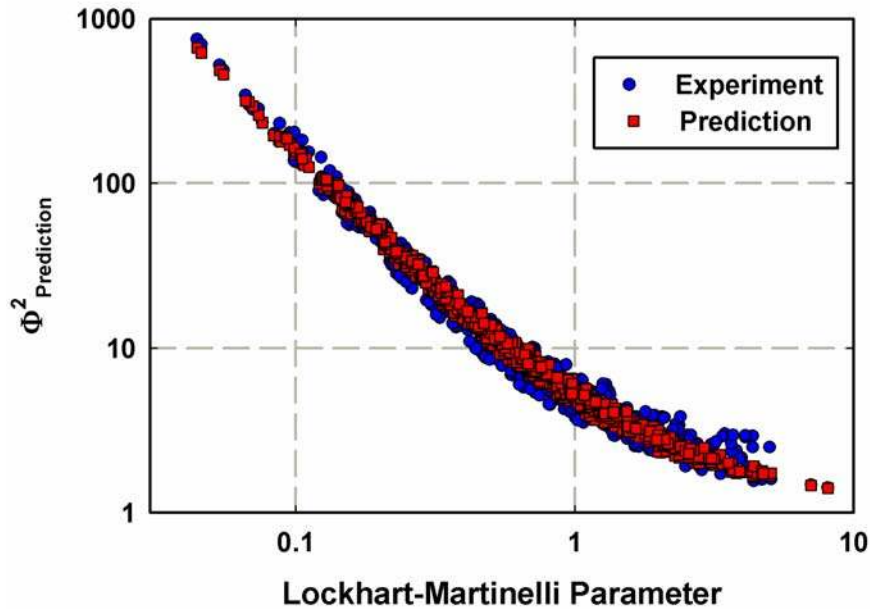
Figure 5.28: Experimental and Predicted Two-phase Multiplier versus X

The pressure drop predictions of this model are shown in Figure 5.29. Overall, 85% of the data are predicted within ± 25%. Figure 5.30 and Figure 5.31 show the individual predictions for each test section and reduced pressure. It should be noted that the model predicts the data smoothly for the entire data set and captures the trends well.
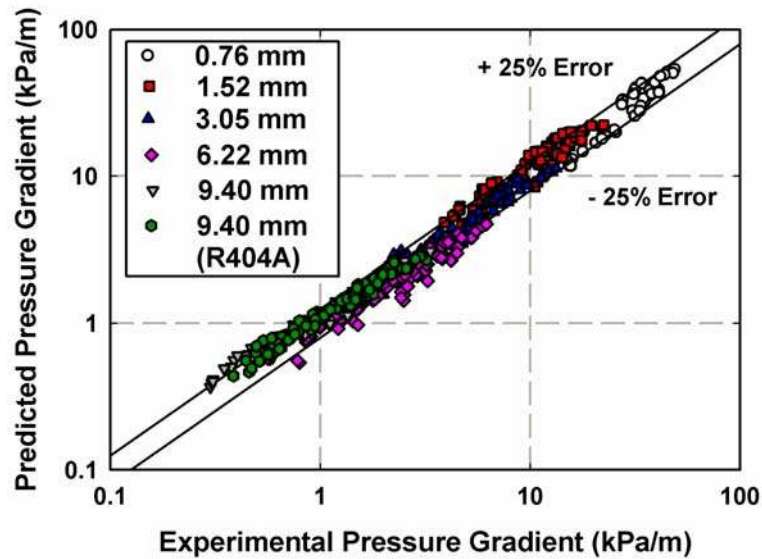
Figure 5.29: Overall Pressure Gradient Predictions

In the 0.76 mm at G = 400 kg/m^2-s and P_r = 0.9, it appears that the model predicts a decrease in pressure gradient with an increase in x. This, however, is only a local phenomenon as the only two data points for the low mass flux fall in the transition region from laminar to turbulent flow (determined by the liquid Reynolds number, which is used in the Churchill friction factor equation to determine $(dP/dz)_L$). This will be illustrated further in a subsequent discussion of the model. An overview of the average deviations is provided in Table 5.5.

The pressure drop model developed here accurately represents all observed trends in the experimental data. As seen in Figure 5.32, the pressure gradient increases with an increase in mass flux (upper left plot in Figure 5.32) and an increase in quality due to an increase in vapor velocity, which results in higher shear rates between the liquid and the vapor.

121
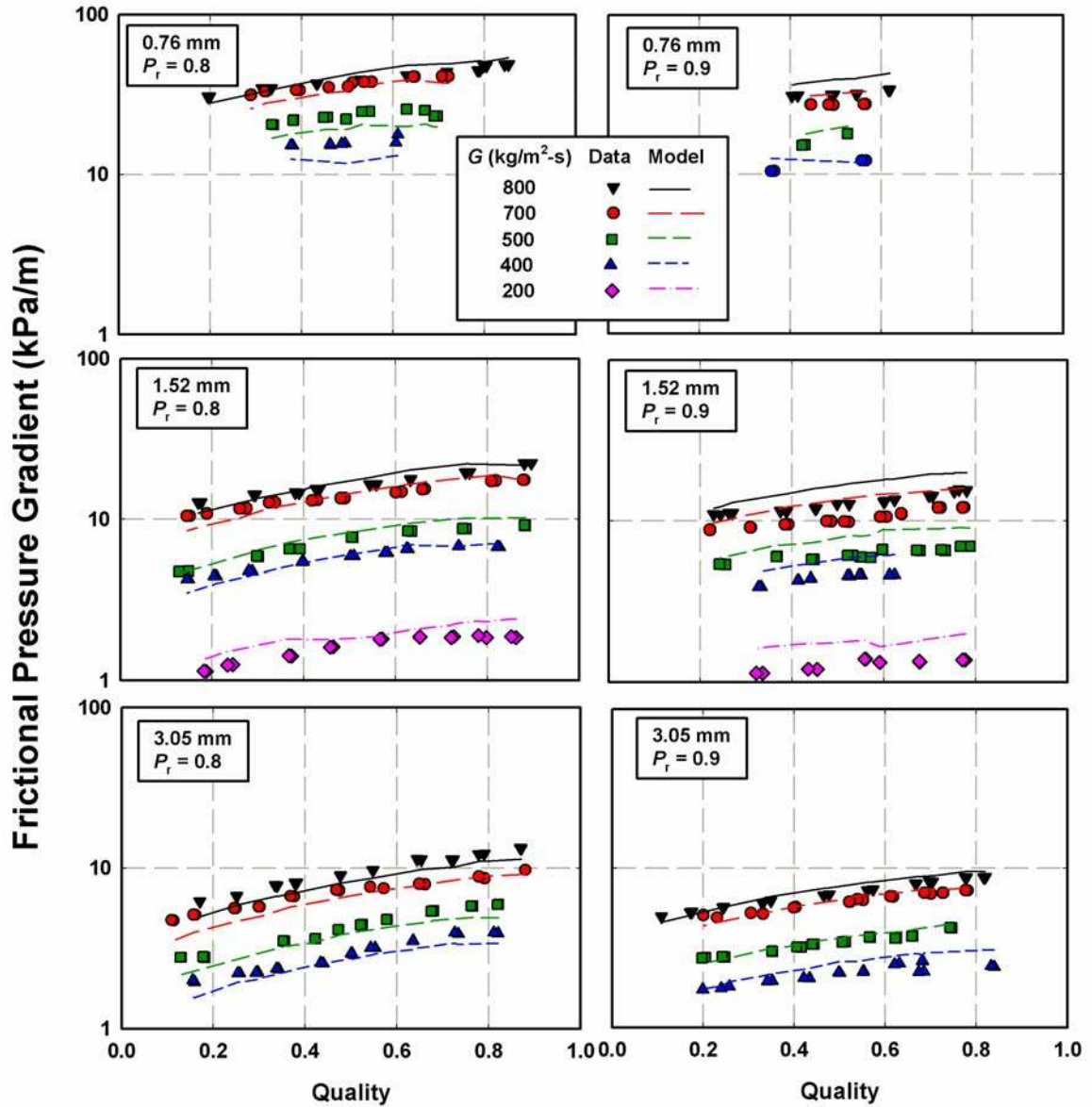
Figure 5.30: (d*P*/d*z*)$_f$ Predictions for *D* = 0.76, 1.52 and 3.05 mm

In addition, with an increase in reduced pressure, the model predicts lower pressure gradients (upper right plot), which is a result of the diminishing differences between the liquid and vapor phases.
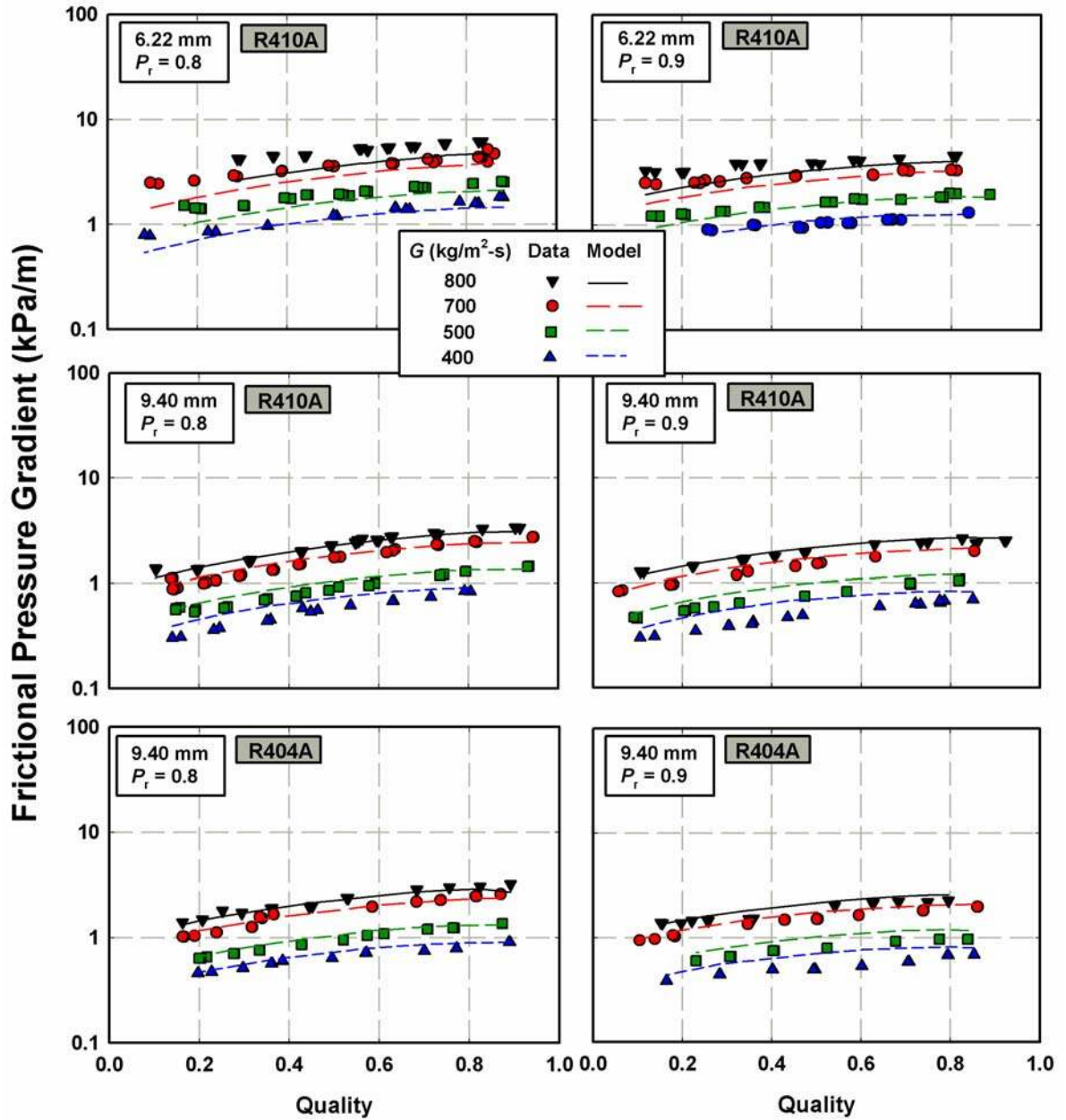
Figure 5.31: (d*P*/d*z*)$_f$ Predictions for *D* = 6.22 and 9.40 mm

As seen in the lower left plot in Figure 5.32, the pressure gradient increases with a decrease in diameter, as expected. Figure 5.33 shows the predictions for a tube with *D* = 0.76 mm.

Table 5.5: Pressure Drop Model Predictions

D (mm)	Average Deviation (%)	Data < 25% Deviation (%)
0.76	14.4	95.1
1.52	18.4	63.2
3.05	10.2	96.8
6.22	16.5	78.5
9.40 (R410A)	14.4	84.4
9.40 (R404A)	11.7	91.1
Overall	**14.1**	**84.5**
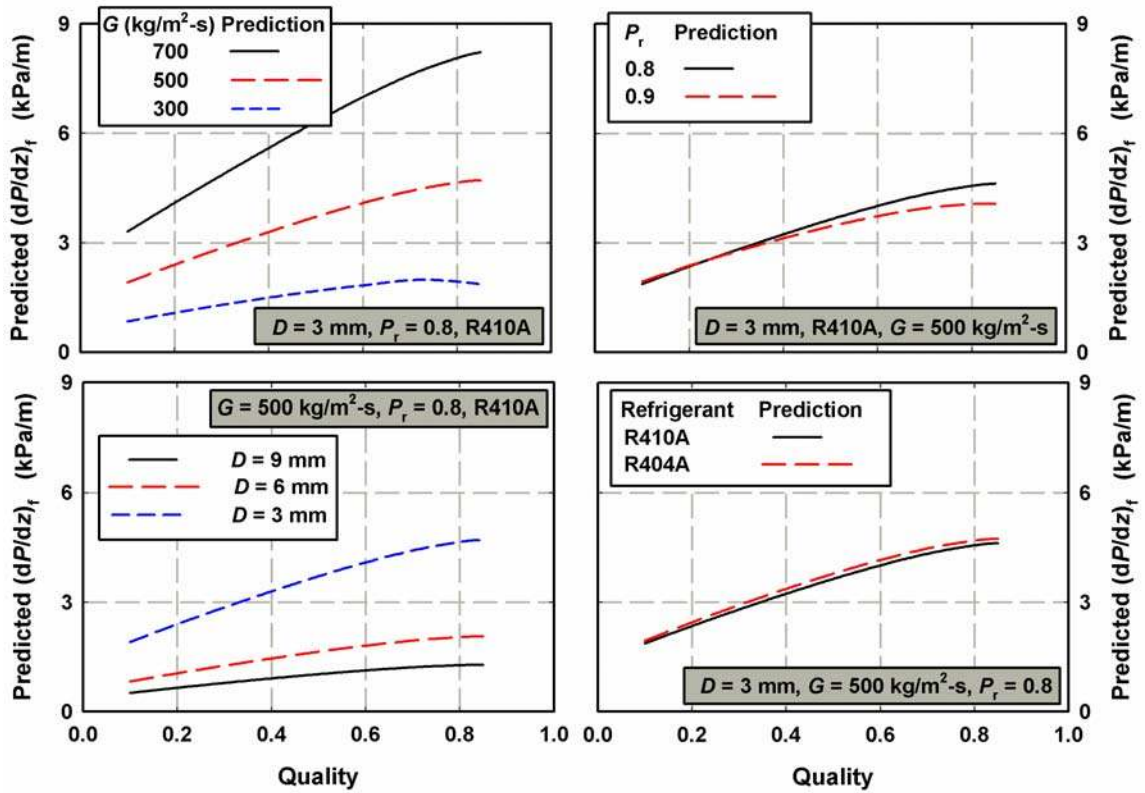
Figure 5.32: Illustration of Pressure Drop Model Trends

Furthermore, the pressure gradient for R404A is slightly higher than the pressure gradient for R410A, because the viscosities and densities are higher for R404A than for R410A, as shown in Table 5.6. The Churchill friction factor correlation can be applied to laminar, turbulent and transitional flow.

Table 5.6: Property Comparison R410A and R404A

P_r	Fluid	μ_l (μPa·s)	μ_v (μPa·s)	ρ_l (kg/m^3)	ρ_v (kg/m^3)	k_l (mW/mK)	k_v (mW/mK)
0.8	R410A	67.27	19.93	804.6	206.0	74.00	33.97
	R404A	70.83	20.14	796.4	209.4	52.08	31.22
0.9	R410A	57.13	22.40	723.7	265.5	72.63	45.20
	R404A	60.48	22.81	721.0	268.7	51.65	38.56

It should be noted that the liquid Reynolds number for $G = 400$ kg/m^2-s at $P_r = 0.8$ ranges from 464 to 4022 at $x = 0.90$ and $x = 0.11$, respectively. The transition from laminar to turbulent flow (for the liquid component) is reflected in the friction factor prediction, resulting in the small dips in the predicted pressure gradients in Figure 5.33.
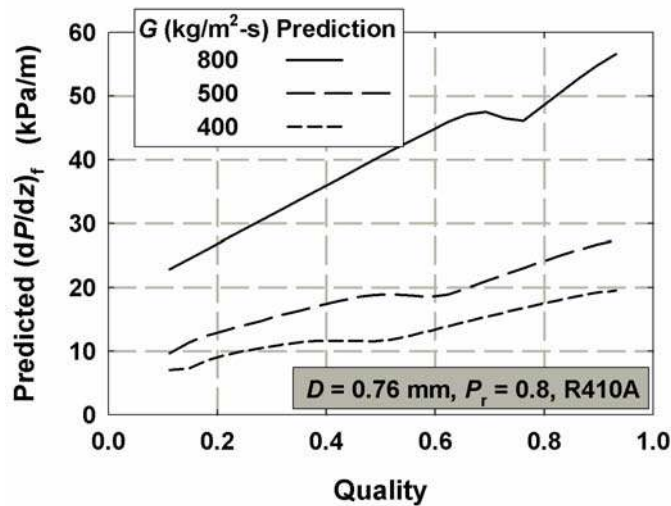
Figure 5.33: Pressure Gradient Prediction for Small Diameter Tube

5.3.2 Heat Transfer Model

Most of the heat transfer data (927 out of 953 points) to be modeled are in annular and wavy flow. In the following discussion, the wavy flow model is presented first, followed by the annular flow model.

Wavy Flow Model

Wavy flow is characterized by vapor condensing on the perimeter of the upper portion of the inner wall and then accumulating in a liquid pool at the bottom of the tube. The condensation on the walls is modeled as gravity-driven film condensation, whereas the pool of liquid at the bottom of the tube is characterized by forced convective axial flow. The schematic in Figure 5.34 illustrates this flow.
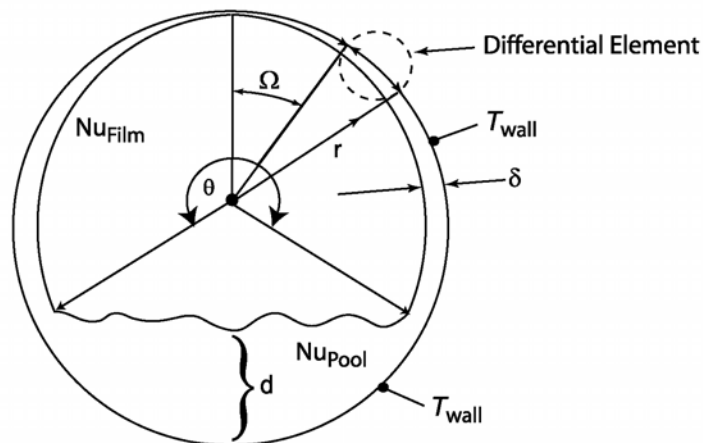
Figure 5.34: Wavy Flow Schematic

The overall Nusselt number, Nu_{wavy}, for this flow is the sum of the convective flow in the bottom, Nu_{Pool}, and the condensation on the upper part of the tube, Nu_{Film}, as seen in Equation 5.50.

$$\text{Nu}_{\text{wavy}} = \left(\frac{\theta}{2\pi}\right)\text{Nu}_{\text{Film}} + \left(1 - \frac{\theta}{2\pi}\right)\text{Nu}_{\text{Pool}} \qquad (5.50)$$

The angle θ can be estimated by Equation 5.51, because the amount of liquid in axial flow at the bottom of the tube is much greater than the liquid condensing on the inner walls in upper part of the tube. Figure 5.35 shows the corresponding areas, which can be calculated as follows:

$$Area_{\text{L}} = \underbrace{\left(\frac{2\pi - \theta}{2}\left(\frac{D}{2}\right)^2\right)}_{Area_{\text{slice}}} - \underbrace{\left(\frac{1}{2} \cdot \frac{D}{2} \cdot \frac{D}{2} \cdot \sin(2\pi - \theta)\right)}_{Area_{\text{triangle}}} \qquad (5.51)$$

$$Area_{\text{L}} = \frac{D^2}{8}\left[(2\pi - \theta) - \sin(2\pi - \theta)\right]$$
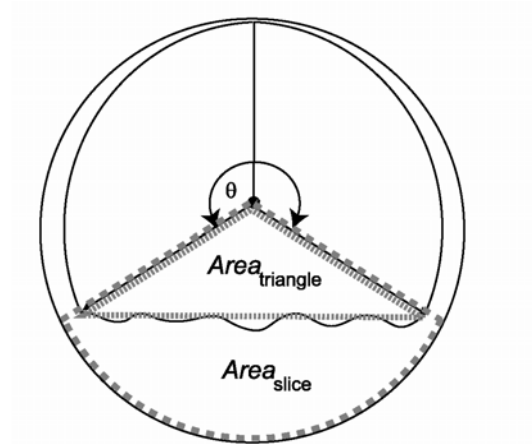
Figure 5.35: Area occupied by Liquid

The area of the liquid, $Area_{\text{L}}$, is determined from a void fraction model, which defines the area occupied by the vapor, $Area_{\text{V}}$, to the total cross-sectional area of the tube, $Area_{\text{total}} = (\pi/4)D^2$. In the present model, Baroczy's (1965) void fraction model, as shown in Equation 4.48, is used.

$$\alpha = \frac{Area_V}{Area_{total}} \tag{5.52}$$

The total area is the sum of the area of the vapor and the area occupied by the liquid:

$$Area_{total} = Area_V + Area_L \tag{5.53}$$

So, $Area_L$ can be written in terms of the void fraction as:

$$Area_L = (1-\alpha) Area_{total} \tag{5.54}$$

The angle θ in Equation 5.51 can be deduced once the cross-sectional area occupied by the liquid is estimated.

Nu_{Film} has been derived analytically by different researchers (Chato, 1962; Cavallini *et al.*, 2002; Mitra, 2005) with varying assumptions, as outlined in the literature comparison section. The derivation of Nu_{Film}, and the corresponding assumptions for gravity-driven film condensation for the data in this study are as follows: for the differential element shown in Figure 5.36, a momentum balance in the direction tangential to the inner wall ($\hat{x}$ direction in Figure 5.36), yields the velocity distribution, u, in that direction.
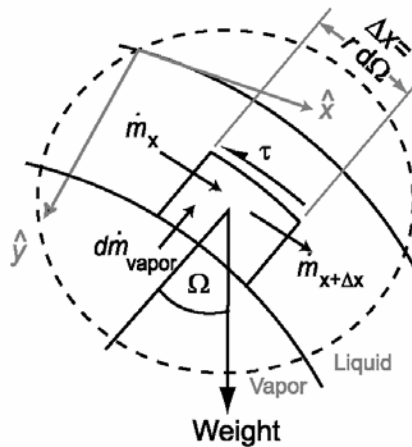
Figure 5.36: Differential Element for Film Condensation

It is assumed that the pressure gradient in the direction perpendicular to the inner wall ($\hat{y}$ direction in Figure 5.36) is negligible $\left(\left(dP/dy\right)\approx0\right)$. By applying the no-slip boundary conditions at the wall $\left(u\left(y=0\right)=0\right)$ and assuming negligible shear stress at the liquid-vapor interface $\left(\left(du/dy\right)_{y=\delta}=0\right)$, the resulting velocity profile after integration is given in Equation 5.55

$$u\left(y\right)=\frac{\left(\rho_1-\rho_v\right)g\sin\left(\Omega\right)}{\mu_1}\left(\delta y-\frac{y^2}{2}\right) \tag{5.55}$$

The velocity profile is now used to determine the mass flow rate per unit length $\dot{m}'$:

$$\dot{m}'=\int_0^\delta\rho_1udy=\frac{\rho_1\left(\rho_1-\rho_v\right)g\sin\left(\Omega\right)\delta^3}{3\mu_1} \tag{5.56}$$

It should be noted that the expression for $\dot{m}'$ so far only considers half of the tube (symmetry around the vertical axis may be applied to compute the total condensation rate). Next, an energy balance is applied to the differential element. It is assumed that the heat transfer to the wall is by pure conduction in the film. Furthermore, at the liquid-vapor interface, heat transfer occurs by condensation. Subcooling is accounted for with $i'_{fg}=i_{fg}+c_{P,1}\left(T_{r,sat}-T_{r,inner\,wall}\right)$:

$$i'_{fg}\frac{d\dot{m}'}{dx}=i'_{fg}\frac{d\dot{m}'}{\left(D/2\right)d\Omega}=k_1\frac{T_{r,sat}-T_{r,inner\,wall}}{\delta} \tag{5.57}$$

It should be noted that the continuity equation was used in the forgoing expression to replace $\left(d\dot{m}'_{vapor}/dx\right)$ with $\left(d\dot{m}'/dx\right)$. Equation 5.56 is now solved for δ and then substituted into Equation 5.57; integration yields a new equation for $\dot{m}'$:

$$\dot{m}' = \left(\frac{2}{3}\right)^{3/4} \left(\frac{1}{3}\right)^{1/4} \left[\left(\frac{Dk_l\left(T_{r,sat} - T_{r,inner\ wall}\right)}{i'_{fg}}\right)^3 \left(\frac{g\rho_l\left(\rho_l - \rho_v\right)}{\mu_l}\right)\right]^{1/4} \left(\int_0^{\theta/2} \sin^{1/3}\left(\Omega\right)d\Omega\right)^{3/4} \quad (5.58)$$

The average heat transfer coefficient for film condensation, h_{Film}, can now be determined, considering condensation on both sides of the tube as:

$$\left(2\dot{m}'\right)i_{fg} = \theta\left(\frac{D}{2}\right)\left(T_{r,sat} - T_{r,inner\ wall}\right)h_{Film} \quad (5.59)$$

Substituting Equation 5.58 into Equation 5.59 and considering the Nusselt number for film condensation $\mathrm{Nu}_{Film} = Dh_{Film}/k_l$, yields:

$$\mathrm{Nu}_{Film} = \left(\frac{4}{\theta}\right)\left(\frac{2}{3}\right)^{3/4}\left(\frac{1}{3}\right)^{1/4}\left[\frac{D^3 g\rho_l\left(\rho_l - \rho_v\right)i'_{fg}}{\left(T_{r,sat} - T_{r,inner\ wall}\right)\mu_l k_l}\right]^{1/4} \underbrace{\left(\int_0^{\theta/2} \sin^{1/3}\left(\Omega\right)d\Omega\right)^{3/4}}_{C_{Film}} \quad (5.60)$$

The expression in Equation 5.60 can be further simplified by substituting the Rayleigh and Jacob numbers. The Rayleigh number is the product of the Grashof and Prandtl numbers and is given in Equation 5.61.

$$\mathrm{Ra} = \frac{D^3 g\rho_l\left(\rho_l - \rho_v\right)c_{P,l}}{\mu_l k_l} \quad (5.61)$$

The Jacob number, Ja, is a measure of sensible heat per unit mass of condensed liquid in the film to the latent heat, or enthalpy, associated with the phase change, and is given in Equation 5.62.

$$\mathrm{Ja} = \frac{\left(T_{r,sat} - T_{r,inner\ wall}\right)c_{P,l}}{i_{fg}} \quad (5.62)$$

Furthermore, the integral in Equation 5.60 can be approximated with its average value for all data points. The expression for the integral is $C_{Film} = 0.860 \pm 0.006$ (with minimum

and maximum values of 0.841 and 0.866 respectively). Equation 5.60 is now simplified to:

$$\mathrm{Nu}_{\mathrm{Film}} = \left(\frac{1.93}{\theta}\right)\left(\mathrm{Ra}\cdot\left(\frac{1}{\mathrm{Ja}}+1\right)\right)^{1/4} \tag{5.63}$$

From Equation 5.60, it is should be noted that $\mathrm{Nu}_{\mathrm{Film}}$ is proportional to $\left(i_{\mathrm{fg}}\right)^{1/4}$. With an increase in reduced pressure, the latent heat of vaporization decreases, which should therefore lead to a decrease in the film condensation heat transfer coefficient as P_r increases.

The condensate liquid pool at the bottom of the tube is assumed to follow single-phase, turbulent behavior. For the data under consideration, the liquid Reynolds number ranges from 2,971 to 113,100 in the wavy flow regime. Due to the coexistence of vapor, a two-phase multiplier is used in conjunction with a Dittus-Boelter type Nusselt number correlation and a diameter multiplier.

$$\mathrm{Nu}_{\mathrm{Pool}} = a\,\mathrm{Re}_{\mathrm{L}}^{0.8}\cdot\mathrm{Pr}_{\mathrm{L}}^{1/3}\cdot\left[1+\left(\frac{x}{1-x}\right)\left(\frac{\rho_{\mathrm{l}}}{\rho_{\mathrm{v}}}\right)^{b}\right]\left(\frac{D}{D_{\mathrm{baseline}}}\right)^{c} \tag{5.64}$$

For the baseline diameter, D_{baseline}, the largest tube from this study was chosen ($D_{\mathrm{baseline}} = 9.40$ mm) since wavy flow is more dominant in the larger tubes than in the smaller ones. The two-phase multiplier (term in brackets) has been proposed by different authors in modeling heat transfer in two-phase flow (Cavallini and Zecchin, 1974; Jiang, 2004; Mitra, 2005). From regression analysis, the variables *a, b* and *c* were determined to be: *a* = 0.018, *b* = 1.24 and *c* = 0.34.

$$\mathrm{Nu_{Pool}} = 0.018 \cdot \mathrm{Re}_L^{0.8} \cdot \mathrm{Pr}_L^{1/3} \cdot \left[1 + \left(\frac{x}{1-x}\right)\left(\frac{\rho_l}{\rho_v}\right)^{1.24}\right]\left(\frac{D}{9.398 \text{ mm}}\right)^{0.34} \quad (5.65)$$

The Nusselt number correlations for the film condensation and the liquid pool are both substituted into Equation 5.50 to yield:

$$\mathrm{Nu_{wavy}} = \left(\frac{1.93}{2\pi}\right)\left(\mathrm{Ra} \cdot \left(\frac{1}{\mathrm{Ja}} + 1\right)\right)^{1/4}$$
$$+ 0.018\,\mathrm{Re}_L^{0.8} \cdot \mathrm{Pr}_L^{1/3} \cdot \left[1 + \left(\frac{x}{1-x}\right)\left(\frac{\rho_l}{\rho_v}\right)^{1.24}\right]\left(\frac{D}{9.398 \text{ mm}}\right)^{0.34} \cdot \left(1 - \frac{\theta}{2\pi}\right) \quad (5.66)$$

The heat transfer coefficient for wavy flow is now given as: $h_{\mathrm{wavy}} = k_l \cdot \mathrm{Nu_{wavy}} / D$.

Annular Flow Model

Kosky and Staub (1971) established that the heat transfer coefficient for purely annular flow is a function of the shear velocity, the dimensionless temperature profile, T^+ (which is also referred to as the thermal resistance), and the liquid density and specific heat. By rewriting Equation 5.28 in terms of the Nusselt number, the Reynolds and Prandtl number dependence is apparent:

$$\mathrm{Nu} \sim \frac{\mathrm{Re}_{\mathrm{shear}}\,\mathrm{Pr}}{T^+\left(\mathrm{Re}_L, \mathrm{Pr}\right)} \quad (5.67)$$

Dobson and Chato (1998) demonstrated the equivalence of the heat transfer model by Traviss *et al.* (1973), which is similar to Kosky and Staub (1971), to a two-phase multiplier approach for $\mathrm{Re}_L > 1125$ (Equation 5.31). By assuming a symmetric annular film and no entrainment, Dobson and Chato realized that T^+ does not change appreciably for $\mathrm{Re}_L > 1125$. Furthermore, they observed that the liquid film is rarely so thin that the

fully turbulent region is not reached ($\text{Re}_\text{L} > 1125$). The authors proposed a heat transfer model that used the Dittus-Boelter equation (Equation 5.35) in conjunction with a two-phase multiplier. This is very similar to the model proposed by Shah (1979).

The annular flow regime in this study was divided based on the dimensionless shear velocity, which is different from the flow regime transition criterion used by Dobson and Chato (1998), who used the modified Froude number. However, all data points have $\text{Re}_\text{L} > 1125$ implying that the non-dimensional thermal resistance is approximately constant and a fully-turbulent model is justified. The liquid phase Reynolds number, Re_L, in this study ranges from 1313 to 32,320 for tubes with diameters of: 0.76, 1.52 and 3.05 mm, and 2971 to 113,100 for the larger tubes 6.23 and 9.40 mm. The liquid Reynolds numbers are larger due to larger diameters since the Reynolds number is directly proportional to D at any given pressure, quality and mass flux ($\text{Re}_\text{L} = (1-x) GD / \mu_\text{l}$).

In the smaller tubes ($D = 0.76$, 1.52 mm), annular flow is sustained for a wide quality and mass flux range (227 annular flow points out of 248 points for $D = 0.76$ and 1.52 mm). Also, in the smaller diameter tubes, surface tension effects are more predominant. Thus, the wavy flow regime ceases to exist and the annular flow regime directly transitions to the intermittent flow regime. In the larger tubes, however, annular flow transitions to wavy flow, because gravitational effects are considerable. A model that accounts for all these physical phenomena and the respective transitions to different regimes for this wide range of diameters could not be developed based on the data obtained in this study and

those of Jiang (2004) and Mitra (2005). Therefore, an empirical model based on the liquid-phase Reynolds and Prandtl number and a two-phase multiplier is proposed to capture those different trends and flow conditions in the following form:

$$Nu_{annular} = a \cdot Re_L^{4/5} \cdot Pr_L^{1/3} \cdot \left[1 + \left(\frac{x}{1-x} \right)^b \left(\frac{\rho_l}{\rho_v} \right)^c \right] \qquad (5.68)$$

Regression analysis resulted in the following correlation, where the two-phase multiplier closely resembles the Martinelli parameter without a viscosity ratio.

$$Nu_{annular} = 0.0133 \cdot Re_L^{4/5} \cdot Pr_L^{1/3} \cdot \left[1 + \left(\frac{x}{1-x} \right)^{0.80} \left(\frac{\rho_l}{\rho_v} \right)^{0.88} \right] \qquad (5.69)$$

Transition Region

A transition region between the annular and wavy flow regime was also defined to ensure a smooth transition between the annular and wavy flow *h* predictions. Thus, based on the definition of annular flow $(J_G > 2.5)$ by Cavallini *et al.* (2002), data between $J_{G,max,wavy} < J_G < J_{G,min,annular}$ were deemed to be in transitional flow, where $J_{G,max,wavy} \simeq 2.0$ and $J_{G,min,annular} \simeq 3.0$. The heat transfer coefficients in this region are determined using an interpolation scheme proposed by Mitra (2005):

$$Nu_{transitional} = \left(\frac{J_G - J_{G,wavy}}{J_{G,annular} - J_{G,wavy}} \right) Nu_{annular} + \left(\frac{J_{G,annular} - J_G}{J_{G,annular} - J_{G,wavy}} \right) Nu_{wavy} \qquad (5.70)$$

Overall, 13% of the data (128 out of 952 points) fall within the transition region.

Model Predictions

Overall, 91% of the data are predicted within ± 25%, where the predicted versus observed

Nusselt numbers are shown in Figure 5.37. Table 5.7 summarizes the average model

deviations for the different diameters, while Table 5.8 provides the deviations for the

different flow regimes.
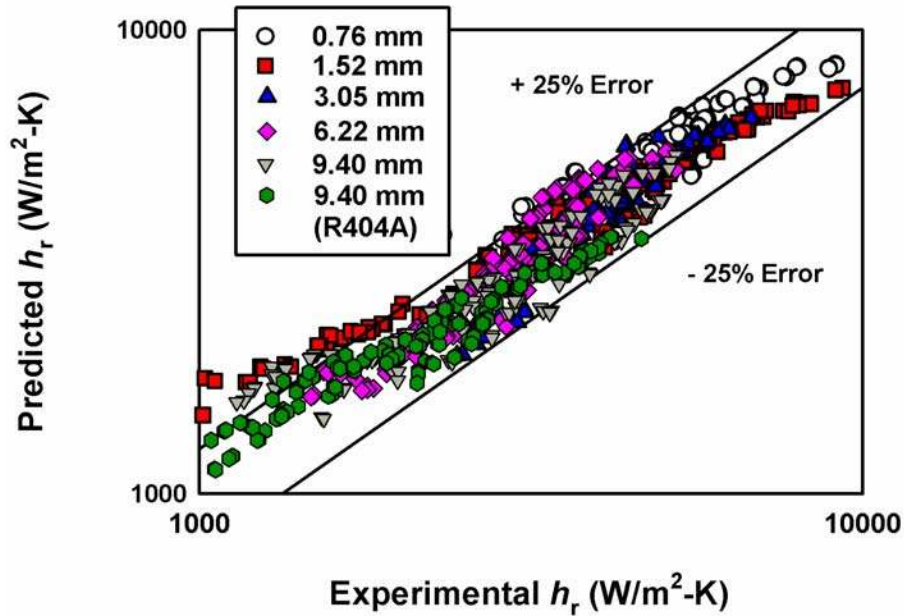
Figure 5.37: Overall Nusselt Number Predictions

Table 5.7: Heat Transfer Model Predictions for different D

D (mm)	Average Deviation (%)	Data < 25% Deviation (%)
0.76	14.6	87.8
1.52	18.5	84.2
3.05	7.5	96.8
6.22	8.9	94.3
9.40 (R410A)	12.0	86.9
9.40 (R404A)	11.8	94.4
Overall	12.0	90.7

Table 5.8: Heat Transfer Model Predictions for different Flow Regimes

Flow Regime	Average Deviation (%)	Data < 25% Deviation (%)
Annular	9.7	94.4
Wavy	16.6	84.3
Transitional	11.4	91.5

The predictions for all test sections are shown in Figures 5.38 and 5.39. In the absence of an intermittent flow heat transfer model, it is recommended that the annular flow model be applied to the few data points that fall within the intermittent flow regime in the 1.52 and 3.05 mm test sections. It can be seen that heat transfer coefficients are predicted well in the wavy and annular flow regimes. In addition, the predictions in the transition region in between are smooth without any discontinuities or jumps. It should be noted that the heat transfer coefficients in Figure 5.38 corresponding to the lower mass fluxes (mostly in the wavy flow regime) in this study are slightly overpredicted – these data points, however, also correspond to the highest uncertainties in this study. The trends predicted by the models are discussed next.

With a decrease in diameter, wavy flow ceases to be dominant. To clearly illustrate the model trends for annular and wavy flow, a diameter of $D = 6$ mm, which is larger than investigated by this author, is used in Figure 5.40. The plots in the left column of the figure show the predictions for the wavy flow model only. The right column shows the predictions for the annular flow. It will be shown in Figure 5.41 how the two models are implemented together with a transition region.
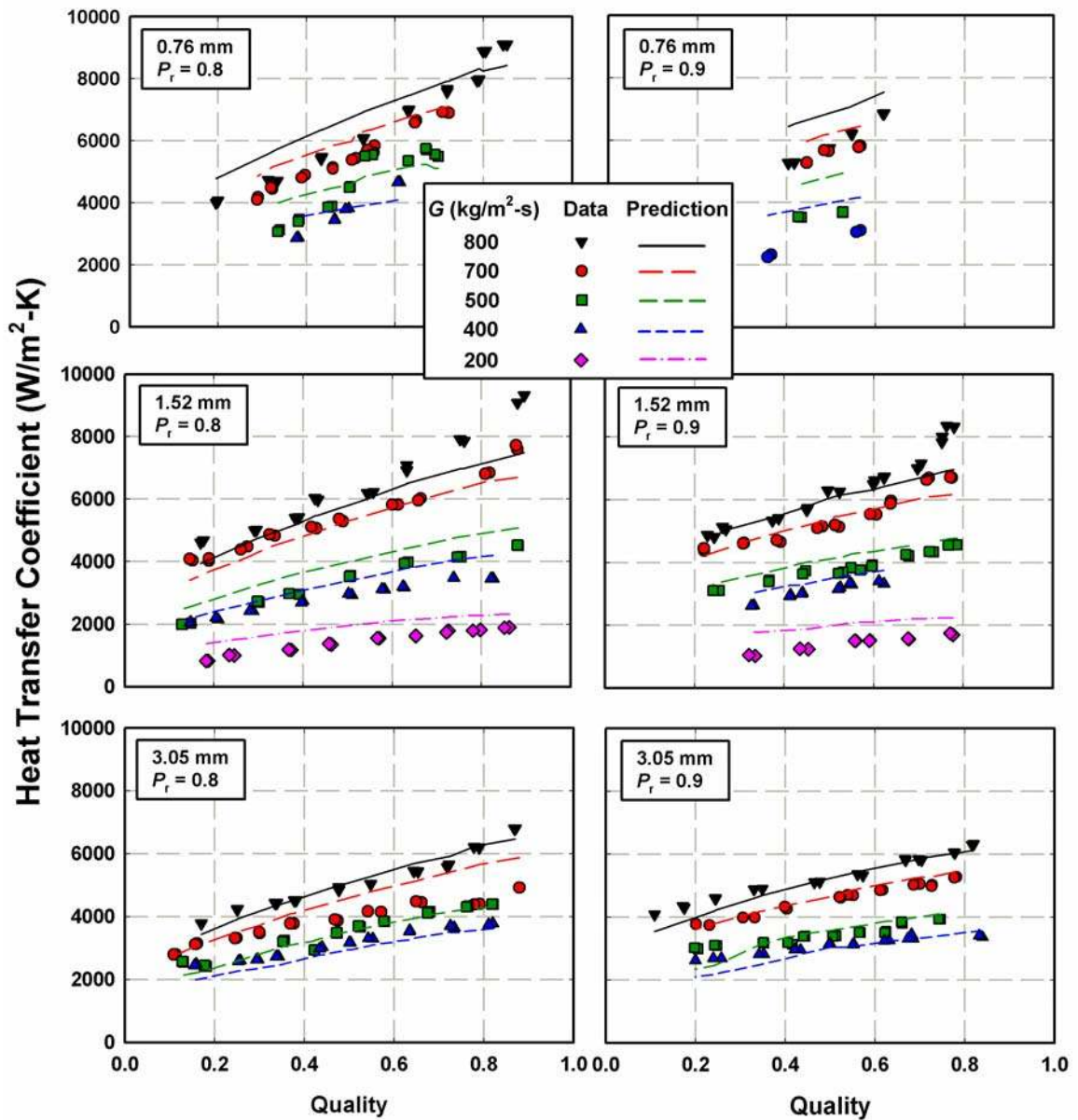
Figure 5.38: Predicted *h* for 0.76, 1.52 and 3.05 mm Test Sections

In the first row of plots in Figure 5.40, the annular and wavy flow models predict an increase in *h* with increasing *x* and *G* due to higher flow velocities and shear rates. The second row illustrates that the reduced pressure has little impact on *h*.
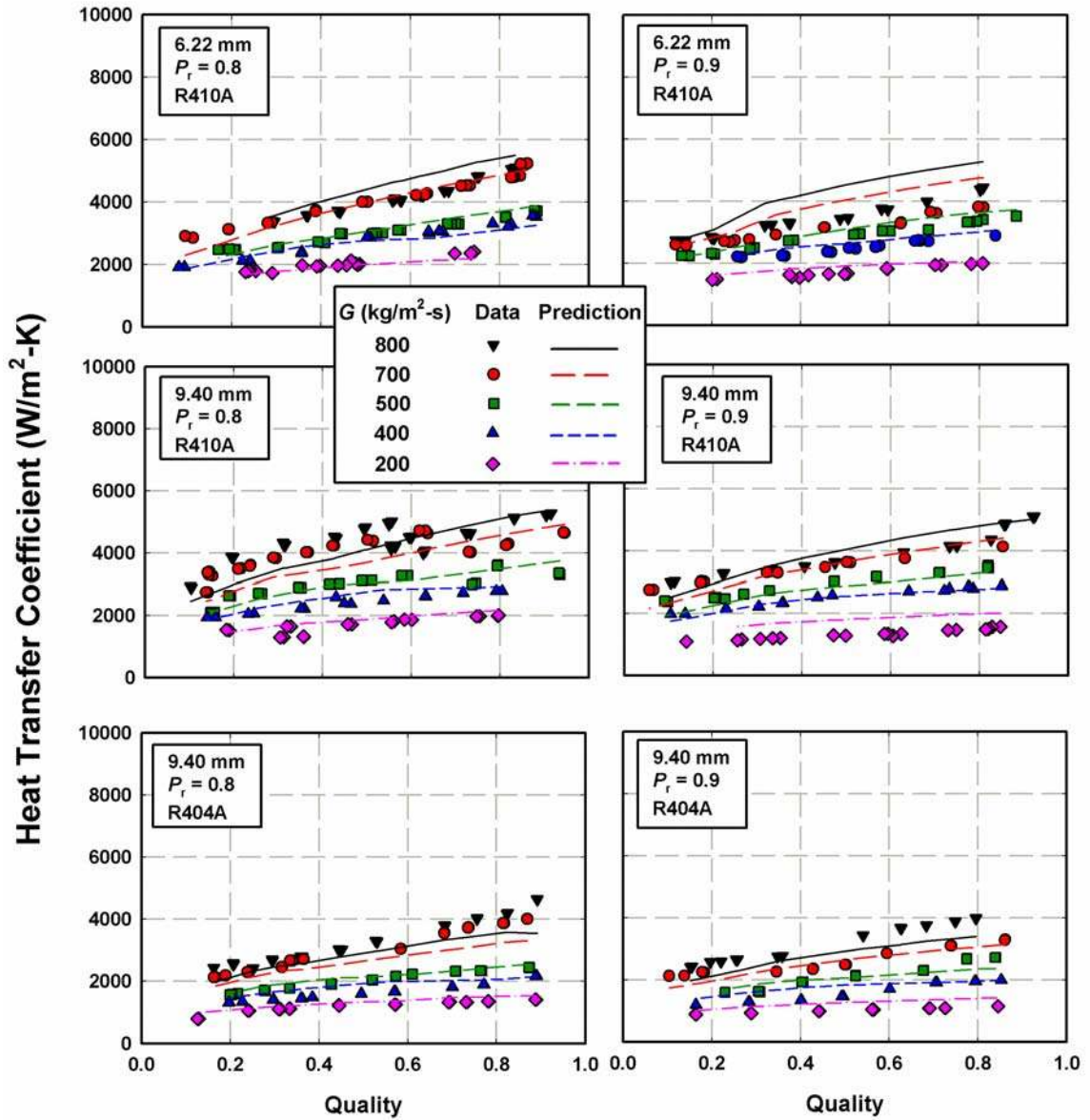
Figure 5.39: Predicted *h* for 6.22 and 9.40 mm Test Sections

For annular flow, a slight decrease in h is predicted with increasing reduced pressure at high qualities. The wavy flow shows negligible variation with P_r at low qualities. This is in agreement with the experimental observations.
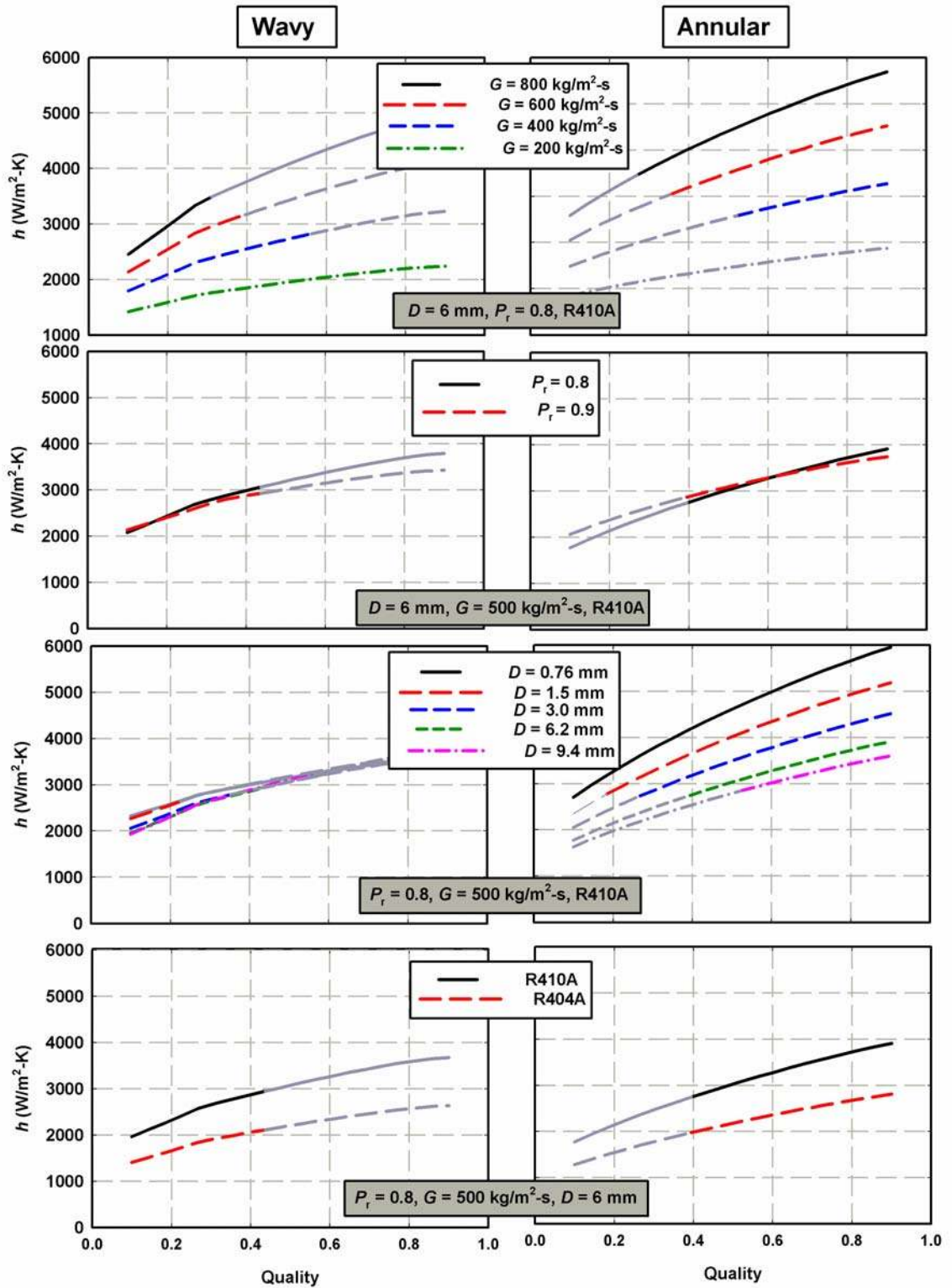
Figure 5.40: *h* Model Trends for Annular and Wavy Flow

139

With increasing P_r from 0.8 to 0.9, the specific heat ratios of the liquid and vapor phases increase by factors of 1.77 and 1.91, respectively. This effect is coupled with a decrease in latent heat by a factor of 1.3. In the third row of the plots, it is apparent that the effect of varying diameter has a more significant effect for annular flow than for wavy flow. Annular flow is shear driven flow. As predicted in the pressure drop model, smaller diameters increase the shear rate and correspond to higher heat transfer rates. These effects are not active in wavy flow. In the last row in the figure, the effect of refrigerant properties is demonstrated. Both the annular and wavy flow models predict a lower heat transfer coefficient for refrigerant R404A. As seen in Table 5.6, the viscosity and density of the two refrigerants are close in value, however, the thermal conductivity of R410A is significantly higher than that of R404A, leading to a higher heat transfer coefficient. At $P_r = 0.8$ and 0.9, the liquid conductivity of R410A is 42% and 41% higher, respectively, than the conductivity of R404A. Since the refrigerant is in contact with the tube wall through a liquid layer, the liquid conductivity has a significant influence on the overall heat transfer coefficient.

Figure 5.41 shows a representative plot for predicting h in the annular and wavy flow regime, in addition to the transition region. For $x > 0.41$ (in this particular example), the flow is in the annular flow regime. The model predicts a smooth transition to wavy flow for data between $0.28 < x < 0.41$ (corresponding to $2.0 < J_G < 3.0$). For qualities $x <$ 0.28, the wavy flow model applies.
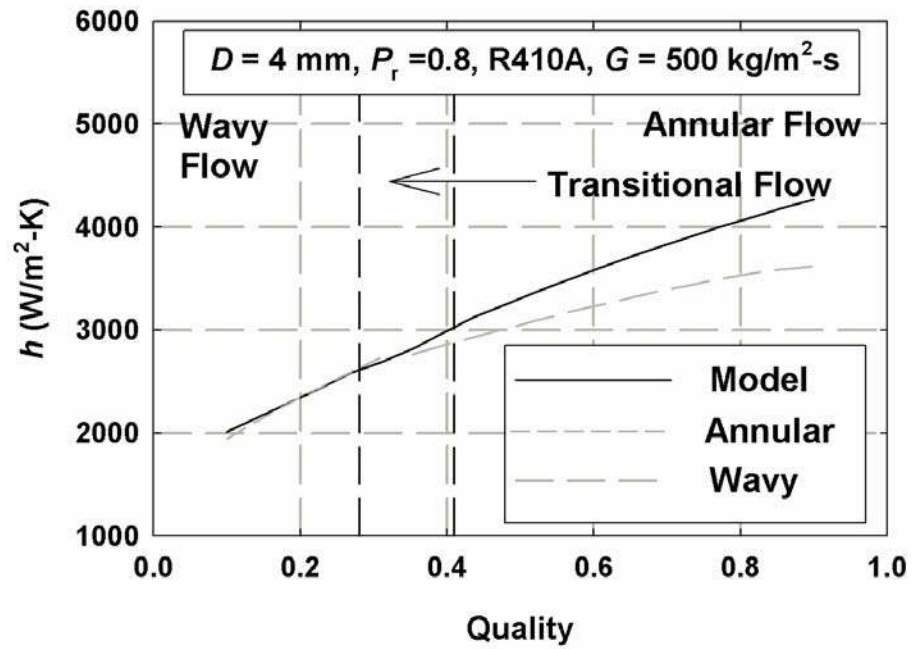
Figure 5.41: Representative *h* Prediction with Annular, Wavy and Transition Region

CHAPTER 6 - SUPERCRITICAL PRESSURE DROP AND HEAT TRANSFER RESULTS AND MODEL DEVELOPMENT

This chapter provides a detailed discussion of the experimental heat transfer and pressure drop results for the supercritical cooling experiments. A comprehensive comparison with the literature is provided, followed by the model development. The experimental results from Jiang (2004) and Mitra (2005) are also incorporated into the database used model development.

6.1 Heat Transfer and Pressure Drop Results

The local heat transfer coefficients, along with the frictional pressure gradients, are plotted versus the average refrigerant temperature in Figures 6.1 – 6.3 for all mass fluxes and pressures. The heat transfer results will be discussed first, followed by the pressure drop results.

6.1.1 Heat Transfer Coefficient

At lower temperatures, the refrigerant has thermo-physical properties of a liquid, and then it drastically transitions to a gas-like fluid in the vicinity of the critical transition temperatures. The transition temperature at the critical pressure is 71.4°C; at $P_r = 1.1$ and $P_r = 1.2$, the pseudo-critical transition temperatures are $T_{\text{pseudo-critical}} = 76.1°C$ and 80.4°C, respectively (Lemmon *et al.*, 2002). These temperatures are also shown in the figures. It should be noted that the heat transfer coefficients show a sharp peak close to $T_{\text{pseudo-critical}}$.
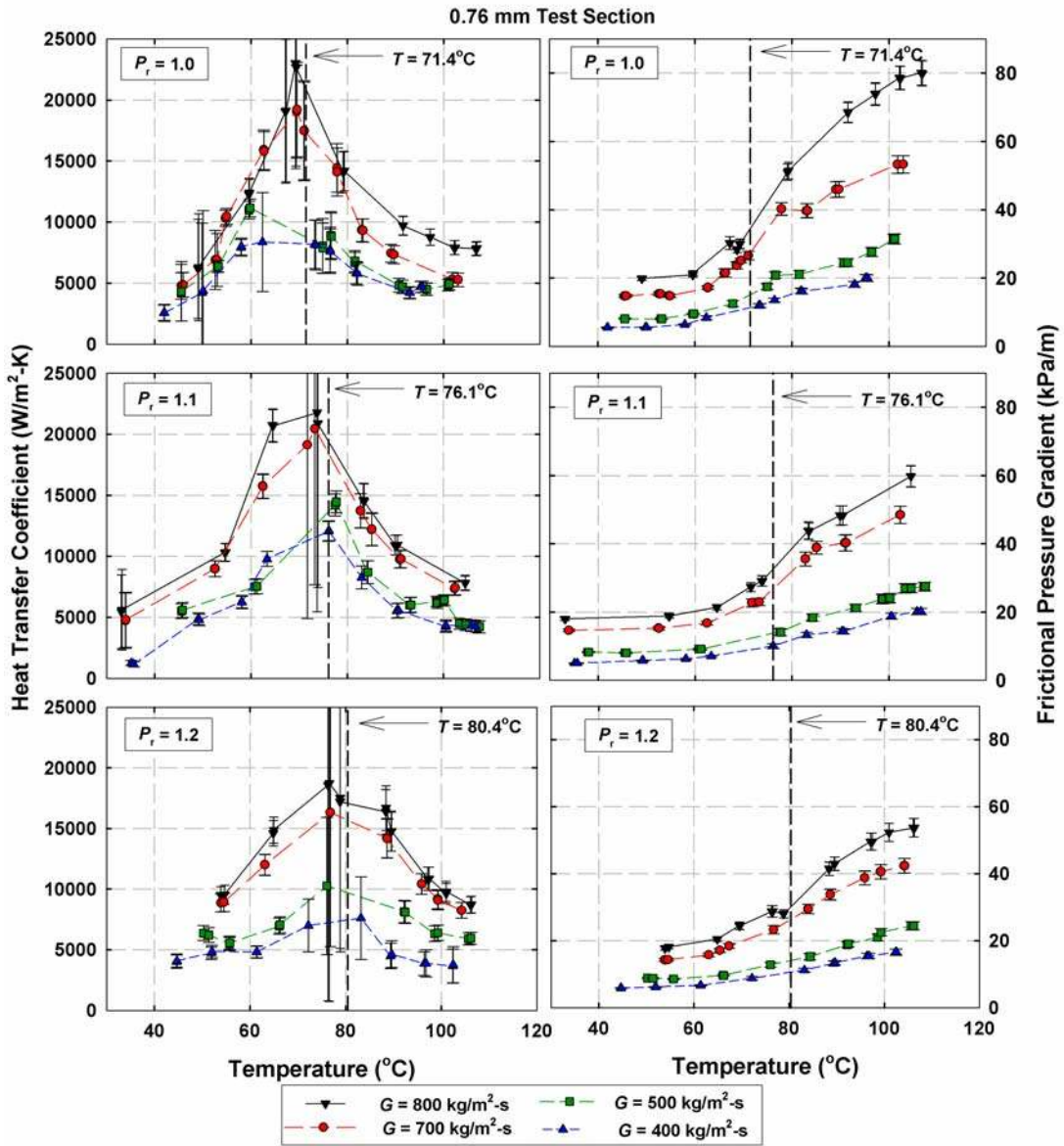
Figure 6.1: *h* and (d*P*/d*z*)_f versus *T*, 0.76 mm Test Section
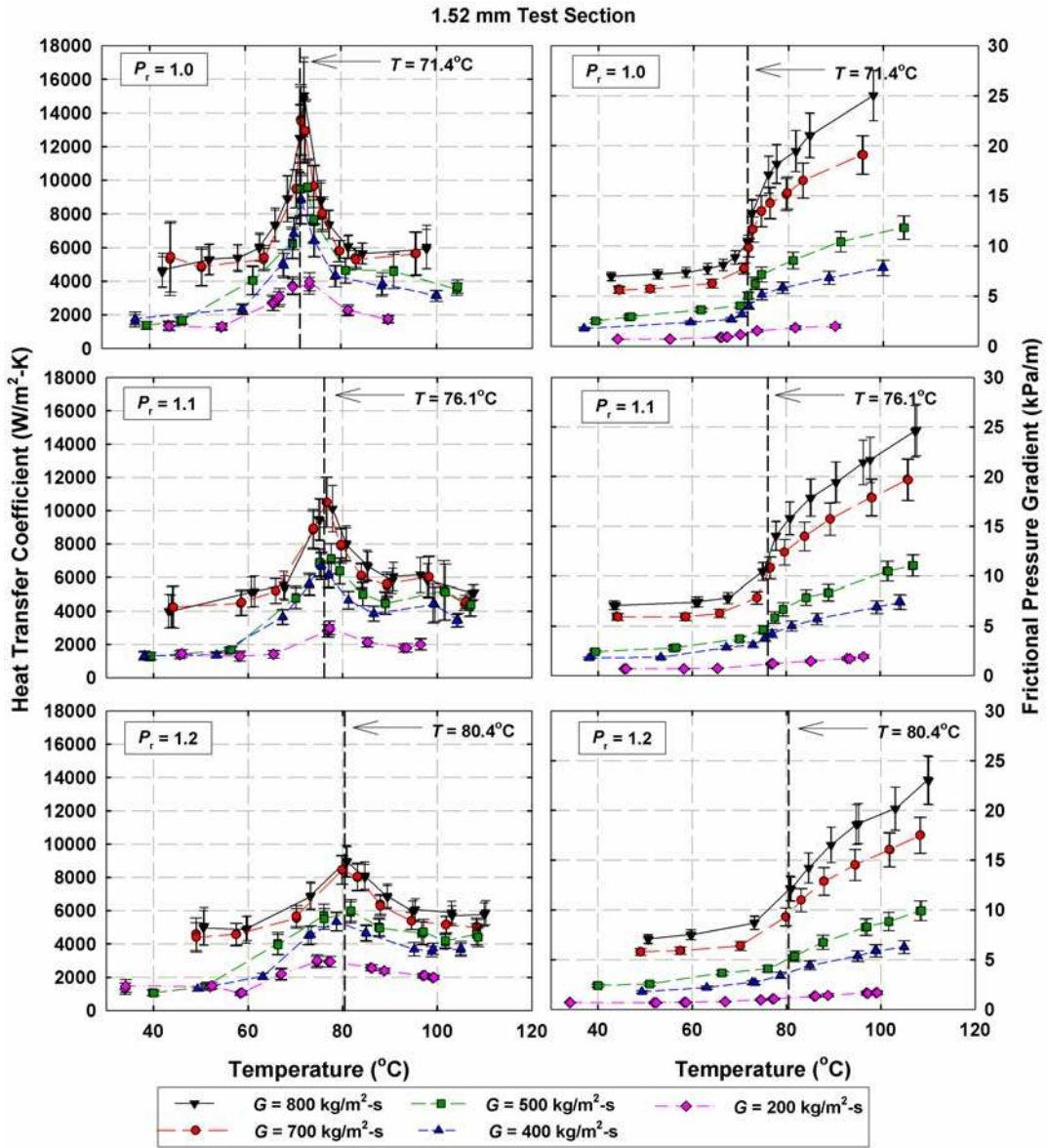
Figure 6.2: *h* and (d*P*/d*z*)$_f$ versus *T*, 1.52 mm Test Section
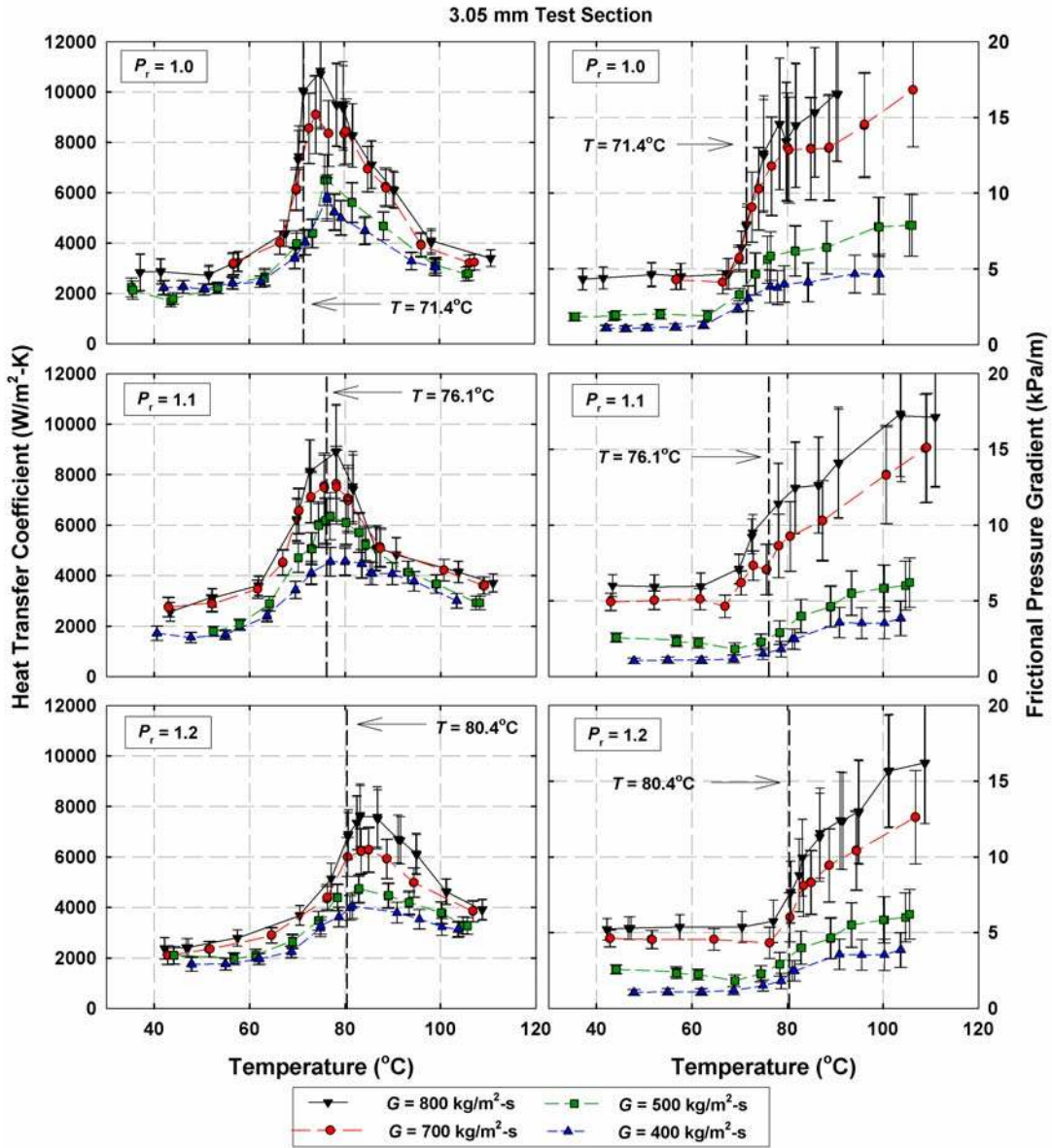
Figure 6.3: *h* and (d*P*/d*z*)_f versus *T*, 3.05 mm Test Section

The property variations for the temperature range of interest is this study are shown in Figure 2.1. The drastic change in thermo-physical properties in the vicinity of the critical temperature leads to the peaks in heat transfer coefficients. For example, for $D = 1.52$ mm at $P_r = 1.0$ for the data point at $T = 66.25°C$, the specific heat is $c_P = 3.12$ kJ/kg-K, whereas at $T = 72.75°C$, $c_P = 21.89$ kJ/kg-K. The viscosity and density abruptly decrease from 64.9×10^{-6} to 27.8×10^{-6} kg/m-s and 789.6 to 372.8 kg/m^3. Similarly, the thermal conductivity decreases from 0.073 to 0.0066 W/m-K. For this mass flux, $G = 800$ kg/m^2-s, the decrease in viscosity results in an increase in Reynolds number from 18815 to 43522. Similarly, the Prandtl number changes from 2.78 to 9.26. The net effect is that the heat transfer coefficient increases from 7297 to 14810 W/m^2-K.

The temperature of the refrigerant in the center of the tube (the bulk flow) is always higher than that of the refrigerant at the inner wall of the tube for all cooling experiments. The temperature gradient between the bulk and wall becomes significant in the vicinity of the critical temperature, as the properties at the wall will be more liquid-like (due to the lower temperatures), and the bulk flow is at a gas-like state. As the temperature near the wall decreases toward the critical temperature, the likelihood of a liquid-like film near the wall increases.

Pitla *et al.* (1998) state that Shitsman (1963), Tanaka *et al.* (1971) and Krasnoshchekov *et al.* (1970) observed an improvement in the heat transfer when the wall temperature was less than the critical temperature and the fluid bulk temperature was greater than the critical temperature. Krasnoshchekov *et al.* (1970) attributed the higher heat transfer rate

to the formation of a liquid-like layer near the wall of the tube. As seen in Chapter 5, thin-film formation in annular flow leads to very high heat transfer coefficients, especially since the thermal conductivity of the liquid-like layer surrounding the gas-like core is higher than the conductivity of the bulk flow. As the bulk and wall flow both approach gas-like properties, the heat transfer coefficient rapidly decreases and the flow exhibits a single-phase gas behavior.

The temperature difference between the inner wall and the bulk flow affects the properties, even for temperatures not in the vicinity of the transition temperatures. For example, a 4°C difference between the bulk and the wall, where T_{bulk} =59°C and T_{wall} =55°C, corresponds to a difference in density of $\Delta \rho = \rho_{bulk} - \rho_{wall} = (911.6 - 876.7)$ kg/m^3 = 34.9 kg/m^3 (Lemmon *et al.*, 2002). This density difference could result in differential forces between the phases in large diameter tubes, which might lead to a more stratified flow, where the denser fluid accumulates at the bottom of the tube. Similar to two-phase flow, the gravitational effects cease to be dominant in smaller diameters, such that the flow of the denser fluid surrounds the inner tube, with a core flow of lower density fluid. Therefore, the heat transfer coefficients increase with a decrease in diameter.

Furthermore, the bulk-to-wall temperature difference could lead to natural convection in the flow. The Grashof number, Gr, as shown in Equation 6.1 is evaluated for $T_{avg} = (T_{bulk} + T_{wall})/2$. For the data in this study, Gr ranged from 1246 to 32.6×10^6 and from 1.25×10^6 to 980.8×10^6 for the data by Jiang (2004) and Mitra (2005).

$$Gr = \frac{\rho_{avg}\left(\rho_{wall} - \rho_{bulk}\right)gD^3}{\mu_{avg}^2} \tag{6.1}$$

To investigate the effects of natural convection, the Grashof number is divided by Re_{bulk}^2.

Small values of Gr/Re_{bulk}^2 indicate that the heat transfer is dominated by forced convection. For $Gr/Re_{bulk}^2 \sim 1$, natural and forced convection effects are equally important. Figure 6.4 shows the Gr/Re_{bulk}^2 for different mass fluxes and diameters. It is observed that Gr/Re_{bulk}^2 increases with a decrease in G and an increase in D. With a decrease in G, the flow velocities decrease, thereby decreasing the impact of forced convection. The maximum value of Gr/Re_{bulk}^2 for $D = 0.76 - 3.05$ mm is 0.0224. Similarly, the maximum value of Gr/Re_{bulk}^2 for $D = 6.22 - 9.40$ mm is 0.1776. It was therefore assumed that natural convection effects are negligible for all data.
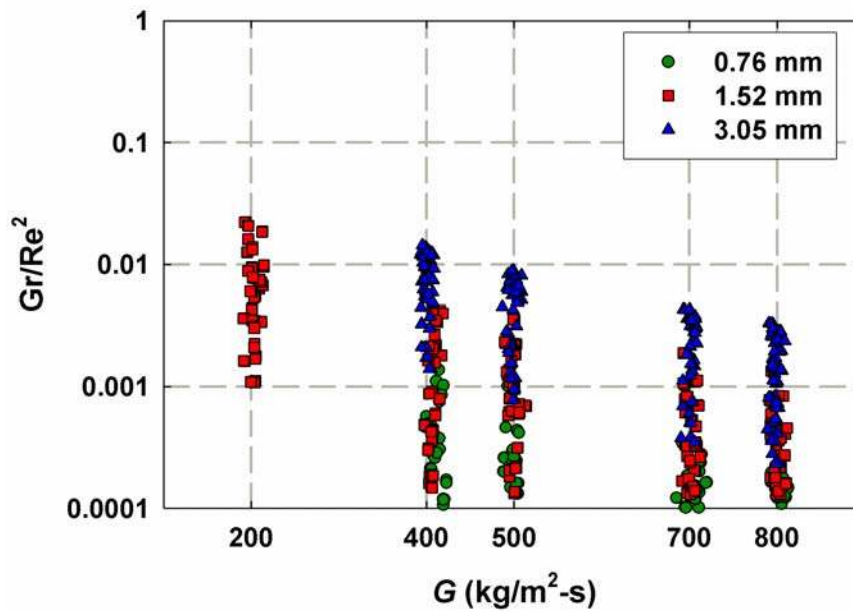
Figure 6.4: Gr/Re^2 for Different Mass Fluxes, *D* = 0.76 – 3.05 mm

An increase in pressure results in a shift of the peak in the heat transfer coefficient to higher temperatures, to coincide with the transition temperatures. The magnitude of the heat transfer coefficients decrease, as the property differences between the gas-like fluid and liquid-like fluid diminish. For example, the specific heat decreases by a factor of 1.65, for a change in pressure from $P_r = 1.1$ to $P_r = 1.2$ at the transition temperatures. Figure 6.10 illustrates the effects of different pressures for $D = 1.52$ mm at three different mass fluxes. The different transition temperatures for the different pressures are indicated in the figure.

The effect of varying diameter is shown in Figure 6.6 for a reduced pressure of 1.1 and three different mass fluxes. The heat transfer coefficient increases with a decrease in D for all mass fluxes. It should be observed there is a significant increase from $D = 1.52$ mm to $D = 0.76$ mm, especially at the higher mass fluxes.

The average uncertainty in the heat transfer coefficients in all three test sections was 14.9%. It should be noted that 96% of the data have uncertainties of less than 30%. There are only a few (33 out of 770) data points in the vicinity of the critical temperature where the uncertainty exceeds 30% due to very high refrigerant heat transfer coefficients and a correspondingly low resistance ratio. Table 6.1 summarizes the uncertainties and resistance ratios for all test sections.
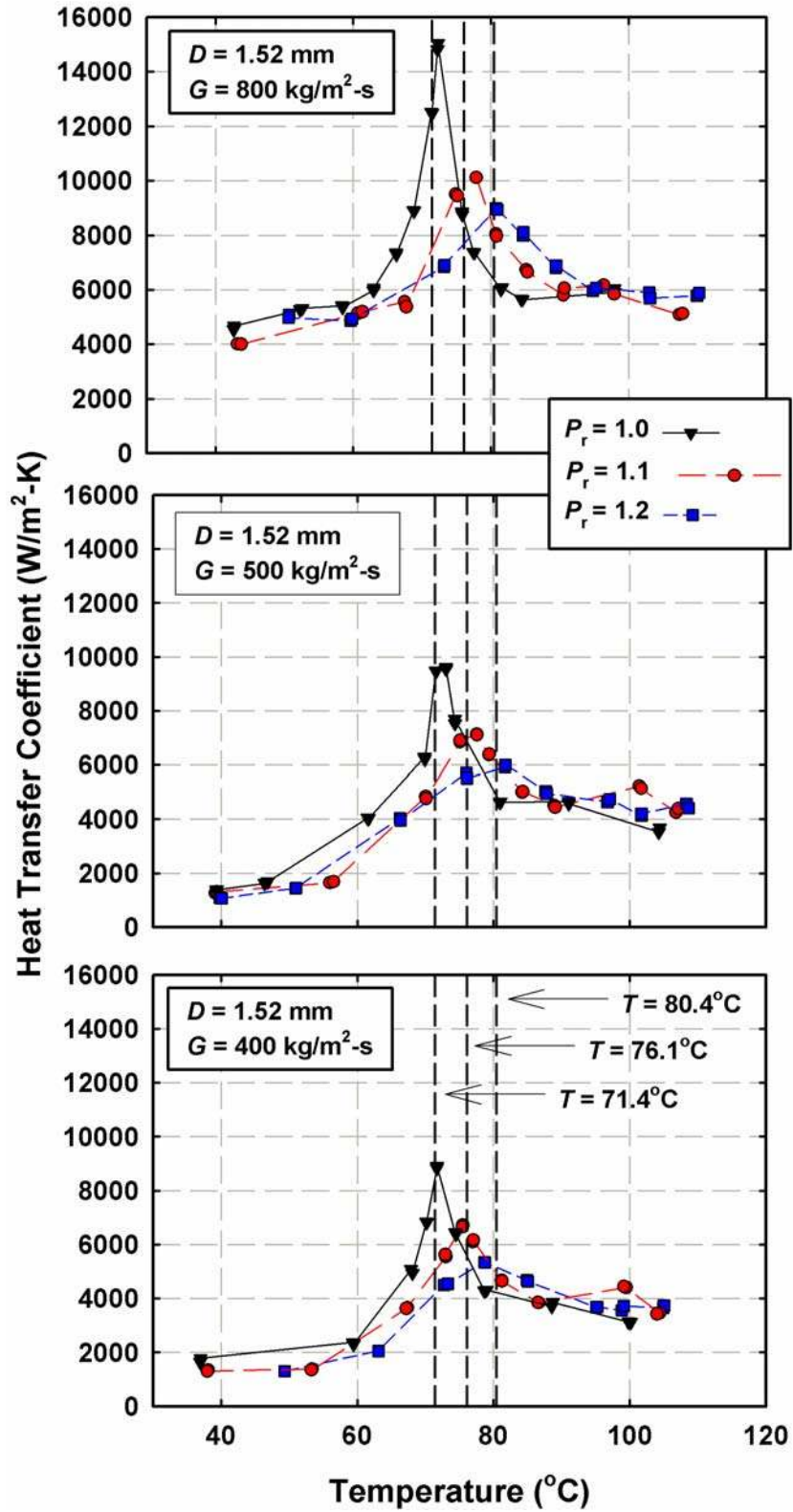
Figure 6.5: Effects of P_r on h for different Mass Fluxes, D = 1.52 mm
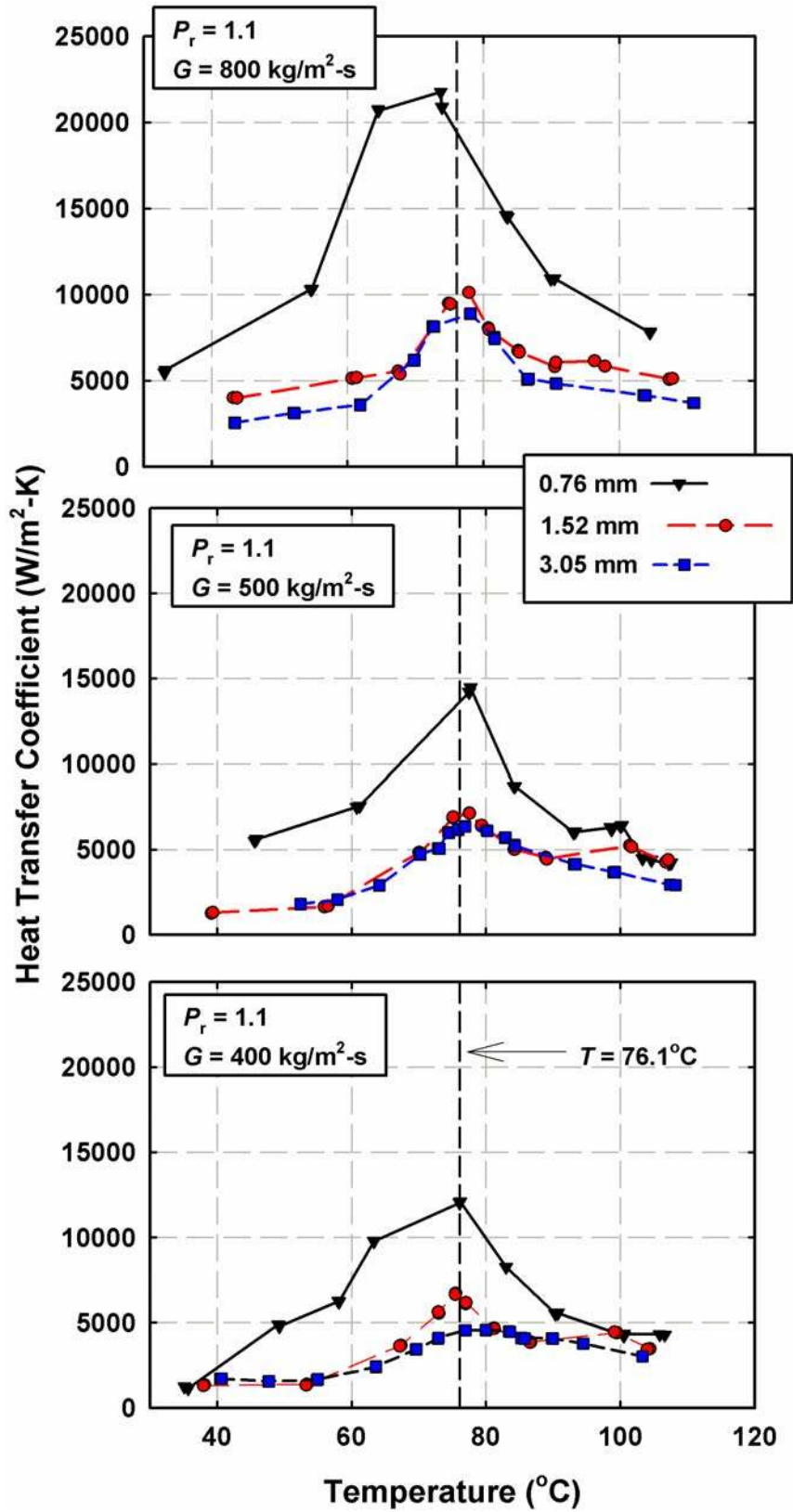
Figure 6.6: Effects of *D* on *h* for different Mass Fluxes, P_r = 1.1

151

The lowest resistance ratio, $R_{ratio} = 1.30$, was encountered in the 3.05 mm test section at $P_r = 1.0$, $G = 795.1$ kg/m²-s and $T_r = 75.01$°C. This corresponds to the highest refrigerant heat transfer coefficient measured in the 3.05 mm test section: $h_r = 10,837$ W/m²-K (Figure 6.3). The highest resistance ratio, $R_{ratio} = 36.47$, occurred in the 1.52 mm test section at one of the lowest h_r measured in the test section ($P_r = 1.2$, $G = 200.5$ kg/m²-s and $T_r = 58.3$°C, $h_r = 1,032$ W/m²-K).

Table 6.1: Average Resistance Ratio and Uncertainty in h_r

Test Section	P_r	$R_{ratio} \pm STD$	$\dfrac{U_{h_r}}{h_r} \pm STD$ (%)
0.76 mm	1.0	7.0 ± 3.2	21.8 ± 24.7
	1.1	7.1 ± 4.2	15.3 ± 17.6
	1.2	7.8 ± 4.3	19.4 ± 21.7
1.52 mm	1.0	11.4 ± 6.5	15.6 ± 4.8
	1.1	14.2 ± 8.0	14.9 ± 4.8
	1.2	13.3 ± 7.3	11.8 ± 3.8
3.05 mm	1.0	3.3 ± 1.2	13.5 ± 3.2
	1.1	3.4 ± 1.3	12.8 ± 2.9
	1.2	3.8 ± 1.2	12.4 ± 2.1
Average	**All**	$\mathbf{8.1 \pm 4.9}$	$\mathbf{14.9 \pm 11.7}$

Figure 6.7 shows a mass flux versus resistance ratio plot for all supercritical experiments. It should be noted that the resistance ratio increase with a decrease in mass flux for all test sections, due to the decrease in the refrigerant heat transfer coefficient. In the 3.05

mm test section, the heat transfer coefficients determined by the thermal amplification technique were verified by means of the measured wall-temperatures. Figure 6.8 shows representative wall-temperatures in the 3.05 mm test section. The average deviation of all wall-temperature measurements was 1.8°C, with a minimum and maximum deviation ranging from 0.3 to 3.9°C. It should be noted that the deviations in the temperature measurements are more significant in the vicinity of the transition temperature, where the flow transitions from a gas-like phase to a liquid-like phase. Comparison plots of the heat transfer coefficients from the thermal amplification technique and the wall temperature measurements are shown in Figure 6.9. The deviation between the two heat transfer coefficients ranged from -1.50% to 16.97% with an average of 8.28%.
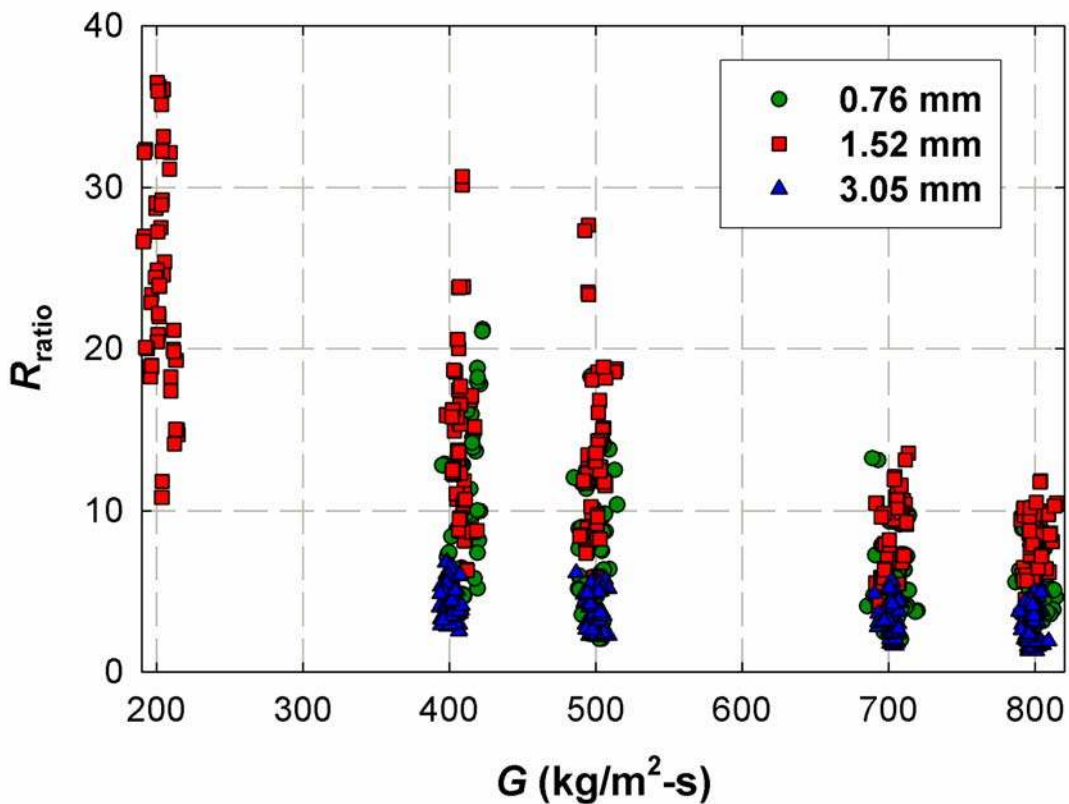
Figure 6.7: Resistance Ratio versus Mass Flux
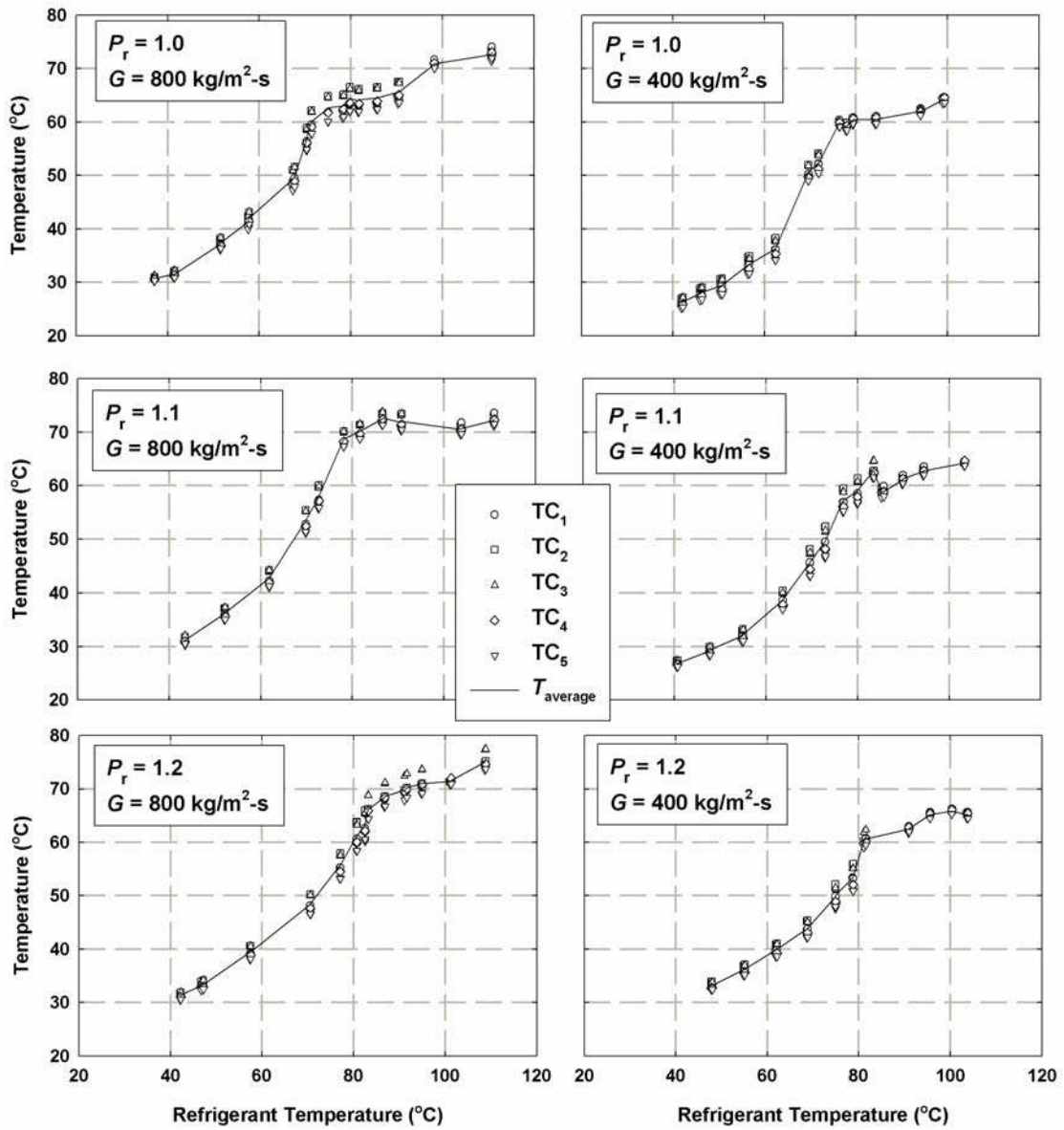
Figure 6.8: Representative Wall-Temperature Measurements, *D* = 3.05 mm

154
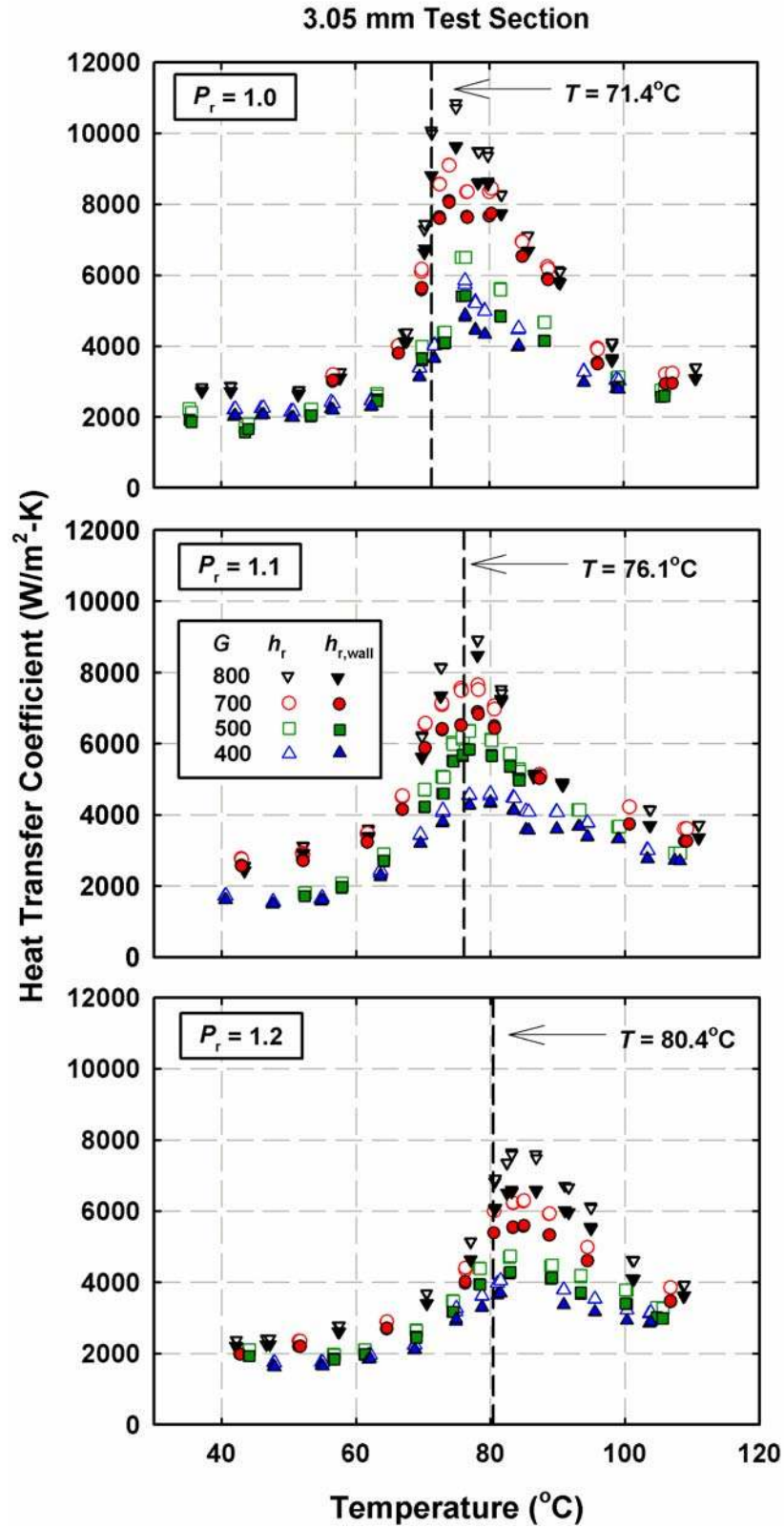
Figure 6.9: Comparison of h_r and $h_{r,wall}$ versus Temperature

6.1.2 Pressure Drop

The frictional pressure gradients show an increase with increasing temperatures and mass flux. As the refrigerant transitions from the liquid-like to the gas-like state, the density decreases significantly which in turn leads to an increase in flow velocity. For a 2°C temperature change from $T = 70°$ to $T = 72°$ at the critical pressure (4902 kPa), the density changes from $\rho = 691$ kg/m^3 to $\rho = 339$ kg/m^3 (Lemmon *et al.*, 2002). With an increase in pressure, the sharp increase in pressure drop coincides with the transition temperature. Since the transition temperature increases with increase in P_r, the experimental pressure gradient for a given temperature for $T > T_{critical}$ decreases. At the higher reduced pressures, the fluid properties do not exhibit the abrupt changes or peaks characteristic of the critical pressure. Therefore, the pressure gradient decreases with an increase in P_r. A direct comparison of the effects of reduced pressure on the pressure gradient data for $D = 1.52$ mm at different mass fluxes is shown in Figure 6.10.

The pressure gradient also increases with a decrease in diameter as illustrated in Figure 6.11. As observed in the heat transfer comparison plot, there is a significant increase in the pressure gradient from $D = 1.52$ mm to $D = 0.76$ mm. It should be noted that at a given mass flux, the flow velocity is constant. Therefore, the pressure gradient is inversely proportional to the tube diameter, which would imply an increase in pressure drop by a factor of two between $D = 1.52$ mm and $D = 0.76$ mm. In addition, there are somewhat smaller differences in friction factor. The coupled effects of f and D lead to the rise in pressure gradient seen in Figure 6.11.
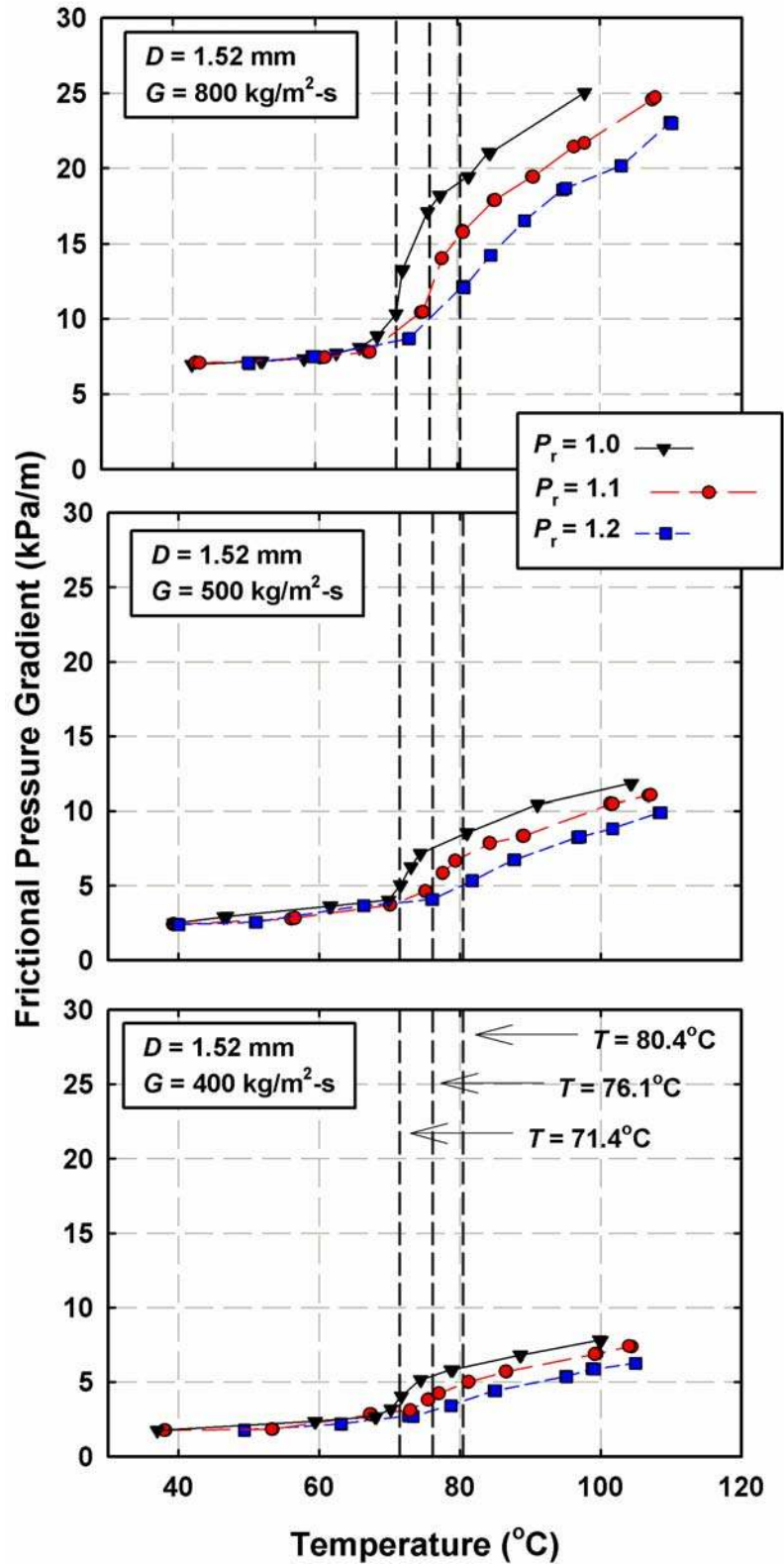
Figure 6.10: Effects of P_r on ΔP_f for different Mass Fluxes, D = 1.52 mm
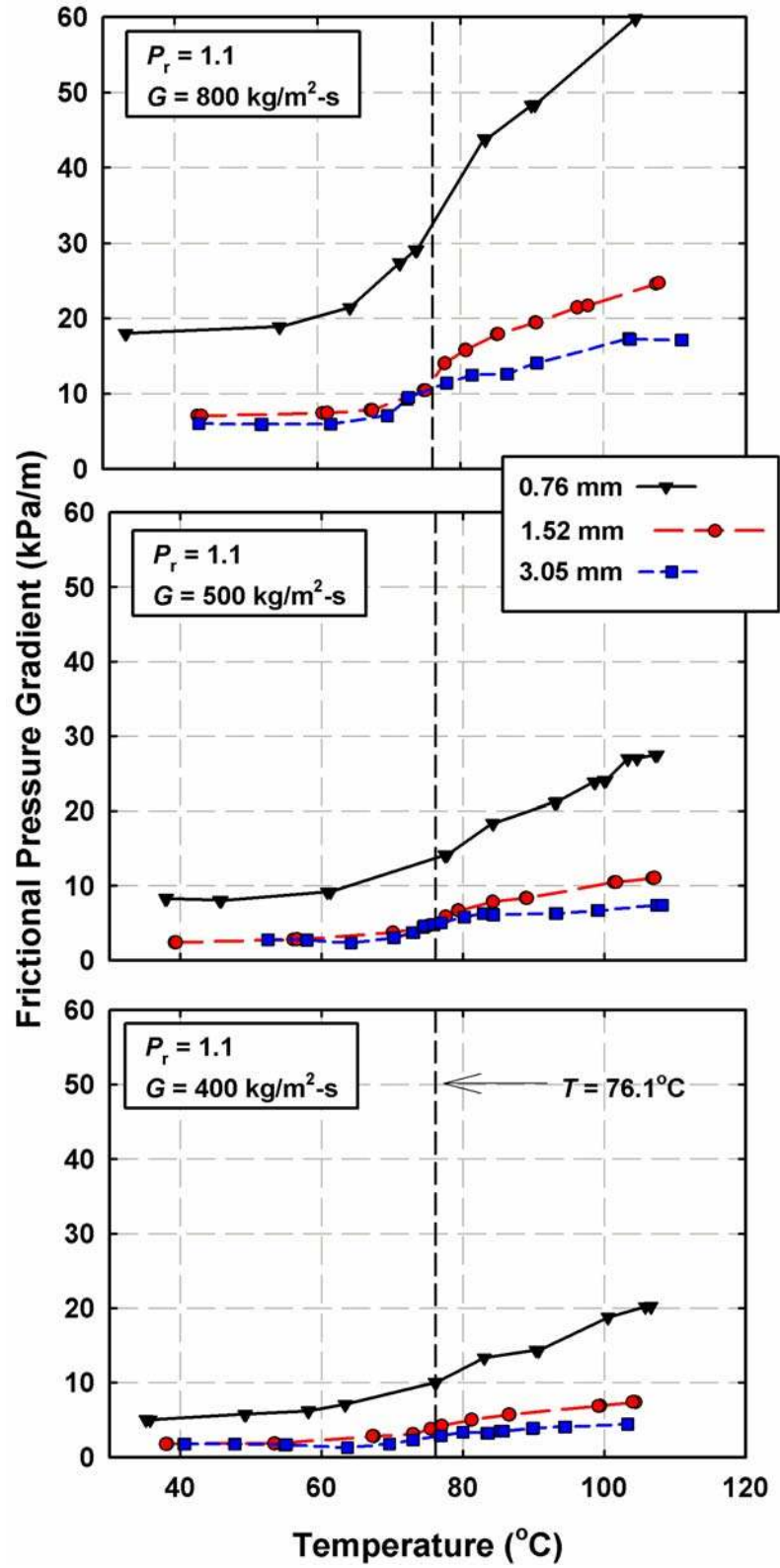
Figure 6.11: Effects of *D* on Δ*P*$_f$ for different Mass Fluxes, *P*$_r$ = 1.1

As outlined in Chapter 4, the frictional pressure gradient was deduced from the measured pressure drop which included deceleration and end effects. Because the density variations are significant in the vicinity of $T_{\text{pseudo-critical}}$, the deceleration component is much larger around this temperature.

For example, the deceleration pressure drop at $T = 52.3°$ is $\Delta P_{\text{deceleration}} = 0.04$ kPa ($\Delta P_{\text{deceleration}} / \Delta P_{\text{measured}} = 1.1\%$), whereas at $T = 72.2°$, $\Delta P_{\text{deceleration}} = 0.80$ kPa ($\Delta P_{\text{deceleration}} / \Delta P_{\text{measured}} = 11.8\%$) in the $D = 1.52$ mm test section ($G = 800$ kg/m^2-s, $P_{\text{r}} = 1.0$). Figure 6.12 shows the relative contributions of the deceleration pressure component, as well as the frictional pressure drop and the end effects for all data in this study. In some cases, the deceleration pressure drop contribution is significant enough that $\Delta P_{\text{f}} / \Delta P_{\text{measured}} > 100\%$. For example, for $D = 1.52$ mm, $G = 695.4$ kg/m^2-s at $P_{\text{r}} = 1.0$ and $T = 74.3°$, $\Delta P_{\text{deceleration}} / \Delta P_{\text{measured}} = 16.0\%$, whereas $\Delta P_{\text{endeffects}} / \Delta P_{\text{measured}} = 14.0\%$. For this data point, therefore, $\Delta P_{\text{f}} / \Delta P_{\text{measured}} = 1 + \left(\Delta P_{\text{deceleration}} / \Delta P_{\text{measured}} \right) - \left(\Delta P_{\text{endeffects}} / \Delta P_{\text{measured}} \right) = 102\%$. The overall uncertainty for the frictional pressure gradient was 12.1%, where the individual uncertainties of the test sections are shown in Table 6.2.
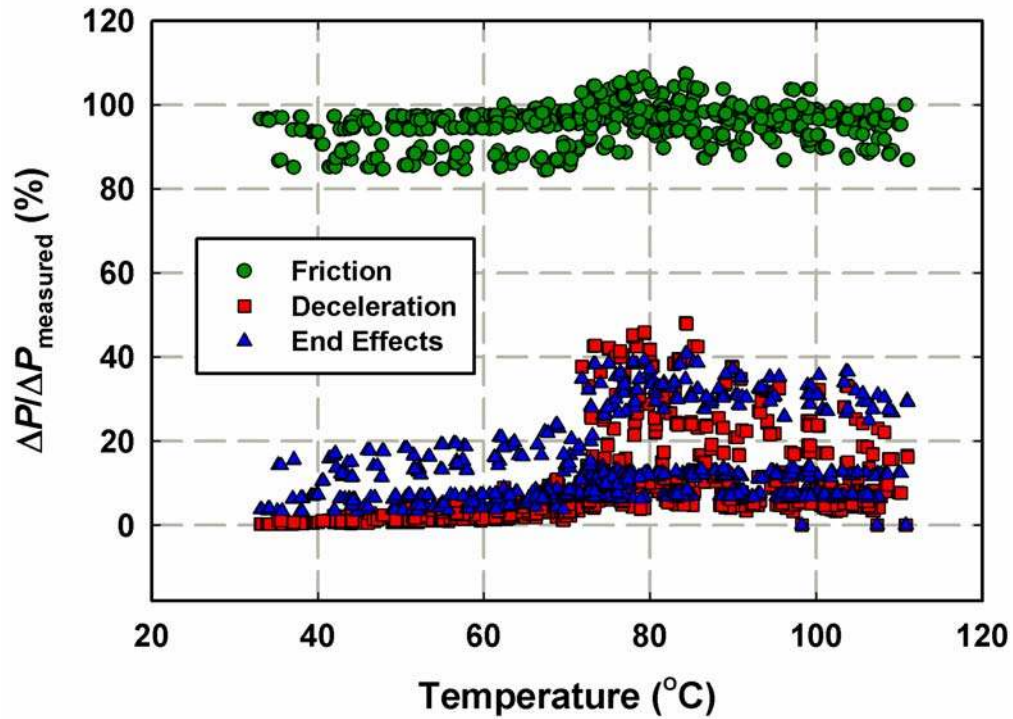
Figure 6.12: Relative Pressure Drop Contributions

Table 6.2: Relative Pressure Drop Contributions

Test Section	P_r	$\dfrac{\Delta P_f}{\Delta P_{measured}}(\%)$	$\dfrac{\Delta P_{deceleration}}{\Delta P_{measured}}(\%)$	$\dfrac{\Delta P_{endeffects}}{\Delta P_{measured}}(\%)$	$\dfrac{U_{\Delta P_f}}{\Delta P_f}(\%)$
0.76 mm	1.0	**97.8**	3.7	5.9	4.1
	1.1	**98.1**	4.4	6.3	4.4
	1.2	**98.0**	4.2	6.2	4.3
1.52 mm	1.0	**96.9**	6.5	9.6	8.2
	1.1	**96.9**	7.0	10.1	8.6
	1.2	**97.5**	7.9	10.4	8.8
3.05 mm	1.0	**93.3**	18.4	25.1	21.6
	1.1	**93.2**	17.4	24.2	20.8
	1.2	**91.4**	17.8	26.4	22.9
Average	**All**	**95.7**	**10.2**	**14.5**	**12.1**

6.2 Comparison with the Literature

Most of the available correlations for supercritical heat transfer and pressure drop are either single-phase flow correlations, or were developed for supercritical steam heating (instead of cooling) and CO_2. In this section, the applicable models will be compared with the data.

6.2.1 Pressure Drop

Filonenko (1954), Kuraeva and Protopopov (1974)

Filonenko's (1954) friction factor correlation was developed for single phase flow and is given in Equation 6.2. The range of applicability spans: $3000 \leq \mathrm{Re} \leq 5 \times 10^6$. It has been used by researchers to predict the pressure drop of a supercritical fluid, by using either the bulk flow Reynolds number, or the Reynolds number corresponding to the properties of the fluid at the inner wall temperature.

$$f_{\text{Filonenko}} = \frac{1}{\left(0.79 \ln\left(\mathrm{Re}\right) - 1.64\right)^2} \tag{6.2}$$

Kuraeva and Protopopov (1974) modified Filonenko's (1954) single-phase friction factor correlation with a ratio of the bulk and wall viscosities, as well as a term involving Grashof and Reynolds numbers to account for free convection effects. For Re < 10^5, $f_0 = f_{\text{Filonenko}}$ and for Re > 10^5, $f_0 = 0.02$. Then, the friction factor, $f_{\text{K-P}}$, is predicted as given in Equation 6.3:

$$f_{\text{K-P}} = f_0 \left(\frac{\mu_{\text{wall}}}{\mu_{\text{bulk}}} \right)^{0.22} \qquad\qquad \text{for } \text{Gr}/\text{Re}^2 < 5\times10^{-4}$$

$$f_{\text{K-P}} = \left(f_0 \left(\frac{\mu_{\text{wall}}}{\mu_{\text{bulk}}} \right)^{0.22} \right)\left(2.15 \left(\frac{\text{Gr}}{\text{Re}^2} \right)^{0.1} \right) \quad \text{for } 5\times10^{-4} < \text{Gr}/\text{Re}^2 \le 0.3$$

(6.3)

The overall predictions and a sample comparison plot of the predictions of this pressure drop model and the present data are provided in Figure 6.13. The pressure drop model by Kuraeva and Protopopov (1974) follows the trend of the data; it however, mostly underpredicts the data in this study by 17%. The data by Jiang (2004) and Mitra (2005) in the 9.40 and 6.22 mm tubes deviate on average by 69%.
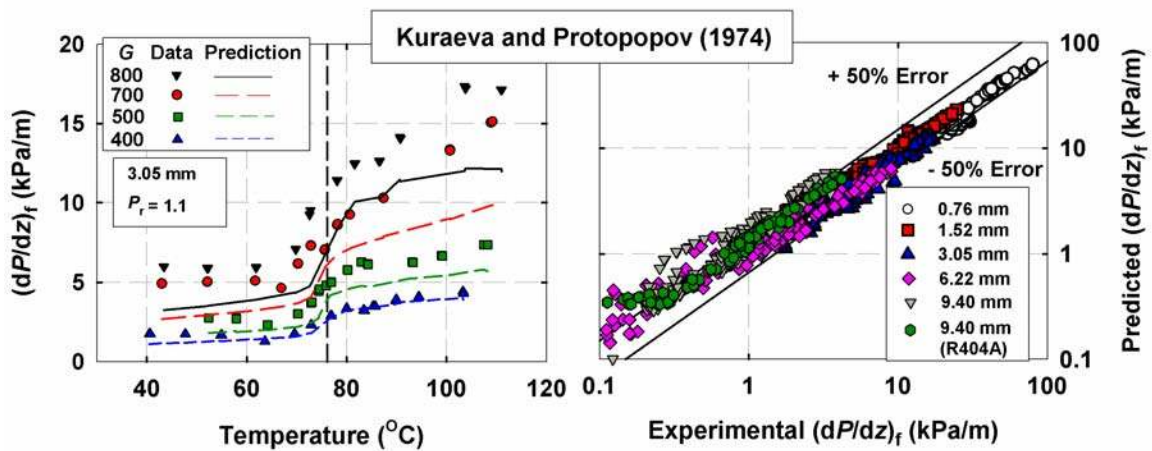
Figure 6.13: Pressure Drop Comparison with Kuraeva and Protopopov (1974)

Churchill (1977), Mitra (2005)

Churchill's friction factor correlation (1977) was developed for single-phase flow, spanning all flow regimes (laminar, turbulent and transitional). The correlation was

introduced in Equation 4.50. Researchers have used the Churchill correlation in conjunction with property multipliers to predict the friction factor in supercritical flow. Mitra (2005) proposed the use of a viscosity multiplier to capture the effects of varying properties from the bulk temperature to the wall temperature. In addition, a diameter ratio was introduced to account for the two different tube diameters investigated:

$$f_{\text{Mitra}} = a \cdot f_{\text{Churchill}} \cdot \left(\frac{\mu_{\text{wall}}}{\mu_{\text{bulk}}} \right)^{b} \cdot \left(\frac{D}{D_{\text{baseline}}} \right)^{c} \tag{6.4}$$

The constants a, b, and c correspond to different flow regimes (liquid-like, pseudo-critical transition and gas-like) assigned based on the specific work of thermal expansion. Figure 6.14 shows comparisons between the predictions of the models of Churchill and Mitra with the data from the present study. The pressure gradient is determined from the friction factor as shown here:

$$\frac{dP}{dz}_{\text{f}} = \frac{1}{2} \cdot f \cdot \frac{G^2}{\rho_{\text{bulk}}} \cdot \frac{1}{D} \tag{6.5}$$

Churchill's model follows the trend of the data well; it however, underpredicts the data from the present study by 28%; in the 6.22 and 9.40 mm tubes (Jiang 2004, Mitra 2005), the model deviates on average by 36%. The Churchill correlation was developed for single-phase flow, while the current study investigates the pressure gradient close to the pseudo-critical transition temperatures. Mitra's correlation overpredicts the data in this study on average by 208%. The deviation increases with a decrease in diameter, primarily because application of this model developed for $D > 6.22$ mm represents a significant extrapolation when used for $D = 0.76$ mm. However, the trends of the data are captured well.
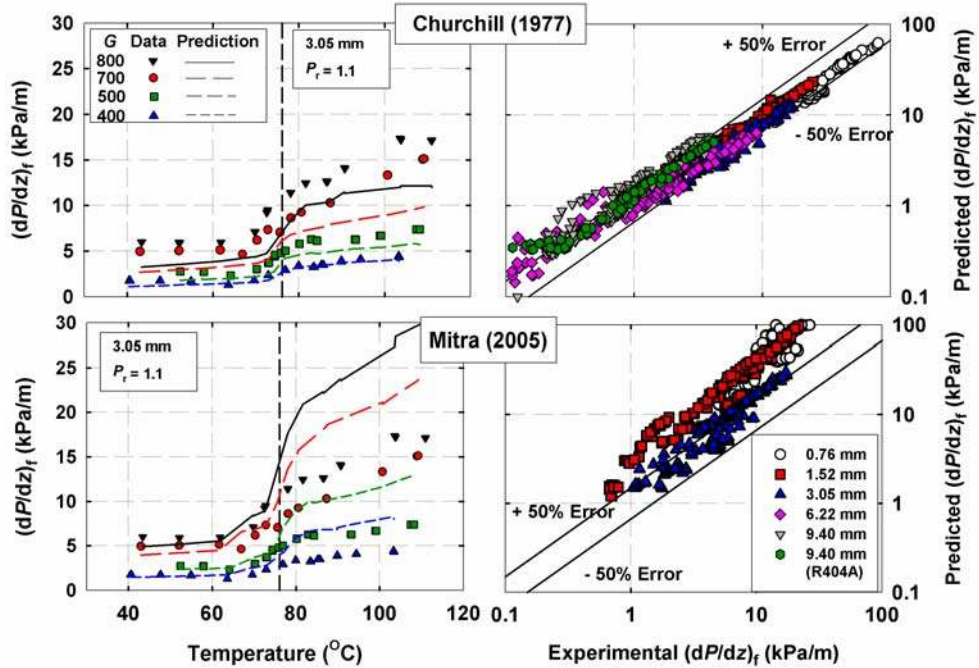
Figure 6.14: Pressure Drop Comparison with Churchill (1977), Mitra (2005)

Summary of Pressure Drop Correlations

Table 6.3 summarizes the average deviations for data collected by this author and by Jiang (2004) and Mitra (2005) from relevant pressure drop correlations in the literature. Well studied single-phase correlations are usually modified to account for the property differences between the bulk and wall temperatures.

Table 6.3: Summary of Predictive Capabilities of Pressure Drop Models in the Literature

Study	Avg. Deviation (%)	Comments
Kuraeva and Protopopov (1974)	31	Deviation increases with increase in diameter
Churchill (1977)	32	Deviation increases with increase in diameter
Mitra (2005)	208	Deviation increases with decrease in diameter (only compared to data from this study)

6.2.2 Heat Transfer

Krasnoshchekov et al. (1970)

Krasnoshchekov *et al.* (1970) suggested the use of density and specific heat multipliers in conjunction with the model by Petukov *et al.* (1961) to predict the heat transfer during supercritical cooling of carbon dioxide:

$$\text{Nu}_{\text{wall}} = \frac{h_r D}{k_{\text{wall}}} = \left(\frac{\rho_{\text{wall}}}{\rho_{\text{bulk}}}\right)^n \left(\frac{c_{P,\text{avg}}}{c_{P,\text{wall}}}\right)^m \left(\frac{\text{Re} \cdot \text{Pr} \cdot \left(f_{\text{Filonenko}} / 8\right)}{12.7 \left(f_{\text{Filonenko}} / 8\right)^{0.5} \left(\text{Pr}^{2/3} - 1\right) + 1.07}\right)_{\text{wall}} \tag{6.6}$$

The exponents *n* and *m* are functions of the reduced pressure, P_r. The predictions of this model do not follow the trends in the data from the present study, since the single-phase model by Petukov *et al.* (1961) relies primarily on the wall properties. The use of wall properties to evaluate $f_{\text{Filonenko}}$ is perhaps not appropriate to represent the data. It should also be noted that the Nusselt number correlation in Equation 6.6 relies on k_{wall}, rather than k_{bulk}. The comparison plot is shown in Figure 6.15. The average deviation is 44%.
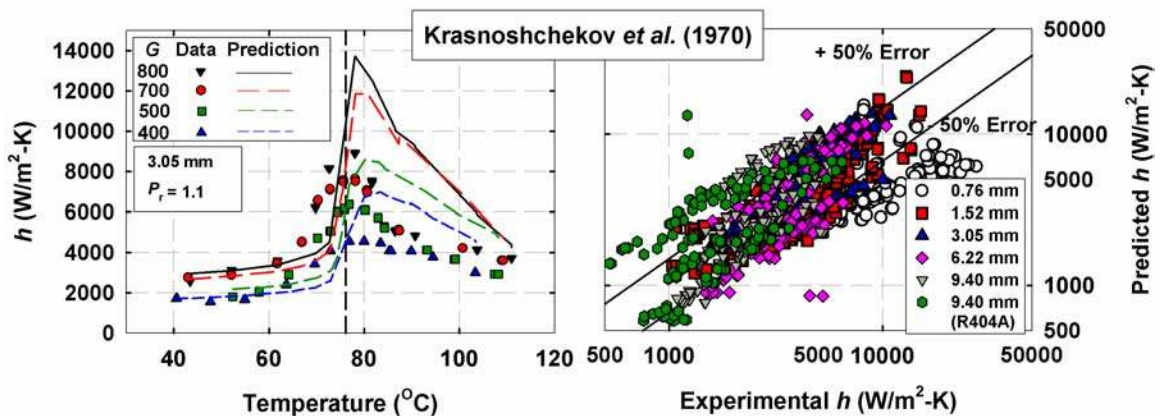
Figure 6.15: *h* Comparison with Krasnoshcheckov *et al.* (1970)

Gnielinski (1976), Pitla et al. (2002)

Gnielinski (1976) proposed the following single-phase convection correlation for turbulent flow in circular tubes:

$$\text{Nu}_{\text{Gnielinski}} = \frac{\left(f_{\text{Filonenko}}/8\right)\left(\text{Re}-1000\right)\text{Pr}}{1.07+12.7\left(f_{\text{Filonenko}}/8\right)^{0.5}\left(\text{Pr}^{2/3}-1\right)} \tag{6.7}$$

The range of applicability for this correlation is stated to be $0.5 < \text{Pr} < 2000$ and $3000 \leq \text{Re} \leq 5\times10^{6}$. Pitla *et al.* (2002) proposed the use of the average of the Gnielinski correlation evaluated at the wall and the bulk of the flow with a conductivity multiplier as shown in Equation 6.8:

$$\text{Nu}_{\text{Pitla}} = \left(\frac{\text{Nu}_{\text{Gnielinski,wall}}+\text{Nu}_{\text{Gnielinski,bulk}}}{2}\right)\left(\frac{k_{\text{wall}}}{k_{\text{bulk}}}\right) \tag{6.8}$$

The model proposed by Pitla *et al.* does not represent the trends in the current data well, especially in the larger diameter tubes at high temperatures as seen in Figure 6.16. For temperatures exceeding the critical temperature, the specific heat decreases. Since the Nusselt number, however, is the average of the wall and the bulk properties, the bulk specific heat decreases, whereas the specific heat based on the wall temperature could continue to increase if the wall temperature is still below the critical temperature. This leads to unrealistic multiple peaks in the heat transfer prediction. Gnielinski's correlation follows the trend in the present data, but exhibits deviations from the heat transfer coefficients, especially in the smaller tubes. The average deviation for Gnielinski's and Pitla's models are 31 and 51%, respectively.
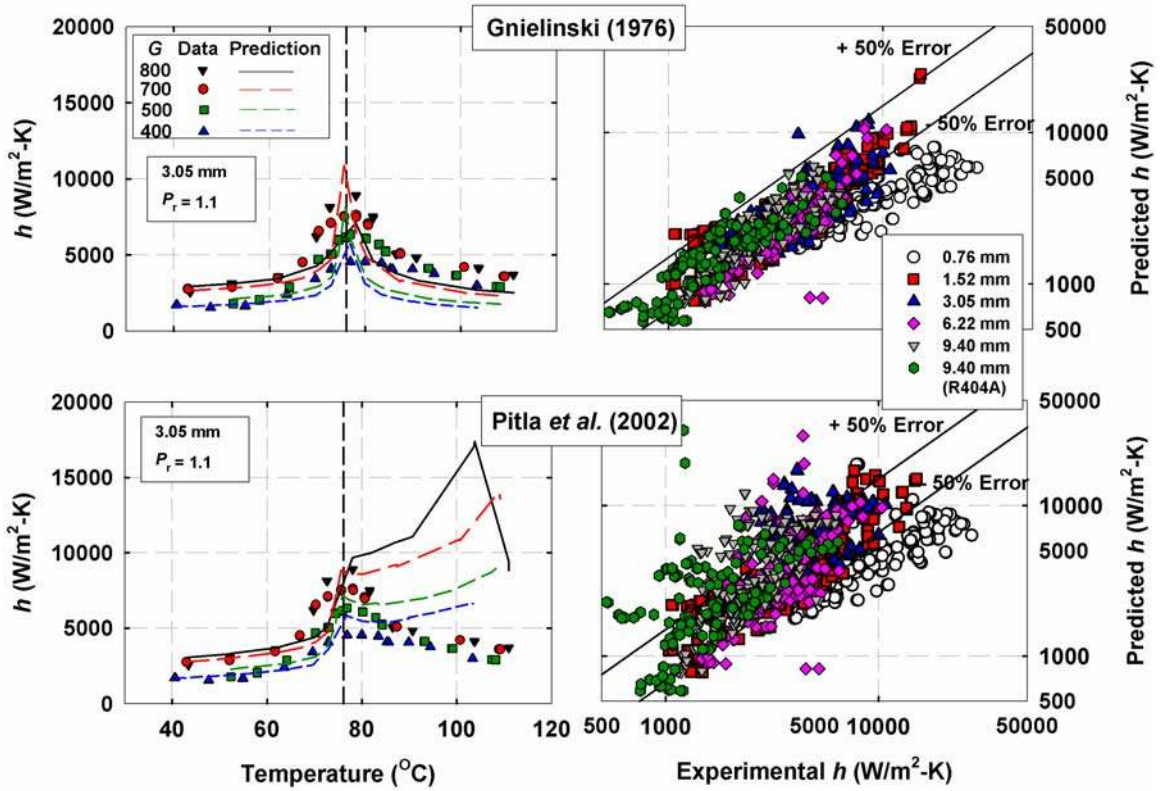
Figure 6.16: *h* Comparison with Gnielinski (1976) and Pitla *et al.* (2002)

Churchill (1977), Mitra (2005)

Mitra (2005) modified the single-phase Nusselt number correlation developed by Churchill (1977) with a wall-to-bulk specific heat multiplier in conjunction with a diameter ratio.

$$\mathrm{Nu}_{\mathrm{Mitra}} = a \cdot \mathrm{Nu}_{\mathrm{Churchill}} \cdot \left(\frac{c_{\mathrm{P,wall}}}{c_{\mathrm{P,bulk}}} \right)^{b} \cdot \left(\frac{D}{D_{\mathrm{baseline}}} \right)^{c} \tag{6.9}$$

where Churchill's correlation is given in Equation 6.10:

$$
\mathrm{Nu}_{\mathrm{Churchill}} = \left[4.364^{10} + \left(\frac{\exp\left(\dfrac{2200 - \mathrm{Re}}{365}\right)}{4.364^2} + \frac{1}{\left[6.3 + \dfrac{0.079\left(f_{\mathrm{Mitra}}/8\right)^{0.5}\mathrm{Re}\cdot\mathrm{Pr}}{\left(1 + \mathrm{Pr}^{0.8}\right)^{5/6}} \right]^2} \right)^{-5} \right]^{1/10} \qquad (6.10)
$$

It should be noted that Re and Pr are evaluated at the bulk temperature. Furthermore, the friction factor correlation developed by Mitra (2005) is used in Equation 6.10, rather than the original friction factor by Churchill (1977). The variables *a*, *b*, and *c* depend on the flow regime, which is defined by the bulk-flow temperature of the refrigerant. The three flow regimes are: liquid-like (at low temperatures), pseudo-critical-transition (in the vicinity of the transition temperature) and gas-like (at high temperatures). The deviations between the predictions of Mitra's model and the current heat transfer data are attributed to reasons similar to those presented in the discussion of the corresponding pressure drop model to diameters much smaller than those used by Mitra, which results in significant differences in the diameter ratio term. Since the pressure drop model already overpredicts the data with a decrease in *D*, the heat transfer model is bound to overpredict the experimental data. Figure 6.17 shows a comparison between the predictions of Mitra's and Churchill's models and the current data. The average deviation between all data and Churchill's model is 32%, while the deviation from Mitra's model, it is 65%.

Summary of Heat Transfer Correlations

Table 6.4 summarizes the average deviations for data collected by this author and by Jiang (2004) and Mitra (2005) from relevant heat transfer correlations in the literature.
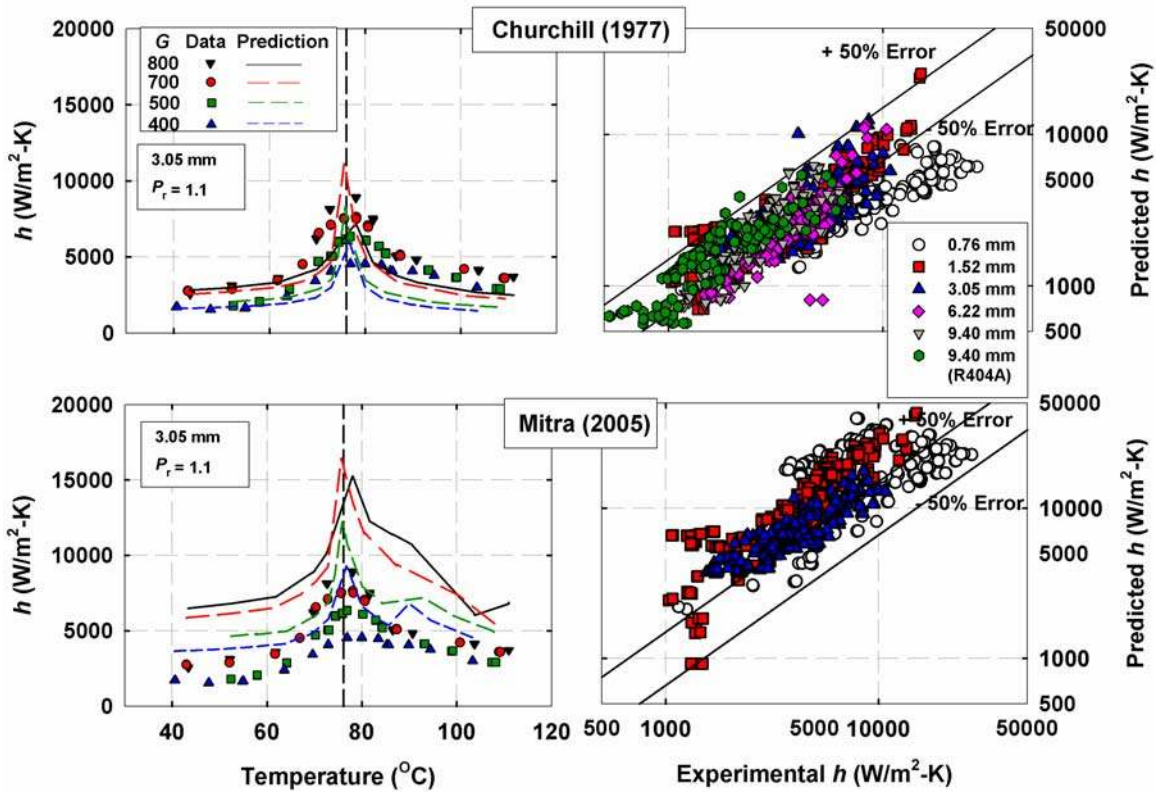
Figure 6.17: *h* Comparison with Churchill (1977) and Mitra (2005)

Table 6.4: Summary of Predictive Capabilities of Heat Transfer Models in the Literature

Study	Avg. Deviation (%)	Comments
Krasnoshchekov *et al.* (1970)	44	Does not predict trends well
Gnielinski (1976)	31	Deviation increases with decrease in diameter
Pitla *et al.* (2002)	51	Unrealistic peaks in gas-like region
Churchill (1977)	32	Follows trends well; deviation increases with decrease in diameter
Mitra (2005)	65	Deviation increases with decrease in diameter (only compared to data from this study)

6.3 Model Development

To capture the variations in the thermo-physical properties of the refrigerant as it transitions from a liquid-like state to gas-like state, researchers have proposed different flow regimes (Kurganov, 1998a, 1998b; Jiang, 2004; Mitra, 2005). A discussion about the appropriate division to accurately capture the property variations is presented first, followed by a development of pressure drop and heat transfer models based on these flow regimes.

6.3.1 Flow Regime Definition

The flow in the supercritical region is a strong function of the thermophysical properties, which could affect the corresponding flow mechanisms. At temperatures below the transition temperature, the viscosity, density and conductivity gradually decrease with an increase in temperature. In the vicinity of the transition temperature, the changes in properties are more abrupt. For temperatures much larger than the transition temperature, the properties gradually approach ideal gas behavior. To interpret such variations in the vicinity of the transition temperature where the properties are changing drastically, Kurganov (1998a; 1998b) proposed the specific work of thermal expansion, E_0, as a dimensionless criterion for assigning flow regimes.

$$E_0 = P\left(\frac{\partial(1/\rho)}{\partial i}\right)_P = \frac{P\beta}{\rho c_P} \tag{6.11}$$

E_0 represents the ratio of the flow work to the heat convected out during the cooling process. Kurganov studied heating of CO_2, however, Mitra (2005) implemented E_0 to

divide his R410A and R404A data into three flow regimes. The variations in E_0 with temperature and enthalpy for R410A are shown in Figure 6.18.
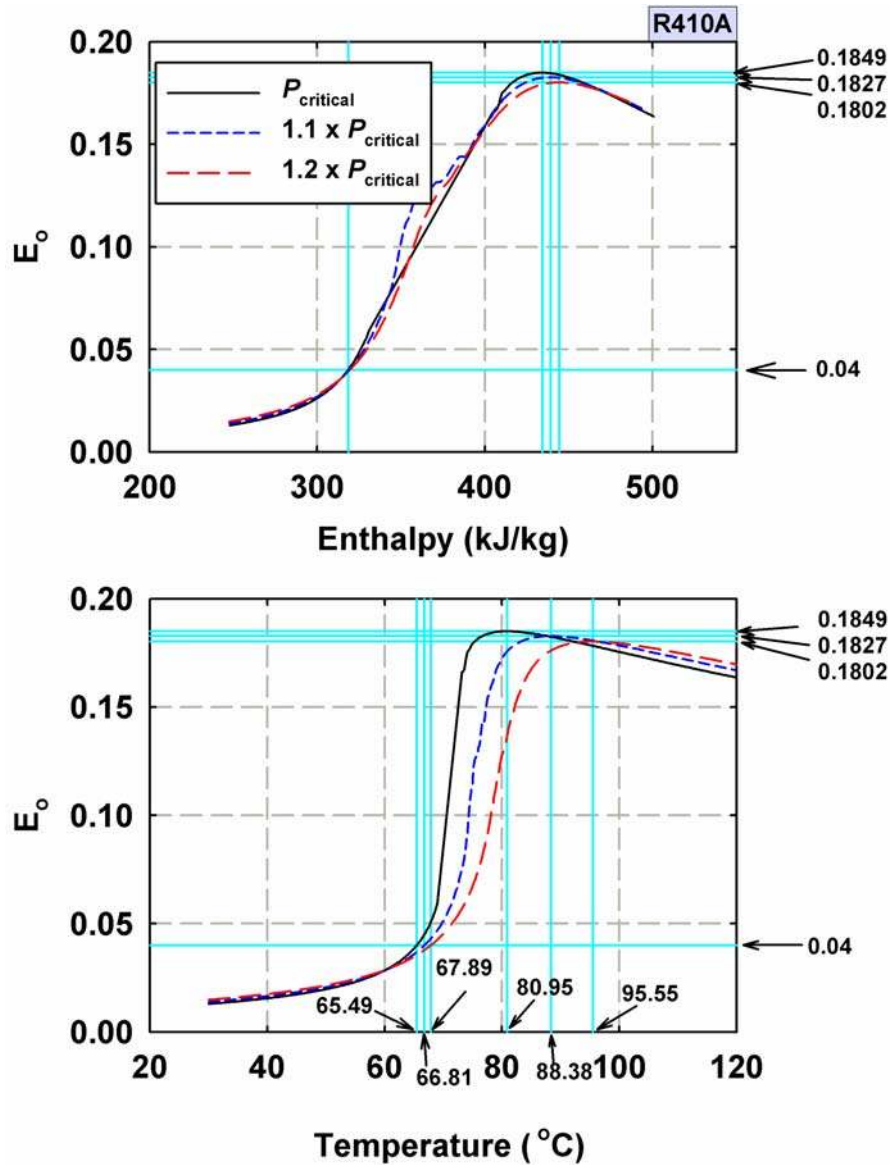
Figure 6.18: E_0 versus Enthalpy and Temperature for R410A (Mitra 2005)

The flow is considered to be in the liquid-like region for $E_0 < 0.04$. The liquid-like region is characteristic of gradual property changes with temperature. The flow is considered to

be in the pseudo-critical transition (PCT) region for $E_0 > 0.04$ until it reaches a maximum value. In the PCT, the flow transitions from a liquid-like state to a gas-like state. The PCT region is marked by rapid changes in E_0 with respect to enthalpy or temperature. The maximum value may be interpreted as the onset of the gas-like regime. In the gas-like state, property changes are small. It should be noted that E_0 is directly proportional to the volumetric thermal expansion coefficient. As the fluid tends to ideal gas behavior, E_0 is found to be proportional to $1/T$ in this regime.

Table 6.5 summarizes the transition temperatures for the different refrigerants and reduced pressures considered in this study.

Table 6.5: Flow Regime Boundaries for R410A and R404A (Mitra 2005)

Fluid	P_r	Liquid-Like Regime	Pseudo-Critical Transition Regime	Gas-Like Regime
R410A	1.0	$T < 65.49°C$	$65.49°C \leq T \leq 80.95°C$	$T > 80.95°C$
	1.1	$T < 66.81°C$	$66.81°C \leq T \leq 88.38°C$	$T > 88.38°C$
	1.2	$T < 67.89°C$	$67.89°C \leq T \leq 95.55°C$	$T > 95.55°C$
R404A	1.0	$T < 64.25°C$	$64.25°C \leq T \leq 74.45°C$	$T > 74.45°C$
	1.1	$T < 65.05°C$	$65.05°C \leq T \leq 81.55°C$	$T > 81.55°C$
	1.2	$T < 65.70°C$	$65.70°C \leq T \leq 88.35°C$	$T > 88.35°C$

The flow regime division based on temperatures for each reduced pressure will be used as a foundation to develop the pressure drop and heat transfer models, which are discussed next.

6.3.2 Pressure Drop Model

It was noted in the comparison of the data with models in the literature that the deviation of $f_{\text{Churchill}}$ increases with increasing diameter. Mitra (2005) proposed a viscosity and diameter multiplier based on experiments on 6.22 and 9.40 mm tubes. As stated previously, this model overpredicts the data. From the experimental results in this study, it was observed that the deviation from Churchill's model decreases at smaller diameter tubes. The increased deviation with increasing diameter is a direct result of the bulk-to-wall temperature difference. The fluid at the wall is at a lower temperature than the bulk flow, leading to a viscosity difference which results in additional shear and higher pressure gradients. The viscosity ratio, $\mu_{\text{wall}} / \mu_{\text{bulk}}$, for all data is shown in Figure 6.19 along with the corresponding temperature difference $T_{\text{bulk}} - T_{\text{wall}}$. It should be noted that the viscosity ratio is higher in the large diameter tubes due to the higher difference between the bulk and wall temperatures. Based on this discussion, the pressure drop data from the present study as well as those from the work of Jiang (2004) and Mitra (2005) were correlated using the following definition of the friction factor, which is in turn a modified version of Churchill's (1977) friction factor to account for bulk-to-wall property variations.

$$\left(\frac{dP}{dz}\right)_{\text{f}} = \frac{1}{2} \cdot f \cdot \frac{G^2}{\rho_{\text{bulk}}} \cdot \frac{1}{D} \tag{6.12}$$

$$f = a \cdot f_{\text{Churchill}} \cdot \left(\frac{\mu_{\text{wall}}}{\mu_{\text{bulk}}}\right)^b \tag{6.13}$$
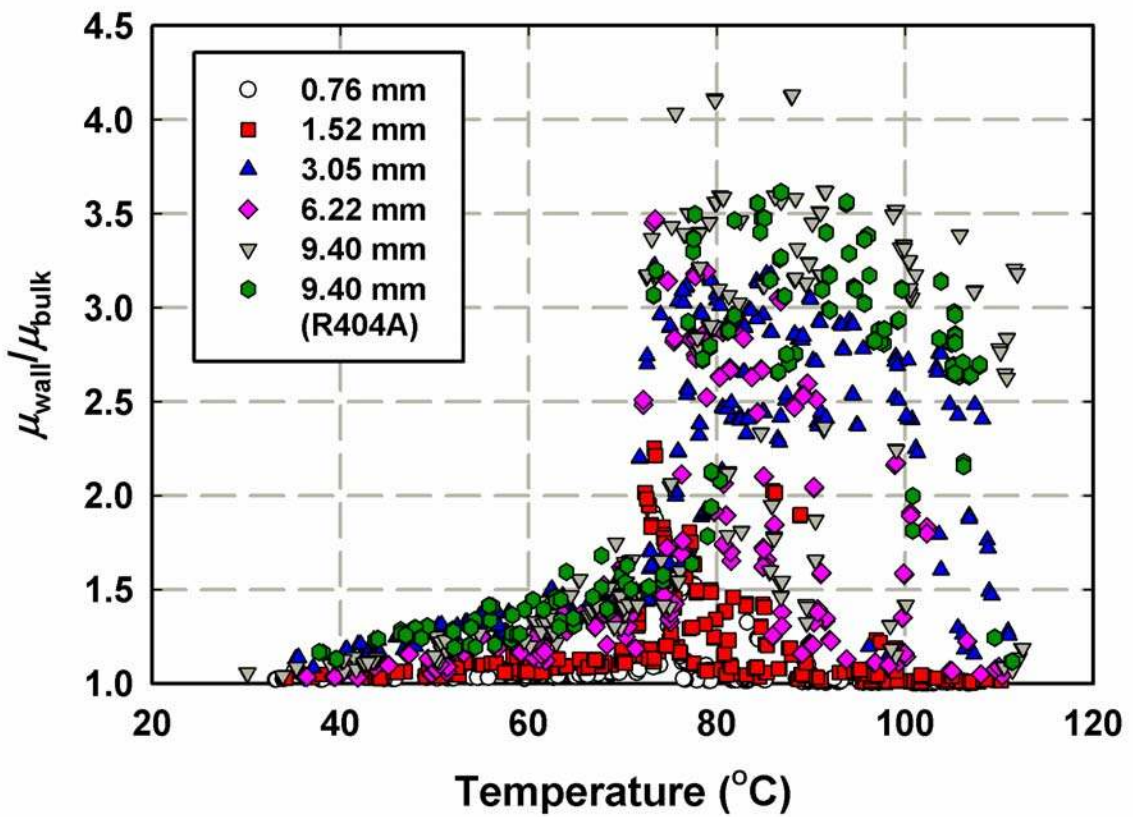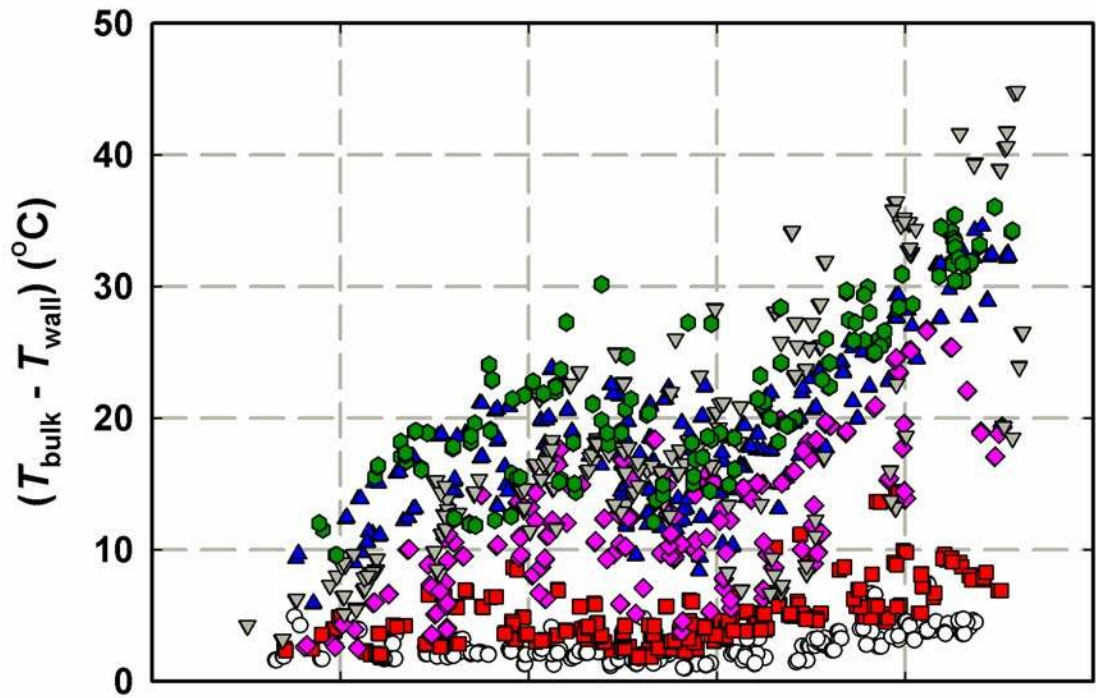
Figure 6.19: Viscosity Ratio and T_{wall} versus T_{bulk}

The parameters *a* and *b* in the above expression for friction factor are determined from regression analysis for the three different flow regimes. The resulting values for each regime are shown in Table 6.6.

Table 6.6: Parameters in Friction Factor Correlation

Flow Regime	a	b
Liquid-Like	1.16	0.91
PCT	1.31	0.25
Gas-Like	1.19	0.17

The Churchill friction factor is given in Equation 4.50. It should be noted that no explicit diameter dependence is introduced in the model as initially proposed by Mitra (2005). In the liquid-like region, the viscosity gradually decreases with increasing temperature and the friction factor is very sensitive to small temperature or viscosity differences between the bulk and wall flow due to the high exponent of $b = 0.91$. In the PCT region, the viscosity ratio can rapidly ramp up, as seen in Figure 6.19, when the bulk temperature is higher than the critical temperature and the wall temperature below the transition temperature. Therefore, the value for *b* in the PCT region decreases from 0.91 (in the liquid-like region) to $b = 0.25$, while the constant *a* increases from 1.16 to $a = 1.31$. It should be noted that constant *a* has similar values for the liquid-like and the gas-like regimes, $a = 1.16$ and 1.19, respectively. In the gas-like region, the viscosity ratio

exponent, b, decreases to $b = 0.17$. In the gas-like region, the viscosity does not change significantly with increasing temperatures. It should be noted that in supercritical cooling, the wall temperature is always lower than the bulk temperature; therefore, the wall-to-bulk viscosity ratio is always greater than unity. Figure 6.20 shows the overall prediction of the pressure gradient model for all data.
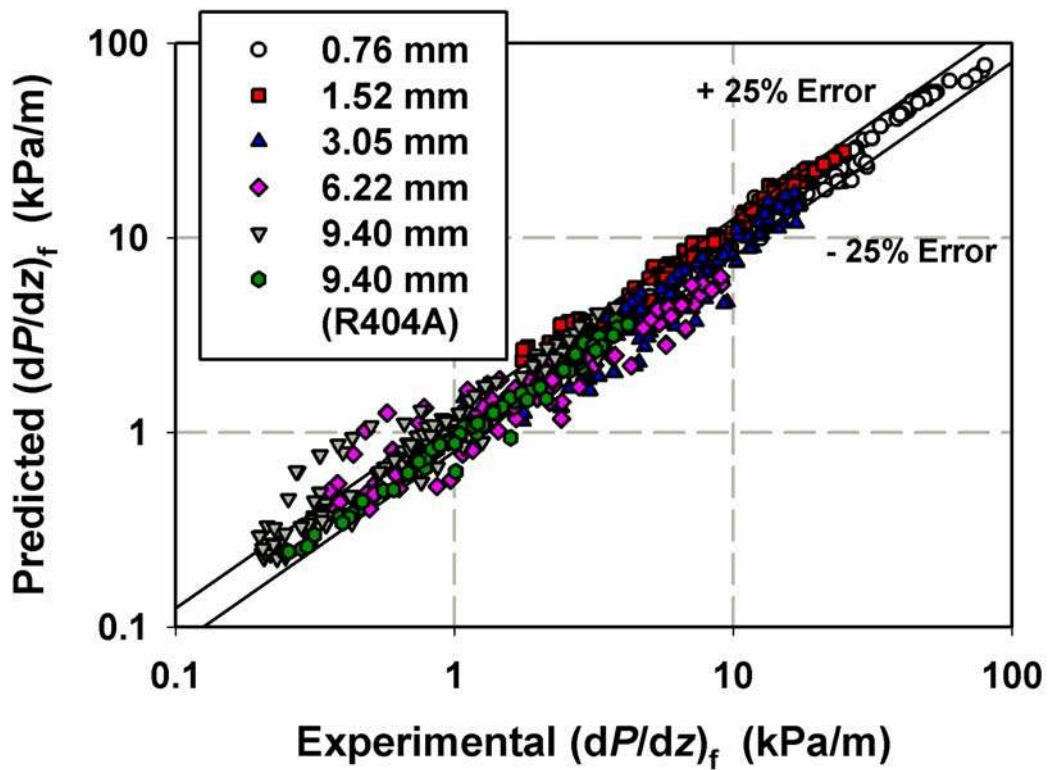
Figure 6.20: Overall Pressure Gradient Prediction

Overall, the model predicts 74% of the data in this study within ± 25%. The average deviation is 19%. The individual comparison plots for the data taken by this author are shown in Figure 6.21. Figure 6.22 shows the predictions for the data of Jiang (2004) and

Mitra (2005). The parametric variation in pressure drop resulting from this model will be discussed after the development of the heat transfer model.

Table 6.7: Prediction Statistics for Pressure Drop Model

Flow Regime	Average Deviation (%)	Data < 25% Deviation (%)
Liquid-Like	16	76
Pseudo-Critical-Transition	22	72
Gas-Like	16	76

.

6.3.3 Heat Transfer Model

The single-phase Nusselt number correlation by Churchill (1977) predicts the trends in the data well, although the deviations for small diameter tubes are significant. To further investigate the correlation between single-phase flow and the quasi single-phase flow in the supercritical state, the experimentally determined Nusselt numbers are plotted as a function of Re_{bulk} in Figure 6.23. The data were divided into two flow regimes based on the transition temperature. The data that are considered to be in the pseudo-critical-transition region are in solid colored symbols in the figure. The Reynolds numbers ranged from 2631 to 370,790 with 90.6% of the data (1437 points of out 1586) in the fully turbulent regime ($Re_{bulk} > 10,000$). Only a few points (149 or 9.4% of the data) are in the transitional flow between turbulent and laminar ($2100 < Re_{bulk} < 10,000$) and these are almost all in the liquid-like region. (Few data with $Re_{bulk} < 10,000$ are in the liquid-like region).
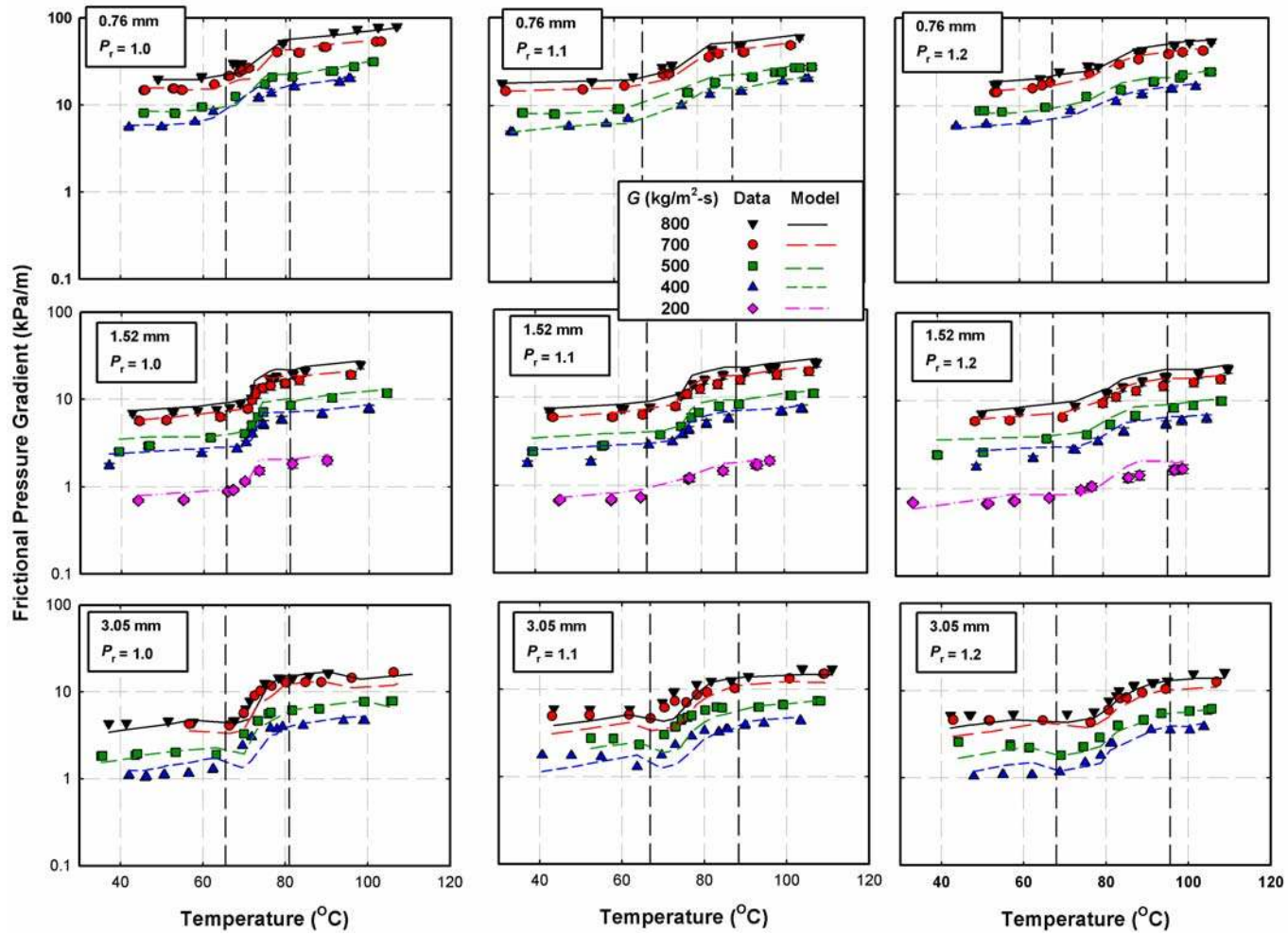
Figure 6.21: Pressure Gradient Prediction for *D* = 0.76 to 3.05 mm
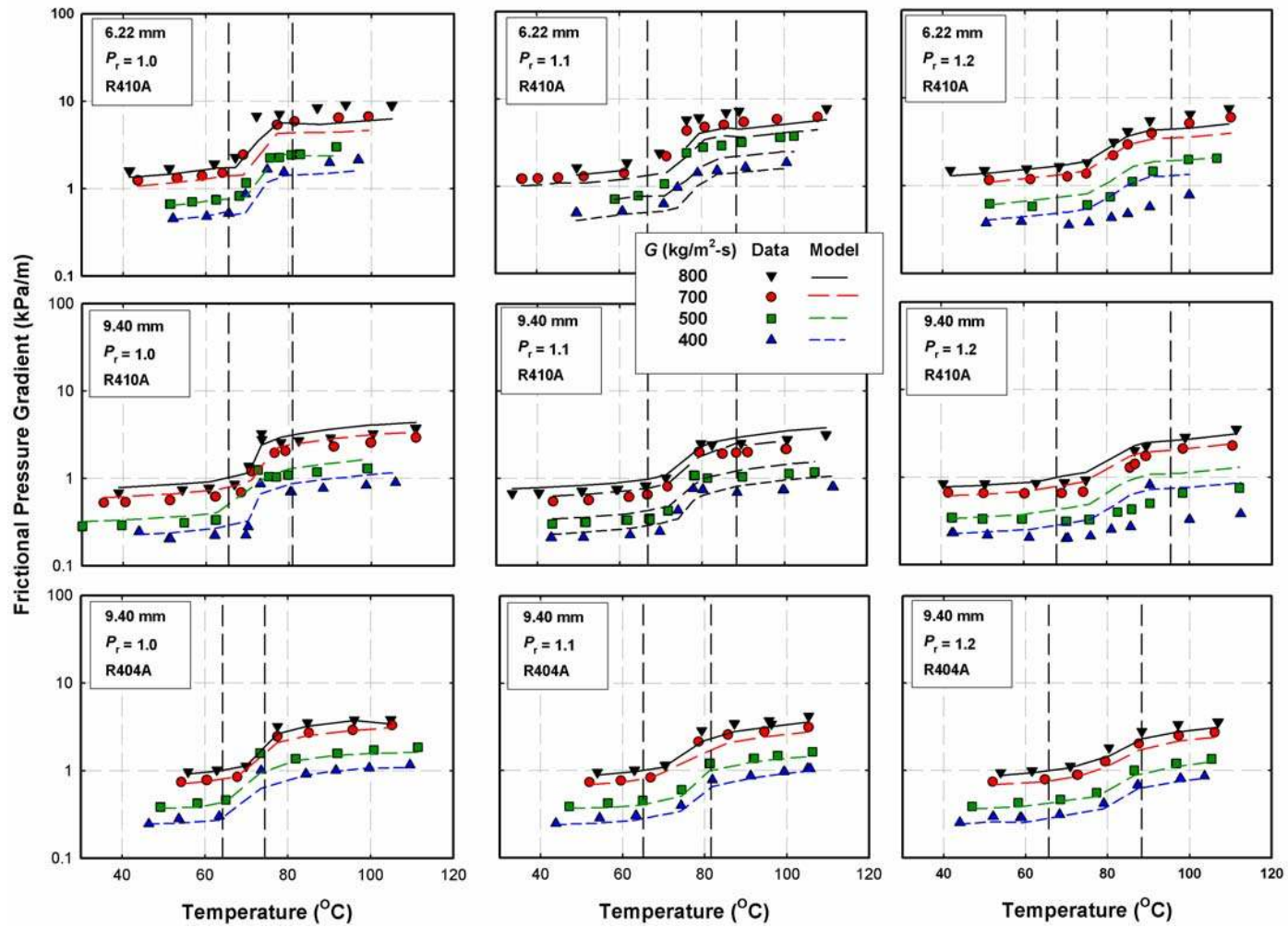
Figure 6.22: Pressure Gradient Prediction for Data of Jiang (2004) and Mitra (2005)
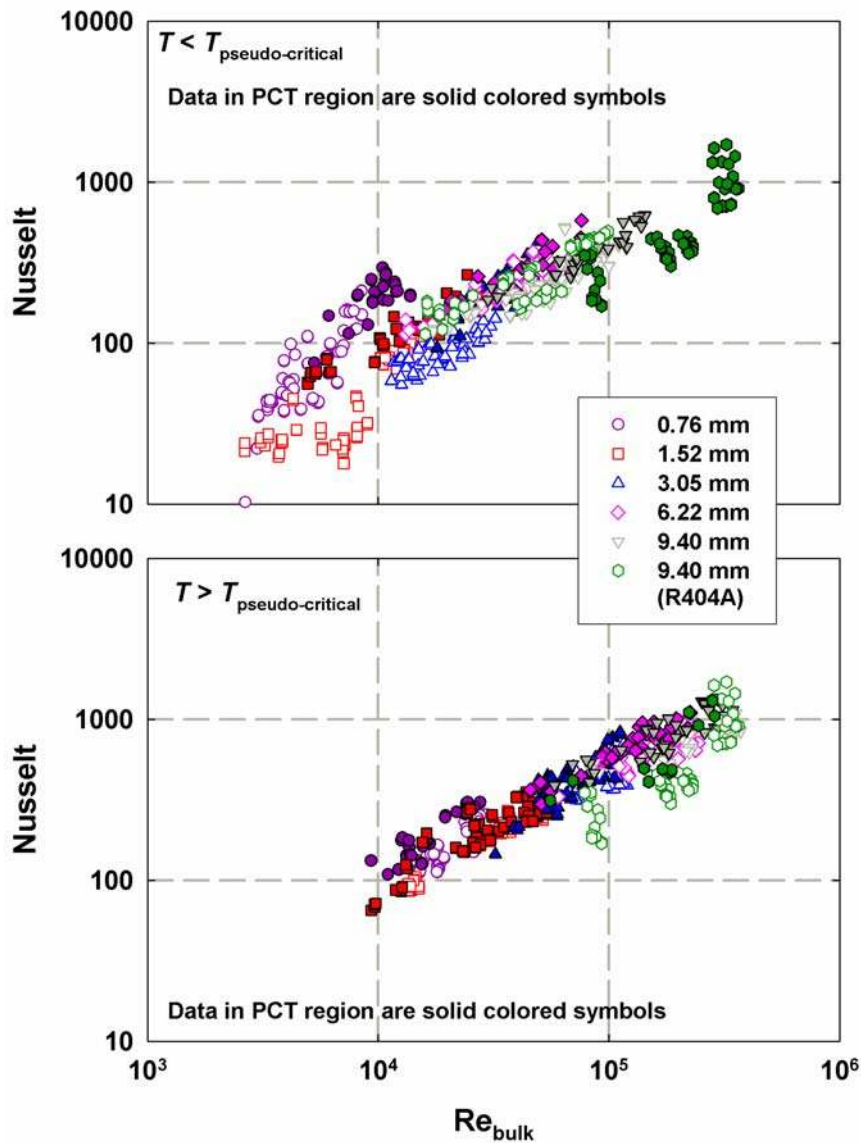
Figure 6.23: Experimental Nu versus Re$_{bulk}$

It should be observed in Figure 6.23 that for temperatures below the transition temperature, the dependence of the data on Re$_{bulk}$ changes with decreasing D. This is probably due to a change in the behavior of the flow. In smaller tubes, gravitational effects are not as significant, leading to a flow similar to annular flow (discussed in

Chapter 5), where the denser fluid surrounds the bulk flow. The higher conductivity of the fluid at the inner wall favors the heat transfer. In larger tubes, the flow may lack the highly conductive layer at the inner wall. For temperatures above the transition temperature, the Reynolds number dependence on D is not as dominant.

To model the heat transfer coefficients, Churchill's (1977) Nusselt number is used as a starting point, because it is valid for transitional and turbulent flow. The friction factor correlation developed in the previous section is substituted into Equation 6.10 to account for the property variations in the three different flow regimes: liquid-like, pseudo-critical transition, and gas-like.

$$\mathrm{Nu}_{\substack{\text{modified} \\ \text{Churchill}}} = \left[4.364^{10} + \left(\frac{\exp\left[\dfrac{2200 - \mathrm{Re}_{\text{bulk}}}{365} \right]}{4.364^2} + \left(6.3 + \frac{0.079 \cdot \left(\dfrac{f_{\text{modified}}}{8} \right)^{1/2} \cdot \mathrm{Re}_{\text{bulk}} \cdot \mathrm{Pr}_{\text{bulk}}}{\left(1 + \mathrm{Pr}_{\text{bulk}}^{0.8} \right)^{5/6}} \right)^{-2} \right)^{-5} \right]^{1/10}$$

To account for the increasing Nu at smaller diameters and lower Reynolds numbers, a $\mathrm{Re}_{\text{bulk}}$ multiplier is used in conjunction with $\mathrm{Nu}_{\substack{\text{modified Churchill}}}$, such that the proposed model has the form:

$$\mathrm{Nu} = a \cdot \mathrm{Nu}_{\substack{\text{modified} \\ \text{Churchill}}} \cdot \mathrm{Re}_{\text{bulk}}^{b + c/D^*} \tag{6.14}$$

where $D^* = \left(D / D_{\text{ref}} \right)$ and $D_{\text{ref}} = 9.40$ mm. The parameters a, b and c are determined from regression analysis for temperatures below and above the transition temperatures: $T < T_{\text{transition}}$ and $T > T_{\text{transition}}$.

Table 6.8: Regression Parameters for Heat Transfer Model

Flow Regime	a	b	c
$T < T_{transition}$	0.56	0.022	0.010
$T > T_{transition}$	0.19	0.118	0.011

Figure 6.24 shows the comparison of the experimental Nusselt number versus the predicted Nusselt number in this model. Overall, the model predicts 64% of the heat transfer coefficients within ± 25%; the average deviation for all data is 22%. Table 6.9 shows the prediction statistics of the heat transfer model.
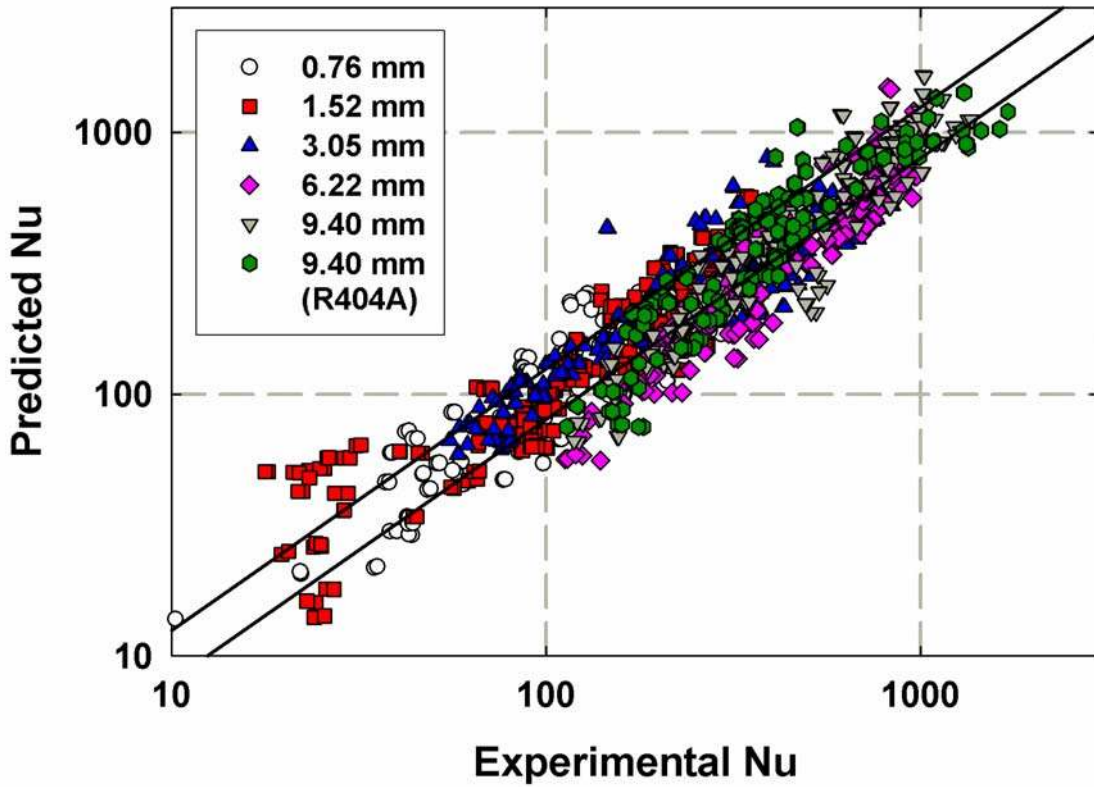
Figure 6.24: Overall Nusselt Number Prediction

Table 6.9: Prediction Statistics for Heat Transfer Model

Flow Regime	Average Deviation (%)	Data < 25% Deviation (%)
$T < T_{transition}$	22	66
$T > T_{transition}$	23	62

The predicted Nusselt numbers for all data are compared with the experimental values in Figure 6.25. In Figure 6.26, the individual trends in h as a function of T for the data taken by this author are shown. Similarly, Figure 6.27 shows the model predictions for the data taken by Jiang (2004) and Mitra (2005). Overall, the model captures all observed trends well.
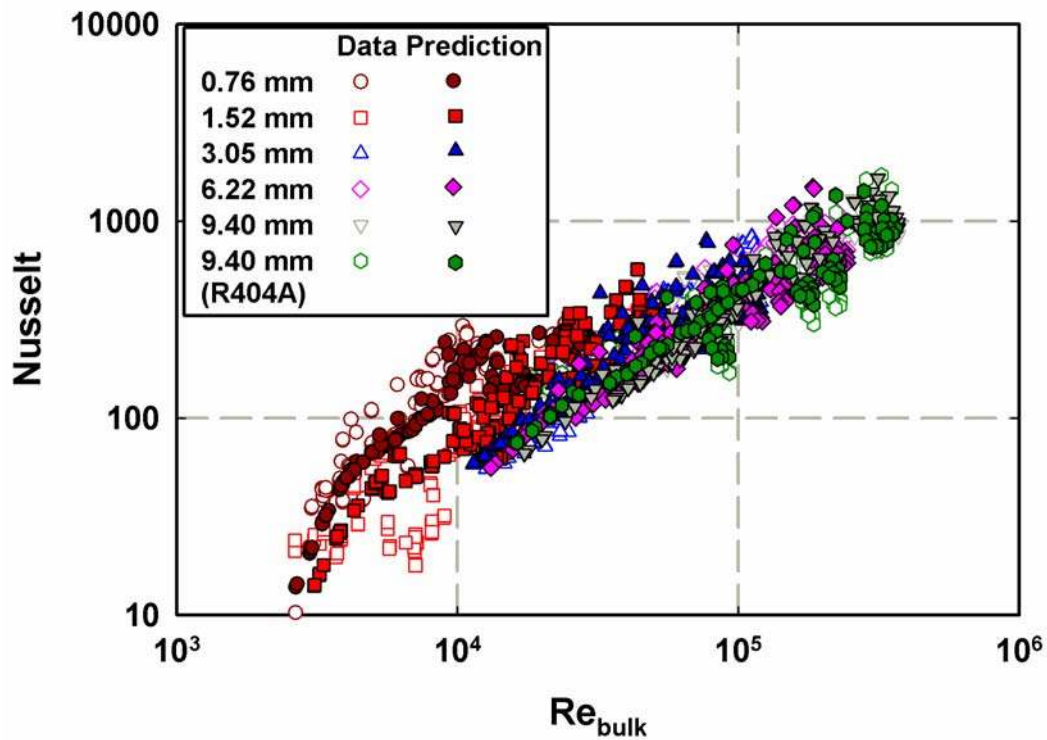
Figure 6.25: Predicted Nu versus Re$_{bulk}$
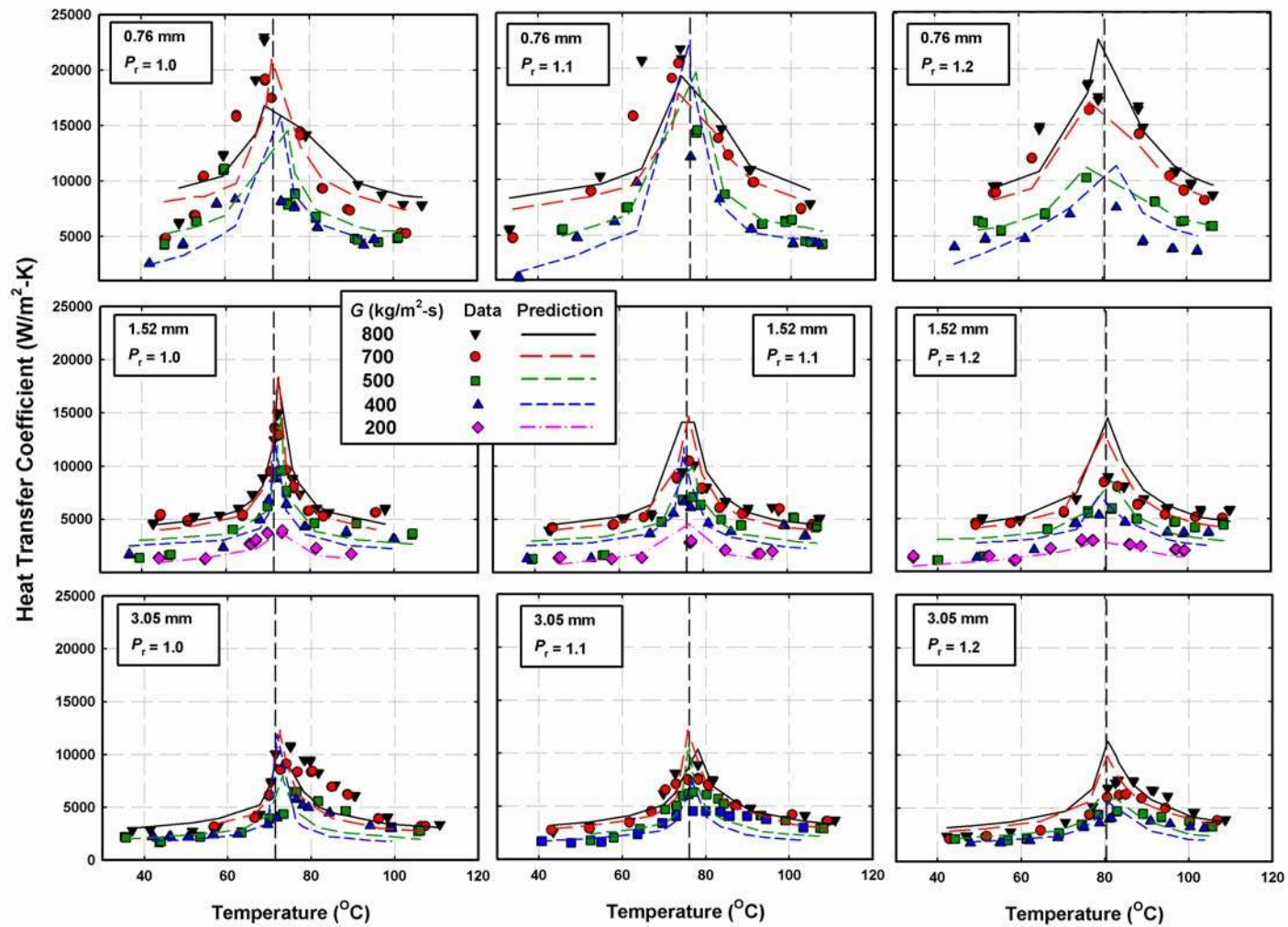
Figure 6.26: *h* Prediction for *D* = 0.76 to 3.05 mm
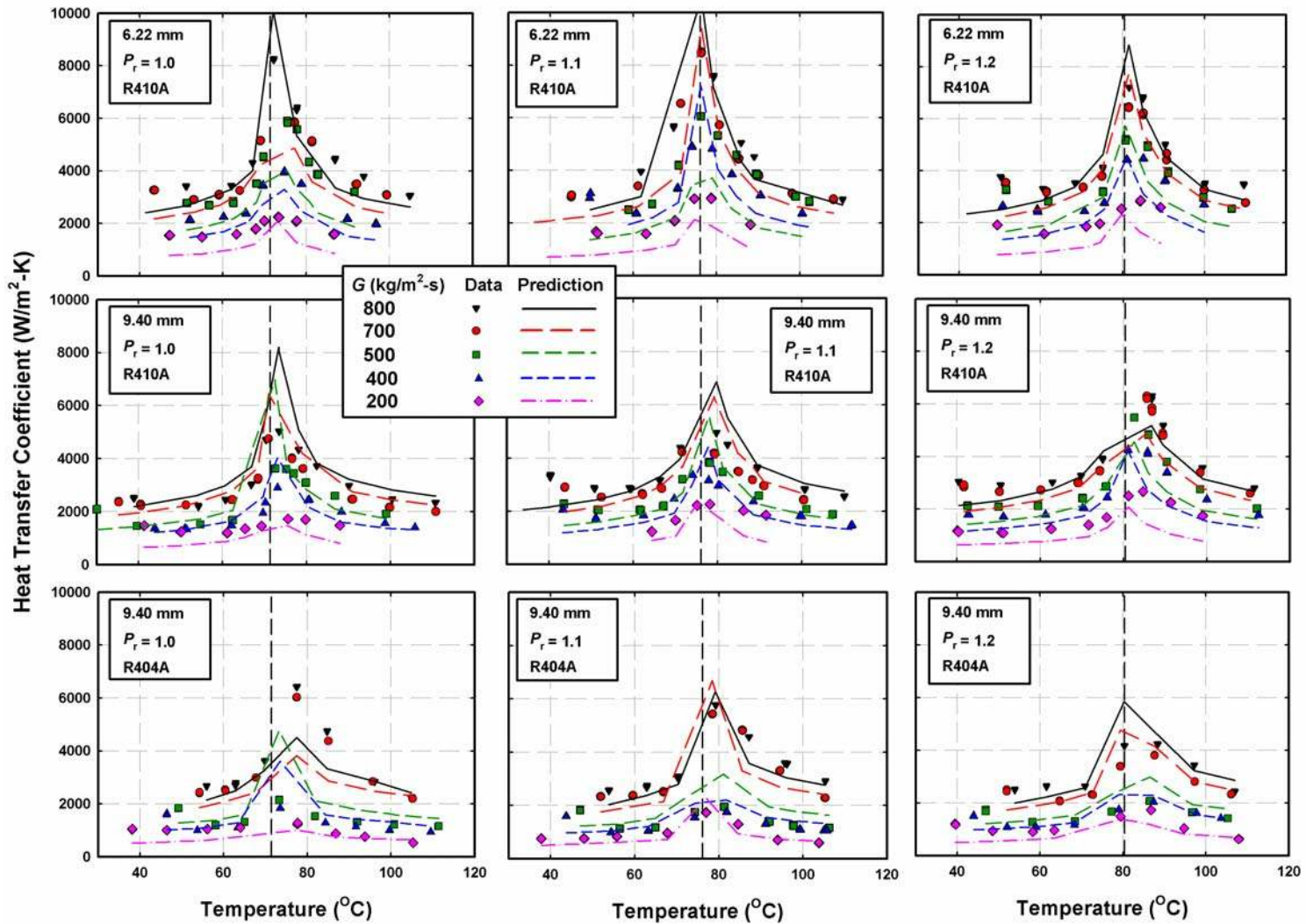
Figure 6.27: *h* Prediction for Data of Jiang (2004) and Mitra (2005)

The predictive capabilities of the friction factor and heat transfer models are discussed in the following section.

6.3.4 Parametric Evaluation and Interpretation of the Pressure Drop and Heat Transfer Models

To investigate the predictive capabilities of the models developed in this study, the friction factor and Nusselt number are plotted versus Re_{bulk} for three different tubes and reduced pressures $P_r = 1.0 - 1.2$ in Figure 6.28. Five representative temperatures are chosen to correspond to: the liquid-like flow regime ($T = 50°C$), the PCT regime with the bulk and wall temperature below the transition temperature ($T = T_{transition} - 2°C$), the bulk temperature above $T_{transition}$ and the wall temperature below the transition temperature ($T = T_{transition} + 2°C$), and two more temperatures in the gas-like regime: $T = T_{transition} + 21°C$ and $T = 120°C$. The assumed temperature differences between the bulk and wall temperatures for the three different diameters, $D = 0.76$, 3.05, and 9.40 mm, are 4°, 8° and 12°C, respectively. Increasing temperature differences are chosen for increasing diameters to reflect the lower heat transfer coefficients in these tubes. The Reynolds number ranges plotted in these graphs coincide with the experimentally obtained Re_{bulk} for the different tubes.

As expected, the friction factor continuously decreases, and the Nusselt number increases with increasing Reynolds number. In the friction factor plot, the effect of the temperature difference between T_{bulk} and T_{wall} becomes apparent. With an increase in $\Delta T = T_{bulk} - T_{wall}$

at any Reynolds number, the friction factor increases as a result of the increased shear within the flow.
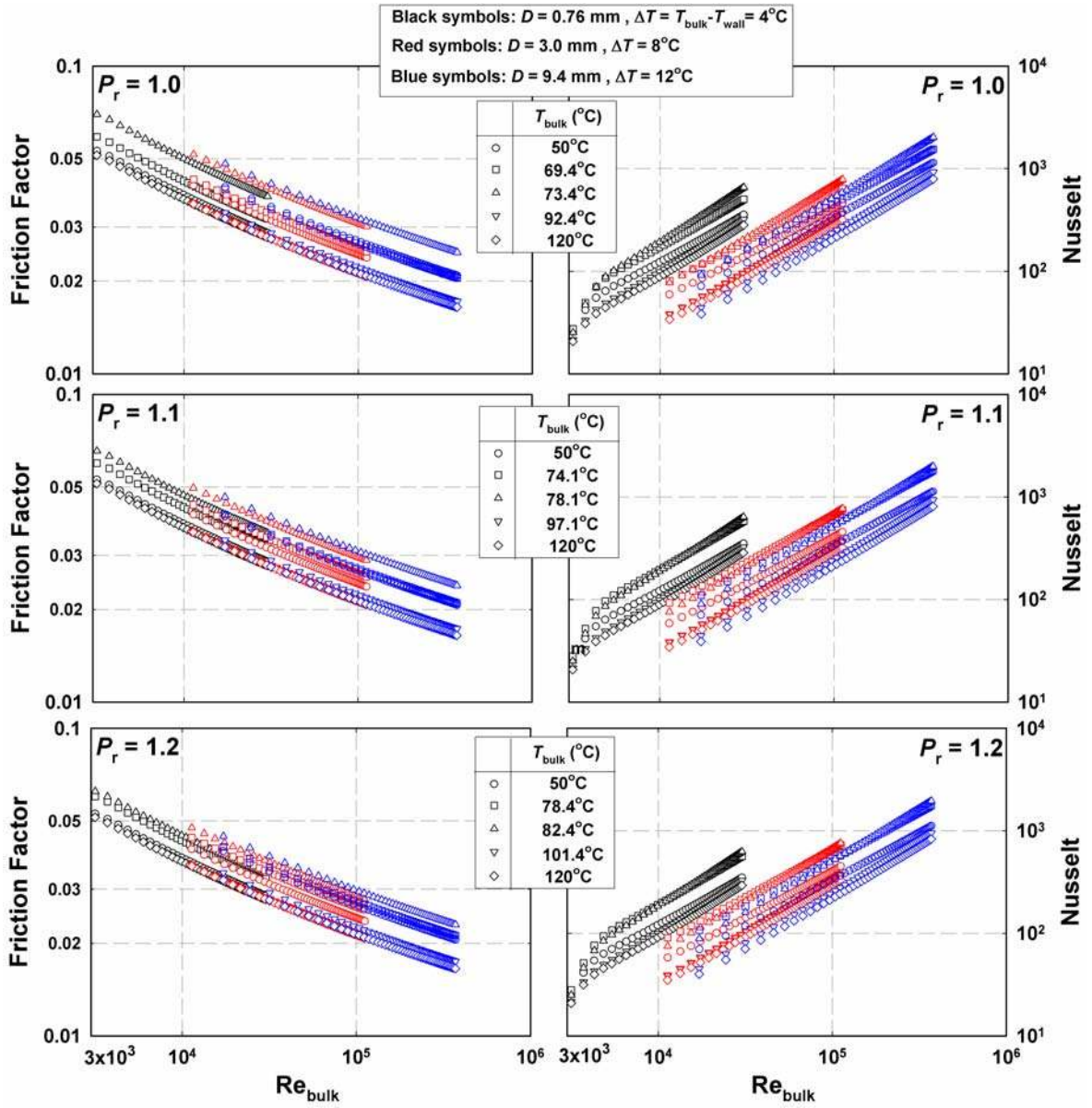
Figure 6.28: Friction Factor and Nu versus Re$_{bulk}$

Furthermore, it should be noted that the friction factor increases as the temperature of the flow approaches the transition temperature. When the bulk flow is above and the wall temperature below the transition temperature, the friction factor reaches a maximum, as the property differences between the two phases are most significant. When both the bulk and the wall flow are in the gas-like state, the friction factor coincides with the liquid-phase prediction. The same trend is observed for the Nusselt number. For the transition region, a higher Nu is predicted than for temperatures in the liquid-like and gas-like phases. The property variations between the bulk and wall temperatures are directly incorporated in the Nusselt number correlation, as the modified Churchill friction factor correlation with property correction factors is used in calculating the Nusselt number. For decreasing diameter, the Nusselt number increases due to the formation of a more conductive layer of fluid on the inner wall. It is suspected that gravitational effects result in a stratified flow for larger diameter tubes. These observations apply for the entire pressure range under investigation.

A parametric study was also conducted with one parameter varied at a time, keeping all others constant. For this parametric analysis, experimental data are used to assign bulk-to-wall temperature differences for each diameter and mass flux in each flow regime (liquid-like, PCT, and gas-like). The abrupt changes in slopes in these graphs correspond to changes in bulk-to-wall temperature difference and the associated steep changes in properties in the critical region. Table 6.10 shows the temperature differences used in these plots.

Table 6.10: Bulk-to-Wall Temperature Differences used in Parametric Study

	G (kg/m^2-s)	Liquid-Like (°C)	PCT (°C)	Gas-Like (°C)
	300	2.8	2.7	4.5
$D = 1$ mm	500	2.1	2.1	3.9
	700	2.3	1.6	3.2
	300	5.2	4.0	8.2
$D = 1.5$ mm	500	4.6	3.3	6.7
	700	2.9	3.5	6.2
	300	10.6	12.3	20.2
$D = 5$ mm	500	10.7	11.1	20.5
	700	6.0	7.7	16.8
	300	10.6	12.3	20.2
$D = 6$ mm	500	10.7	11.1	20.5
	700	6.0	7.7	16.8
	300	12.5	16.4	31.8
$D = 9$ mm	500	11.3	15.6	28.7
	700	11.4	14.9	27.8

Figure 6.29 shows the effect of varying diameter. With a decreasing diameter, the predicted pressure gradients and heat transfer coefficients increase for all mass fluxes. Figure 6.30 illustrates the effect of varying G. Increasing the mass flux corresponds to higher flow velocities, which increase the shear rate and lead to higher pressure gradients and heat transfer coefficients. The effects of pressure are characterized in Figure 6.31. The figure illustrates that the pressure gradients are the highest at the lowest pressure.

Also, the transition from liquid-like to the PCT region, and from the PCT region to the gas-like region, occur at higher temperatures corresponding to the increase in transition temperatures with pressure. In the liquid-like regime, the pressure gradients are essentially constant, as the thermo-physical properties do not vary significantly for the reduced pressure range of $P_r = 1.0 - 1.2$ and the temperature range in that flow regime. With the onset of changing properties in the pseudo-critical-transition region, a sharp increase in pressure gradient is predicted. The gas-like regime shows a steady increase with increasing temperature as the fluid slowly approaches ideal gas behavior. The peaks in the heat transfer coefficient coincide with the transition temperatures. The magnitude of the peaks decreases with an increase in P_r. This corresponds to the decrease in specific heat with increasing pressure as the fluid moves away from near-critical behavior. Figure 6.32 compares the effects of varying refrigerant properties. It is clear that the pressure gradient is only weakly dependent on the fluid type, with the pressure drops for the two fluids being almost the same. In the liquid-like regime, the pressure gradient for R404A is slightly higher than for R410A, since the viscosity is higher for R404A. For the temperature range $35°C \leq T \leq 60°C$, the viscosity ratio of $\mu_{R404A} / \mu_{R410A}$ at $P_r = 1.1$ is 1.06 on average. In the transition and gas-like region, the pressure gradients are close to one-another and cross at times. It should be noted that the temperatures dividing the flow regime, based on the fluid properties, differ slightly for R404A and R410A. For $P_r = 1.1$, the pseudo-critical-transition region for R404A is $65.05°C \leq T \leq 81.55°C$. For R410A, the temperature range is $66.81°C \leq T \leq 88.38°C$. The shift of flow regime onset to different temperatures in combination with the bulk-to-wall temperature differences used as inputs have the above-mentioned effect on the pressure gradient predictions. The heat

transfer coefficients for R404A are consistently lower than those for R410A due to the lower thermal conductivity. For example at $P_r = 1.0$, the thermal conductivity of R404A is 30% lower than the conductivity of R410A in the liquid-like regime.
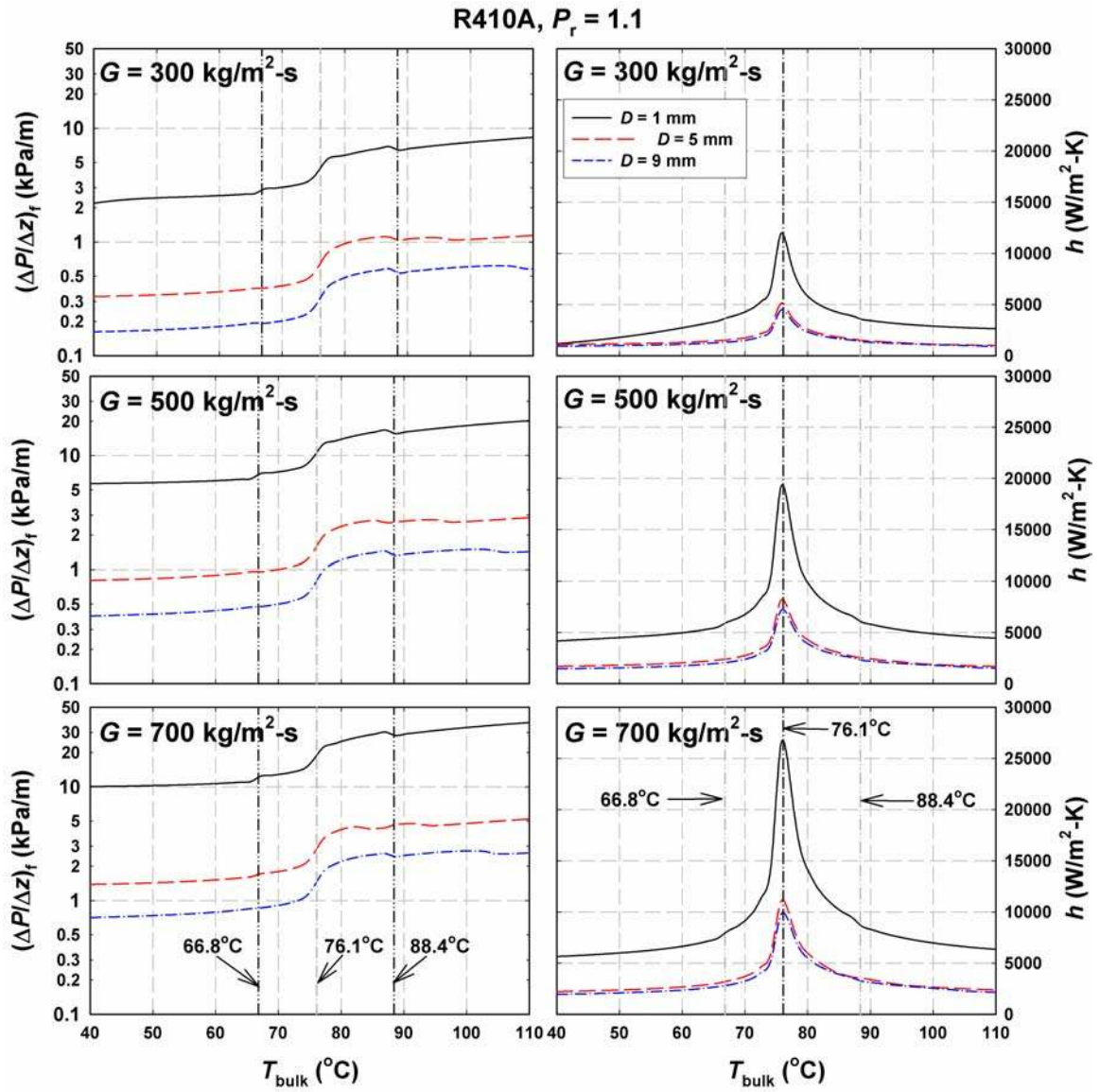
Figure 6.29: Influence of *D* on *h* and ΔP
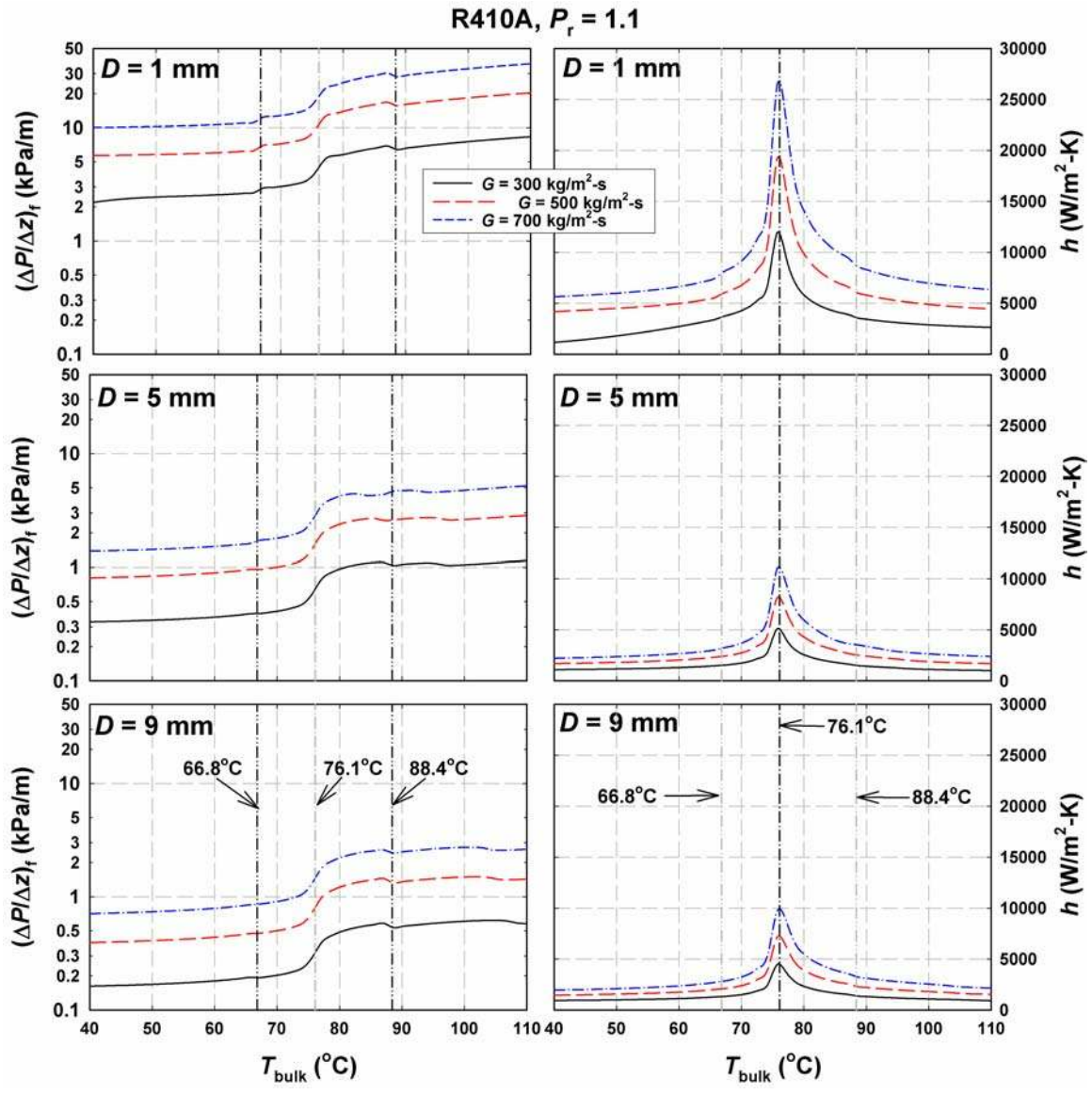
Figure 6.30: Influence of *G* on *h* and Δ*P*
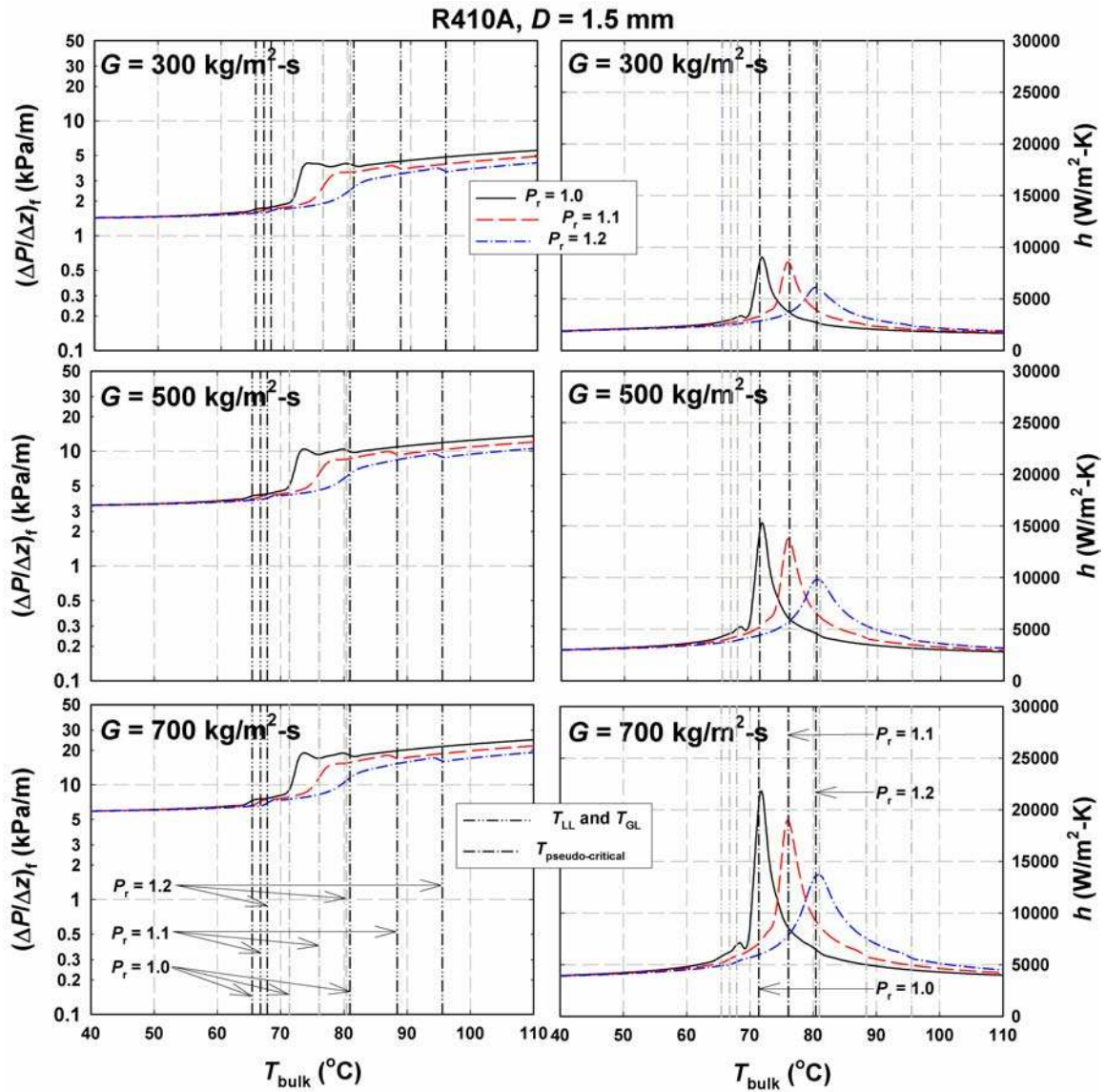
Figure 6.31: Influence of P_r on h and ΔP
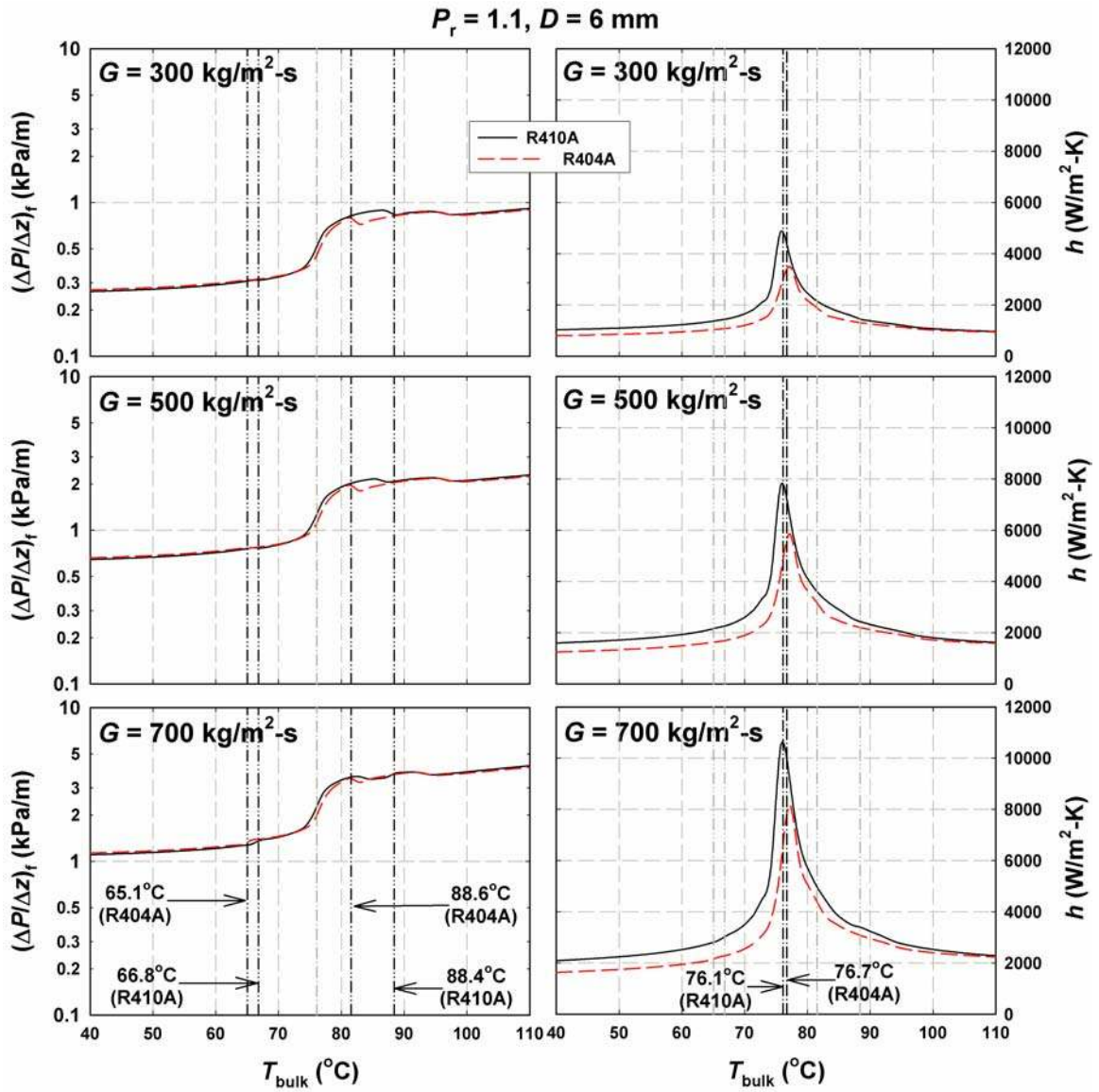
Figure 6.32: Influence of Refrigerant on h and ΔP

CHAPTER 7 - CONCLUSIONS

A comprehensive study of heat transfer and pressure drop in zero ozone-depletion-potential (ODP) refrigerant blends in small diameter tubes was conducted during condensation near the critical pressure at 0.8, $0.9 \times P_{critical}$ and gas cooling at 1.0, 1.1, $1.2 \times P_{critical}$. Heat transfer coefficients and pressure drops for R410A were determined experimentally during condensation across the entire vapor-liquid dome in three different round tubes ($D = 3.05, 1.52, 0.76$ mm) over a mass flux range of $200 < G < 800$ kg/m^2-s. A thermal amplification technique was used to accurately determine the heat duty for condensation in small quality increments or supercritical cooling across small temperature changes while ensuring low uncertainties in the refrigerant heat transfer coefficients. The data from this study were used in conjunction with data obtained under similar operating conditions for refrigerants R404A and R410A in tubes of diameter 6.22 and 9.40 mm to develop models to predict heat transfer and pressure drop in tubes with diameters ranging from 0.76 to 9.40 mm during condensation. Similarly, in the supercritical states, heat transfer and pressure drop models were developed to account for the sharp variations in the thermophysical properties near the critical point.

Based on the existing flow regime maps in the literature, it was assumed that condensation would occur in the annular or wavy flow regime. The flow was assigned to annular or wavy flow regimes, with the transition occurring at $J_G = 2.5$, as proposed by Cavallini *et al.* (2002). For implementation of the heat transfer model, $J_G > 3.0$ corresponds to purely annular flow, while for $J_G < 2.0$, the wavy flow regime model

should be used. An interpolation technique is used for $2.0 < J_G < 3.0$. The wavy flow heat transfer model considers film condensation with subcooling on the inner wall in addition to the forced convection in the liquid pool at the bottom of the tube.

$$\mathrm{Nu}_{\mathrm{wavy}} = \frac{h_{\mathrm{wavy}} D}{k_1} = \left(\frac{1.93}{2\pi}\right)\left(\mathrm{Ra}\cdot\left(\frac{1}{\mathrm{Ja}}+1\right)\right)^{1/4}$$
$$+ 0.018\,\mathrm{Re}_L^{0.8}\cdot\mathrm{Pr}_L^{1/3}\cdot\left[1+\left(\frac{x}{1-x}\right)\left(\frac{\rho_1}{\rho_v}\right)^{1.24}\right]\left(\frac{D}{9.398\ \mathrm{mm}}\right)^{0.34}\cdot\left(1-\frac{\theta}{2\pi}\right)$$

where θ is a function of Baroczy's (1965) void fraction model: $\theta = f\left(\alpha_{\mathrm{Baroczy}}\right)$.

The annular flow model assumes symmetric shear driven flow with no entrainment.

$$\mathrm{Nu}_{\mathrm{annular}} = \frac{h_{\mathrm{annular}} D}{k_1} = 0.0133\cdot\mathrm{Re}_L^{4/5}\cdot\mathrm{Pr}_L^{1/3}\cdot\left[1+\left(\frac{x}{1-x}\right)^{0.80}\left(\frac{\rho_1}{\rho_v}\right)^{0.88}\right]$$

The two-phase pressure drop is modeled by means of the liquid pressure gradient and a two-phase multiplier. The two-phase multiplier is a function of the Reynolds number, Martinelli parameter and the confinement number.

$$\phi_L^2 = 1 + \frac{24\cdot\mathrm{Re}_L^{-0.3}\cdot N_{\mathrm{conf}}^{-0.4}}{X} + \frac{1}{X^2}$$

This pressure drop model is applicable for all flow regimes. Overall, the heat transfer and pressure models predicted 91% and 85% of the data within 25%, respectively. The average deviations for the two models were 12 and 14%.

To account for the sharp variations in the thermophysical properties in the supercritical region, the flow was divided into three different regimes by means of the specific work of thermal expansion, as introduced by Kurganov (1998a, 1998b). Churchill's (1977)

friction factor correlation was modified with a bulk-to-wall viscosity multiplier to account for the corresponding variations in the properties of the fluid.

$$f = a \cdot f_{\text{Churchill}} \cdot \left(\frac{\mu_{\text{wall}}}{\mu_{\text{bulk}}} \right)^b$$

The heat transfer model used the modified friction factor in Churchill's (1977) Nusselt number correlation. To account for the increase in Nusselt numbers for the small diameter tubes, a Reynolds number multiplier with a diameter dependent exponent was used as follows:

$$\text{Nu} = a \cdot \text{Nu}_{\substack{\text{modified} \\ \text{Churchill}}} \cdot \text{Re}_{\text{bulk}}^{b + c/D^*}$$

where $D^* = (D/D_{\text{ref}})$ and $D_{\text{ref}} = 9.40$ mm. The pressure drop and heat transfer models predicted 74% and 64% of the data within 25%, respectively. The average deviations were 19% and 22%, respectively.

The understanding gained from this study will aid the HVAC industry in developing safe, cost-effective, and energy efficient high-temperature-lift space-conditioning and water-heating systems with less adverse impact on the environment.

Recommendations for Future work:

The work presented here establishes a comprehensive basis for the evaluation of heat transfer and pressure drop at near-critical condensing and supercritical cooling conditions. However, the models were based on heat transfer and pressure drop measurements, but without direct visualization of the flow mechanisms. It is therefore suggested that flow visualization experiments be conducted during condensation at high

reduced pressures, which will corroborate the inferences made about the applicable flow mechanisms for the models developed in the present study. The models are implicitly depend on the void fractions in condensing flows, for which correlations from the literature were used here. Measurement of void fractions at the high reduced pressures of interest in the present study would further improve the heat transfer and pressure drop predictions. Similarly, flow visualization experiments at supercritical conditions would assist in better delineation of the liquid-like, gas-like and pseudo-critical transition regimes, and perhaps reveal the potential for stratification of the flow under specific conditions, particularly in the larger diameter tubes. It should be noted that flow visualization experiments for condensation and supercritical cooling pose several challenges. The test sections need to be transparent and able to withstand pressures up to 5900 kPa (P_r = 1.2 for R410A). Furthermore, visualization must be of condensing or supercritical cooling, not simply of adiabatic flow, and the heat duty in the transparent visualization section must be measured. Such experiments were conducted by Coleman and Garimella (2003) for the condensation of R134a in $1 < D_h < 5$ mm channels, although the highest pressure tested was only 1725 kPa.

Finally, the present study was conducted with refrigerant R410A as the working fluid, and also included some data collected by previous investigators on refrigerant R404A. The models developed in this study would benefit from experiments on other fluids with different properties, so that their range of applicability can be extended further.

APPENDIX A – UNCERTAINTY PROPAGATION

An EES code was developed to estimate all necessary uncertainties in the data analysis. To illustrate the propagation of the uncertainties, sample calculations are shown below. The uncertainties are denoted by a U with the appropriate subscript. For example., the refrigerant heat transfer coefficient uncertainty is labeled U_{h_r}. The sample calculations below accompany the condensation calculations in the 3.05 mm test section (Run 29 on 06 September 2005), presented in Chapter 4.

A.1 Heat Duty Uncertainty

The heat duty in the test section, is given by Equation 4.16: $\dot{Q}_{test} = \dot{Q}_{sec} + \dot{Q}_{loss,ambient} - \dot{Q}_{pump}$, and is a function of the heat duty in the secondary heat exchanger, $\dot{Q}_{sec}$, the heat losses to the ambient, $\dot{Q}_{loss,ambient}$, and the heat input by the water pump, $\dot{Q}_{pump}$ and the corresponding uncertainties. The uncertainties in $\dot{Q}_{loss,ambient}$ and $\dot{Q}_{pump}$ are assumed to be $\pm 50\%$ of the calculated values. The uncertainty in the secondary heat exchanger heat duty, $U_{\dot{Q}_{sec}}$, is a function of the mass flow rate as well as the water enthalpies at the inlet and outlet of the heat exchanger. The uncertainties in enthalpy at the inlet, $i_{w,sec,in}$, and outlet, $i_{w,sec,out}$, are assumed to be functions of the respective water temperature uncertainties only:

$$\left(U_{\dot{Q}_{sec}}\right)^2 = \left(\frac{\partial \dot{Q}_{sec}}{\partial \dot{m}_{sec}} U_{\dot{m}_{sec}}\right)^2 + \left(\frac{\partial \dot{Q}_{sec}}{\partial i_{w,sec,in}} U_{i_{w,sec,in}}\right)^2 + \left(\frac{\partial \dot{Q}_{sec}}{\partial i_{w,sec,out}} U_{i_{w,sec,out}}\right)^2 \quad (8.1)$$

By differentiation, Equation 8.1 simplifies to:

$$\left(U_{\dot{Q}_{sec}}\right)^2 = \left(\Delta i_{w,sec} \cdot U_{\dot{m}_{sec}}\right)^2 + \left(\dot{m}_{sec} \cdot U_{i_{w,sec,in}}\right)^2 + \left(\dot{m}_{sec} \cdot U_{i_{w,sec,out}}\right)^2$$

The Coriolis mass flow meter uncertainty is ± 0.15% of the measured value, resulting in $U_{\dot{m}_{sec}} = 0.002 \times 10^{-3}$ kg/s (Table 4.2). The uncertainties in the enthalpies are determined in Equations 8.2 and 8.3.

$$\left(U_{i_{w,sec,in}}\right)^2 = \left(\frac{\partial i_{w,sec,in}}{\partial T_{w,sec,in}} U_{T_{w,sec,in}}\right)^2 = \left(c_p U_{T_{w,sec,in}}\right)^2 \tag{8.2}$$

$$\left(U_{i_{w,sec,out}}\right)^2 = \left(\frac{\partial i_{w,sec,out}}{\partial T_{w,sec,out}} U_{T_{w,sec,out}}\right)^2 = \left(c_p U_{T_{w,sec,out}}\right)^2 \tag{8.3}$$

The temperature measurement uncertainty at the inlet and outlet are $U_{T_{w,sec,in}} = U_{T_{w,sec,out}} = 0.5°C$, resulting in: $\left(U_{i_{w,sec,in}}\right)^2 = \left(U_{i_{w,sec,out}}\right)^2 = 2.1$ kJ/kg. Substituting all quantities into Equation 8.1 yields:

$$\left(U_{\dot{Q}_{sec}}\right)^2 = \left(51.03 \text{ kJ/kg} \cdot 2 \times 10^{-6} \text{ kg/s}\right)^2 + 2\left(1.697 \times 10^{-3} \text{ kg/s} \cdot 2.1 \text{ kJ/kg}\right)^2$$
$$= 2.54 \times 10^{-5} \text{ kW}^2$$

As stated in Chapter 4, $U_{\dot{Q}_{sec}} = 5.02$ W (5.8%).

The test section heat duty uncertainty is given in Equation 8.4:

$$\left(U_{\dot{Q}_{test}}\right)^2 = \left(\frac{\partial \dot{Q}_{test}}{\partial \dot{Q}_{sec}} U_{\dot{Q}_{sec}}\right)^2 + \left(\frac{\partial \dot{Q}_{test}}{\partial \dot{Q}_{loss,ambient}} U_{\dot{Q}_{loss,ambient}}\right)^2 + \left(\frac{\partial \dot{Q}_{test}}{\partial \dot{Q}_{pump}} U_{\dot{Q}_{pump}}\right)^2 \tag{8.4}$$

Differentiating Equation 8.4, results in:

$$\left(U_{\dot{Q}_{test}}\right)^2 = \left(U_{\dot{Q}_{sec}}\right)^2 + \left(U_{\dot{Q}_{loss,ambient}}\right)^2 + \left(U_{\dot{Q}_{pump}}\right)^2$$

The uncertainties in the heat losses to the ambient, $U_{\dot{Q}_{loss,ambient}}$, and the heat input by the water pump, $U_{\dot{Q}_{pump}}$, are assumed to be ± 50% of their corresponding values. As stated in

Chapter 4, $U_{\dot{Q}_{\text{loss,ambient}}}$ = 9 W and $U_{\dot{Q}_{\text{pump}}}$ = 5.04W. Substituting all uncertainties into Equation 8.4 gives:

$$\left(U_{\dot{Q}_{\text{test}}}\right)^2 = \left(5.02 \text{ W}\right)^2 + \left(9 \text{ W}\right)^2 + \left(5.04 \text{ W}\right)^2 = 132 \text{ W}^2$$

This leads to an uncertainty in the test section heat duty of $U_{\dot{Q}_{\text{test}}}$ = 11.5 W (12.1%). From

Equation 4.27: $\dot{Q}_{\text{test}} = \left(UA\right)\left(\text{LMTD}\right)$, and U_{LMTD} = 0.35°C, which yields an uncertainty in

the overall heat conductance: U_{UA} = 1.06 W/K (12.6%).

A.2 Heat Transfer Coefficient Uncertainty

Neglecting the uncertainties in the effective heat transfer area, the wall resistance and the heat transfer correlations at the test section ends, the refrigerant heat transfer coefficient uncertainty is a function of the uncertainties in UA and h_{annulus}.

$$\left(U_{h_{\text{r}}}\right)^2 = \left(\frac{\partial h_{\text{r}}}{\partial h_{\text{annulus}}} U_{h_{\text{annulus}}}\right)^2 + \left(\frac{\partial h_{\text{r}}}{\partial UA} U_{UA}\right)^2 \tag{8.5}$$

In this case, h_{annulus} = 10100 W/m²-K, with an assumed uncertainty of ± 25%: $U_{h_{\text{annulus}}}$ = 2525 W/m²-K. The refrigerant-side heat transfer coefficient uncertainty is determined to be $U_{h_{\text{r}}}$ = 1069 W/m²-K. For the heat transfer coefficient of h_{r} = 5440 W/m²-K, this represents an uncertainty of 19.6%.

A.3 Frictional Pressure Drop Uncertainty

The frictional pressure drop is deduced from Equation 4.40:

$\Delta P_{\text{measured}} = \Delta P_{\text{f}} - \left|\Delta P_{\text{deceleration}}\right| + \Delta P_{\text{contraction}} - \Delta P_{\text{expansion}}$.

The uncertainty in the frictional pressure drop, $U_{\Delta P_f}$, is determined by Equation 8.6:

$$\left(U_{\Delta P_f}\right)^2 = \left(\frac{\partial \Delta P_f}{\partial \Delta P_{\text{measured}}} U_{\Delta P_{\text{measured}}}\right)^2 + \left(\frac{\partial \Delta P_f}{\partial \Delta P_{\text{deceleration}}} U_{\Delta P_{\text{deceleration}}}\right)^2$$
$$+ \left(\frac{\partial \Delta P_f}{\partial \Delta P_{\text{contraction}}} U_{\Delta P_{\text{contraction}}}\right)^2 + \left(\frac{\partial \Delta P_f}{\partial \Delta P_{\text{expansion}}} U_{\Delta P_{\text{expansion}}}\right)^2 \tag{8.6}$$

where the uncertainties in the deceleration, contraction and expansion pressure drops are assumed to be ± 50% of the calculated values. The measured pressure drop uncertainty, $U_{\Delta P_{\text{measured}}}$, is ± 0.075% of the span of the differential pressure transducer. Equation 8.6 reduces to the following expression:

$$\left(U_{\Delta P_f}\right)^2 = \left(U_{\Delta P_{\text{measured}}}\right)^2 + \left(U_{\Delta P_{\text{deceleration}}}\right)^2 + \left(U_{\Delta P_{\text{contraction}}}\right)^2 + \left(U_{\Delta P_{\text{expansion}}}\right)^2 \tag{8.7}$$

For the data point of interest, $U_{\Delta P_{\text{contraction}}} = 0.7895$ kPa, $U_{\Delta P_{\text{expansion}}} = 0.2302$ kPa and $U_{\Delta P_{\text{measured}}} = 0.0046$ kPa. Substituting the respective uncertainties into Equation 8.7 gives:

$$\left(U_{\Delta P_f}\right)^2 = \left(0.0046 \text{ kPa}\right)^2 + \left(0.2025 \text{ kPa}\right)^2 + \left(0.7895 \text{ kPa}\right)^2 + \left(0.2302 \text{ kPa}\right)^2$$

The uncertainty, $U_{\Delta P_f}$, is 0.847 kPa. It is apparent that uncertainty in the measured pressure drop is small compared to the other values; it contributes only 0.5% of the total uncertainty. Neglecting any error in measurement in the length of the test section ($L_{\text{test}} = 323.8$ mm), the frictional pressure gradient uncertainty is $U_{\nabla P_f} = 2.616$ kPa/m ($U_{\nabla P_f} / \nabla P_f = 23\%$). The average uncertainty in all test sections for condensing flow is 11.5%, with the highest uncertainties in the 3.05 mm test section due to the lower contribution of frictional pressure drop in this large diameter test section compared to the end effects.

APPENDIX B – PHASE CHANGE HEAT TRANSFER AND PRESSURE DROP

IN 3.05 mm TEST SECTION: SAMPLE CALCUALATIONS

Table B.1 - Measured Variables

Primary Loop	
$T_{w,test,in}$ (°C)	49.69
$T_{w,test,out}$ (°C)	50.01
$\dot{V}_{w,prim}$ (m³/s)	6.618×10^{-5}

Secondary Loop	
$T_{w,sec,i}$ (°C)	36.84
$T_{w,sec,o}$ (°C)	49.05
$\dot{m}_{w,sec}$ (kg/s)	1.697×10^{-3}

Pre-Condenser	
$T_{w,pre,in}$ (°C)	30.07
$T_{w,pre,out}$ (°C)	66.54
$\dot{V}_{w,pre}$ (m³/s)	3.787×10^{-6}

Post-Condenser	
$T_{w,post,in}$ (°C)	30.10
$T_{w,post,out}$ (°C)	59.32
$\dot{V}_{w,post}$ (m³/s)	3.33×10^{-6}

Refrigerant Loop	
$P_{r,pre,in}$ (kPa)	3927
$P_{r,test,in}$ (kPa)	3926
$P_{r,test,out}$ (kPa)	3926
$P_{r,post,out}$ (kPa)	3924
$\Delta P_{r,test}$ (kPa)	4.362
$T_{r,pre,in}$ (°C)	100.30
$\Delta T_{sup,pre}$ (°C)	39.21
$T_{r,pre,out}$ (°C)	62.17
$T_{r,test,in}$ (°C)	61.37
$Error_{r,test,in}$ (°C)	0.30
$T_{r,test,out}$ (°C)	61.01
$Error_{r,test,out}$ (°C)	0.06
$T_{r,post,in}$ (°C)	60.20
$T_{r,post,out}$ (°C)	56.78
$\Delta T_{sub,post}$ (°C)	4.19
$\dot{m}_r$ (kg/s)	5.847×10^{-3}

Table B.2 – Other Parameters

Data Point	
P_r	0.8008
$P_{critical}$ (kPa)	4903
G (kg/m²-s)	801.3
$x_{r,test,avg}$	0.6531
Date of Experiment	06 Sept 05
Run of Experiment	29

Assumed Variables	
P_w (kPa)	275.8
$T_{ambient}$ (°C)	23.0
$P_{ambient}$ (kPa)	101.0
ε_{ins}	0.85

Heat Transfer Calculations: 06 September 2005 – Run 29		
Inputs	**Equations**	**Results**
Heat Losses in Pre-Condenser (Shell-and-Tube)		
$D_{pre,o,s}$ = 38.1 mm $D_{pre,i,s}$ = 34.8 mm $D_{pre,ins,s}$ = 100 mm $k_{pre,s}$ = 14.9 W/m-K (SS) k_{ins} = 0.043 W/m-K $L_{pre,s}$ = 460 mm ε_{ins} = 0.85 σ = 5.67 x 10^{-8} W/m^2-K^4 $T_{ambient}$ = 23.0°C g = 9.81 kg-m/s^2 $P_{ambient}$ = 101 kPa $T_{w,pre,in}$ = 30.07°C $T_{w,pre,out}$ = 66.54°C	$R_{wall} = \dfrac{\ln\left(\dfrac{D_{pre,o,s}}{D_{pre,i,s}}\right)}{2\pi k_{pre,s} L_{pre,s}}$	R_{wall} = 2.103 ×10^{-3} K/W
	$R_{ins} = \dfrac{\ln\left(\dfrac{D_{pre,ins,s}}{D_{pre,o,s}}\right)}{2\pi k_{ins} L_{pre,s}}$	R_{ins} = 7.756 K/W
	$R_{radiation} = \dfrac{1}{\varepsilon_{ins}\pi D_{pre,ins,s} L_{pre,s}\sigma\left(T^2_{ins} + T^2_{ambient}\right)\left(T_{ins} + T_{ambient}\right)}$	$R_{radiation}$ = 1.362 K/W T_{ins} = 25.64°C (solved by iteration)
	$T_{avg} = (T_{ins} + T_{ambient})/2$	T_{avg} = 24.32°C
	$Pr_{air}, \nu_{air}, \alpha_{air}, k_{air}, \beta_{air} = f\left(T_{avg}, P_{ambient}\right)$	Pr_{air} =0.7297 , ν_{air} = 1.560 ×10^{-5} m^2/s α_{air} = 2.138 ×10^{-5} m^2/s, k_{air} = 0.02546 W/m-K β_{air} = 0.003362 1/K
	By assuming a negligible convective resistance in coolant: $T_{inner\,wall} = (T_{w,pre,in} + T_{w,pre,out})/2$	$T_{inner\,wall}$ = 48.31°C
	$Ra = \dfrac{g\beta_{air}\left(T_{ins} - T_{ambient}\right)D^3_{pre,\,ins,\,s}}{\nu_{air}\alpha_{air}}$	Ra = 261200

Heat Transfer Calculations: 06 September 2005 – Run 29		
Inputs	**Equations**	**Results**
	$$\mathrm{Nu} = \frac{h_{\text{nat.conv.}} D_{\text{ins}}}{k_{\text{air}}} = \left(0.60 + \frac{0.387 \mathrm{Ra}^{1/6}}{\left[1 + \left(\frac{0.559}{\mathrm{Pr}_{\text{air}}} \right)^{9/16} \right]^{8/27}} \right)^2$$ (Churchill and Chu, 1975)	$\mathrm{Nu} = 10.08$ $h_{\text{nat.conv.}} = 2.565$ W/m^2-K
	$R_{\text{nat.conv.}} = \dfrac{1}{h_{\text{nat.conv.}} \pi D_{\text{ins}} L_{\text{pre, s}}}$	$R_{\text{nat.conv.}} = 2.695$ K/W
	$\dot{Q}_{\text{loss, pre}} = \dfrac{\left(T_{\text{inner wall}} - T_{\text{ambient}} \right)}{R_{\text{wall}} + R_{\text{ins}} + \left(\dfrac{R_{\text{nat.conv.}} R_{\text{radiation}}}{R_{\text{nat.conv.}} + R_{\text{radiation}}} \right)}$	$\dot{Q}_{\text{loss, pre}} = 2.921$ W
Heat Losses in Post-Condenser (Shell-and-Tube)		
$D_{\text{post,o,s}} = 38.1$ mm $D_{\text{post,i,s}} = 34.8$ mm $D_{\text{post,ins,s}} = 100$ mm $k_{\text{post,s}} = 14.9$ W/m-K $k_{\text{ins}} = 0.043$ W/m-K $L_{\text{post,s}} = 206$ mm $\varepsilon_{\text{ins}} = 0.85$	$R_{\text{wall}} = \dfrac{\ln\left(\dfrac{D_{\text{post,o,s}}}{D_{\text{post,i,s}}} \right)}{2 \pi k_{\text{post,s}} L_{\text{post,s}}}$	$R_{\text{wall}} = 4.689 \times 10^{-3}$ K/W
	$R_{\text{ins}} = \dfrac{\ln\left(\dfrac{D_{\text{post,ins,s}}}{D_{\text{post,o,s}}} \right)}{2 \pi k_{\text{ins}} L_{\text{post,s}}}$	$R_{\text{ins}} = 17.3$ K/W
	$R_{\text{radiation}} = \dfrac{1}{\varepsilon_{\text{ins}} \pi D_{\text{post,ins,s}} L_{\text{post,s}} \sigma \left(T^2_{\text{ins}} + T^2_{\text{ambient}} \right)\left(T_{\text{ins}} + T_{\text{ambient}} \right)}$	$R_{\text{radiation}} = 3.043$ K/W $T_{\text{ins}} = 25.30°C$ (solved by iteration)
	$T_{\text{avg}} = (T_{\text{ins}} + T_{\text{ambient}})/2$	$T_{\text{avg}} = 24.15°C$

Heat Transfer Calculations: 06 September 2005 – Run 29		
Inputs	**Equations**	**Results**
σ = 5.67 x 10^{-8} W/m^2-K^4 $T_{ambient}$ = 23.0°C g = 9.81 m/s^2 $P_{ambient}$ = 101 kPa $T_{w,post,in}$ = 30.10°C $T_{w,post,out}$ = 59.32°C	$Pr_{air}, \nu_{air}, \alpha_{air}, k_{air}, \beta_{air} = f\left(T_{avg}, P_{ambient}\right)$	Pr_{air} =0.7298 , ν_{air} = 1.559 ×10^{-5} m^2/s α_{air} = 2.136 ×10^{-5} m^2/s, k_{air} = 0.02545 W/m-K β_{air} = 0.003364 1/K
	By assuming a negligible convective resistance in coolant: $T_{inner\ wall} = (T_{w,post,in} + T_{w,post,out})/2$	$T_{inner\ wall}$ = 44.71°C
	$Ra = \dfrac{g\beta_{air}\left(T_{ins} - T_{ambient}\right)D^3_{post,\ ins,\ s}}{\nu_{air}\alpha_{air}}$	Ra = 227800
	$Nu = \dfrac{h_{nat.conv.}D_{ins}}{k_{air}} = \left(0.60 + \dfrac{0.387Ra^{1/6}}{\left(1 + \left(\dfrac{0.559}{Pr_{air}}\right)^{9/16}\right)^{8/27}}\right)^2$ (Churchill and Chu, 1975)	Nu = 9.71 $h_{nat.conv.}$ = 2.471 W/m^2-K
	$R_{nat.conv.} = \dfrac{1}{h_{nat.conv.}\pi D_{ins}L_{post,\ s}}$	$R_{nat.conv.}$ = 6.238 K/W
	$\dot{Q}_{loss,\ post} = \dfrac{\left(T_{inner\ wall} - T_{ambient}\right)}{R_{wall} + R_{ins} + \left(\dfrac{R_{nat.conv.}R_{radiation}}{R_{nat.conv.} + R_{radiation}}\right)}$	$\dot{Q}_{loss,\ post}$ = 1.123 W
Heat Losses in Refrigerant Tubing from Pre-Condenser Outlet to Test Section Inlet		

Heat Transfer Calculations: 06 September 2005 – Run 29

Inputs	Equations	Results
$D_{\text{tube,r,i}} = 10.2$ mm	$R_{\text{wall}} = \dfrac{\ln\left(\dfrac{D_{\text{tube,r,o}}}{D_{\text{tube,r,i}}}\right)}{2\pi k_{\text{tube,r}} L_{\text{r,pre-to-test}}}$	$R_{\text{wall}} = 2.451 \times 10^{-3}$ K/W
$D_{\text{tube,r,o}} = 12.7$ mm		
$D_{\text{r,ins}} = 100$ mm		
$k_{\text{tube,r}} = 15.5$ W/m-K	$R_{\text{ins}} = \dfrac{\ln\left(\dfrac{D_{\text{r,ins}}}{D_{\text{tube,r,o}}}\right)}{2\pi k_{\text{ins}} L_{\text{r,pre-to-test}}}$	$R_{\text{ins}} = 8.353$ K/W
$L_{\text{r,pre-to-test}} = 914$ mm		
$k_{\text{ins}} = 0.043$ W/m-K		
$k_{\text{ins}} = 0.043$ W/m-K	$R_{\text{radiation}} = \dfrac{1}{\varepsilon_{\text{ins}} \pi D_{\text{r,ins}} L_{\text{pre-to-test}} \sigma \left(T^2_{\text{ins}} + T^2_{\text{ambient}}\right)\left(T_{\text{ins}} + T_{\text{ambient}}\right)}$	$R_{\text{radiation}} = 0.6880$ K/W $T_{\text{ins}} = 25.05°$C (solved by iteration)
$\varepsilon_{\text{ins}} = 0.85$	$T_{\text{avg}} = (T_{\text{ins}} + T_{\text{ambient}})/2$	$T_{\text{avg}} = 24.03°$C
$\sigma = 5.67 \times 10^{-8}$ W/m²-K⁴	$\text{Pr}_{\text{air}}, \nu_{\text{air}}, \alpha_{\text{air}}, k_{\text{air}}, \beta_{\text{air}} = f\left(T_{\text{avg}}, P_{\text{ambient}}\right)$	$\text{Pr}_{\text{air}} = 0.7298$, $\nu_{\text{air}} = 1.557 \times 10^{-5}$ m²/s $\alpha_{\text{air}} = 2.133 \times 10^{-5}$ m²/s, $k_{\text{air}} = 0.02544$ W/m-K $\beta_{\text{air}} = 0.003365$ 1/K
$T_{\text{ambient}} = 23.0°$C		
$g = 9.81$ m/s²		
$P_{\text{ambient}} = 101$ kPa	By assuming a negligible convective resistance in coolant: $T_{\text{inner wall}} = (T_{\text{r,pre,out}} + T_{\text{r,test,in}})/2$	$T_{\text{inner wall}} = 61.77°$C
$T_{\text{r,pre,out}} = 62.17°$C		
$T_{\text{r,test,in}} = 61.37°$C	$\text{Ra} = \dfrac{g\beta_{\text{air}}\left(T_{\text{ins}} - T_{\text{ambient}}\right)D^3_{\text{r,ins}}}{\nu_{\text{air}}\alpha_{\text{air}}}$	$\text{Ra} = 203300$
	$\text{Nu} = \dfrac{h_{\text{nat.conv.}} D_{\text{ins}}}{k_{\text{air}}} = \left(0.60 + \dfrac{0.387 \text{Ra}^{1/6}}{\left(1 + \left(\dfrac{0.559}{\text{Pr}_{\text{air}}}\right)^{9/16}\right)^{8/27}}\right)^2$ (Churchill and Chu, 1975)	$\text{Nu} = 9.416$ $h_{\text{nat.conv.}} = 2.395$ W/m²-K

Heat Transfer Calculations: 06 September 2005 – Run 29		
Inputs	**Equations**	**Results**
	$$R_{\text{nat.conv.}} = \frac{1}{h_{\text{nat.conv.}}\pi D_{\text{ins}}L_{\text{r,pre-to-test}}}$$	$R_{\text{nat.conv.}}$ = 1.452 K/W
	$$\dot{Q}_{\text{loss, pre-to-test}} = \frac{\left(T_{\text{inner wall}} - T_{\text{ambient}}\right)}{R_{\text{wall}} + R_{\text{ins}} + \left(\dfrac{R_{\text{nat.conv.}}R_{\text{radiation}}}{R_{\text{nat.conv.}} + R_{\text{radiation}}}\right)}$$	$\dot{Q}_{\text{loss, pre-to-test}}$ = 4.395 W
Heat Losses in Refrigerant Tubing from Test Section Outlet to Post-Condenser Inlet		
$D_{\text{tube,r,i}}$ = 10.2 mm $D_{\text{tube,r,o}}$ = 12.7 mm $D_{\text{r,ins}}$ = 100 mm $k_{\text{tube,r}}$ = 15.5 W/m-K k_{ins} = 0.043 W/m-K $L_{\text{r,test-to-post}}$ = 914 mm ε_{ins} = 0.85 σ = 5.67 x 10^{-8} W/m^2-K^4 T_{ambient} = 23.0°C g = 9.81 kg-m/s^2 P_{ambient} = 101 kPa $T_{\text{r,test,out}}$ = 61.01°C	$$R_{\text{wall}} = \frac{\ln\left(\dfrac{D_{\text{tube,r,o}}}{D_{\text{tube,r,i}}}\right)}{2\pi k_{\text{tube,r}}L_{\text{r,test-to-post}}}$$	R_{wall} = 2.454 $\times10^{-3}$ K/W
	$$R_{\text{ins}} = \frac{\ln\left(\dfrac{D_{\text{r,ins}}}{D_{\text{tube,r,o}}}\right)}{2\pi k_{\text{ins}}L_{\text{r,test-to-post}}}$$	R_{ins} = 8.353 K/W
	$$R_{\text{radiation}} = \frac{1}{\varepsilon_{\text{ins}}\pi D_{\text{r,ins}}L_{\text{test-to-post}}\sigma\left(T^2_{\text{ins}} + T^2_{\text{ambient}}\right)\left(T_{\text{ins}} + T_{\text{ambient}}\right)}$$	$R_{\text{radiation}}$ = 0.6882 K/W T_{ins} = 24.99°C (solved by interation)
	$T_{\text{avg}} = (T_{\text{ins}} + T_{\text{ambient}})/2$	T_{avg} = 24.00 °C
	$\text{Pr}_{\text{air}}, \nu_{\text{air}}, \alpha_{\text{air}}, k_{\text{air}}, \beta_{\text{air}} = f\left(T_{\text{avg}}, P_{\text{ambient}}\right)$	Pr_{air} = 0.7298, ν_{air} = 1.557 $\times10^{-5}$ m^2/s α_{air} = 2.133 $\times10^{-5}$ m^2/s, k_{air} = 0.02544 W/m-K β_{air} = 0.003365 1/K
	By assuming a negligible convective resistance in coolant: $T_{\text{inner wall}} = (T_{\text{r,test,out}} + T_{\text{r,post,in}})/2$	$T_{\text{inner wall}}$ = 60.61°C

Heat Transfer Calculations: 06 September 2005 – Run 29		
Inputs	**Equations**	**Results**
$T_{r,post,in} = 60.20°C$	$\mathrm{Ra} = \dfrac{g\beta_{air}\left(T_{ins} - T_{ambient}\right)D_{r,ins}^3}{\nu_{air}\alpha_{air}}$	$\mathrm{Ra} = 197800$
	$\mathrm{Nu} = \dfrac{h_{nat.conv.}D_{ins}}{k_{air}} = \left(0.60 + \dfrac{0.387\mathrm{Ra}^{1/6}}{\left(1 + \left(\dfrac{0.559}{\mathrm{Pr}_{air}}\right)^{9/16}\right)^{8/27}}\right)^2$ (Churchill and Chu, 1975)	$\mathrm{Nu} = 9.346$ $h_{nat.conv.} = 2.377$ W/m²-K
	$R_{nat.conv.} = \dfrac{1}{h_{nat.conv.}\pi D_{ins}L_{r,test-to-post}}$	$R_{nat.conv.} = 1.464$ K/W
	$\dot{Q}_{loss,\,test-to-post} = \dfrac{\left(T_{inner\,wall} - T_{ambient}\right)}{R_{wall} + R_{ins} + \left(\dfrac{R_{nat.conv.}R_{radiation}}{R_{nat.conv.} + R_{radiation}}\right)}$	$\dot{Q}_{loss,\,test-to-post} = 4.262$ W
Heat Losses in Secondary Heat Exchanger (Shell-and-Tube)		
$D_{sec,o} = 25.4$ mm $D_{sec,i} = 22.9$ mm $D_{sec,ins} = 100$ mm $k_{sec} = 14.9$ W/m-K $k_{ins} = 0.043$ W/m-K	$R_{wall} = \dfrac{\ln\left(\dfrac{D_{sec,o}}{D_{sec,i}}\right)}{2\pi k_{sec}L_{sec}}$	$R_{wall} = 6.369 \times 10^{-3}$ K/W
	$R_{ins} = \dfrac{\ln\left(\dfrac{D_{sec,ins}}{D_{sec,o}}\right)}{2\pi k_{ins}L_{sec}}$	$R_{ins} = 29.32$ K/W

Heat Transfer Calculations: 06 September 2005 – Run 29

Inputs	Equations	Results
L_{sec} = 173 mm	$R_{radiation} = \dfrac{1}{\varepsilon_{ins}\pi D_{sec,ins}L_{sec}\sigma\left(T^2_{ins}+T^2_{ambient}\right)\left(T_{ins}+T_{ambient}\right)}$	$R_{radiation}$ = 3.646 K/W
ε_{ins} = 0.85		T_{ins} = 24.58°C (solved by iteration)
σ = 5.67 x 10^{-8} W/m^2-K^4	$T_{avg} = (T_{ins} + T_{ambient})/2$	T_{avg} = 23.79°C
	$Pr_{air}, \nu_{air}, \alpha_{air}, k_{air}, \beta_{air} = f\left(T_{avg}, P_{ambient}\right)$	Pr_{air} = 0.7299 , ν_{air} = 1.555 ×10^{-5} m^2/s
$T_{ambient}$ = 23.0°C		α_{air} = 2.130 ×10^{-5} m^2/s, k_{air} = 0.02542 W/m-K
g = 9.81 m/s^2		β_{air} = 0.003368 1/K
$P_{ambient}$ = 101 kPa	By assuming a negligible convective resistance in coolant: $T_{inner\ wall} = (T_{w,sec,in}+T_{w,sec,out})/2$	$T_{inner\ wall}$ = 42.95°C
$T_{w,sec,in}$ = 36.84°C		
$T_{w,sec,out}$ = 49.05°C	$Ra = \dfrac{g\beta_{air}\left(T_{ins}-T_{ambient}\right)D^3_{sec,\ ins}}{\nu_{air}\alpha_{air}}$	Ra = 157600
	$Nu = \dfrac{h_{nat.conv.}D_{sec,ins}}{k_{air}} = \left(0.60+\dfrac{0.387Ra^{1/6}}{\left(1+\left(\dfrac{0.559}{Pr_{air}}\right)^{9/16}\right)^{8/27}}\right)^2$ (Churchill and Chu, 1975)	Nu = 8.799 $h_{nat.conv.}$ = 2.237 W/m^2-K
	$R_{nat.conv.} = \dfrac{1}{h_{nat.conv.}\pi D_{ins}L_{sec}}$	$R_{nat.conv.}$ = 8.227 K/W
	$\dot{Q}_{loss,\ sec} = \dfrac{\left(T_{inner\ wall}-T_{ambient}\right)}{R_{wall}+R_{ins}+\left(\dfrac{R_{nat.conv.}R_{radiation}}{R_{nat.conv.}+R_{radiation}}\right)}$	$\dot{Q}_{loss,\ sec}$ = 0.6261 W
Heat Losses in Primary Loop		

Heat Transfer Calculations: 06 September 2005 – Run 29		
Inputs	**Equations**	**Results**
$D_{\text{tube,r,i}} = 10.2$ mm	$R_{\text{wall}} = \dfrac{\ln\left(\dfrac{D_{\text{tube,r,o}}}{D_{\text{tube,r,i}}}\right)}{2\pi k_{\text{tube,r}} L_{\text{prim,equiv}}}$	$R_{\text{wall}} = 3.452 \times 10^{-4}$ K/W
$D_{\text{tube,r,o}} = 12.7$ mm		
$D_{\text{r,ins}} = 76$ mm	$R_{\text{ins}} = \dfrac{\ln\left(\dfrac{D_{\text{r,ins}}}{D_{\text{tube,r,o}}}\right)}{2\pi k_{\text{ins}} L_{\text{prim,equiv}}}$	$R_{\text{ins}} = 1.456$ K/W
$k_{\text{tube,r}} = 15.3$ W/m-K		
$k_{\text{ins}} = 0.043$ W/m-K		
$L_{\text{prim,equiv}} = 4.548$ m		
$\varepsilon_{\text{ins}} = 0.85$	$R_{\text{radiation}} = \dfrac{1}{\varepsilon_{\text{ins}} \pi D_{\text{r,ins}} L_{\text{prim,equiv}} \sigma \left(T^2_{\text{ins}} + T^2_{\text{ambient}}\right)\left(T_{\text{ins}} + T_{\text{ambient}}\right)}$	$R_{\text{radiation}} = 0.182$ K/W $T_{\text{ins}} = 25.06°$C (solved by interation)
$\sigma = 5.67 \times 10^{-8}$ W/m^2-K^4	$T_{\text{avg}} = (T_{\text{ins}} + T_{\text{ambient}})/2$	$T_{\text{avg}} = 24.03°$C
$T_{\text{ambient}} = 23.0°$C	$\text{Pr}_{\text{air}}, \nu_{\text{air}}, \alpha_{\text{air}}, k_{\text{air}}, \beta_{\text{air}} = f\left(T_{\text{avg}}, P_{\text{ambient}}\right)$	$\text{Pr}_{\text{air}} = 0.7298$, $\nu_{\text{air}} = 1.558 \times 10^{-5}$ m^2/s $\alpha_{\text{air}} = 2.135 \times 10^{-5}$ m^2/s, $k_{\text{air}} = 0.02544$ W/m-K $\beta_{\text{air}} = 0.003365$ 1/K
$g = 9.81$ m/s^2		
$P_{\text{ambient}} = 101$ kPa		
$T_{\text{w,test,in}} = 49.69°$C	By assuming a negligible convective resistance in coolant: $T_{\text{inner wall}} = (T_{\text{w,test,in}} + T_{\text{w,test,out}})/2$	$T_{\text{inner wall}} = 48.31°$C
$T_{\text{w,test,out}} = 50.01°$C	$\text{Ra} = \dfrac{g\beta_{\text{air}}\left(T_{\text{ins}} - T_{\text{ambient}}\right)D^3_{\text{r, ins}}}{\nu_{\text{air}}\alpha_{\text{air}}}$	$\text{Ra} = 89810$
	$\text{Nu} = \dfrac{h_{\text{nat.conv.}} D_{\text{r,ins}}}{k_{\text{air}}} = \left(0.60 + \dfrac{0.387\text{Ra}^{1/6}}{\left[1 + \left(\dfrac{0.559}{\text{Pr}_{\text{air}}}\right)^{9/16}\right]^{8/27}}\right)^2$ (Churchill and Chu, 1975)	$\text{Nu} = 7.593$ $h_{\text{nat.conv.}} = 2.542$ W/m^2-K

Heat Transfer Calculations: 06 September 2005 – Run 29		
Inputs	**Equations**	**Results**
	$R_{\text{nat.conv.}} = \dfrac{1}{h_{\text{nat.conv.}} \pi D_{\text{r,ins}} L_{\text{prim,equiv}}}$	$R_{\text{nat.conv.}} = 0.3621$ K/W
	$\dot{Q}_{\text{loss, prim}} = \dfrac{\left(T_{\text{inner wall}} - T_{\text{ambient}}\right)}{R_{\text{wall}} + R_{\text{ins}} + \left(\dfrac{R_{\text{nat.conv.}} R_{\text{radiation}}}{R_{\text{nat.conv.}} + R_{\text{radiation}}}\right)}$	$\dot{Q}_{\text{loss, prim}} = 17.00$ W
Water Heat Transfer Coefficient Test Section Annulus		
$T_{\text{w,test,in}} = 49.69°C$	$T_{\text{w,test,avg}} = (T_{\text{w,test,in}} + T_{\text{wtest,out}})/2$	$T_{\text{w,test,avg}} = 49.85°C$
$T_{\text{w,test,out}} = 50.01°C$	$\Pr_{\text{w}}, \nu_{\text{w}}, \rho_{\text{w}}, k_{\text{w}} = f\left(T_{\text{w,test,avg}}, P_{\text{w}}\right)$	$\Pr_{\text{w}} = 3.562$, $\nu_{\text{w}} = 5.548 \times 10^{-7}$ m^2/s $k_{\text{w}} = 0.6435$ W/m-K
$P_{\text{w}} = 275.8$ kPa		
$D_{\text{annulus,i}} = 10.2$ mm	$A_{\text{annulus}} = 0.25\pi\left(D_{\text{annulus, i}}^2 - D_{\text{test, o}}^2\right)$	$A_{\text{annulus}} = 5.022 \times 10^{-5}$ m^2
$D_{\text{test,o}} = 6.35$ mm	$V_{\text{annulus}} = \dfrac{\dot{V}_{\text{w, prim}}}{A_{\text{annulus}}}$	$V_{\text{annulus}} = 1.318$ m/s
$\dot{V}_{\text{w, prim}} = 6.618 \times 10^{-5}$ (m^3/s)	$D_{\text{hydraulic}} = D_{\text{annulus, i}} - D_{\text{test, o}}$	$D_{\text{hydraulic}} = 3.861$ mm
	$\text{Re}_{\text{annulus}} = \dfrac{V_{\text{annulus}} D_{\text{hydraulic}}}{\nu_{\text{w, prim}}}$	$\text{Re}_{\text{annulus}} = 9171$
	$r^* = D_{\text{test, o}} / D_{\text{annulus, i}}$	$r^* = 0.6225$
	if: $\text{Re}_{\text{annulus}} \geq \text{Re}_{\text{CU}} = 2963.02 + 334.16 r^*$, then:	$\text{Re}_{\text{CU}} = 3171$
	$\text{Nu}_{\text{turbulent}} = 0.025\left(\text{Re}_{\text{annulus}}^{0.78} \Pr_{\text{w}}^{0.48} \left(r^*\right)^{-0.14}\right)$ (Garimella and Christensen, 1995)	$\text{Nu}_{\text{turbulent}} = 60.58$
	$h_{\text{annulus}} = \dfrac{\text{Nu}_{\text{turbulent}} k_{\text{w}}}{D_{\text{hydraulic}}}$	$h_{\text{annulus}} = 10100$ W/m^2-K

Heat Transfer Calculations: 06 September 2005 – Run 29		
Inputs	**Equations**	**Results**
Heat Losses in Test Section		
$h_{annulus} = 10100$ W/m²-K	$R_{annulus,o} = \dfrac{1}{h_{annulus}\pi D_{annulus,i}L_{annulus}}$	$R_{annulus,o} = 2.026 \times 10^{-2}$ K/W
$L_{annulus} = 152.4$ mm		
$D_{annulus,i} = 10.2$ mm	$R_{wall} = \dfrac{\ln\left(\dfrac{D_{annulus,o}}{D_{annulus,i}}\right)}{2\pi k_{annulus}L_{annulus}}$	$R_{wall} = 1.529 \times 10^{-3}$ K/W
$D_{annulus,o} = 12.7$ mm		
$D_{test,ins} = 100$ mm		
$k_{annulus} = 14.9$ W/m-K	$R_{ins} = \dfrac{\ln\left(\dfrac{D_{test,ins}}{D_{annulus,o}}\right)}{2\pi k_{ins}L_{annulus}}$	$R_{ins} = 50.12$ K/W
$k_{ins} = 0.043$ W/m-K		
$\varepsilon_{ins} = 0.85$	$R_{radiation} = \dfrac{1}{\varepsilon_{ins}\pi D_{test,ins}L_{annulus}\sigma\left(T^2_{ins}+T^2_{ambient}\right)\left(T_{ins}+T_{ambient}\right)}$	$R_{radiation} = 4.141$ K/W
$\sigma = 5.67 \times 10^{-8}$ W/m²-K⁴		$T_{ins} = 24.46$°C (solved by iteration)
$T_{ambient} = 23.0$°C	$T_{avg} = (T_{ins} + T_{ambient})/2$	$T_{avg} = 23.73$°C
$g = 9.81$ m/s²	$Pr_{air}, \nu_{air}, \alpha_{air}, k_{air}, \beta_{air} = f\left(T_{avg}, P_{ambient}\right)$	$Pr_{air} = 0.7301$, $\nu_{air} = 1.548 \times 10^{-5}$ m²/s
		$\alpha_{air} = 2.120 \times 10^{-5}$ m²/s, $k_{air} = 0.02536$ W/m-K
$P_{ambient} = 101$ kPa		$\beta_{air} = 0.003377$ 1/K
$T_{w,test,in} = 49.69$°C	$T_{w,test,avg} = (T_{w,test,in}+T_{wtest,out})/2$	$T_{w,test,avg} = 49.85$°C
$T_{w,test,out} = 50.01$°C	$Ra = \dfrac{g\beta_{air}\left(T_{ins}-T_{ambient}\right)D^3_{test,ins}}{\nu_{air}\alpha_{air}}$	$Ra = 147400$

Heat Transfer Calculations: 06 September 2005 – Run 29		
Inputs	**Equations**	**Results**
	$$\text{Nu} = \frac{h_{\text{nat.conv.}} D_{\text{test,ins}}}{k_{\text{air}}} = \left(0.60 + \frac{0.387 \text{Ra}^{1/6}}{\left(1 + \left(\frac{0.559}{\text{Pr}_{\text{air}}} \right)^{9/16} \right)^{8/27}} \right)^2$$	$\text{Nu} = 8.644$ $h_{\text{nat.conv.}} = 2.192$ W/m²-K
	$$R_{\text{nat.conv.}} = \frac{1}{h_{\text{nat.conv.}} \pi D_{\text{test,ins}} L_{\text{annulus}}}$$	$R_{\text{nat.conv.}} = 9.527$ K/W
	$$\dot{Q}_{\text{loss,test}} = \frac{\left(T_{\text{w,test,avg}} - T_{\text{ambient}} \right)}{R_{\text{annulus,o}} + R_{\text{wall}} + R_{\text{ins}} + \left(\frac{R_{\text{nat.conv.}} R_{\text{radiation}}}{R_{\text{nat.conv.}} + R_{\text{radiation}}} \right)}$$	$\dot{Q}_{\text{loss,test}} = 0.5062$ W
Average Test Section Quality		
$P_{\text{w}} = 275.8$ kPa	$i_{\text{w,pre,in}} = f\left(T_{\text{w,pre,in}}, P_{\text{w}} \right)$	$i_{\text{w,pre,in}} = 126.3 \times 10^3$ J/kg
$T_{\text{w,pre,in}} = 30.07°\text{C}$	$i_{\text{w,pre,out}} = f\left(T_{\text{w,pre,out}}, P_{\text{w}} \right)$	$i_{\text{w,pre,out}} = 278.8 \times 10^3$ J/kg
$T_{\text{w,pre,out}} = 66.54°\text{C}$	$\rho_{\text{w, pre, in}} = \left(T_{\text{w,pre,in}}, P_{\text{w}} \right)$	$\rho_{\text{w, pre, in}} = 995.7$ kg/m³
$\dot{V}_{\text{w, pre}} = 3.787 \times 10^{-6}$ m³/s	$\dot{m}_{\text{w, pre}} = \rho_{\text{w, pre, in}} \dot{V}_{\text{w, pre}}$	$\dot{m}_{\text{w, pre}} = 3.770 \times 10^{-3}$ kg/s
	$\dot{Q}_{\text{pre}} = \dot{m}_{\text{w, pre}} \left(i_{\text{w, pre, out}} - i_{\text{w, pre, in}} \right) + \dot{Q}_{\text{loss, pre}}$	$\dot{Q}_{\text{pre}} = 577.9$ W
$\dot{Q}_{\text{loss, pre}} = 2.921$ W	$T_{\text{r,pre,in,sat}} = f\left(P_{\text{r,pre,in}}, x = 1 \right)$	$T_{\text{r,pre,in,sat}} = 61.09°\text{C}$
$T_{\text{r, pre, in}} = 100.30°\text{C}$	$\Delta T_{\text{sup,pre}} = T_{\text{r,pre,in}} - T_{\text{r,pre,in,sat}}$	$\Delta T_{\text{sup,pre}} = 39.21°\text{C}$
	$i_{\text{r, pre, in}} = i\left(T_{\text{r, pre, in}}, P_{\text{r, pre, in}} \right)$	$i_{\text{r, pre, in}} = 486.0 \times 10^3$ J/kg

Heat Transfer Calculations: 06 September 2005 – Run 29		
Inputs	**Equations**	**Results**
$P_{r,\,pre,\,in} = 3927$ kPa	$i_{r,\,pre,\,out} = \left(i_{r,\,pre,\,in} - \dfrac{\dot{Q}_{pre}}{\dot{m}_r} \right)$	$i_{r,\,pre,\,out} = 387.2 \times 10^3$ J/kg
$\dot{m}_r = 5.847 \times 10^{-3}$ kg/s		
$\dot{Q}_{loss,\,pre\text{-}to\text{-}test} = 4.395$ W	$i_{r,test,\,in} = \left(i_{r,\,pre,\,out} - \dfrac{\dot{Q}_{loss,\,pre\text{-}to\text{-}test}}{\dot{m}_r} \right)$	$i_{r,test,\,in} = 386.4 \times 10^3$ J/kg
$P_{r,\,test,\,in} = 3926$ kPa	$x_{r,\,test,\,in} = f\left(P_{r,\,test,\,in},\, i_{r,\,test,\,in} \right)$	$x_{r,\,test,\,in} = 0.7317$
$T_{w,\,post,\,in} = 30.10°C$	$i_{w,\,post,\,in} = i\left(T_{w,\,post,\,in},\, P_w \right)$	$i_{w,\,post,\,in} = 126.4 \times 10^3$ J/kg
$T_{w,\,post,\,out} = 59.32°C$	$i_{w,\,post,\,out} = f\left(T_{w,\,post,\,out},\, P_w \right)$	$i_{w,\,post,\,out} = 248.6 \times 10^3$ J/kg
$\dot{V}_{w,\,post} = 3.333 \times 10^{-6}$ m³/s	$\rho_{w,\,post,\,in} = f\left(T_{w,\,post,\,in},\, P_w \right)$	$\rho_{w,\,post,\,in} = 995.7$ kg/m³
$\dot{Q}_{loss,\,post} = 1.123$ W	$\dot{m}_{w,\,post} = \rho_{w,\,post,\,in} \dot{V}_{w,\,post}$	$\dot{m}_{w,\,post} = 3.319 \times 10^{-3}$ kg/s
	$\dot{Q}_{post} = \dot{m}_{w,\,post}\left(i_{w,\,post,\,out} - i_{w,\,post,\,in} \right) + \dot{Q}_{loss,\,post}$	$\dot{Q}_{post} = 406.5$ W
$T_{r,\,post,\,out} = 56.78°C$	$T_{r,post,out,sat} = f\left(P_{r,post,out},\, x = 0 \right)$	$T_{r,post,out,sat} = 60.97°C$
$P_{r,\,post,\,out} = 3924$ kPa	$\Delta T_{sub,post} = T_{r,post,out} - T_{r,post,out,sat}$	$\Delta T_{sub,post} = 4.19°C$
$\dot{Q}_{loss,\,test\text{-}to\text{-}post} = 4.262$ W	$i_{r,\,post,\,out} = f\left(T_{r,\,post,\,out},\, P_{r,\,post,\,out} \right)$	$i_{r,\,post,\,out} = 300.3 \times 10^3$ J/kg
$P_{r,\,test,\,out} = 3926$ kPa	$i_{r,\,post,\,in} = \left(i_{r,\,post,\,out} + \dfrac{\dot{Q}_{post}}{\dot{m}_r} \right)$	$i_{r,\,post,\,in} = 369.8 \times 10^3$ J/kg
	$i_{r,\,test,\,out} = \left(i_{r,\,post,\,in} + \dfrac{\dot{Q}_{loss,\,test\text{-}to\text{-}post}}{\dot{m}_r} \right)$	$i_{r,\,test,\,out} = 370.6 \times 10^3$ J/kg
	$x_{test,\,out} = f\left(P_{r,\,test,\,out},\, i_{r,\,test,\,out} \right)$	$x_{test,\,out} = 0.5746$

Heat Transfer Calculations: 06 September 2005 – Run 29		
Inputs	**Equations**	**Results**
	$x_{\text{test, avg}} = \dfrac{x_{\text{test, in}} + x_{\text{test, out}}}{2}$	$x_{\text{test, avg}} = 0.6531$
Refrigerant Heat Transfer Coefficient in Test Section		
$T_{\text{w,sec,i}} = 33.0\ °\text{C}$	$i_{\text{w,sec,o}} = f\left(T_{\text{w,sec,o}}, P_{\text{w}}\right)$	$i_{\text{w,sec,o}} = 205.6 \times 10^3\ \text{J/kg}$
$T_{\text{w,sec,o}} = 46.0\ °\text{C}$	$i_{\text{w,sec,i}} = f\left(T_{\text{w,sec,i}}, P_{\text{w}}\right)$	$i_{\text{w,sec,i}} = 154.6 \times 10^3\ \text{J/kg}$
$P_{\text{w}} = 275.8\ \text{kPa}$	$\dot{Q}_{\text{sec}} = \dot{m}_{\text{w,sec}}\left(i_{\text{w,sec,o}} - i_{\text{w,sec,i}}\right)$	$\dot{Q}_{\text{sec}} = 86.61\ \text{W}$
$\dot{m}_{\text{w,sec}} = 1.697 \times 10^{-3}\ \text{kg/s}$	$\dot{Q}_{\text{loss, ambient}} = \dot{Q}_{\text{loss, test}} + \dot{Q}_{\text{loss, prim}} + \dot{Q}_{\text{loss, sec}}$	$\dot{Q}_{\text{loss, ambient}} = 18.14\ \text{W}$
$\dot{Q}_{\text{loss,test}} = 0.5062\ \text{W}$	$\dot{Q}_{\text{pump}} = 9.0397\dot{V}_{\text{w,prim,gpm}} + 0.1304\dot{V}_{\text{w,prim,gpm}}^2 + 0.4034\dot{V}_{\text{w,prim,gpm}}^3$	$\dot{Q}_{\text{pump}} = 10.09\ \text{W}$
$\dot{Q}_{\text{loss, prim}} = 17.00\ \text{W}$		
$\dot{Q}_{\text{loss, sec}} = 0.6261\ \text{W}$	$\dot{Q}_{\text{test}} = \dot{Q}_{\text{sec}} + \dot{Q}_{\text{loss,ambient}} - \dot{Q}_{\text{pump}}$	$\dot{Q}_{\text{test}} = 94.65\ \text{W}$
$\dot{V}_{\text{w,prim,gpm}} = 1.049\ \text{gpm}$	$T_{\text{r,test,in,sat}} = f\left(i_{\text{r,test,in}}, P_{\text{r,test,in}}\right)$	$T_{\text{r,test,in,sat}} = 61.07°\text{C}$
	$Error_{\text{r,test,in}} = T_{\text{r,test,in}} - T_{\text{r,test,in,sat}}$	$Error_{\text{r,test,in}} = 0.30°\text{C}$
$i_{\text{r,test,in}} = 386.4 \times 10^3\ \text{J/kg}$	$T_{\text{r,test,out,sat}} = f\left(i_{\text{r,test,out}}, P_{\text{r,test,out}}\right)$	$T_{\text{r,test,out,sat}} = 61.07°\text{C}$
$P_{\text{r,test,in}} = 3926\ \text{kPa}$	$Error_{\text{r,test,out}} = T_{\text{r,test,out}} - T_{\text{r,test,out,sat}}$	$Error_{\text{r,test,out}} = 0.06°\text{C}$
$i_{\text{r,test,out}} = 370.6 \times 10^3\ \text{J/kg}$	$\text{LMTD} = \dfrac{\left(T_{\text{r,test,in,sat}} - T_{\text{w,test,out}}\right) - \left(T_{\text{r,test,out,sat}} - T_{\text{w,test,in}}\right)}{\ln\left[\dfrac{\left(T_{\text{r,test,in,sat}} - T_{\text{w,test,out}}\right)}{\left(T_{\text{r,test,out,sat}} - T_{\text{w,test,in}}\right)}\right]}$	$\text{LMTD} = 11.22°\text{C}$
$P_{\text{r,test,out}} = 3926\ \text{kPa}$		
$T_{\text{r,test,in}} = 61.37°\text{C}$	$\left(UA\right) = \dfrac{\dot{Q}_{\text{test}}}{\left(\text{LMTD}\right)}$	$UA = 8.433\ \text{W/K}$

Heat Transfer Calculations: 06 September 2005 – Run 29		
Inputs	**Equations**	**Results**
$T_{\text{r,test,out}} = 61.01°\text{C}$ $k_{\text{test}} = 398.3$ W/m-K $T_{\text{w,test,in}} = 49.69°\text{C}$	$R_{\text{wall}} = \dfrac{\ln\left(\dfrac{D_{\text{test,o}}}{D_{\text{test,i}}}\right)}{2\pi k_{\text{test}}\left(L_{\text{annulus}} + 2\cdot\left(L_{\text{reducer}} + L_{\text{tee}}\right)\right)}$	$R_{\text{wall}} = 1.306 \times 10^{-3}$ K/W
$T_{\text{w,test,out}} = 50.01°\text{C}$ $P_{\text{w}} = 275.8$ kPa	$R_{\text{annulus,i}} = \dfrac{1}{h_{\text{annulus}}\pi D_{\text{test,o}} L_{\text{annulus}}}$	$R_{\text{annulus,i}} = 3.258 \times 10^{-2}$ K/W
	$T_{\text{w,test,avg}} = (T_{\text{w,test,in}} + T_{\text{wtest,out}})/2$	$T_{\text{w,test,avg}} = 49.85°\text{C}$
$h_{\text{annulus}} = 10100$ W/m^2-K $D_{\text{test,i}} = 3.048$ mm	$\text{Pr}_{\text{w}}, \nu_{\text{w}}, \rho_{\text{w}}, k_{\text{w}}, \beta_{\text{w}}, \alpha_{\text{w}} = f\left(T_{\text{w,test,avg}}, P_{\text{w}}\right)$	$\text{Pr}_{\text{w}} = 3.562$, $\nu_{\text{w}} = 5.548 \times 10^{-7}$ m^2/s $k_{\text{w}} = 0.6435$ W/m-K, $\beta_{\text{w}} = 0.0004567$ 1/K $\alpha_{\text{w}} = 1.558 \times 10^{-7}$ m^2/s
$D_{\text{test,o}} = 6.350$ mm $L_{\text{annulus}} = 152.4$ mm	$\dfrac{\text{Ra}}{L^3} = \dfrac{g\beta_{\text{w}}\left(T_{\text{wall,o}} - T_{\text{w,test,avg}}\right)}{\nu_{\text{w}}\alpha_{\text{w}}}$	$\dfrac{\text{Ra}}{L^3} = 1.619 \times 10^9$, $T_{\text{wall,o}} = 52.97°\text{C}$ (by iteration)
$L_{\text{reducer}} = 22.86$ mm $L_{\text{tee}} = 13.21$ mm $D_{\text{reducer}} = 9.25$ mm	$\text{Ra}^{*}_{\text{reducer}} = \left(\dfrac{\text{Ra}}{L^3}\right)\cdot\dfrac{\ln^4\left(\dfrac{D_{\text{reducer}}}{D_{\text{test,o}}}\right)}{\left(D_{\text{test,o}}^{-3/5} + D_{\text{reducer}}^{-3/5}\right)^5}$ (Incropera and DeWitt, 1996)	$\text{Ra}^{*}_{\text{reducer}} = 44.18$
$D_{\text{tee}} = 10.41$ mm $x_{\text{test, avg}} = 0.6531$	$\text{Ra}^{*}_{\text{tee}} = \left(\dfrac{\text{Ra}}{L^3}\right)\cdot\dfrac{\ln^4\left(\dfrac{D_{\text{tee}}}{D_{\text{test,o}}}\right)}{\left(D_{\text{test,o}}^{-3/5} + D_{\text{tee}}^{-3/5}\right)^5}$	$\text{Ra}^{*}_{\text{tee}} = 154.2$

Heat Transfer Calculations: 06 September 2005 – Run 29

Inputs	Equations	Results
	for: $100 \leq \mathrm{Ra}^*_{\mathrm{reducer}} \leq 10^7$ $$k_{\mathrm{effective,reducer}} = (k_{\mathrm{w}}) \cdot 0.386 \left(\frac{\mathrm{Pr_w}}{0.861 + \mathrm{Pr_w}} \right)^{1/4} \left(\mathrm{Ra}^*_{\mathrm{reducer}} \right)^{1/4}$$ for: $\mathrm{Ra}^*_{\mathrm{reducer}} \leq 100$ $k_{\mathrm{effective,reducer}} = k_{\mathrm{w}}$ (Irvine and Hartnett, 1975)	$k_{\mathrm{effective,reducer}} = k_{\mathrm{w}} = 0.6435$ W/m-K
	for: $100 \leq \mathrm{Ra}^*_{\mathrm{tee}} \leq 10^7$ $$k_{\mathrm{effective,tee}} = (k_{\mathrm{w}}) \cdot 0.386 \left(\frac{\mathrm{Pr_w}}{0.861 + \mathrm{Pr_w}} \right)^{1/4} \left(\mathrm{Ra}^*_{\mathrm{tee}} \right)^{1/4}$$ for: $\mathrm{Ra}^*_{\mathrm{tee}} \leq 100$ $k_{\mathrm{effective,tee}} = k_{\mathrm{w}}$	$k_{\mathrm{effective,tee}} = 0.8293$ W/m-K
	$$R_{\mathrm{reducer}} = \frac{\ln\left(\dfrac{D_{\mathrm{reducer}}}{D_{\mathrm{test,o}}} \right)}{2\pi k_{\mathrm{effective,reducer}} L_{\mathrm{reducer}}}$$	$R_{\mathrm{reducer}} = 4.070$ K/W
	$$R_{\mathrm{tee}} = \frac{\ln\left(\dfrac{D_{\mathrm{tee}}}{D_{\mathrm{test,o}}} \right)}{2\pi k_{\mathrm{effective,tee}} L_{\mathrm{tee}}}$$	$R_{\mathrm{tee}} = 7.188$ K/W
	$$\frac{1}{R_{\mathrm{conv,equiv.}}} = \frac{1}{R_{\mathrm{annulus,i}}} + 2 \cdot \left(\frac{1}{R_{\mathrm{tee}}} + \frac{1}{R_{\mathrm{reducer}}} \right)$$	$R_{\mathrm{conv,equiv.}} = 3.178 \times 10^{-2}$ K/W

Heat Transfer Calculations: 06 September 2005 – Run 29		
Inputs	**Equations**	**Results**
	$h_r = \dfrac{1}{\left[(UA)^{-1} - R_{wall} - R_{conv,equiv.}\right] \cdot \left[\pi D_{test,i}\left(L_{annulus} + 2\cdot\left(L_{reducer} + L_{tee}\right)\right)\right]}$	$h_r = 5440$ W/m^2-K
	$R_r = \dfrac{1}{h_r \pi D_{test,i}\left(L_{annulus} + 2\cdot\left(L_{reducer} + L_{tee}\right)\right)}$	$R_r = 8.550 \times 10^{-2}$ K/W
	$R_{ratio} = \dfrac{R_r}{R_{wall} + R_{conv,equiv.}}$	$R_{ratio} = 2.584$
	$\dot{Q}_{test} = \dfrac{\left(\left(T_{r,test,in,sat} + T_{r,test,out,sat}\right)/2 - T_{wall,o}\right)}{R_r + R_{wall}}$	$T_{wall,o} = 52.86°C$
	$\dot{Q}_{reducer} = 2\cdot\dfrac{\left(T_{wall,o} - T_{w,test,avg}\right)}{R_{reducer}}$	$\dot{Q}_{reducer} = 1.478$ W (1.6% of $\dot{Q}_{annulus}$)
	$\dot{Q}_{tee} = 2\cdot\dfrac{\left(T_{wall,o} - T_{w,test,avg}\right)}{R_{tee}}$	$\dot{Q}_{tee} = 0.8291$ W (0.9% of $\dot{Q}_{annulus}$)
	$\dot{Q}_{annulus} = \dfrac{\left(T_{wall,o} - T_{w,test,avg}\right)}{R_{annulus,i}}$	$\dot{Q}_{annulus} = 92.35$ W
	$P_{r,test,avg} = \dfrac{P_{r,test,in} + P_{r,test,out}}{2}$	$P_{r,test,avg} = 3926$ kPa
	$i_{r,fg} = f\left(P_{r,test,avg}, x_{r,test,avg}\right)$	$i_{r,fg} = 101.2 \times 10^3$ J/kg
	$\Delta x = \dfrac{\dot{Q}_{test}}{\dot{m}_r \cdot i_{r,fg}}$	$\Delta x = 0.16$

Heat Transfer Calculations: 06 September 2005 – Run 29		
Inputs	**Equations**	**Results**
Refrigerant Heat Transfer Coefficient in Test Section – Based on Measured Wall Temperature		
$T_{wall,1} = 51.42°C$	$T_{wall,avg} = \dfrac{T_{wall,1} + T_{wall,2} + T_{wall,3} + T_{wall,4} + T_{wall,5}}{5}$	$T_{wall,avg} = 51.83°C$
$T_{wall,2} = 52.50°C$		
$T_{wall,3} = 52.71°C$	$\text{LMTD} = \dfrac{\left(T_{r,test,in,sat} - T_{wall,avg}\right) - \left(T_{r,test,out,sat} - T_{wall,avg}\right)}{\ln\left[\dfrac{\left(T_{r,test,in,sat} - T_{wall,avg}\right)}{\left(T_{r,test,out,sat} - T_{wall,avg}\right)}\right]}$	$\text{LMTD} = 9.243°C$
$T_{wall,4} = 51.46°C$		
$T_{wall,5} = 51.06°C$	$(UA) = \dfrac{\dot{Q}_{test}}{(\text{LMTD})}$	$UA = 10.24$ W/K
$T_{r,test,in,sat} = 61.05°C$	$h_{r,wall} = \dfrac{1}{\left[(UA)^{-1} - R_{wall}\right] \cdot}$	
$T_{r,test,out,sat} = 61.04°C$	$\left[\pi D_{test,i}\left(L_{annulus} + 2 \cdot \left(L_{reducer} + L_{tee}\right)\right)\right]$	$h_{r,wall} = 4828$ W/m^2-K
$\dot{Q}_{test} = 94.65$ W		
$R_{wall} = 1.306 \times 10^{-2}$ K/W	$\Delta h = \dfrac{h_r - h_{r,wall}}{h_r}$	$\Delta h = 11.25$ %

Pressure Drop Calculations: 06 September 2005 – Run 29		
Inputs	**Equations**	**Results**
$D_{reducer}$ = 9.25 mm	$A_{ratio,1} = \dfrac{A_{reducer}}{A_{tee}} = \left(\dfrac{D_{reducer}}{D_{tee}}\right)^2$	$A_{ratio,1}$ = 0.7889
D_{tee} = 10.41 mm		
$D_{contraction}$ = 4.83 mm	$A_{ratio,2} = \dfrac{A_{contraction}}{A_{reducer}} = \left(\dfrac{D_{contraction}}{D_{reducer}}\right)^2$	$A_{ratio,2}$ = 0.2722
$D_{test, i}$ = 3.048 mm		
$\dot{m}_r$ = 5.847 ×10⁻³ kg/s	$A_{ratio,3} = \dfrac{A_{test}}{A_{contraction}} = \left(\dfrac{D_{test,i}}{D_{contraction}}\right)^2$	$A_{ratio,3}$ = 0.3989
$x_{r,test,in}$ = 0.7317		
$P_{r,test,in}$ = 3926 kPa	$G = \dfrac{\dot{m}_r}{A_{test}} = \dfrac{\dot{m}_r}{0.25 \cdot \pi \cdot D_{test,i}^2}$	G = 801.3 kg/m²-s
$x_{r,test,out}$ = 0.5746	$G_{contraction} = G \cdot A_{ratio,3}$	$G_{contraction}$ = 319.6 kg/m²-s
$P_{r,test,out}$ = 3926 kPa	$G_{reducer} = G \cdot A_{ratio,3} \cdot A_{ratio,2}$	$G_{reducer}$ = 87.01 kg/m²-s
	$G_{tee} = G \cdot A_{ratio,3} \cdot A_{ratio,2} \cdot A_{ratio,1}$	G_{tee} = 68.64 kg/m²-s
B = 0.25		
$\Delta P_{measured}$ = 4.362 kPa	$C_{C,1} = \dfrac{1}{0.639\left[1-\left(A_{ratio,1}\right)\right]^{1/2}+1}$ (Chisholm, 1983)	$C_{C,1}$ = 0.7731
L_{test} = 323.8 mm		
	$C_{C,2} = \dfrac{1}{0.639\left[1-\left(A_{ratio,2}\right)\right]^{1/2}+1}$ (Chisholm, 1983)	$C_{C,2}$ = 0.6472
	$C_{C,3} = \dfrac{1}{0.639\left[1-\left(A_{ratio,3}\right)\right]^{1/2}+1}$ (Chisholm, 1983)	$C_{C,3}$ = 0.6687

Pressure Drop Calculations: 06 September 2005 – Run 29		
Inputs	**Equations**	**Results**
	$(\rho_l, \mu_l)_{in} = f(x_{r,test,in}, P_{r,test,in})$	$\rho_{l,in} = 804.0 \text{ kg/m}^3$, $\mu_{l,in} = 6.715 \times 10^{-5} \text{ kg/m-s}$
	$(\rho_v, \mu_v)_{in} = f(x_{r,test,in}, P_{r,test,in})$	$\rho_{v,in} = 209.6 \text{ kg/m}^3$, $\mu_{v,in} = 2.006 \times 10^{-5} \text{ kg/m-s}$
	$(\rho_l, \mu_l)_{out} = f(x_{r,test,out}, P_{r,test,out})$	$\rho_{l,out} = 804.0 \text{ kg/m}^3$, $\mu_{l,out} = 6.715 \times 10^{-5} \text{ kg/m-s}$
	$(\rho_v, \mu_v)_{out} = f(x_{r,test,out}, P_{r,test,out})$	$\rho_{v,out} = 209.6 \text{ kg/m}^3$, $\mu_{v,out} = 2.006 \times 10^{-5} \text{ kg/m-s}$
	$\psi_H = 1 + \left(\dfrac{\rho_{l,in}}{\rho_{v,in}} - 1\right) x_{r,test,in}$ (Hewitt *et al.*, 1994)	$\psi_H = 3.075$
	$\Delta P_{contraction,1} = \dfrac{G^2_{reducer}}{2\rho_{l,in}} \left(1 - A^2_{ratio,1} + \left(\dfrac{1}{C_{C,1}} - 1\right)^2\right)\psi_H$ (Hewitt *et al.*, 1994)	$\Delta P_{contraction,1} = 6.713 \times 10^{-3} \text{ kPa}$
	$\Delta P_{contraction,2} = \dfrac{G^2_{contraction}}{2\rho_{l,in}} \left(1 - A^2_{ratio,2} + \left(\dfrac{1}{C_{C,2}} - 1\right)^2\right)\psi_H$ (Hewitt *et al.*, 1994)	$\Delta P_{contraction,2} = 0.2389 \text{ kPa}$
	$\Delta P_{contraction,3} = \dfrac{G^2}{2\rho_{l,in}} \left(1 - A^2_{ratio,3} + \left(\dfrac{1}{C_{C,3}} - 1\right)^2\right)\psi_H$ (Hewitt *et al.*, 1994)	$\Delta P_{contraction,3} = 1.334 \text{ kPa}$
	$\Delta P_{contraction} = \Delta P_{contraction,1} + \Delta P_{contraction,2} + \Delta P_{contraction,3}$	$\Delta P_{contraction} = 1.579 \text{ kPa (36.2\% of } \Delta P_{measured})$
	$\psi_s = 1 + \left(\dfrac{\rho_{l,out}}{\rho_{v,out}} - 1\right)\left[Bx_{r,test,out}\left(1 - x_{r,test,out}\right) + x^2_{r,test,out}\right]$ (Chisholm, 1983)	$\psi_s = 2.110$

Pressure Drop Calculations: 06 September 2005 – Run 29		
Inputs	**Equations**	**Results**
	$$\Delta P_{\text{expansion,3}} = \frac{G^2 A_{\text{ratio,3}}\left(1 - A_{\text{ratio,3}}\right)\psi_S}{\rho_{\text{l,out}}}$$ (Hewitt *et al.*, 1994)	$\Delta P_{\text{expansion,3}} = 0.4039$ kPa
	$$\Delta P_{\text{expansion,2}} = \frac{G_{\text{contraction}}^2 A_{\text{ratio,2}}\left(1 - A_{\text{ratio,2}}\right)\psi_S}{\rho_{\text{l,out}}}$$ (Hewitt *et al.*, 1994)	$\Delta P_{\text{expansion,2}} = 0.0531$ kPa
	$$\Delta P_{\text{expansion,1}} = \frac{G_{\text{reducer}}^2 A_{\text{ratio,1}}\left(1 - A_{\text{ratio,1}}\right)\psi_S}{\rho_{\text{l,out}}}$$ (Hewitt *et al.*, 1994)	$\Delta P_{\text{expansion,1}} = 3.307 \times 10^{-3}$ kPa
	$\Delta P_{\text{expansion}} = \Delta P_{\text{expansion,1}} + \Delta P_{\text{expansion,2}} + \Delta P_{\text{expansion,3}}$	$\Delta P_{\text{expansion}} = 0.4604$ kPa (10.6% of $\Delta P_{\text{measured}}$)
	$$\alpha_{\text{r,test,in}} = \left[1 + \left(\frac{1 - x_{\text{r,test,in}}}{x_{\text{r,test,in}}}\right)^{0.74}\left(\frac{\rho_{\text{v,in}}}{\rho_{\text{l,in}}}\right)^{0.65}\left(\frac{\mu_{\text{l,in}}}{\mu_{\text{v,in}}}\right)^{0.13}\right]^{-1}$$ (Baroczy, 1965)	$\alpha_{\text{r,test,in}} = 0.8114$
	$$\alpha_{\text{r,test,out}} = \left[1 + \left(\frac{1 - x_{\text{r,test,out}}}{x_{\text{r,test,out}}}\right)^{0.74}\left(\frac{\rho_{\text{v,out}}}{\rho_{\text{l,out}}}\right)^{0.65}\left(\frac{\mu_{\text{l,out}}}{\mu_{\text{v,out}}}\right)^{0.13}\right]^{-1}$$ (Baroczy, 1965)	$\alpha_{\text{r,test,out}} = 0.7189$

Pressure Drop Calculations: 06 September 2005 – Run 29		
Inputs	**Equations**	**Results**
	$$\left\|\Delta P_{\text{deceleration}}\right\| = \left\| \left\| G^2 \left[\frac{x^2}{\rho_{v,\text{out}}\alpha} + \frac{(1-x)^2}{\rho_{l,\text{out}}(1-\alpha)} \right] \right\|_{\substack{\alpha = \alpha_{r,\text{ test, out}} \\ x = x_{r,\text{ test, out}}}} - \left\| G^2 \left[\frac{x^2}{\rho_{v,\text{in}}\alpha} + \frac{(1-x)^2}{\rho_{l,\text{in}}(1-\alpha)} \right] \right\|_{\substack{\alpha = \alpha_{r,\text{ test, in}} \\ x = x_{r,\text{ test, in}}}} \right\|$$ (Carey, 1992)	$\left\|\Delta P_{\text{deceleration}}\right\| = 0.4050$ kPa (9.3% of $\Delta P_{\text{measured}}$)
	$\Delta P_{\text{measured}} = \Delta P_{f} - \left\|\Delta P_{\text{deceleration}}\right\| + \Delta P_{\text{contraction}} - \Delta P_{\text{expansion}}$	$\Delta P_{f} = 3.648$ kPa (86.6% of $\Delta P_{\text{measured}}$)
	$\nabla P_{f} = \dfrac{\Delta P_{f}}{L_{\text{test}}}$	$\nabla P_{f} = 11.27$ kPa/m

APPENDIX C - PHASE CHANGE HEAT TRANSFER AND PRESSURE DROP

IN 1.52 mm TEST SECTION: SAMPLE CALCULATIONS
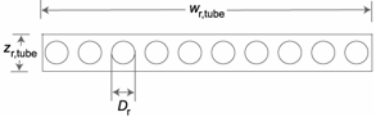
Table C.1 – Measured Variables
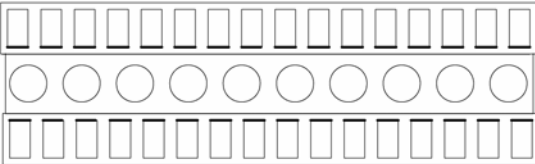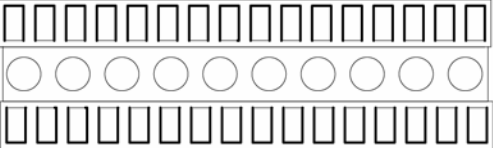
Primary Loop	
$T_{w,test,in,top}$ (˚C)	57.47
$T_{w,test,out,top}$ (˚C)	57.98
$T_{w,test,in,bottom}$ (˚C)	57.27
$T_{w,test,out,bottom}$ (˚C)	57.87
$\dot{V}_{w,prim}$ (m³/s)	1.01×10^{-4}
Secondary Loop	
$T_{w,sec,i}$ (˚C)	16.56
$T_{w,sec,o}$ (˚C)	56.71
$\dot{m}_{w,sec}$ (kg/s)	1.408×10^{-3}
Refrigerant Loop	
$P_{r,test,in}$ (kPa)	3933
$P_{r,test,out}$ (kPa)	3932
$\Delta P_{r,test}$ (kPa)	7.444
$T_{r,test,in}$ (˚C)	61.11
$T_{r,test,out}$ (˚C)	60.80
$\dot{m}_r$ (kg/s)	1.459×10^{-2}
Assumed Variables	
P_w (kPa)	275.8
$T_{ambient}$ (˚C)	23
ε_{ins}	0.85

Table C.2 – Other Parameters

Data Point	
P_r	0.8021
$P_{critical}$ (kPa)	4903
G (kg/m²-s)	800.0
Date of Experiment	10 June 06
Run of Experiment	26
Heat Losses	
$\dot{Q}_{loss,sec}$ (W)	0.4269
$\dot{Q}_{loss,primary}$ (W)	22.32
Quality	
$x_{r,test,in}$	0.3736
$x_{r,test,out}$	0.2189
$x_{r,test,avg}$	0.2962
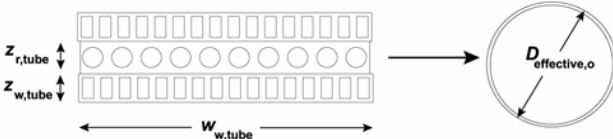
Heat Transfer Calculations: 10 June 2006 – Run 26		
Inputs	**Equations**	**Results**
Various Dimensions in Refrigerant Tube		
$D_{r,port}$ = 1.524 mm	$A_{r,cross} = \dfrac{\pi}{4} \cdot D_{r,port}^2 \cdot n_r$	$A_{r,cross}$ = 1.824 $\times 10^{-5}$ m^2
$L_{r,h}$ = 0.3048 m (12 in.)	$A_{r,surface} = \pi \cdot D_r \cdot L_{r,h} \cdot n_r$	$A_{r,surface}$ = 0.01459 m^2
n_r = 10	$t_{r,tube} = \dfrac{\left(z_{r,tube} - D_r\right)}{2}$	$t_{r,tube}$ = 0.383 mm
$z_{r,tube}$ = 2.290 mm		
$w_{r,tube}$ =19.05 mm		
	$t_{r,port} = \dfrac{\left(w_{r,tube} - 2 \cdot t_{r,tube} - n_r \cdot D_{r,port}\right)}{n_r - 1}$	$t_{r,port}$ = 0.338 mm
Various Dimensions in Water Tube		
$z_{w,port}$ = 1.397 mm	$A_{w,cross} = 2 \cdot z_{w,port} \cdot w_{w,port} \cdot n_w$ (for top and bottom tube)	$A_{w,cross}$ = 3.406 $\times 10^{-5}$ m^2
$w_{w,port}$ = 0.762 mm	$D_{w,port,hydraulic} = \dfrac{4 \cdot z_{w,port} \cdot w_{w,port}}{2 \cdot \left(z_{w,port} + w_{w,port}\right)}$	$D_{w,port,hydraulic}$ = 0.986 mm
n_w = 16		
$z_{w,tube}$ = 1.905 mm	$t_{w,tube} = \dfrac{\left(z_{w,tube} - z_{w,port}\right)}{2}$	$t_{w,tube}$ = 0.254 mm
$w_{w,tube}$ = 19.84 mm	$t_{w,port} = \dfrac{\left(w_{w,tube} - 2 \cdot t_{w,tube} - n_w \cdot w_{w,port}\right)}{n_w - 1}$	$t_{w,port}$ = 0.476 mm
	$A_{w,direct} = 2n_w \cdot L_{r,h} \cdot w_{w,port}$	$A_{w,direct}$ = 7.432 $\times 10^{-3}$ m^2

Heat Transfer Calculations: 10 June 2006 – Run 26		
Inputs	**Equations**	**Results**
	$$A_{w,\text{indirect}} = 2n_w \cdot L_{r,h} \cdot \left(2z_{w,\text{port}} + w_{w,\text{port}}\right)$$	$A_{w,\text{indirect}} = 3.468 \times 10^{-2}\,\text{m}^2$
Conductive Thermal Resistance		
$L_{r,h} = 0.3048$ m (12 in.) $n_r = 10$ $t_{r,\text{port}} = 0.338$ mm $D_{r,\text{port}} = 1.524$ mm $w_{r,\text{tube}} = 19.05$ mm $n_w = 16$ $t_{w,\text{port}} = 0.4758$ mm $w_{w,\text{port}} = 0.762$ mm $w_{w,\text{tube}} = 19.837$ mm $t_{r,\text{tube}} = 0.383$ mm	$$A_{r,\text{tube,i}} = 2 \cdot L_{r,h}\left((n_r - 1)t_{r,\text{port}} + (\pi/2)D_{r,\text{port}} \cdot n_r\right)$$	$A_{r,\text{tube,i}} = 0.01645\,\text{m}^2$
	$$A_{r,\text{tube,o}} = 2 \cdot L_{r,h} \cdot w_{r,\text{tube}}$$	$A_{r,\text{tube,o}} = 0.01161\,\text{m}^2$
	$$A_{w,\text{tube,i}} = 2 \cdot L_{r,h}\left((n_w - 1)t_{w,\text{port}} + w_{w,\text{port}} \cdot n_w\right)$$	$A_{w,\text{tube,i}} = 0.01178\,\text{m}^2$
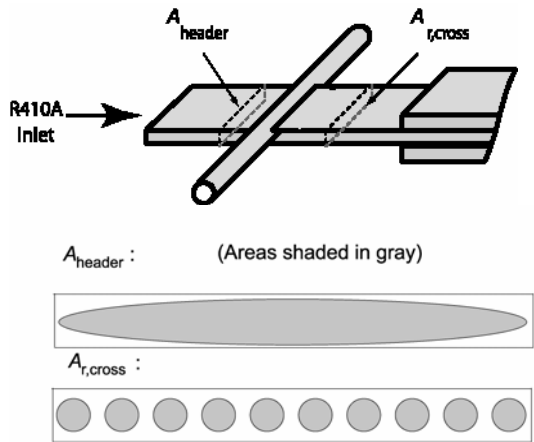
Heat Transfer Calculations: 10 June 2006 – Run 26		
Inputs	**Equations**	**Results**
$t_{w,tube} = 0.254$ mm $k_{Al} = 237.9$ W/m-K	$A_{w,tube,o} = 2 \cdot L_{r,h} \cdot w_{w,tube}$	$A_{w,tube,o} = 0.01209$ m^2
	(assuming that conduction area is average of water and refrigerant side inner and outer areas) $A_{conduction} = \dfrac{A_{r,tube,i} + A_{r,tube,o} + A_{w,tube,i} + A_{w,tube,o}}{4}$	$A_{conduction} = 0.01298$ m^2
	$R_{conduction} = \dfrac{t_{r,tube} + t_{w,tube}}{k_{Al} \cdot A_{conduction}}$	$R_{conduction} = 3.303 \times 10^{-4}$ K/W
Convective Thermal Resistance in Water Tube		
$T_{w,test,in,top} = 57.47°C$ $T_{w,test,out,top} = 57.98°C$ $T_{w,test,in,bottom} = 57.27°C$ $T_{w,test,out,bottom} = 57.87°C$ $P_w = 275.8$ kPa $\dot{V}_{w,prim} = 1.01 \times 10^{-4}$ m^3/s $A_{w,cross} = 3.406 \times 10^{-5}$ m^2	$T_{w,prim,avg} = \dfrac{\left(\begin{array}{c} T_{w,test,in,top} + T_{w,test,in,bottom} \\ + T_{w,test,out,top} + T_{w,test,out,bottom} \end{array} \right)}{4}$	$T_{w,test,avg} = 57.65°C$
	$Pr_w, \mu_w, \rho_w, k_w = f\left(P_w, T_{w,prim,avg}\right)$	$Pr_w = 3.102$, $\mu_w = 4.835 \times 10^{-4}$ kg/m-s, $\rho_w = 984.5$ kg/m^3, $k_w = 0.6521$ W/m-K
	$V_w = \dfrac{\dot{V}_{w,prim}}{A_{w,cross}}$	$V_w = 2.963$ m/s
	$Re_w = \dfrac{\rho_w V_w D_{w,port,hydraulic}}{\mu_w}$	$Re_w = 5950$

Heat Transfer Calculations: 10 June 2006 – Run 26		
Inputs	**Equations**	**Results**
$D_{w,port,hydraulic} = 0.986$ mm	$f = 8\left[\left(\dfrac{8}{Re_w}\right)^{12} + \left\{2.457\ln\left(\left[\dfrac{7}{Re_w}\right]^{0.9} + 0.27\left(\dfrac{e_{w,port}}{D_{w,port,hydraulic}}\right)\right)^{16} + \left[\dfrac{37530}{Re_w}\right]^{16}\right\}^{-1.5}\right]^{1/12}$ (Churchill, 1977)	$f = 0.03717$
$\left(\dfrac{e_{w,port}}{D_{w,port,hydraulic}}\right) = 0.0009$ (Coleman, 2000)	$Nu_w = \left[4.364^{10} + \left(\dfrac{\exp\left[\dfrac{2200 - Re_w}{365}\right]}{4.364^2} + \left(6.3 + \dfrac{0.079 \cdot \left(\dfrac{f}{8}\right)^{1/2} \cdot Re_w \cdot Pr}{\left(1 + Pr^{0.8}\right)^{5/6}}\right)^{-2}\right)\right]$ (Churchill, 1977)	$Nu_w = 41.45$
$L_{r,h} = 0.3048$ m (12 in.) $t_{w,port} = 0.4758$ mm $k_{Al} = 237.9$ W/m-K		
$z_{w,port} = 1.397$ mm	$h_w = \dfrac{k_w Nu_w}{D_{w,port,hydraulic}}$	$h_w = 27410$ W/m^2-K
$A_{w,direct} = 7.432 \times 10^{-3}$ m^2 $A_{w,indirect} = 3.468 \times 10^{-2}$ m^2	$M = \sqrt{\dfrac{h_w \cdot 2\left(L_{r,h} + t_{w,port}\right)}{k_{Al} \cdot \left(L_{r,h} \cdot t_{w,port}\right)}}$	$M = 697.4$ m^{-1}
	$\eta_{w,fin} = \dfrac{\tanh\left(M \cdot \left(z_{w,port} + w_{w,port}/2\right)\right)}{M \cdot \left(z_{w,port} + w_{w,port}/2\right)}$	$\eta_{w,fin} = 0.6818$
	$A_w = A_{w,direct} + \eta_{w,fin} A_{w,indirect}$	$A_w = 0.03108$ m^2
	$R_w = \dfrac{1}{h_w A_w}$	$R_w = 11.74 \times 10^{-4}$ K/W
Heat Losses to Ambient in Test Section		
$w_{w,tube} = 19.84$ mm $z_{w,tube} = 1.905$ mm $z_{r,tube} = 2.290$ mm	$D_{effective,o} = \dfrac{\left(2 \cdot w_{w,tube} + 4 \cdot z_{w,tube} + 2z_{r,tube}\right)L_{r,h}}{\pi \cdot L_{r,h}}$	$D_{effective,o} = 16.51$ mm

Heat Transfer Calculations: 10 June 2006 – Run 26		
Inputs	**Equations**	**Results**
$L_{r,h}$ = 0.3048 m		
$t_{w,tube}$ = 0.254 mm		
k_{Al} = 237.9 W/m-K		
D_{ins} = 0.1 m	$D_{effective,i} = D_{effective,o} - 2 \cdot t_{w,tube}$	$D_{effective,i}$ =16.00 mm
k_{ins} = 0.043 W/m-K	$R_{conduction,outer} = \dfrac{\ln\left(\dfrac{D_{effective,\,o}}{D_{effective,\,i}}\right)}{2\pi k_{Al} L_{r,h}}$	$R_{conduction,outer}$ = 6.858 × 10^{-5} K/W
ε_{ins} = 0.8		
σ = 5.67 ×10^{-8} W/m^2-K^4		
$T_{w,test,avg}$ = 57.65˚C	$R_{ins} = \dfrac{\ln\left(\dfrac{D_{ins}}{D_{effective,o}}\right)}{2\pi k_{ins} L_{r,h}}$	R_{ins} = 21.87 K/W
$T_{ambient}$ = 23˚C		
g = 9.81 m/s^2	$R_{radiation} = \dfrac{1}{\pi D_{test,ins} L_{r,h} \varepsilon_{ins} \sigma \left(T_{ins}^2 + T_{ambient}^2\right)\left(T_{ins} + T_{ambient}\right)}$	$R_{radiation}$ = 2.064 K/W
R_{w} = 10.68 ×10^{-4} K/W		
	$Pr_{air}, \nu_{air}, \alpha_{air}, \beta_{air}, k_{air} = f\left(P_{ambient}, T_{ambient}\right)$	Pr_{air} = 0.73, ν_{air} = 1.548 ×10^{-5} m^2/s, α_{air} = 2.11 ×10^{-5} m^2/s, β_{air} = 0.003377 1/K k_{air} = 0.02536 W/m-K
	$Ra = \dfrac{g\beta\left(T_{ins} - T_{ambient}\right)D_{ins}^3}{\nu_{air}\alpha_{air}}$	Ra = 210 ×10^3 T_{ins} = 25.08˚C (solved by iteration)

Heat Transfer Calculations: 10 June 2006 – Run 26		
Inputs	**Equations**	**Results**
	$\text{Nu} = \dfrac{h_{\text{nat.conv.}} D_{\text{ins}}}{k_{\text{air}}} = \left(0.60 + \dfrac{0.387 \text{Ra}^{1/6}}{\left(1 + \left(\dfrac{0.559}{\text{Pr}_{\text{air}}} \right)^{9/16} \right)^{8/27}} \right)^2$ (Churchill and Chu, 1975)	$\text{Nu} = 9.50$ $h_{\text{nat.conv.}} = 2.41$ W/m^2-K
	$R_{\text{nat.conv.}} = \dfrac{1}{h_{\text{nat.conv.}} \pi D_{\text{ins}} L_{\text{r,h}}}$	$R_{\text{nat.conv.}} = 4.332$ K/W
	$\dot{Q}_{\text{loss, test}} = \dfrac{T_{\text{w,test,avg}} - T_{\text{ambient}}}{R_{\text{w}} + R_{\text{conduction,outer}} + R_{\text{ins}} + \dfrac{R_{\text{radiation}} R_{\text{nat.conv.}}}{R_{\text{radiation}} + R_{\text{nat.conv.}}}}$	$\dot{Q}_{\text{loss, test}} = 1.489$ W
Refrigerant Heat Transfer Coefficient		
$\dot{V}_{\text{w,prim,gpm}} = 1.6$ gpm $(\dot{V}_{\text{w, prim}} = 1.01 \times 10^{-4}$ m^3/s)	$\dot{Q}_{\text{pump}} = 3.3957 \dot{V}^3_{\text{w,prim,gpm}} - 1.4044 \dot{V}^2_{\text{w,prim,gpm}}$ $\qquad + 10.651 \dot{V}_{\text{w,prim,gpm}}$	$\dot{Q}_{\text{pump}} = 27.36$ W
$\dot{Q}_{\text{loss, test}} = 1.489$ W	$\dot{Q}_{\text{loss, ambient}} = \dot{Q}_{\text{loss, test}} + \dot{Q}_{\text{loss, primary}} + \dot{Q}_{\text{loss, sec}}$	$\dot{Q}_{\text{loss,ambient}} = 24.23$ W
	$i_{\text{w, sec, o}} = f\left(T_{\text{w, sec, o}}, P_{\text{w}} \right)$	$i_{\text{w, sec, o}} = 237.6 \times 10^3$ J/kg
$\dot{Q}_{\text{loss, primary}} = 22.32$ W	$i_{\text{w, sec, i}} = f\left(T_{\text{w, sec, i}}, P_{\text{w}} \right)$	$i_{\text{w, sec, i}} = 69.76 \times 10^3$ J/kg
$\dot{Q}_{\text{loss, sec}} = 0.4269$ W	$\dot{Q}_{\text{sec}} = \dot{m}_{\text{w, sec}} \left(i_{\text{w, sec, o}} - i_{\text{w, sec, i}} \right)$	$\dot{Q}_{\text{sec}} = 236.4$ W
$T_{\text{w,sec,i}} = 16.56°\text{C}$	$\dot{Q}_{\text{test}} = \dot{Q}_{\text{sec}} + \dot{Q}_{\text{loss,ambient}} - \dot{Q}_{\text{pump}}$	$\dot{Q}_{\text{test}} = 233.3$ W

Heat Transfer Calculations: 10 June 2006 – Run 26		
Inputs	**Equations**	**Results**
$T_{w,\,sec,\,o} = 56.71°C$	$T_{w,test,in,avg} = \dfrac{\left(T_{w,test,in,top} + T_{w,test,in,bottom}\right)}{2}$	$T_{w,test,in,avg} = 57.37°C$
$P_w = 275.8 \text{ kPa}$		
$\dot{m}_{w,\,sec} = 1.408 \times 10^{-3} \text{ kg/s}$	$T_{w,test,out,avg} = \dfrac{\left(T_{w,test,out,top} + T_{w,test,out,bottom}\right)}{2}$	$T_{w,test,out,avg} = 57.93°C$
$T_{r,test,in} = 61.11°C$		
$T_{r,test,out} = 60.80°C$	$T_{r,test,in,sat} = f\left(x_{r,test,in}, P_{r,test,in}\right)$	$T_{r,test,in,sat} = 61.10°C$
$T_{w,test,in,top} = 57.47°C$	$Error_{r,test,in} = T_{r,test,in} - T_{r,test,in,sat}$	$Error_{r,test,in} = 0.01°C$
$T_{w,test,out,top} = 57.98°C$	$T_{r,test,out,sat} = f\left(x_{r,test,out}, P_{r,test,out}\right)$	$T_{r,test,out,sat} = 61.07°C$
$T_{w,test,in,bottom} = 57.27°C$	$Error_{r,test,out} = T_{r,test,out} - T_{r,test,in,out}$	$Error_{r,test,out} = -0.27°C$
$T_{w,test,out,bottom} = 57.87°C$	$\text{LMTD} = \dfrac{\left(T_{r,test,in,sat} - T_{w,test,out,avg}\right) - \left(T_{r,test,out,sat} - T_{w,test,in,avg}\right)}{\ln\left[\dfrac{\left(T_{r,test,in,sat} - T_{w,test,out,avg}\right)}{\left(T_{r,test,out,sat} - T_{w,test,in,avg}\right)}\right]}$	$\text{LMTD} = 3.493°C$
$x_{r,test,in} = 0.3736$		
$x_{r,test,out} = 0.2189$		
$P_{r,test,in} = 3933 \text{ kPa}$	$(UA) = \dfrac{\dot{Q}_{test}}{(\text{LMTD})}$	$UA = 66.8 \text{ W/K}$
$P_{r,test,out} = 3932 \text{ kPa}$		
$R_w = 10.68 \times 10^{-4} \text{ K/W}$	$h_r = \dfrac{1}{\left[(UA)^{-1} - R_{conduction} - R_w\right] A_{r,surface}}$	$h_r = 5088 \text{ W/m}^2\text{-K}$
$R_{conduction} = 2.295 \times 10^{-4} \text{ K/W}$		
$A_{r,surface} = 0.01459 \text{ m}^2$	$R_r = \dfrac{1}{h_r A_{r,surface}}$	$R_r = 13.57 \times 10^{-3} \text{ K/W}$
	$R_{ratio} = \dfrac{R_r}{R_w + R_{conduction}}$	$R_{ratio} = 8.953$

Pressure Drop Calculations: 10 June 2006 – Run 26		
Inputs	**Equations**	**Results**
$A_{\text{header}} = 0.05328 \text{ m}^2$ $A_{\text{r,cross}} = 1.824 \times 10^{-5} \text{ m}^2$ $\dot{m}_r = 1.459 \times 10^{-2} \text{ kg/s}$ $x_{\text{r,test,in}} = 0.3736$ $P_{\text{r,test,in}} = 3933 \text{ kPa}$ $x_{\text{r,test,out}} = 0.2189$ $P_{\text{r,test,out}} = 3932 \text{ kPa}$ $B = 0.25$ $\Delta P_{\text{measured}} = 7.444 \text{ kPa}$ $L_{\text{r,P}} = 508.0 \text{ mm}$	$A_{\text{ratio}} = \dfrac{A_{\text{header}}}{A_{\text{r,cross}}}$ 	$A_{\text{ratio}} = 0.5307$
	$G = \dfrac{\dot{m}_r}{A_{\text{r,cross}}}$	$G = 800.0 \text{ kg/m}^2\text{-s}$
	$C_C = \dfrac{1}{0.639\left[1-\left(A_{\text{ratio}}\right)\right]^{1/2}+1}$ (Chisholm, 1983)	$C_C = 0.6955$
	$\left(\rho_l, \mu_l\right)_{\text{in}} = f\left(x_{\text{r,test,in}}, P_{\text{r,test,in}}\right)$	$\rho_{l,\text{in}} = 803.1 \text{ kg/m}^3$, $\mu_{l,\text{in}} = 6.705 \times 10^{-5} \text{ kg/m-s}$
	$\left(\rho_v, \mu_v\right)_{\text{in}} = f\left(x_{\text{r,test,in}}, P_{\text{r,test,in}}\right)$	$\rho_{v,\text{in}} = 210.3 \text{ kg/m}^3$, $\mu_{v,\text{in}} = 2.007 \times 10^{-5} \text{ kg/m-s}$

Pressure Drop Calculations: 10 June 2006 – Run 26		
Inputs	**Equations**	**Results**
	$\left(\rho_{l},\mu_{l}\right)_{out}=f\left(x_{r,test,out},P_{r,test,out}\right)$	$\rho_{l,out}=803.2$ kg/m^3, $\mu_{l,out}=6.711\times10^{-5}$ kg/m-s
	$\left(\rho_{v},\mu_{v}\right)_{out}=f\left(x_{r,test,out},P_{r,test,out}\right)$	$\rho_{v,out}=210.2$ kg/m^3, $\mu_{v,out}=2.005\times10^{-5}$ kg/m-s
	$\psi_{H}=1+\left(\dfrac{\rho_{l,in}}{\rho_{v,in}}-1\right)x_{r,test,in}$ (Hewitt *et al.*, 1994)	$\psi_{H}=2.053$
	$\Delta P_{contraction}=\dfrac{G^{2}}{2\rho_{l,in}}\left(1-A_{ratio}^{2}+\left(\dfrac{1}{C_{C}}-1\right)^{2}\right)\psi_{H}$ (Hewitt *et al.*, 1994)	$\Delta P_{contraction}=0.7444$ kPa
	$\psi_{s}=1+\left(\dfrac{\rho_{l,out}}{\rho_{v,out}}-1\right)\left[Bx_{r,test,out}\left(1-x_{r,test,out}\right)+x_{r,test,out}^{2}\right]$ (Chisholm, 1983)	$\psi_{s}=1.256$
	$\Delta P_{expansion}=\dfrac{G^{2}A_{ratio}\left(1-A_{ratio}\right)\psi_{S}}{\rho_{l,out}}$ (Hewitt *et al.*, 1994)	$\Delta P_{expansion}=0.2492$ kPa
	$\alpha_{in}=\left[1+\left(\dfrac{1-x_{r,test,in}}{x_{r,test,in}}\right)^{0.74}\left(\dfrac{\rho_{v,in}}{\rho_{l,in}}\right)^{0.65}\left(\dfrac{\mu_{l,in}}{\mu_{v.in}}\right)^{0.13}\right]^{-1}$ (Baroczy, 1965)	$\alpha_{in}=0.5822$
	$\alpha_{out}=\left[1+\left(\dfrac{1-x_{r,test,out}}{x_{r,test,out}}\right)^{0.74}\left(\dfrac{\rho_{v,out}}{\rho_{l,out}}\right)^{0.65}\left(\dfrac{\mu_{l,out}}{\mu_{v,out}}\right)^{0.13}\right]^{-1}$ (Baroczy, 1965)	$\alpha_{out}=0.4435$

Pressure Drop Calculations: 10 June 2006 – Run 26		
Inputs	**Equations**	**Results**
	$$\left\| \Delta P_{\text{deceleration}} \right\| = \left\| \left\| G^2 \left[\frac{x^2}{\rho_{v,\text{out}} \alpha} + \frac{(1-x)^2}{\rho_{l,\text{out}} (1-\alpha)} \right] \right\|_{\substack{\alpha = \alpha_{r,\text{test, out}} \\ x = x_{r,\text{test, out}}}} - \left\| G^2 \left[\frac{x^2}{\rho_{v,\text{in}} \alpha} + \frac{(1-x)^2}{\rho_{l,\text{in}} (1-\alpha)} \right] \right\|_{\substack{\alpha = \alpha_{r,\text{test, in}} \\ x = x_{r,\text{test, in}}}} \right\|$$ (Carey, 1992)	$\left\| \Delta P_{\text{deceleration}} \right\| = 0.2755$ kPa
	$\Delta P_{\text{measured}} = \Delta P_{f} - \left\| \Delta P_{\text{deceleration}} \right\| + \Delta P_{\text{contraction}} - \Delta P_{\text{expansion}}$	$\Delta P_{f} = 7.224$ kPa
	$\nabla P_{f} = \dfrac{\Delta P_{f}}{L_{r,P}}$	$\nabla P_{f} = 14.22$ kPa/m

APPENDIX D - PHASE CHANGE HEAT TRANSFER AND PRESSURE DROP

MODELS

Data Point in Annular Flow	
P_r	0.8008
$P_{r,test}$ (kPa)	3926
$P_{critical}$ (kPa)	4903
G (kg/m^2-s)	801.3
$x_{r,test,avg}$	0.6531
$T_{r,sat}$ (°C)	61.07
T_{wall} (°C)	52.98
Date of Experiment	06 Sept 05
Run of Experiment	29
$h_{experimental}$ (W/m^2-K)	5440
$\nabla P_{experimental}$ (kPa/m)	11.27
D (mm)	3.048
Refrigerant	R410A

Data Point in Wavy Flow	
P_r	0.8005
$P_{r,test}$ (kPa)	3924
$P_{critical}$ (kPa)	4903
G (kg/m^2-s)	400.8
$x_{r,test,avg}$	0.3567
$T_{r,sat}$ (°C)	61.05
T_{wall} (°C)	55.09
Date of Experiment	N/A
Run of Experiment	N/A
$h_{experimental}$ (W/m^2-K)	2405
$\nabla P_{experimental}$ (kPa/m)	0.9633
D (mm)	6.223
Refrigerant	R410A

Two-Phase Pressure Drop and Heat Transfer Models		
Inputs	**Equations**	**Results**
Common Variables and Properties - Annular Flow		
$P_{r,test}$ = 3926 kPa G = 801.3 kg/m^2-s D = 3.048 mm $x_{r,test,avg} = x = 0.6531$ $\varepsilon = \dfrac{e}{D} = 0.0005$	$\mu_l, \rho_l, \mathrm{Pr}_L, c_P, k_l, i_{fg} = f\left(P_{r,test}, x = 0\right)$	μ_l = 67.19 ×10^{-6} kg/m-s, ρ_l = 804.0 kg/m^3, Pr_L = 3.036, c_P = 3343 J/kg-K, i_{fg} =101.2 kJ/kg k_l = 0.07398 W/m-K
	$\mu_v, \rho_v = f\left(P_{r,test}, x = 1\right)$	μ_v = 20.04 ×10^{-6} kg/m-s, ρ_v = 209.6 kg/m^3
	$\sigma = f\left(P_{r,test}, x\right)$	σ = 80.83 ×10^{-5} N/m

Two-Phase Pressure Drop and Heat Transfer Models		
Inputs	**Equations**	**Results**
	$$\alpha = \left[1+\left(\frac{1-x}{x}\right)^{0.74}\left(\frac{\rho_v}{\rho_l}\right)^{0.65}\left(\frac{\mu_l}{\mu_v}\right)^{0.13}\right]^{-1}$$	$\alpha = 0.7658$
	$$\text{Re}_L = \frac{(1-x)GD}{\mu_l}$$	$\text{Re}_L = 12610$
	$$\text{Re}_G = \frac{xGD}{\mu_v}$$	$\text{Re}_G = 79600$
	$$f_L = 8\left[\left(\frac{8}{\text{Re}_L}\right)^{12}+\left\{2.457\ln\left(\left[\frac{7}{\text{Re}_L}\right]^{0.9}+0.27\left(\frac{e}{D}\right)\right)^{16}+\left[\frac{37530}{\text{Re}_L}\right]^{16}\right\}^{-1.5}\right]^{1/12}$$	$f_L = 0.03008$
	$$f_G = 8\left[\left(\frac{8}{\text{Re}_G}\right)^{12}+\left\{2.457\ln\left(\left[\frac{7}{\text{Re}_G}\right]^{0.9}+0.27\left(\frac{e}{D}\right)\right)^{16}+\left[\frac{37530}{\text{Re}_G}\right]^{16}\right\}^{-1.5}\right]^{1/12}$$	$f_G = 0.02106$
	$$\left(\frac{dP}{dz}\right)_L = \left(\frac{1}{2}\cdot f_L\cdot\frac{\left((1-x)G\right)^2}{\rho_l\cdot D}\right)$$	$\left(\dfrac{dP}{dz}\right)_L = 0.4741$ kPa/m
	$$\left(\frac{dP}{dz}\right)_G = \left(\frac{1}{2}\cdot f_G\cdot\frac{(xG)^2}{\rho_v\cdot D}\right)$$	$\left(\dfrac{dP}{dz}\right)_G = 4.513$ kPa/m
Common Variables and Properties - Wavy Flow		
$P_{r,test} = 3920$ kPa $G = 397.2$ kg/m²-s $D = 6.223$ mm	$$\mu_l,\rho_l,\text{Pr}_L,c_p,k_l,i_{fg} = f\left(P_{r,test},x=0\right)$$	$\mu_l = 67.22\times10^{-6}$ kg/m-s, $\rho_l =$ 804.2 kg/m³, $\text{Pr}_L = 3.034$, $c_p =$ 3339 J/kg-K, $i_{fg} = 101.3$ kJ/kg $k_l = 0.07398$ W/m-K

Two-Phase Pressure Drop and Heat Transfer Models		
Inputs	**Equations**	**Results**
$x_{\text{r,test,avg}} = x = 0.5108$ $\varepsilon = \dfrac{e}{D} = 0.00025$	$\mu_v, \rho_v = f\left(P_{\text{r,test}}, x = 1\right)$	$\mu_v = 20.04 \times 10^{-6}$ kg/m-s, $\rho_v = 209.5$ kg/m^3
	$\sigma = f\left(P_{\text{r,test}}, x\right)$	$\sigma = 81.60 \times 10^{-5}$ N/m
	$\alpha = \left[1 + \left(\dfrac{1-x}{x}\right)^{0.74}\left(\dfrac{\rho_v}{\rho_l}\right)^{0.65}\left(\dfrac{\mu_l}{\mu_v}\right)^{0.13}\right]^{-1}$	$\alpha = 0.5697$
	$\text{Re}_L = \dfrac{(1-x)GD}{\mu_l}$	$\text{Re}_L = 23870$
	$\text{Re}_G = \dfrac{xGD}{\mu_v}$	$\text{Re}_G = 44400$
	$f_L = 8\left[\left(\dfrac{8}{\text{Re}_L}\right)^{12} + \left\{2.457\ln\left(\left[\dfrac{7}{\text{Re}_L}\right]^{0.9} + 0.27\left(\dfrac{e}{D}\right)\right)^{16} + \left[\dfrac{37530}{\text{Re}_L}\right]^{16}\right\}^{-1.5}\right]^{1/12}$	$f_L = 0.02539$
	$f_G = 8\left[\left(\dfrac{8}{\text{Re}_G}\right)^{12} + \left\{2.457\ln\left(\left[\dfrac{7}{\text{Re}_G}\right]^{0.9} + 0.27\left(\dfrac{e}{D}\right)\right)^{16} + \left[\dfrac{37530}{\text{Re}_G}\right]^{16}\right\}^{-1.5}\right]^{1/12}$	$f_G = 0.02226$
	$\left(\dfrac{dP}{dz}\right)_L = \left(\dfrac{1}{2} \cdot f_L \cdot \dfrac{\left((1-x)G\right)^2}{\rho_l \cdot D}\right)$	$\left(\dfrac{dP}{dz}\right)_L = 0.1687$ kPa/m
	$\left(\dfrac{dP}{dz}\right)_G = \left(\dfrac{1}{2} \cdot f_G \cdot \dfrac{(xG)^2}{\rho_v \cdot D}\right)$	$\left(\dfrac{dP}{dz}\right)_G = 0.1745$ kPa/m
Pressure Drop Model – Annular Flow		

Two-Phase Pressure Drop and Heat Transfer Models		
Inputs	**Equations**	**Results**
$\sigma = 80.83 \times 10^{-5}$ N/m $\rho_l = 804.0$ kg/m^3 $\rho_v = 209.6$ kg/m^3 $D = 3.048$ mm $\text{Re}_L = 12610$ $\left(\dfrac{dP}{dz}\right)_L = 0.4741$ kPa/m $\left(\dfrac{dP}{dz}\right)_G = 4.513$ kPa/m $\nabla P_{\text{experimental}} = 11.27$ kPa/m	$N_{\text{conf}} = \dfrac{\left[\dfrac{\sigma}{g\left(\rho_l - \rho_v\right)}\right]^{1/2}}{D}$	$N_{\text{conf}} = 0.1222$
	$C = 24 \cdot \text{Re}_L^{-0.3} \cdot N_{\text{conf}}^{-0.4}$	$C = 3.275$
	$\dfrac{dP_f}{dz} = \left(\dfrac{dP}{dz}\right)_L + C\left[\left(\dfrac{dP}{dz}\right)_L \cdot \left(\dfrac{dP}{dz}\right)_G\right]^{1/2} + \left(\dfrac{dP}{dz}\right)_G$	$\dfrac{dP_f}{dz} = \nabla P_f = 9.778$ kPa/m
	$Error = \dfrac{\left(\nabla P_f - \nabla P_{\text{experimental}}\right)}{\nabla P_{\text{experimental}}}$	$Error = 13.2\%$
Heat Transfer Model – Annular Flow		
$\text{Re}_L = 12610$ $\text{Pr}_L = 3.036$ $x_{\text{r,test,avg}} = x = 0.6531$ $\rho_l = 804.0$ kg/m^3 $\rho_v = 209.6$ kg/m^3 $D = 3.048$ mm	$\text{Nu}_{\text{annular}} = 0.0133 \cdot \text{Re}_L^{4/5} \cdot \text{Pr}_L^{1/3} \cdot \left[1 + \left(\dfrac{x}{1-x}\right)^{0.80}\left(\dfrac{\rho_l}{\rho_v}\right)^{0.88}\right]$	$\text{Nu}_{\text{annular}} = 235.7$
	$h = \text{Nu}_{\text{annular}} \dfrac{k_l}{D}$	$h = 5721$ W/m^2-K
	$Error = \dfrac{\left(h - h_{\text{experimental}}\right)}{h_{\text{experimental}}}$	$Error = 5.2\%$

Two-Phase Pressure Drop and Heat Transfer Models		
Inputs	**Equations**	**Results**
k_l = 0.07398 W/m-K $h_{experimental}$ = 5440 W/m²-K		
Pressure Drop Model – Wavy Flow		
σ = 81.60 ×10⁻⁵ N/m ρ_l = 804.2 kg/m³ ρ_v = 209.5 kg/m³ D = 6.223 mm Re_L = 23870 $\left(\dfrac{dP}{dz}\right)_L$ = 0.1687 kPa/m $\left(\dfrac{dP}{dz}\right)_G$ = 0.1745 kPa/m $\nabla P_{experimental}$ = 0.9633 kPa/m	$N_{conf} = \dfrac{\left[\dfrac{\sigma}{g\left(\rho_l - \rho_v\right)}\right]^{1/2}}{D}$	N_{conf} = 0.06011
	$C = 24 \cdot Re_L^{-0.3} \cdot N_{conf}^{-0.4}$	C = 3.592
	$\dfrac{dP_f}{dz} = \left(\dfrac{dP}{dz}\right)_L + C\left[\left(\dfrac{dP}{dz}\right)_L \cdot \left(\dfrac{dP}{dz}\right)_G\right]^{1/2} + \left(\dfrac{dP}{dz}\right)_G$	$\dfrac{dP_f}{dz} = \nabla P_f = 0.9594$ kPa/m
	$Error = \left(\nabla P_f - \nabla P_{experimental}\right)\Big/ \nabla P_{experimental}$	$Error$ = 0.4 %
Heat Transfer Model – Wavy Flow		
$T_{r,sat}$ = 61.05°C T_{wall} =55.09°C α = 0.5697	$Area_{total} = \dfrac{\pi}{4}D^2$	$Area_{total}$ = 30.42 ×10⁻⁶ m²
	$Area_L = \left(1 - \alpha\right)Area_{total}$	$Area_L$ = 13.09 ×10⁻⁶ m²
	$Area_L = \dfrac{D^2}{8}\left[\left(2\pi - \theta\right) - \sin\left(2\pi - \theta\right)\right]$	θ = 3.362 rad

Two-Phase Pressure Drop and Heat Transfer Models		
Inputs	**Equations**	**Results**
$i_{fg} = 101.3$ kJ/kg	$\mathrm{Ja} = \dfrac{\left(T_{bulk} - T_{r,inner\,wall}\right)c_{P,l}}{i_{fg}}$	$\mathrm{Ja} = 0.1642$
$c_{P,l} = 3339$ J/kg-K	$\mathrm{Ra} = \dfrac{D^3 g \rho_l \left(\rho_l - \rho_v\right)c_{P,l}}{\mu_l k_l}$	$\mathrm{Ra} = 7.591 \times 10^8$
$\rho_l = 804.2$ kg/m^3		
$\mu_l = 67.22 \times 10^{-6}$ kg/m-s	$\mathrm{Nu}_{wavy} = \left(\dfrac{1.93}{2\pi}\right)\left(\mathrm{Ra}\cdot\left(\dfrac{1}{\mathrm{Ja}}+1\right)\right)^{1/4}$	
$k_l = 0.07398$ W/m-K	$\quad + 0.018\,\mathrm{Re}_L^{0.8}\cdot\mathrm{Pr}_L^{1/3}\cdot\left[1+\left(\dfrac{x}{1-x}\right)\left(\dfrac{\rho_l}{\rho_v}\right)^{1.24}\right]\left(\dfrac{D}{9.398\ \mathrm{mm}}\right)^{0.34}\cdot\left(1-\dfrac{\theta}{2\pi}\right)$	$\mathrm{Nu}_{wavy} = 216.0$
$\mathrm{Pr}_L = 3.034$		
$h_{experimental} = 2408$ W/m^2-K	$h = \mathrm{Nu}_{wavy}\dfrac{k_l}{D}$	$h = 2568$ W/m^2-K
	$Error = \dfrac{\left(h - h_{experimental}\right)}{h_{experimental}}$	$Error = 6.6\ \%$

APPENDIX E - SUPERCRITICAL HEAT TRANSFER AND PRESSURE DROP

MODELS

Data Point in Liquid-Like Regime	
P_r	1.108
$P_{r,test}$ (kPa)	5432
$P_{critical}$ (kPa)	4903
G (kg/m²-s)	801.9
$T_{r,test,avg} = T_{bulk}$ (°C)	60.71
T_{wall} (°C)	57.73
Date of Experiment	27 June 06
Run of Experiment	Run 11
$h_{experimental}$ (W/m²-K)	5136
$\nabla P_{experimental}$ (kPa/m)	7.405

Data Point in PCT Regime	
P_r	1.106
$P_{r,test}$ (kPa)	5423
$P_{critical}$ (kPa)	4903
G (kg/m²-s)	792.8
$T_{r,test,avg} = T_{bulk}$ (°C)	67.47
T_{wall} (°C)	64.09
Date of Experiment	27 June 06
Run of Experiment	Run 17
$h_{experimental}$ (W/m²-K)	5555
$\nabla P_{experimental}$ (kPa/m)	7.807

Data Point in Gas-Like Regime	
P_r	1.105
$P_{r,test}$ (kPa)	5418
$P_{critical}$ (kPa)	4903
G (kg/m²-s)	792.4
$T_{r,test,avg} = T_{bulk}$ (°C)	90.51
T_{wall} (°C)	85.71
Date of Experiment	27 June 06
Run of Experiment	Run 44
$h_{experimental}$ (W/m²-K)	5802
$\nabla P_{experimental}$ (kPa/m)	19.45

Supercritical Pressure Drop and Heat Transfer Models		
Inputs	**Equations**	**Results**
Common Variables and Properties – Liquid-Like Regime		
$P_{r,test} = 5432$ kPa $G = 801.9$ kg/m²-s $D = 1.524$ mm $T_{r,test,avg} = T_{bulk} = 60.71°C$ $T_{wall} = 57.73°C$ $\varepsilon = \dfrac{e}{D} = 0.0001$	$\mu_{bulk}, \rho_{bulk}, k_{bulk}, \text{Pr}_{bulk} = f\left(P_{r,test}, T_{bulk} = \right)$	$\mu_{bulk} = 77.39 \times 10^{-6}$ kg/m-s, $\rho_{bulk} =$ 875.1 kg/m³, $k_{bulk} = 0.07751$W/m-K, $\text{Pr}_{bulk} = 2.229$
	$\mu_{wall}, \rho_{wall} = f\left(P_{r,test}, T_{wall} = \right)$	$\mu_{wall} = 81.86 \times 10^{-6}$ kg/m-s, $\rho_{wall} =$ 900.9 kg/m³
	$\text{Re}_{bulk} = \dfrac{GD}{\mu_{bulk}}$	$\text{Re}_{bulk} = 15792$
	$f_{Churchill} = 8\left[\left(\dfrac{8}{\text{Re}_{bulk}}\right)^{12} + \left\{2.457\ln\left(\left[\dfrac{7}{\text{Re}_{bulk}}\right]^{0.9} + 0.27\left(\dfrac{e}{D}\right)\right)^{16} + \left[\dfrac{37530}{\text{Re}_{bulk}}\right]^{16}\right\}^{-1.5}\right]^{1/12}$	$f_{Churchill} = 0.02766$
Common Variables and Properties – PCT Regime		

Supercritical Pressure Drop and Heat Transfer Models

Inputs	Equations	Results
$P_{r,test} = 5423$ kPa $G = 792.8$ kg/m²-s $D = 1.524$ mm $T_{r,test,avg} = T_{bulk} = 67.47°C$ $T_{wall} = 64.09°C$ $\varepsilon = \dfrac{e}{D} = 0.0001$	$\mu_{bulk}, \rho_{bulk}, k_{bulk}, \mathrm{Pr}_{bulk} = f\left(P_{r,test}, T_{bulk} =\right)$	$\mu_{bulk} = 66.07 \times 10^{-6}$ kg/m-s, $\rho_{bulk} =$ 799.9 kg/m³, $k_{bulk} = 0.0729$ W/m-K, $\mathrm{Pr}_{bulk} = 2.572$
	$\mu_{wall}, \rho_{wall} = f\left(P_{r,test}, T_{wall} =\right)$	$\mu_{wall} = 71.98 \times 10^{-6}$ kg/m-s, $\rho_{wall} =$ 841.2 kg/m³
	$\mathrm{Re}_{bulk} = \dfrac{GD}{\mu_{bulk}}$	$\mathrm{Re}_{bulk} = 18290$
	$f_{Churchill} = 8\left[\left(\dfrac{8}{\mathrm{Re}_{bulk}}\right)^{12} + \left\{2.457\ln\left(\left[\dfrac{7}{\mathrm{Re}_{bulk}}\right]^{0.9} + 0.27\left(\dfrac{e}{D}\right)\right)^{16} + \left[\dfrac{37530}{\mathrm{Re}_{bulk}}\right]^{16}\right\}^{-1.5}\right]^{1/12}$	$f_{Churchill} = 0.02667$

Common Variables and Properties in Gas-Like Regime

Inputs	Equations	Results
$P_{r,test} = 5418$ kPa $G = 792.4$ kg/m²-s $D = 1.524$ mm $T_{r,test,avg} = T_{bulk} = 90.51°C$ $T_{wall} = 85.71°C$ $\varepsilon = \dfrac{e}{D} = 0.0001$	$\mu_{bulk}, \rho_{bulk}, k_{bulk}, \mathrm{Pr}_{bulk} = f\left(P_{r,test}, T_{bulk} =\right)$	$\mu_{bulk} = 21.96 \times 10^{-6}$ kg/m-s, $\rho_{bulk} =$ 233.3 kg/m³, $k_{bulk} = 0.03295$ W/m-K, $\mathrm{Pr}_{bulk} = 1.524$
	$\mu_{wall}, \rho_{wall} = f\left(P_{r,test}, T_{wall} =\right)$	$\mu_{wall} = 22.74 \times 10^{-6}$ kg/m-s, $\rho_{wall} =$ 258.2 kg/m³
	$\mathrm{Re}_{bulk} = \dfrac{GD}{\mu_{bulk}}$	$\mathrm{Re}_{bulk} = 54980$
	$f_{Churchill} = 8\left[\left(\dfrac{8}{\mathrm{Re}_{bulk}}\right)^{12} + \left\{2.457\ln\left(\left[\dfrac{7}{\mathrm{Re}_{bulk}}\right]^{0.9} + 0.27\left(\dfrac{e}{D}\right)\right)^{16} + \left[\dfrac{37530}{\mathrm{Re}_{bulk}}\right]^{16}\right\}^{-1.5}\right]^{1/12}$	$f_{Churchill} = 0.02076$

Pressure Drop Model – Liquid-Like Regime

Inputs	Equations	Results
$a = 1.16$	$f_{modified} = a \cdot f_{Churchill} \cdot \left(\dfrac{\mu_{wall}}{\mu_{bulk}}\right)^{b} =$	$f_{modified} = 0.03377$

Supercritical Pressure Drop and Heat Transfer Models		
Inputs	**Equations**	**Results**
$b = 0.91$ $f_{\text{Churchill}} = 0.02766$ $\mu_{\text{bulk}} = 77.39 \times 10^{-6}$ kg/m-s $\mu_{\text{wall}} = 81.86 \times 10^{-6}$ kg/m-s $G = 801.9$ kg/m^2-s $D = 1.524$ mm $\rho_{\text{bulk}} = 875.1$ kg/m^3 $\nabla P_{\text{experimental}} = 7.405$ kPa/m	$\left(\dfrac{\mathrm{d}P}{\mathrm{d}z}\right)_{\text{f}} = \dfrac{1}{2} \cdot f_{\text{modified}} \cdot \dfrac{G^2}{\rho_{\text{bulk}}} \cdot \dfrac{1}{D}$ $Error = \left(\nabla P_{\text{f}} - \nabla P_{\text{experimental}}\right) \Big/ \nabla P_{\text{experimental}}$	$\left(\dfrac{\mathrm{d}P}{\mathrm{d}z}\right)_{\text{f}} = \nabla P_{\text{f}} = 8.142$ kPa/m $Error = 9.9\ \%$
Heat Transfer Model – Liquid-Like Regime		
$f_{\text{modified}} = 0.03377$ $\text{Re}_{\text{bulk}} = 15790$ $\text{Pr}_{\text{bulk}} = 2.229$ $a = 0.56$ $b = 0.022$ $c = 0.010$ $D = 1.524$ mm $k_{\text{bulk}} = 0.07751$ W/m-K	$\text{Nu}_{\substack{\text{modified} \\ \text{Churchill}}} = \left[4.364^{10} + \left(\dfrac{\exp\left[\frac{2200 - \text{Re}_{\text{bulk}}}{365}\right]}{4.364^2} + \left(6.3 + \dfrac{0.079 \cdot \left(\frac{f_{\text{modified}}}{8}\right)^{1/2} \cdot \text{Re}_{\text{bulk}} \cdot \text{Pr}_{\text{bulk}}}{\left(1 + \text{Pr}_{\text{bulk}}^{0.8}\right)^{5/6}} \right)^{-2} \right)^{-5} \right]^{1/10}$	$\text{Nu}_{\text{modified Churchill}} = 80.72$
	$D^* = \dfrac{D}{9.398\text{mm}}$	$D^* = 0.1622$
	$\text{Nu} = a \cdot \text{Nu}_{\text{modified Churchill}} \cdot \text{Re}^{b+c/D^*}$	$\text{Nu} = 101.5$
	$h = \text{Nu}\,\dfrac{k_{\text{bulk}}}{D}$	$h = 5161$ W/m^2-K
	$Error = \left(h - h_{\text{experimental}}\right) \Big/ h_{\text{experimental}}$	$Error = 0.5\ \%$

Supercritical Pressure Drop and Heat Transfer Models		
Inputs	**Equations**	**Results**
$h_{\text{experimental}} = 5136$ W/m²-K		
Pressure Drop Model – PCT Regime		
$a = 1.31$	$f_{\text{modified}} = a \cdot f_{\text{Churchill}} \cdot \left(\dfrac{\mu_{\text{wall}}}{\mu_{\text{bulk}}}\right)^{b} =$	$f_{\text{modified}} = 0.03569$
$b = 0.25$		
$f_{\text{Churchill}} = 0.02667$	$\left(\dfrac{\text{d}P}{\text{d}z}\right)_{\text{f}} = \dfrac{1}{2} \cdot f_{\text{modified}} \cdot \dfrac{G^2}{\rho_{\text{bulk}}} \cdot \dfrac{1}{D}$	$\left(\dfrac{\text{d}P}{\text{d}z}\right)_{\text{f}} = \nabla P_{\text{f}} = 9.201$ kPa/m
$\mu_{\text{bulk}} = 66.07 \times 10^{-6}$ kg/m-s		
$\mu_{\text{wall}} = 71.98 \times 10^{-6}$ kg/m-s		
$G = 792.8$ kg/m²-s		
$D = 1.524$ mm		
$\rho_{\text{bulk}} = 799.9$ kg/m³	$Error = \left(\nabla P_{\text{f}} - \nabla P_{\text{experimental}}\right)\Big/ \nabla P_{\text{experimental}}$	$Error = 17.8$ %
$\nabla P_{\text{experimental}} = 7.807$ kPa/m		
Heat Transfer Model – PCT Regime		
$f_{\text{modified}} = 0.03377$	$\text{Nu}_{\substack{\text{modified} \\ \text{Churchill}}} = \left[4.364^{10} + \left(\dfrac{\exp\left[\frac{2200 - \text{Re}_{\text{bulk}}}{365}\right]}{4.364^2} + \left(6.3 + \dfrac{0.079 \cdot \left(\frac{f_{\text{modified}}}{8}\right)^{1/2} \cdot \text{Re}_{\text{bulk}} \cdot \text{Pr}_{\text{bulk}}}{\left(1 + \text{Pr}_{\text{bulk}}^{0.8}\right)^{5/6}} \right)^{-2} \right)^{-5} \right]^{1/10}$	$\text{Nu}_{\text{modified Churchill}} = 102.2$
$\text{Re}_{\text{bulk}} = 18290$		
$\text{Pr}_{\text{bulk}} = 2.572$		
$a = 0.56$	$D^{*} = \dfrac{D}{9.398\text{mm}}$	$D^{*} = 0.1622$
	$\text{Nu} = a \cdot \text{Nu}_{\text{modified Churchill}} \cdot \text{Re}^{b + c/D^{*}}$	$\text{Nu} = 130.1$

Supercritical Pressure Drop and Heat Transfer Models		
Inputs	**Equations**	**Results**
$b = 0.022$ $c = 0.010$ $D = 1.524$ mm $k_{bulk} = 0.07291$ W/m-K $h_{experimental} = 5555$ W/m²-K	$h = \text{Nu}\,\dfrac{k_{bulk}}{D}$	$h = 6223$ W/m²-K
	$Error = \dfrac{\left(h - h_{experimental}\right)}{h_{experimental}}$	$Error = 12.0\ \%$
Pressure Drop Model – Gas-Like Regime		
$a = 1.19$ $b = 0.17$ $f_{Churchill} = 0.02076$ $\mu_{bulk} = 21.96 \times 10^{-6}$ kg/m-s $\mu_{wall} = 22.74 \times 10^{-6}$ kg/m-s $G = 792.4$ kg/m²-s $D = 1.524$ mm $\rho_{bulk} = 233.3$ kg/m³ $\nabla P_{experimental} = 19.45$ kPa/m	$f_{modified} = a \cdot f_{Churchill} \cdot \left(\dfrac{\mu_{wall}}{\mu_{bulk}}\right)^{b} =$	$f_{modified} = 0.02485$
	$\left(\dfrac{\mathrm{d}P}{\mathrm{d}z}\right)_{f} = \dfrac{1}{2} \cdot f_{modified} \cdot \dfrac{G^{2}}{\rho_{bulk}} \cdot \dfrac{1}{D}$	$\left(\dfrac{\mathrm{d}P}{\mathrm{d}z}\right)_{f} = \nabla P_{f} = 21.95$ kPa/m
	$Error = \dfrac{\left(\nabla P_{f} - \nabla P_{experimental}\right)}{\nabla P_{experimental}}$	$Error = 12.8\ \%$
Heat Tranfer Model – Gas-Like Regime		

Supercritical Pressure Drop and Heat Transfer Models		
Inputs	**Equations**	**Results**
$f_{modified} = 0.02485$ $Re_{bulk} = 54980$ $Pr_{bulk} = 1.524$ $a = 0.19$	$Nu_{\substack{modified \\ Churchill}} = \left[4.364^{10} + \left(\dfrac{\exp\left[\dfrac{2200 - Re_{bulk}}{365}\right]}{4.364^2} + \left(6.3 + \dfrac{0.079 \cdot \left(\dfrac{f_{modified}}{8}\right)^{1/2} \cdot Re_{bulk} \cdot Pr_{bulk}}{\left(1 + Pr_{bulk}^{0.8}\right)^{5/6}} \right)^{-2} \right)^{-5} \right]^{1/10}$	$Nu_{modified\ Churchill} = 184.2$
$b = 0.118$	$D^* = \dfrac{D}{9.398\text{mm}}$	$D^* = 0.1622$
$c = 0.011$	$Nu = a \cdot Nu_{modified\ Churchill} \cdot Re^{b + c/D^*}$	$Nu = 266.0$
$D = 1.524$ mm	$h = Nu\ \dfrac{k_{bulk}}{D}$	$h = 5751$ W/m^2-K
$k_{bulk} = 0.03295$ W/m-K $h_{experimental} = 5802$ W/m^2-K	$Error = \dfrac{\left(h - h_{experimental}\right)}{h_{experimental}}$	$Error = 0.9\ \%$

REFERENCES

Akers, W. W., H. A. Deans and O. K. Crosser (1959), "Condensation Heat Transfer with Horizontal Tubes," *Chemical Engineering Progress Symposium Series*, pp. 171-176.

Bandhauer, T., A. Agarwal and S. Garimella (2005), "Measurement and Modeling of Condensation Heat Transfer Coefficients in Circular Microchannels," *ICMM2005*, Toronto, Ontario, Canada

Bandhauer, T. M. (2002). *Heat Transfer in Microchannel Geometries During Condensation of R-134a*. Mechanical Engineering. Ames, IA, Iowa State University.

Baroczy, C. J. (1965), "Correlation of Liquid Fraction in Two-Phase Flow with Applications to Liquid Metals," *Chem. Eng. Prog. Symp. Series* Vol. 61(57) pp. 179-191.

Boissieux, X., M. R. Heikal and R. A. Johns (2000), "Two-Phase Heat Transfer Coefficients of Three Hfc Refrigerants inside a Horizontal Smooth Tube, Part Ii: Condensation," *International Journal of Refrigeration* Vol. 23(5) pp. 345-352.

Breber, G., J. W. Palen and J. Taborek (1980), "Prediction of Horizontal Tubeside Condensation of Pure Components Using Flow Regime Criteria," *Journal of Heat Transfer, Transactions ASME* Vol. 102(3) pp. 471-476.

Carey, V. P. (1992). *Liquid-Vapor Phase-Change Phenomena: An Introduction to the Themophysics of Vaporization and Condensation Processes in Heat Transfer Equipment*, Taylor and Francis.

Cavallini, A., G. Censi, D. D. Col, L. Doretti, G. A. Longo and L. Rossetto (2002), "Condensation of Halogenated Refrigerants inside Smooth Tubes," *HVAC and R Research* Vol. 8(4) pp. 429-451.

Cavallini, A. and R. Zecchin (1974), "A Dimensionless Correlation for Heat Transfer in Forced Convective Condensation," *Proceedings of the 5th International Heat transfer Conference, JSME*, pp. 309-313.

Chato, S. C. (1962), "Laminar Condensation inside Horizontal and Inclined Tubes,"

ASHRAE Journal Vol. 4(2) pp. 52-60.

Chisholm (1967), "A Theoretical Basis for the Lockhart-Martinelli Correlation for Two-Phase Flow," *International Journal of Heat and Mass Transfer* Vol. 10 pp. 1767-1778.

Chisholm, D. (1973), "Pressure Gradients Due to Friction During the Flow of Evaporationg Two-Phase Mixtures in Smooth Tubes and Channels," *International Journal of Heat and Mass Transfer* Vol. 16(2) pp. 347-358.

Chisholm, D. (1983). *Two-Phase Flow in Pipelines and Heat Exchangers*. New York, Longman.

Churchill, S. W. (1977), "Comprehensive Correlating Equations for Heat, Mass and Momentum Transfer in Fully Developed Flow in Smooth Tubes," *Industrial and Engineering Chemistry, Fundamentals* Vol. 16(1) pp. 109-116.

Churchill, S. W. and H. H. S. Chu (1975), "Correlating Equations for Laminar and Turbulent Free Convection from a Vertical Plate," *International Journal of Heat and Mass Transfer* Vol. 18(11) pp. 1323-1329.

Coleman, J. W. (2000). *Flow Visualization and Pressure Drop in Small Hydraulic Diameter Geometries During Phase Change of Refrigerants*. Mechanical Engineering. Aimes, Iowa State University, Vol. Ph.D.

Coleman, J. W. and S. Garimella (2000a), "Two-Phase Flow Regime Transitions in Microchannel Tubes: The Effect of Hydraulic Diameter," *Procdings of IMECE*, Orlando

Coleman, J. W. and S. Garimella (2000b), "Visualization of Two-Phase Refrigerant Flow During Phase Change.," *Proc. 34th National Heat Transfer Conference*

Coleman, J. W. and S. Garimella (2003), "Two-Phase Flow Regimes in Round, Square and Rectangular Tubes During Condensation of Refrigerant R134a," *International Journal of Refrigeration* Vol. 26(1) pp. 117-128.

Dittus, W. and L. M. K. Boelter (1930), "Heat Transfer in Automobile Radiators of the Tubular Type," *University of California - Publications in Engineering* Vol. 2 p. 443.

Dobson, M. K. and J. C. Chato (1998), "Condensation in Smooth Horizontal Tubes.," *Journal of Heat Transfer* Vol. 120(1) pp. 193-213.

Ebisu, T. and K. Torikoshi (1998), "Heat Transfer Characteristics and Correlations for R-410a Flowing inside a Horizontal Smooth Tube," *ASHRAE Transactions* Vol. 104(2) pp. 556-561.

Eckels, S. J. and M. B. Pate (1991), "Experimental Comparison of Evaporation and Condensation Heat Transfer Coefficients for Hfc-134a and Cfc-12," *International Journal of Refrigeration* Vol. 14(2) pp. 70-77.

El Hajal, J., J. R. Thome and A. Cavallini (2003), "Condensation in Horizontal Tubes, Part 1: Two-Phase Flow Pattern Map," *International Journal of Heat and Mass Transfer* Vol. 46(18) pp. 3349-3363.

Ewing, M. E., J. J. Weinandy and R. N. Christensen (1999), "Observations of Two-Phase Flow Patterns in a Horizontal Circular Channel," *Heat Transfer Engineering* Vol. 20(1) pp. 9-14.

Filonenko, G. K. (1954), "Hydraulic Resistance in Pipes," *Teploenergetika (In Russian)* Vol. 1 pp. 10-44.

Friedel, L. (1979), "Improved Friction Pressure Drop Correlation for Horizontal and Vertical Two Phase Flow," *3R International* Vol. 18(7) pp. 485-491.

Garimella, S., A. Agarwal and J. D. Killion (2005), "Condensation Pressure Drop in Circular Microchannels," *Heat Transfer Engineering* Vol. 26(3) pp. 28-35.

Garimella, S. and T. M. Bandhauer (2001), "Measurement of Condensation Heat Transfer Coefficients in Microchannel Tubes, New York, NY, United States, American Society of Mechanical Engineers, p. 243.

Garimella, S. and R. N. Christensen (1995), "Heat Transfer and Pressure Drop Characteristics of Spirally Fluted Annuli, Part Ii: Heat Transfer," *ASME Journal of Heat Transfer* Vol. 117 pp. 61-68.

Garimella, S., J. D. Killion and J. W. Coleman (2002), "An Experimentally Validated Model for Two-Phase Pressure Drop in the Intermittent Flow Regime for Circular

Microchannels," *Journal of Fluids Engineering, Transactions of the ASME* Vol. 124(1) pp. 205-214.

Garimella, S., J. D. Killion and J. W. Coleman (2003), "An Expermentally Validated Model for Two-Phase Pressure Drop in the Intermittent Flow Regime for Noncircular Microchannels," *Journal of Fluids Engineering, Transactions of the ASME* Vol. 125(5) p. 887.

Ghajar, A. J. and A. Asadi (1986), "Improved Forced Convective Heat Transfer Correlations for Liquids in the near-Critical Region," *AIAA Journal* Vol. 24(12) pp. 2030-2037.

Gnielinski, V. (1976), "New Equations for Heat and Mass Transfer in Turbulent Pipe and Channel Flow," *International Chemical Engineering.* Vol. 16(2) pp. 359-368.

Gonzalez, M. and G. M. Bankobeza (2003). *Handbook for the International Treaties for the Protection of the Ozone Layer*. Sixth Edition Ed. Nairobi, Kenya, United Nations Environment Programme.

Han, D.-H. and K.-J. Lee (2001), "Experiments on Condensation Heat Transfer Characteristics inside a 7 Mm Outside Diameter Microfin Tube with R410a," *35th National Heat Transfer Conference, Anaheim, California*.

Hewitt, G. F., G. L. Shires and T. R. Bott (1994). *Process Heat Transfer*, CRC Press LLC.

Incropera, F. P. and D. P. DeWitt (1996). *Fundamentals of Heat and Mass Transfer*. Fourth Edition Ed., John Wiley & Sons, Inc.

Irvine, T. F. J. and J. P. Hartnett (1975). *Advances in Heat Transfer*. New York, Academic Press.

Jackson, J. D. and J. Fewster (1975). Aere-R8158. Harwell.

Jiang, Y. (2004). *Quasi Single-Phase and Condensation Heat Transfer and Pressure Drop of Refrigerant R404a at Supercritical and near Critical Pressures*. Mechanical Engineering. Ames, Iowa State University, Ph.D.

Kattan, N., J. R. Thome and D. Favrat (1998a), "Flow Boiling in Horizontal Tubes: Part 1 - Development of a Diabatic Two-Phase Flow Pattern Map," *Journal of Heat Transfer, Transactions ASME* Vol. 120(1) pp. 140-147.

Kattan, N., J. R. Thome and D. Favrat (1998b), "Flow Boiling in Horizontal Tubes: Part 2 - New Heat Transfer Data for Five Refrigerants," *Journal of Heat Transfer, Transactions ASME* Vol. 120(1) pp. 148-155.

Kattan, N., J. R. Thome and D. Favrat (1998c), "Flow Boiling in Horizontal Tubes: Part 3 - Development of a New Heat Transfer Model Based on Flow Pattern," *Journal of Heat Transfer, Transactions ASME* Vol. 120(1) pp. 156-165.

Kawahara, A., P. M.-Y. Chung and M. Kawaji (2002), "Investigation of Two-Phase Flow Pattern, Void Fraction and Pressure Drop in a Microchannel," *International Journal of Multiphase Flow* Vol. 28(9) pp. 1411-1435.

Kays, W. M. and E. Y. Leung (1963), "Heat Transfer in Annular Passages: Hydrodynamically Developed Flow with Arbitrarily Prescribed Heat Flux," *International Journal of Heat and Mass Transfer* Vol. 6 pp. 537-557.

Kim, N.-H., J.-P. Cho, J.-O. Kim and B. Youn (2003), "Condensation Heat Transfer of R-22 and R-410a in Flat Alumninum Multi-Channel Tubes with or without Micro-Fins," *International Journal of Refrigeration* Vol. 26 pp. 830-839.

Klein, S. A. (2005). *Engineering Equation Solver*. V7.431-3D, F-Chart Software.

Kosky, P. G. and F. W. Staub (1971), "Local Condensing Heat Transfer Coefficients in the Annular Flow Regime," *AIChe Journal* Vol. 17(5) pp. 1037-1043.

Krasnoshchekov, E. A., I. V. Kuraeva and V. S. Protopopov (1970), "Local Heat Transfer of Carbon Dioxide at Supercritical Pressure under Cooling Conditions.," *Teplofizika Vysokikh Temperatur* Vol. 7(5) pp. 922-930.

Kuraeva, I. V. and V. S. Protopopov (1974), "Mean Friction Coefficients for Turbulent Flow of a Liquid at a Supercritical Pressure in Horizontal Circular Tubes," *Teplofizika Vysokikh Temperatur* Vol. 12(1) pp. 218-220.

Kurganov, V. A. (1998a), "Heat Transfer and Pressure Drop in Tubes under Supercritical Pressure of the Coolant. Part 1: Specifics of the Thermophysical Properties,

Hydrodynamics, and Heat Transfer of the Liquid. Regimes of Normal Heat Transfer," *Thermal Engineering (English translation of Teploenergetika)* Vol. 45(3) pp. 177-185.

Kurganov, V. A. (1998b), "Heat Transfer and Pressure Drop in Tubes under Supercritical Pressure. Part 2. Heat Transfer and Friction at High Heat Fluxes. The Influence of Additional Factors. Enhancement of Deteriorated Heat Transfer," *Thermal Engineering (English translation of Teploenergetika)* Vol. 45(4) pp. 301-310.

Kwon, J. T., Y. C. Ahn and M. H. Kim (2001), "A Modeling of in-Tube Condensation Heat Transfer for a Turbulent Annular Film Flow with Liquid Entrainment," *International Journal of Multiphase Flow* Vol. 27(5) pp. 911-928.

Kwon, J. T. and M. H. Kim (2000), "Modeling and Experiments of in-Tube Condensation Heat Transfer for R22 and Its Alternative Refrigerant," *JSME International Journal, Series B* Vol. 43(4) pp. 596-601.

Lee, H. J. and S. Y. Lee (2001), "Pressure Drop Correlations for Two-Phase Flow within Horizontal Rectangular Channels with Small Heights," *International Journal of Multiphase Flow* Vol. 27(5) pp. 783-796.

Lemmon, E. W., M. O. McLinden and M. L. Huber (2002). *Refprop Version, 7.0 Beta Version*. NIST Standard Reference Database 23, NIST.

Lockhart, R. W. and R. C. Martinelli (1949), "Proposed Correlation of Data for Isothermal Two-Phase Two-Component Flow in a Pipe," *Chem. Eng. Prog. Symp. Series* Vol. 45 p. 39.

Micropump, I. (2000). Micropump Series 5000 Technical Datap.

Mishima, K. and T. Hibiki (1996), "Some Characteristics of Air-Water Two-Phase Flow in Small Diameter Vertical Tubes," *International Journal of Multiphase Flow* Vol. 22(4) pp. 703-712.

Mitra, B. (2005). *Supercritical Gas Cooling and Condensation of Refrigerant R410a at near-Critical Pressures*. Meachanical Enginerring. Atlanta, Georgia Institute of Technology, Ph.D.

Moser, K. W., R. L. Webb and B. Na (1998), "A New Equivalent Reynolds Number Model for Condensation in Smooth Tubes," *Journal of Heat Transfer* Vol. 120 pp. 410-417.

Munson, B. R., D. F. Young and T. H. Okiishi (1998). *Fundamentals of Fluid Mechanics*. 3nd. Ed.

Petukhov, B. S. (1970), "Heat Transfer and Friction in Turbulent Pipe Flow with Variable Physical Properties," *Advances in Heat Transfer* Vol. 6.

Petukov, B. S., E. A. Krasnoshchekov and V. S. Protopopov (1961), "An Investigation of Heat Transfer to Fluids Flowing in Pipes under Supercritical Conditions.," *ASME International Developments in Heat Transfer Part 3* pp. 569-578.

Pitla, S. S., E. A. Groll and S. Ramadhyani (2001a), "Convective Heat Transfer from in-Tube Cooling of Turbulent Supercritical Carbon Dioxide: Part 2 - Experimental Data and Numerical Predictions," *HVAC&R Research* Vol. 7(4) pp. 367-382.

Pitla, S. S., E. A. Groll and S. Ramadhyani (2001b), "Convective Heat Transfer from in-Tube Flow of Turbulent Supercritical Carbon Dioxide: Part 1 - Numerical Analysis," *HVAC&R Research* Vol. 7(4) pp. 345-366.

Pitla, S. S., E. A. Groll and S. Ramadhyani (2002), "New Correlation to Predict the Heat Transfer Coefficient During in-Tube Cooling of Turbulent Supercritical Co_2," *International Journal of Refrigeration* Vol. 25(7) pp. 887-895.

Pitla, S. S., D. M. Robinson, E. A. Groll and S. Ramadhyani (1998), "Heat Transfer from Supercritical Carbon Dioxide in Tube Flow: A Critical Review," *HVAC&R Research* Vol. 4(3).

Rabas, T. J. and B. Arman (2000), "Effect of the Exit Condition on the Performance of in-Tube Condensers," *Heat Transfer Engineering* Vol. 21 pp. 4-14.

Rouhani, S. Z. and E. Axelsson (1970), "Calculation of Void Volume Fraction in the Subcooled and Quality Boiling Regions," *International Journal of Heat and Mass Transfer* Vol. 13 pp. 383-393.

Sardesai, R. G., R. G. Owen and D. J. Pulling (1981), "Flow Regimes for Condensation of a Vapour inside a Horizontal Tube," *Chemical Engineering Science* Vol. 36 pp. 1173-1180.

Shah, M. M. (1979), "A General Correlation for Heat Transfer During Film Condensation inside Pipes," *International Journal of Heat and Mass Transfer* Vol. 22 pp. 547-556.

Shitsman, M. E. (1963), "Impairment of the Heat Transmission at Supercritical Pressures," *Teplofizika Vysokikh Temperatur* Vol. 1(2) pp. 267-275.

Soliman, H. M. (1982), "On the Annular to Wavy Flow Pattern Transition During Condensation inside Horizontal Tubes," *Canadian Journal of Chemical Engineering* Vol. 60 pp. 475-481.

Swagelok (2003). An Installer's Pocket Guide for Swagelok Tube Fittings. Solon, OH, 19 p.

Sweeney, K. A. (1996). *The Heat Transfer and Pressure Drop Behavior of a Zeotropic Refrigerant Mixture in a Micro-Finned Tube*. Dept. Mechanical and Industrial Engineering. Urbana, IL, University of Illionis at Urbana-Champaign.

Taitel, Y. and A. E. Dukler (1976), "A Model for Predicting Flow Regime Transitions in Horizontal and near Horizontal Gas-Liquid Flow," *AIChe Journal* Vol. 22(1) pp. 47-54.

Tanaka, H., N. Nishiwaki, M. Hirate and A. Tsage (1971), "Forced Convection Heat Transfer to a Fluid near Critical Point Flowing in Circular Tube," *International Journal of Heat and Mass Transfer* Vol. 14 pp. 739-750.

Tandon, T. N., H. K. Varma and C. P. Gupta (1982), "A New Flow Regimes Map for Condensation inside Horizontal Tubes," *ASME Journal of Heat Transfer* Vol. 104(4) pp. 763-768.

Tandon, T. N., H. K. Varma and C. P. Gupta (1985), "Prediction of Flow Patterns During Condensation of Binary Mixtures in a Horizontal Tube," *Journal of Heat Transfer, Transactions ASME* Vol. 107(2) pp. 424-430.

Taylor, B. N. and C. E. Kuyatt (1994), "Guidelines for Evaluating and Expressing the Uncertainty of Nist Measurement Results," *National Institute of Standards and Technology* (SP 1297).

Thome, J. R., J. El Hajal and A. Cavallini (2003), "Condensation in Horizontal Tubes, Part 2: New Heat Transfer Model Based on Flow Regimes," *International Journal of Heat and Mass Transfer* Vol. 46(18) pp. 3365-3387.

Tran, T. N., M.-C. Chyu, M. W. Wambsganss and D. M. France (2000), "Two-Phase Pressure Drop of Refrigerants During Flow Boiling in Small Channels: An Experimental Investigation and Correlation Development," *International Journal of Multiphase Flow* Vol. 26(11) pp. 1739-1754.

Traviss, D. P., W. M. Rohsenow and A. B. Baron (1973), "Forced-Convection Condensation inside Tubes: A Heat Transfer Equation for Condenser Design," *ASHRAE Transactions* Vol. 79(Part 1) pp. 157-165.

Walker, J. E., G. A. Whan and R. R. Rothfus (1957), "Fluid Friction in Noncircular Ducts," *AIChE Journal* Vol. 3(4) pp. 484-489.

Webb, R. L. (1998), "Prediction of Condensation and Evaporization in Micro-Fin and Micro-Channel Tubes," *In: Kakac, Bergles, Mayinger, Yuncu Heat Transfer Enhancement of Heat Exchangers* pp. 529-550.

Zivi, S. M. (1964), "Estimation of Steady-State Stream Void-Fraction by Means of the Principle of Minimum Entropy Production," *ASME Journal of Heat Transfer* Vol. 86 pp. 247-252.